In-Situ Measurement of Wind Loads for Roof Edge Metal Configurations

By

Jason Bysice

A thesis presented to the University of Ottawa
in partial fulfilment of
the requirements for the degree of

Master of Applied Science in Civil Engineering

Department of Civil Engineering
University of Ottawa
Ottawa, Ontario, Canada
June 2015

M.A.Sc in Civil Engineering is a joint program
with Carleton University administrated by the
Ottawa-Carleton Institute for Civil Engineering (OCICE)

Abstract

The role of a roof on any building is to separate the interior environment of the building from the exterior environment, thereby making it a crucial component of the building design. Metal roof edges are the first line of defense against wind-induced loads on the roof system; however, data on the nature of these loads acting on the roof edge system is scarce. Previous studies with field measurements of wind pressure acting on the roof edge reported that metal flashings experienced negative pressure. These findings suggest that current building codes in North America (i.e. NBCC and ASCE codes) do not accurately identify wind design loads acting on roof edge systems. The Roof Edge Systems and Technologies (REST) project is a consortium of academia, government and roof industries, which was created to develop testing protocols and design guidelines for roof edges. The work presented in this thesis contributes to the collection and analysis of wind loads acting on metal roof edges, which were installed on the Canada Post building in Vancouver, Canada. The thesis presents the findings and analysis of the measured wind-induced pressure acting on all surfaces of three different edge configurations, namely the Anchor Clip Configuration (ACC), Continuous Cleat Configuration (CCC) and Discontinuous Cleat Configuration (DCC). The analysis showed the presence of negative pressure acting on all three faces of the configurations, in which the type of configuration had minimum effect on the magnitude and nature of the wind-induced loads. Furthermore, the top face of the edge configurations was found to experience the highest suction, and the front face of the edge coping was subjected to a net outward suction force due to the combination of the suction experienced by the coping front face and the positive pressure acting on the cleat. Comparison of these results with current NBCC and ASCE building codes highlight a need to update these codes in order to adequately design metal roof edges against wind action.

Acknowledgements

The road of life is never walked alone, and it is by surrounding ourselves with great and caring people who help encourage us that we are able to succeed in it. I would like to take this opportunity to express my gratitude to all the people who have given their support toward the completion of this thesis.

I would like to express a great deal of gratitude to Dr. Bas A. Baskaran, my supervisor, who has provided his incredible guidance during this work. Dr. Baskaran has given me invaluable knowledge and experience that has led to the success of this paper.

I would also like to express appreciation to Dr. Beatriz Martin-Perez, my co-supervisor, for her amazing support and assistance during this work. Not enough words can be said about all advice she has given that has contributed to the success of this work.

A great deal of thankfulness goes to Nelson, Mike and Andrea who have been working alongside me, giving their support and assistance during my research.

I would like to express my sincere thanks to the thesis examiners Dr. Ghasan Doudak and Dr. David Lau for taking the time to review my thesis and for their valuable comments and feedback. In addition, special thanks to Dr. Magdi Mohareb, the defence chair

Many thanks go to the amazing staff of the NRC including Amor, David, Suda, Steven and others who helped in operating the facilities and offered a wide range of technical support and academic assistance.

To the sponsoring companies and organizations that funded this project and gave technical assistance along with the materials required for the experimental work. Thank you.

Finally, I owe a lot to my family and friends who have supported me endless love and encouragement.

Table of Contents

List of Figures

List of Tables

Chapter 1 : Introduction

1.1 Background

The roof is a crucial part of a building structure as its role is to separate the internal and external environments of the building. It is the first member of a building structure that can experience damage due to strong winds, resulting in individual or composite failure of its components. Roofs can be classified in two ways based on their slope, namely a low-slope or steep-slope roof. Low-slope roofs are installed on commercial buildings such as warehouses, whereas steep-slope roofs are found installed on residential buildings (e.g., gable or hip roof) (Figure 1.1). A low-slope roof is comprised of the roof deck, vapour or air barrier, insulation, cover board and waterproof membrane (Figure 1.2). Once these layers have been put together, roofing systems are classified based on the method of attachment, such as the Adhesive Applied Roofing Systems (AARS), Mechanically Attached Roofing Systems (MARS), Fully-Bonded Roofing Systems (FBRS), and Ballasted Roofing Systems (BRS).

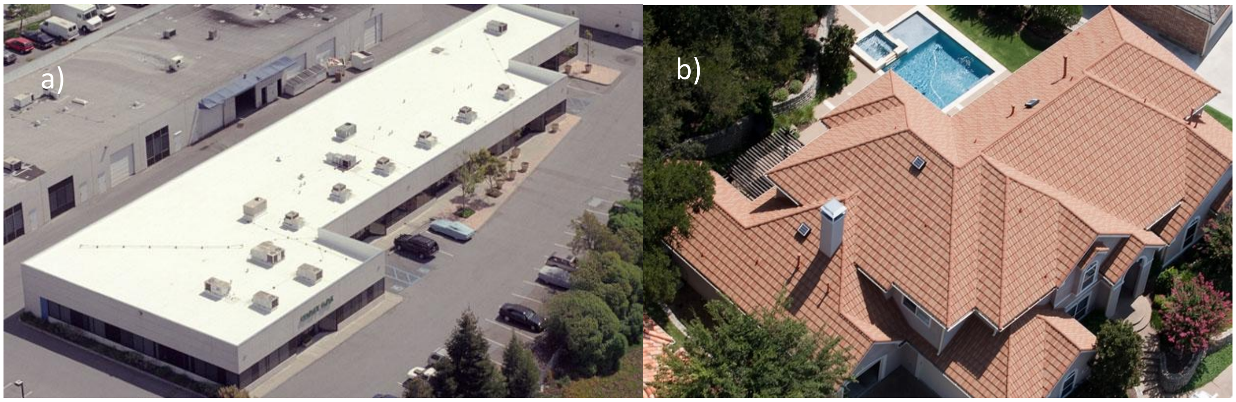

Figure 1.1: Low-slope roofs: (a) commercial roof and (b) residential roof (http://www.visionroofservices.com)

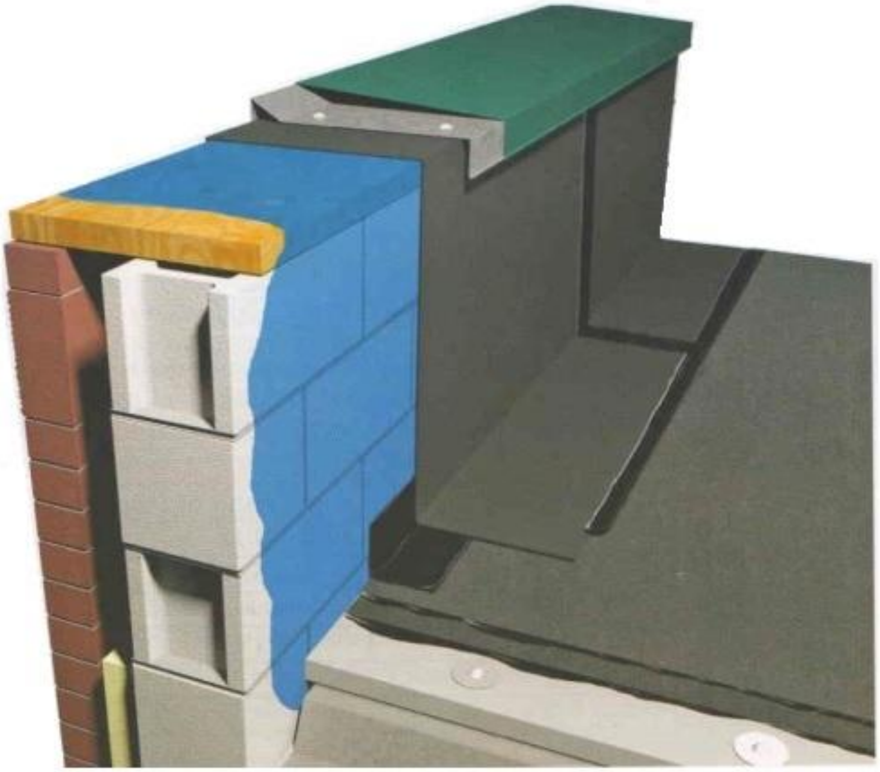

Figure 1.2: Typical low slope roof assembly (Mellott and Diamond, 2015)

Changes in the Earth's climate can lead to extreme weather events such as hurricanes and tornadoes, which cause flooding and high wind speeds. These events can severely damage the roof edge systems of low-rise buildings and result in failure. In October of 2012, Hurricane Sandy caused severe damage to building and the roof envelope, leading to several total roofs collapses (CBC News 2012). Figure 1.3 shows various failures for roof edge system for different components that have been seen in the field.

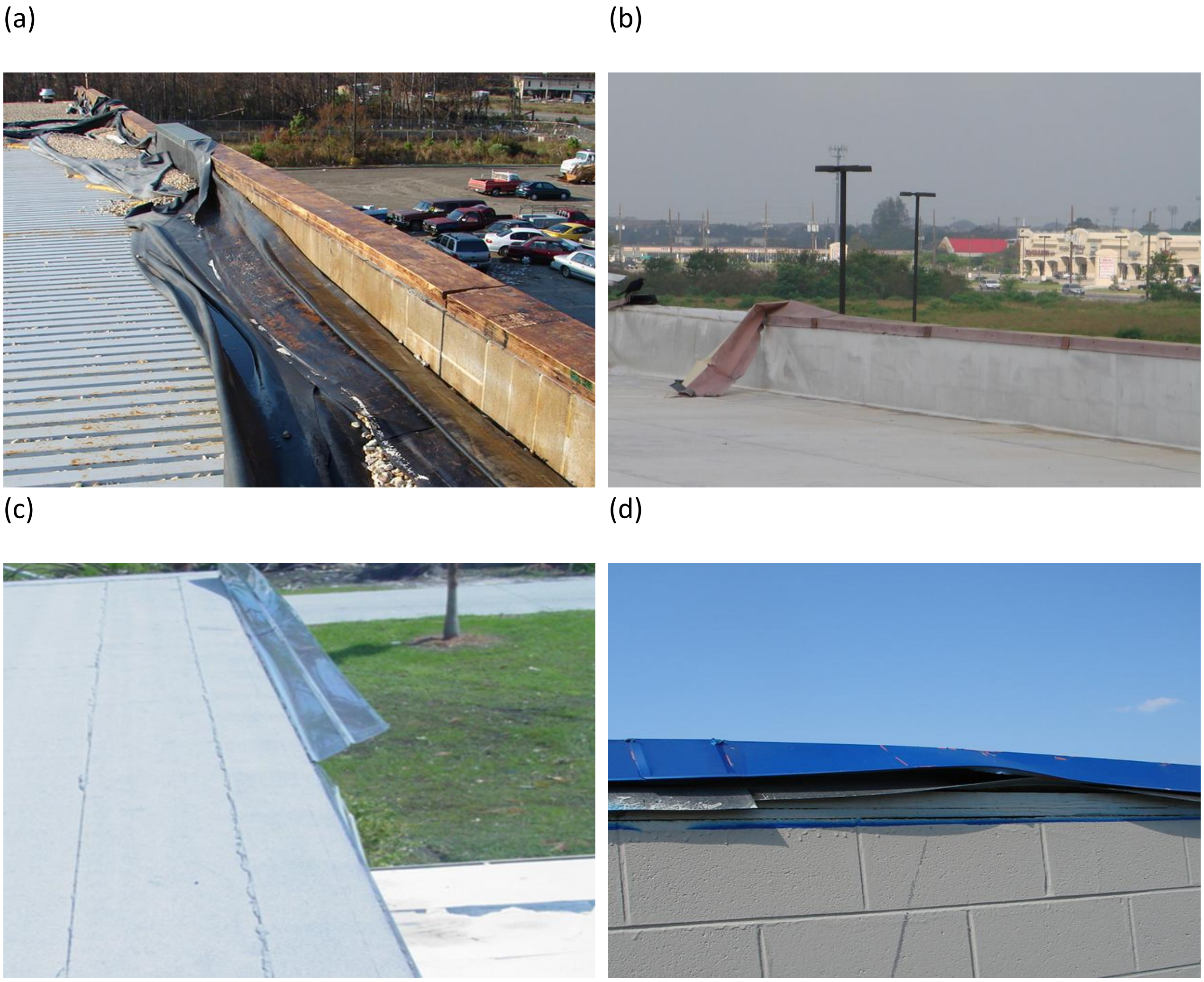

Figure 1.3: Typical roof edge failures during high wind conditions: (a) complete failure, (b) partial failure, (c) cleat failure and (d) coping failure. (Courtesy of NRCC)

1.2 Wind Effects on Roofs

As wind hits a rectangular building, the air flow follows the contours of the structure. The separated air flow is divided into a thin region of high shear and vortices known as a free shear layer (Holmes, 2001). Shear layers are unstable, but reattach to the surface of the roof to create vortices along the roof of the building. The stagnation point is defined as the point of zero air velocity and divides the building into upstream and downstream regions (Figure 1.4). The negative velocities and low pressures of the downstream region indicate the occurrence of a flow separation bubble, whereas the upstream region is characterized by positive wind velocities and high pressure (Holmes, 2001). The dynamics of the wind pressure can be described by static components, such as mean pressure, and fluctuating components, such as dynamic pressure, often modelled as a random process.

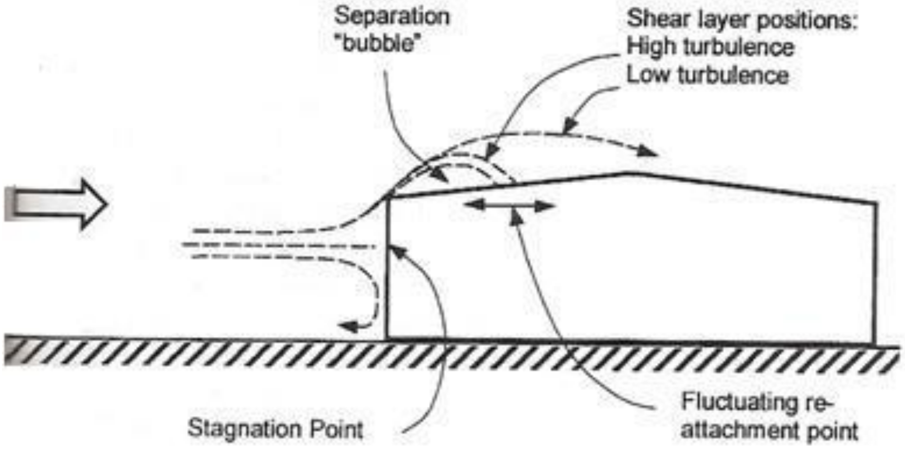

Figure 1.4: Wind flow around a low-slope roof (Holmes, 2001)

A roof surface can be divided into three zones known as the field, edge and corner. The field area of the roof covers the majority of the roof's surface. The edge area of the roof runs along the edge of the building and has a width defined on the basis of the building geometry. The corner area has an equal width as the edge, and the length is twice the width. A parapet is a barrier that is an extension of the wall at the roof's edge and may or may not be included in the roof design. They are widely used on buildings and are specifically a crucial part of low-rise buildings. Parapets not only serve for safety purposes, but they are also used for joining the wall to the roof membrane. The main component of the parapet is the substrate, which can be made of various materials, such as concrete, wood and metal.

As the wind flows over the roof of the building, it generates a negative pressure or suction along the surface of the metal cap of the roof edge system. The design of roof edge components must therefore guarantee that the high suction will not damage the roof edge system. Ideally, roof edge systems should be determined from tests in field experiments of actual roof edge systems, rather than using wind tunnels to determine design loads. The roof edge systems would have scaling issues in wind tunnels and the wind loads in the wind tunnels do not properly show what would happen in the field. Over the service life, a properly designed roof edge system must be able to withstand wind-induced loads greater than the design wind loads.

1.3 Roof Edge Systems

A roof edge is defined as the perimetric part of a roof that serves as termination for roof components to the wall (Figure 1.5). Architects use the entirety of roof edges to add to the aesthetics of the building exterior. The roof edge acts as an effective termination and transition between the roof and wall, so that no component of the roof system is noticeable from the building exterior (Alassafin et al 2014). A typical roof edge system is comprised of metal components such as coping coverings and the cleat/clip, which is a load transferring metal component secured to the parapet by fasteners or nails. In addition, the coping or metal cap is typically attached to the cleat/clip using various attachments (such as snap-on), and then placed over the length of the parapet. The different types of commercially available roof edge systems share similar structural components with slightly different layouts (Figure 1.6).The roof edge system is the first line of defense against wind loads along the roof edge, thereby making it essential that it is adequately designed and installed on the structure. The wind loads (dynamic in nature) acting on the roof edge system must also be properly identified for the design process of the roof edge system.

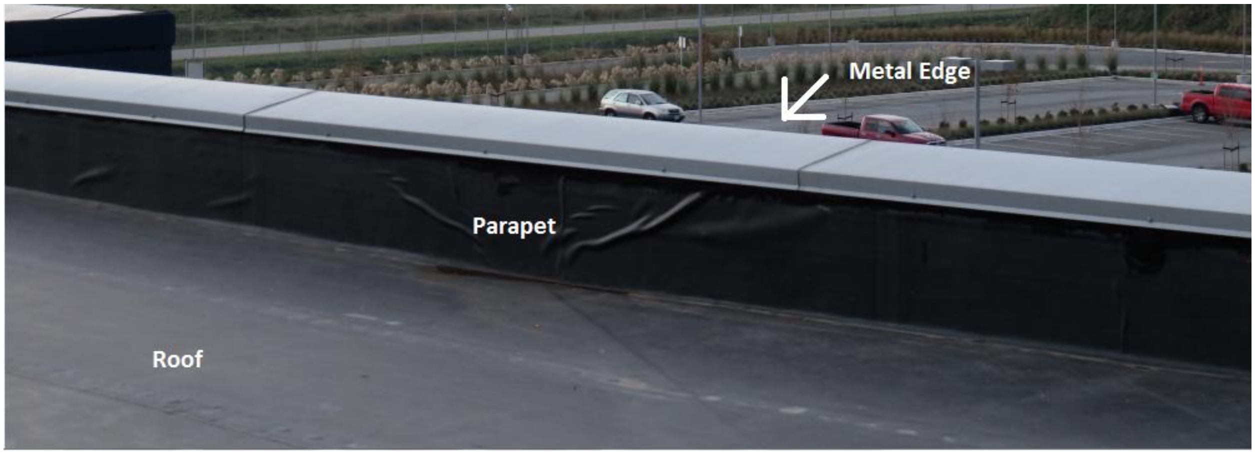

Figure 1.5: Parapet connecting the roof and wall (Courtesy of NRCC)

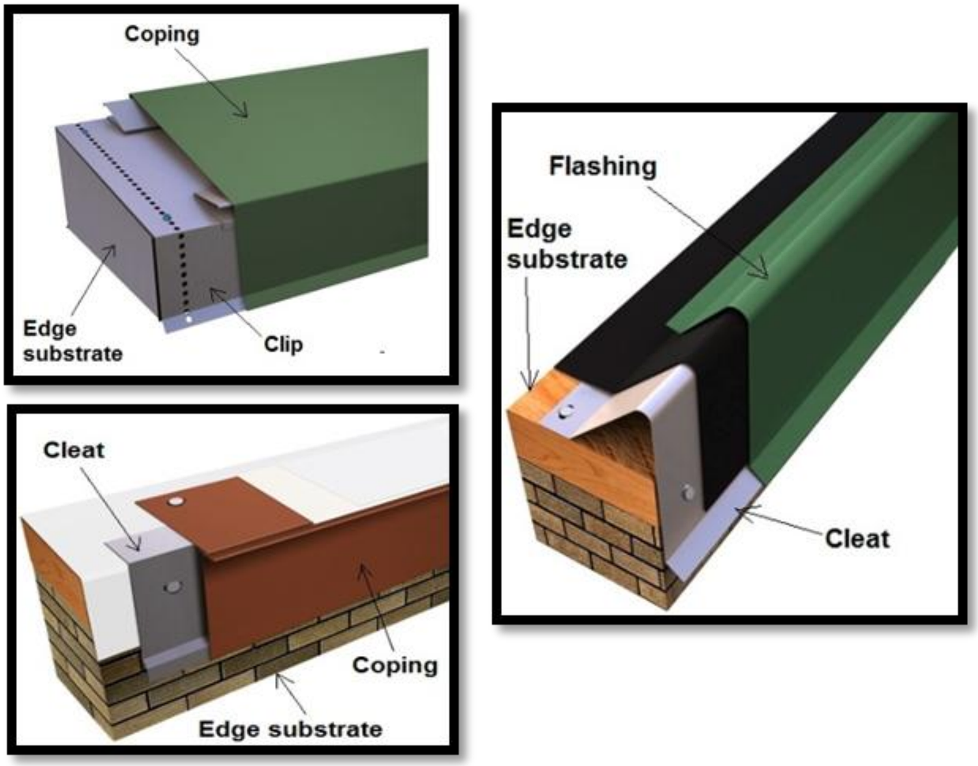

Figure 1.6: Typical roof edge systems installed on commercial roofs

(https://www.metalera.com)

Wind flowing over a roof’s surface generates an uplift force or negative pressure (suction), thereby requiring parapets to alter the wind flow around the structure. Kopp et al. (2005) concluded that a parapet adjusts the wind flow, which results in lower suction over the corner area of the roof by elevating the corner vortices above the roof surface, an effect which is a function of the height of the parapet.

Roof edge systems are used for holding the roof membrane in place along the edge, as well as protecting the roof components from water infiltration. When roof edge systems are poorly finished or not properly installed, even weak wind uplift forces can disturb the roof membrane of the now uncertain roofing system. The roof edge system must therefore be structurally sound to resist high wind loads during its service life.

1.4 Forces on Roof Edges

As wind hits the roof edge, it breaks down into vortices which create large pressure differences at the roof’s perimeter (Figure 1.7). The arrows in Figure 1.7 indicate air flow, vortices and uplift forces. The negative pressure from the wind on the roof edge system surface induces horizontal outward forces and uplift forces (F_1 and F_2 in Figure 1.7, respectively), which cause coping disengagement from the cleat and nail pullout. The pressure differences create suction pressure on the roof membrane, whose associated wind uplift force (F_3 in Figure 1.7) can ultimately blow roofs off buildings.

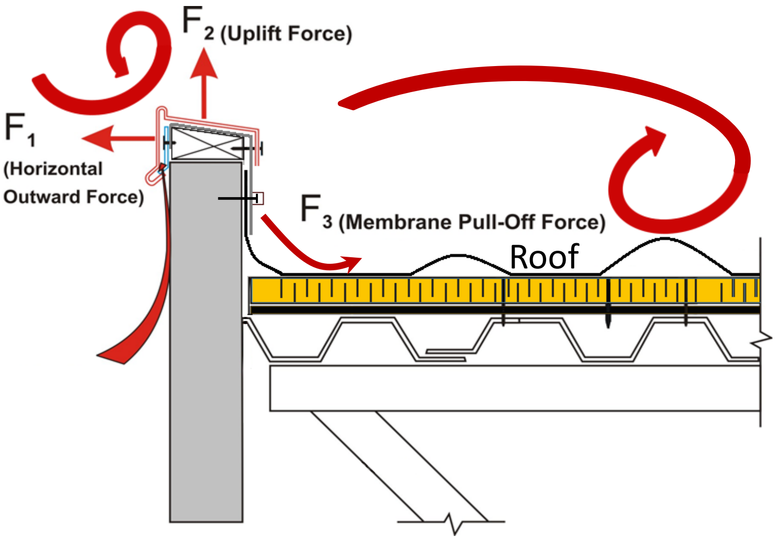

Figure 1.7: Wind-induced forces on roof edges: horizontal outward force F_1, vertical uplift force F_2 and oblique pull-off force F_3

1.5 Roof Edge Systems and Technologies (REST) Project - Overview

Literature regarding the real effect of wind-induced loads acting on the roof edge system is scarce. In the last two decades, only three studies with full-scale measurements have analyzed metal flashings on the roof edge and wind-induced loads on the parapet, all of which experienced negative pressure (Jiang, 1995; McDonald et al., 1997; Bedair, 2009). This negative pressure is thought to be the cause of major failures of roof edge systems as observed by Baskaran et al. (2007), suggesting that current building codes in North America, such as the National Building Code of Canada (NBCC) and the American Society of Civil Engineers (ASCE) code, do not properly identify the wind design loads acting on roof edge systems.

In this context the Roof Edge Systems and Technologies (REST) project was created to develop testing protocols and design guidelines for roof edges. This project was initiated in cooperation with the Natural Sciences and Engineering Research Council (NSERC), as well as project partners including the Department of Civil Engineering of the University of Ottawa, the National Research Council of Canada (NRCC) and members of the Canadian roofing industry (Firestone Building Products, Menzies Metal Products, Soprema Inc. and RCABC, together with contributors JRS Engineering Group and Metal-Era). The REST project consists of the following tasks:

TASK 1: Experimental investigation of

1.1 Components of Roof Edge Systems

1.2 Roof Edge Systems (Interaction with roofing systems)

1.3 In-Situ Roof Edge Systems

TASK 2: Formulation of a numerical model by using finite element analysis.

TASK 3: Development of wind design guide and standards.

1.6 Focus of the Present Study

Alassafin (2013) developed a new experimental setup for full-scale testing of components of roof edge systems in a lab setting under Task 1.1. Hajsaid (2014) further evaluated the roof edge components of different edge configurations installed on parapets of different materials. In Task 1.2, Borzoee (2012) tested the different attachment methods of roof edge systems, and Dabas (2013) developed a numerical model of the roof edge system using finite element analysis for Task 2. The present work is part of Task 1.3. The main objectives of the research include:

1. Evaluating the wind-induced pressure acting on different configurations of metal roof edges installed at a field site, and producing a novel methodology to analyze the measured data.
2. Comparing the results collected from the field site with previous studies, with a focus on the wind-induced loads acting along the roof edge.
3. Comparing the measured results with current building standards and codes for wind loads on roof edges in North America, namely with the National Building Code of Canada (NBCC) and to the American Society of Civil Engineers (ASCE) Code.

1.7 Thesis Outline

This thesis aims to present previous work pertaining to this field of research, discuss the methodology and results of the project, and finally discuss the results of this project. A chapter by chapter summary includes the following:

Chapter 2 describes past work inside the scope of the REST project, including a literature review of existing design guidelines for roof edges, the current building code specifications and previous field experimental studies on roof parapets and metal edges.

Chapter 3 presents the field experiment site and describes the different installed roof edge configurations. This includes details of the building, pressure tap and on-site instrumentation. In addition, it discusses the procedure used to analyze the collected data.

Chapter 4 presents and discusses the measured results of the various roof edge configurations.

Chapter 5 compares the results of the performance of the configurations with other studies and to the current building codes in North America.

Chapter 6 draws the main conclusions of this study and delineates recommendations for future research.

Chapter 2: Literature Review

2.1 Introduction

This chapter reviews the different studies that addressed REST. Taking into account the focus of the present work on wind effects on parapets with metal edges, selected works from literature and building codes have been summarized. The literature that has come from the REST project will be reviewed in Section 2.2. Section 2.3 will look at the existing standards and codes. The experimental studies that concern effects on roofs with and without parapets, on roof metal edges, and on parapets are viewed at in section 2.4.

2.2 REST Project Research Review

The effect of hurricanes on buildings often lead to major failures of roof edges, as demonstrated in a study conducted by Baskaran et al. (2007). The evidence observed from these events suggests that the current building codes do not properly account for wind loads on the roof edge. The NRCC initiated a project, with partners from the University of Ottawa and the Canadian roofing industry that focused on REST. The goal of this project is to develop testing procedures and design guidelines for roof edges. The project was divided into three tasks, the first of which was focused on experimental testing. The first task was further subdivided into (i) experimental lab testing of roof edge components, (ii) experimental lab testing of roof edge systems, and (iii) in-situ testing of roof edge systems.

Experimental lab testing was conducted by Alassafin (2013), in which a new experimental method for testing roof edge components was developed. The experimental setup used a gust simulator device to mimic wind gusts (Figure 2.1) and pressure bags installed along the parapet and underneath the edge coping to simulate wind pressure. The testing method proposed showed multiple failure modes (coping/cleat disengagement, cleat fastener pull-out) and a realistic system rating for the roof edge systems. This was applied to a number of roof edge configurations, namely the continuous cleat configuration (CCC), discontinuous cleat configuration (DCC) and anchor clip configuration (ACC). The resistance of these configurations were then compared to one another, and the results showed that the CCC edge performance was superior in comparison to the DCC and ACC.

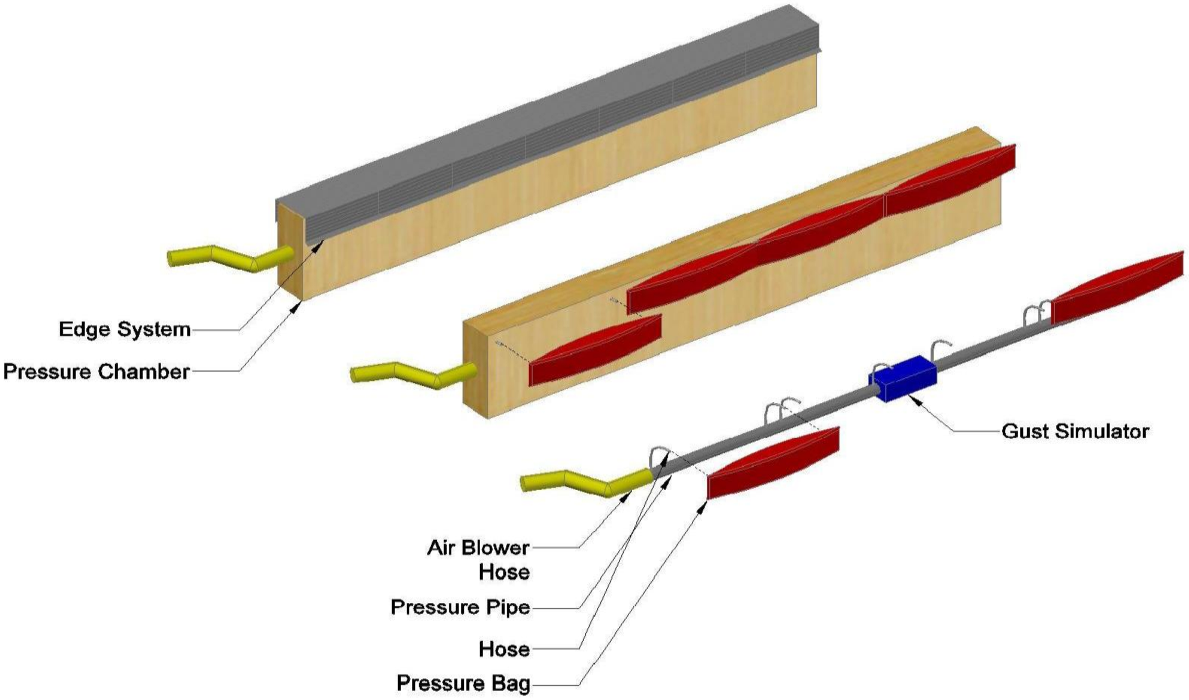

Figure 2.1: Overall view of the experimental setup in Alassafin (2013)

Experimental lab testing of roof edge systems was conducted by Borzoee (2012), in which five single-ply roofing systems were tested using the protocol proposed by the Special Interest Group for Dynamic Evaluation of Roofing Systems (SIGDERS) at the NRCC Dynamic Roofing Facility. The study investigated the performance of five roof systems, each with different attachment methods and membranes. It was observed that the wind-uplift resistance of the tested systems was dependent on the attachment methods (mechanically attached or fully bonded). Of the two attachment methods tested, systems with membranes mechanically attached had a wind rating greater than 50% of those which were fully bonded. In addition, the Thermoplastic Olefin Membrane (TPO) single-ply system had a wind rating 50% higher than the Modified Bitumen (Mod-Bit) membrane, showing that the type of membrane has an effect on the wind uplift rating. In all tested cases, failure of the roofing systems was initiated at the membrane and not at the roof edge. Figure 2.2 shows the billowing of the membrane as well as deformation in the back leg of the roof edge coping.

Figure 2.2: Laboratory testing system for full-scale single ply roofing system mock ups. a) whole system installed, b) close up, from Borzoee (2012)

A field pilot study was conducted by Baskaran et al. (2011) at the NRCC in Ottawa to investigate the in-situ performance of roof metal edge systems, the goal being to experimentally determine the wind pressure acting on each of the faces of a metal edge installed on a roof parapet. Pressure taps were installed on every face of the parapet, and an additional one was located between the parapet and the cleat. The measured pressure varied on a day to day basis due to wind dynamics, and the pressure on the windward face was consistently higher than that on the leeward face. Figure 2.3 illustrates the wind pressure distribution observed in the study, where pressure taps on the outside of the coping covering the parapet (P1 in Figure 2.3) experienced negative pressure. The pilot study also found that because of pressure stagnation between the cleat and parapet, the pressure tap installed in between them (P4 in Figure 2.3) experienced positive pressure. The combined load (negative pressure) of the two pressure taps, located on the front and the cleat, resulted in an increase in the net pullout force of the cleat fasteners. The pressure taps on the front and top faces of the coping recorded the highest pressure for all cases, the pressure coefficients usually ranging from -2 to -3. However, values as high as -6.8 were also recorded.

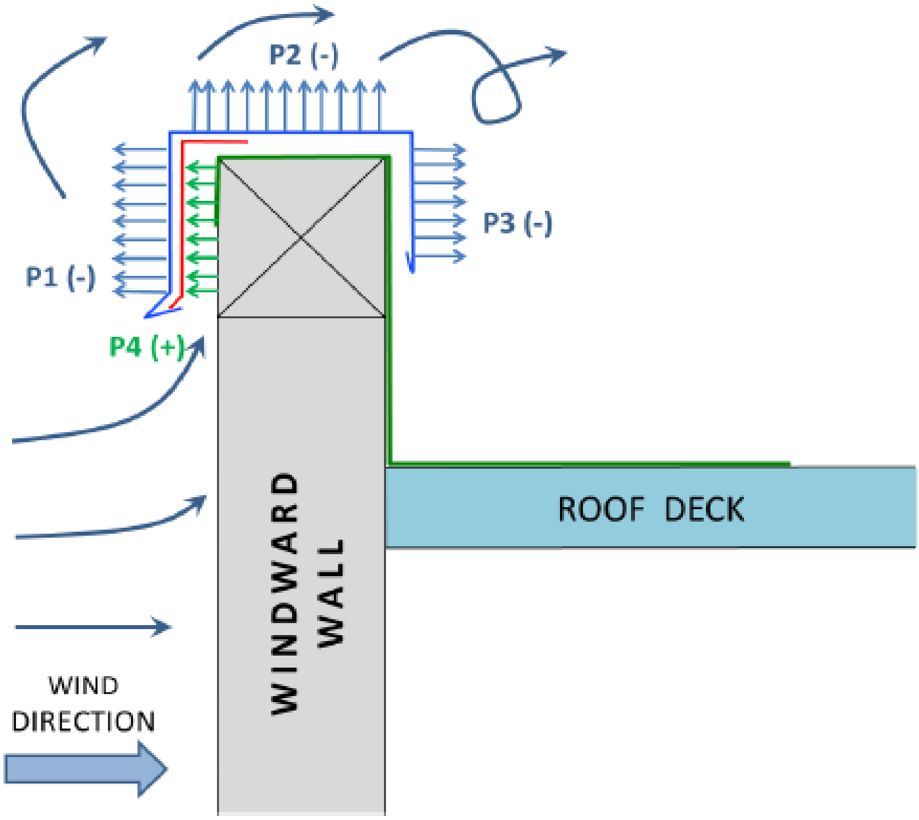

Figure 2.3: Observed pressure distribution on the roof edges, from Baskaran et al. (2011)

2.3 Existing Standards and Codes

2.3.1 ANSI/SPRI/FM4435/ES-1

Building code requirements for the design of metal edges on the roofs do not currently exist. Nevertheless, the ANSI/SPRI/FM4435/ES-1 standard has been created for the design and testing of roof edges. The standard consists of two parts: (i) wind design of edge systems and (ii) edge system testing. Three testing procedures exist to determine the resistance of an edge system, referred to as RE-1, RE-2 and RE-3. Test RE-1 is used to determine how the metal edge would respond to tension in the billowing membrane (Figure 2.4). Test RE-2 is used to determine the resistance of the metal edge when the front face is subjected to a pull-out force (Figure 2.5). Finally, test RE-3 is used to determine the resistance of the metal edge when both the top and front faces of the edge are pulled out simultaneously (Figure 2.6). All three tests use point loads along the metal edge to simulate the wind load.

The RE-1 test applies to mechanically attached roof membranes or ballasted systems, if the distance from the roof edge system to the first row of fasteners is greater than 12 in (305 mm). The setup of the test maintains uniform tension along the length of the membrane, and the length of the membrane and edge contains a minimum of three attachment fasteners at design spacing, or is 3-ft (915 mm) in length, whichever is greater. To simulate the billowing of the membrane, the membrane is pulled at 25° from the horizontal at a loading rate of 2 in/min (50 mm/min), until the membrane or any components are removed and failure occurs (Figure 2.4). The roof edge termination strength is deemed satisfactory if the test force at failure on a minimum 12-in (300 mm) wide sample meets or exceeds the design membrane tension.

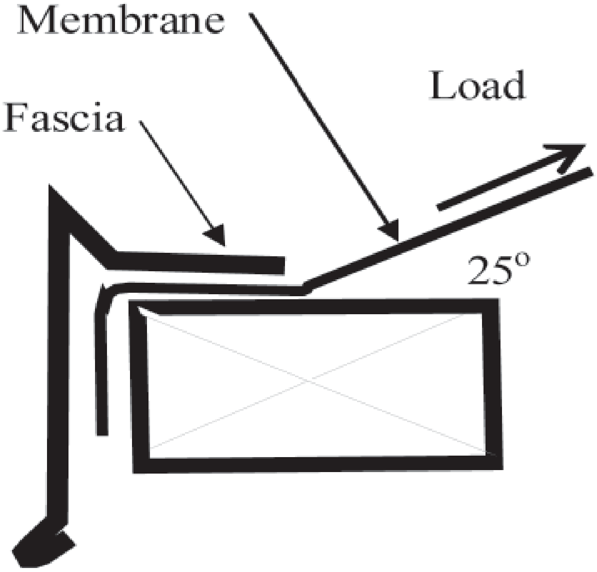

Figure 2.4: Schematic of the RE-1 test (ANSI/SPRI/FM4435/ES-1)

The RE-2 test specimen has the same dimensions as used on an actual building, with the minimum length of the sample being 8-ft (2.4 m). Uniform loading is applied along the vertical face at points no further apart than 12 in (300 mm) from its centerline (Figure 2.5). The loads are applied incrementally, each one held for a minimum of 60 seconds, and the specimen that is unloaded between loads returns so that the sample comes to a complete rest. Load increments applied do not exceed 25 psf (120 kg/m^2) until half the expected failure point, at which point the maximum applied increments is modified to be 10 psf (50 kg/m^2). Loading of each increment is reached in a maximum of 60 seconds up to 150 psf (7.2 kPa), and then increments are reached in a maximum of 120 seconds.

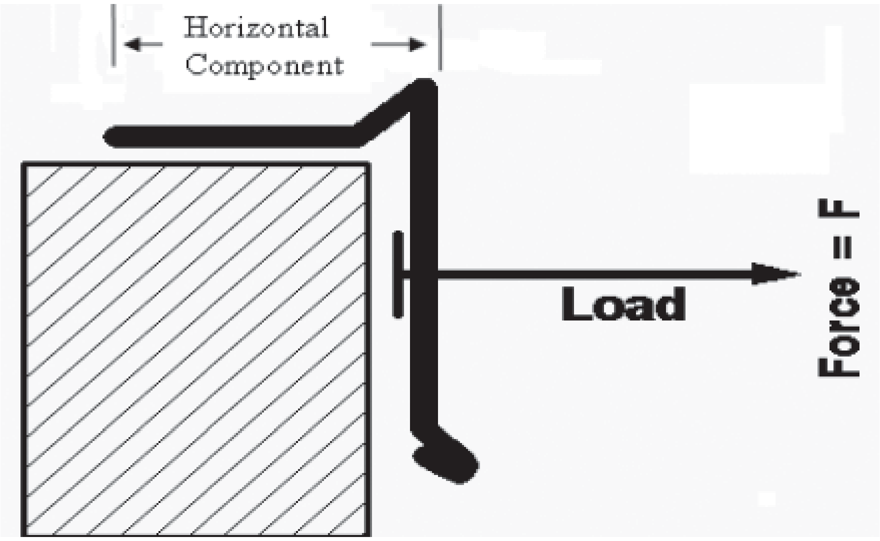

Figure 2.5: Schematic of the RE-2 test (ANSI/SPRI/FM4435/ES-1)

The test specimen used in the RE-3 test is prepared in a similar manner as the specimen for the RE-2 test. Loading on the front and top faces or on the back and top faces is applied at the same time in ratios of (Face Height x Horizontal GC_p) to (Top Width x Vertical GC_p). The external pressure value, GC_p, can be found in ASCE 7-10, Figure 30.4-2. The same loading protocol as the RE-2 test is followed, with the same failure criteria (Figure 2.6).

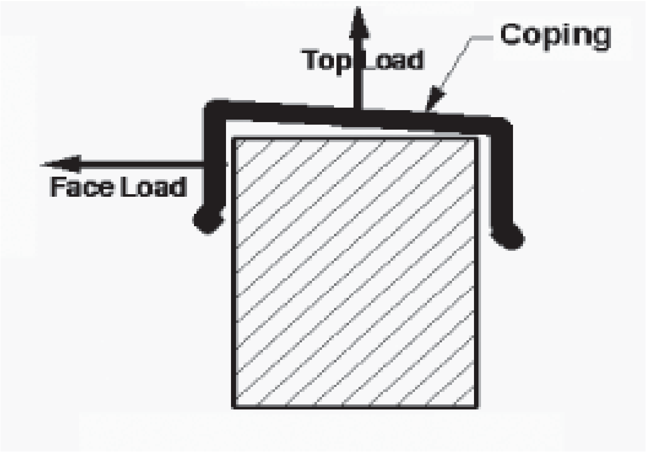

Figure 2.6: Schematic of the RE-3 test –front and top leg pull (ANSI/SPRI/FM4435/ES-1)

2.3.2 **American Society of Civil Engineers (ASCE) Code**

The ASCE 7-10, published in 2010, is the most recent version of the wind standard referenced in most of the United States building code. It specifies the minimum load thresholds, including that induced by wind, used in the design of buildings and other structures. The wind guidelines for building structures were first published in 1988. The analytical procedures for the design of components and cladding for wind loads on any building are included in Chapter 30 of ASCE 7-10, in which Section 30.9 specifically deals with components and cladding elements of parapets for all building types and heights (ASCE 7-10/Section 30.9).

When calculating the design wind loads for a building using Chapter 30, the following requirements must be met for the buildings:

- Buildings are to be regularly shaped, as defined in section 26.2;
- Buildings are not to have response characteristics that are subjected to cross-wind loading, vortex shedding, or instability due to galloping or flutter; and,
- Buildings are not to have a site location for which channeling effects are significant.

The design wind pressure P can be calculated from the following equation (ASCE 7-10/Eq 30.9-1):

$$P = q_p\left[\left(GC_p\right)-\left(GC_{pi}\right)\right] \qquad (2.1)$$

where:

q_p = Velocity pressure evaluated at the top of the parapet (ASCE 7-10/Section 30.3),

GC_p = External pressure coefficient given in ASCE 7-10/Figs. 30.4-1, 30.4-2A to 30.4-2C, 30.4-3, 30.4-4, 30.4-5A, 30.4-5B, 30.4-6, 30.4-7, 27.4-3, and

GC_{pi} = Internal pressure coefficient (ASEC 7-10/ Table 26.11-1).

The velocity pressure at height *z* can be calculated from the following equation:

$$q_p = 0.00256 \times K_z \times K_d \times K_{zt} \times V^2 \text{ (psf), with V in mph} \qquad (2.2a)$$

$$q_p = 0.613 \times K_z \times K_d \times K_{zt} \times V^2 \text{ (Pa), with V in m/s} \qquad (2.2b)$$

where:

K_d = Wind directionality factor (ASCE 7-10/Section 26.6),

K_z = Velocity pressure exposure coefficient (ASCE 7-10/Section 30.3-1),

K_{zt} = Topographic factor (ASCE 7-10/Section 26.8), and

V = Basic wind speed (ASCE 7-10/Section 26.5).

Section 30.9 of the ASCE 7-10 states that two load cases must be considered when designing parapets; (i) load case A, windward parapet, and (ii) load case B, leeward parapet. Figure 2.7, which corresponds to Figure 30.9-1 in the ASCE 7-10, illustrates the two load cases graphically. The two load cases are defined as follows:

1. “Load Case A: Windward parapet shall consist of applying the applicable positive wall pressure from Fig. 30.4-1 [*h* ≤ 60 ft (18.3 m)] or Fig. 30.6-1 [*h* > 60 ft (18.3 m)] to the windward surface of the parapet while applying the applicable negative edge or corner zone roof pressure from Figs. 30.4-2 (A, B, or C), 30.4-3, 30.4-4, 30.4-5 (A or B), 30.4-6, 30.4-7, Fig. 27.4-3 note 4, or Fig. 30.6-1 [*h* > 60 ft (18.3 m)] as applicable to the leeward surface of the parapet” (ASCE7-10/Section 30.9).
2. “Load Case B: Leeward parapet shall consist of applying the applicable positive wall pressure from Fig. 30.4-1 [*h* ≤ 60 ft (18.3 m)] or Fig. 30.6-1 [*h* > 60 ft (18.3 m)] to the windward surface of the parapet, and applying the applicable negative wall pressure from Fig. 30.4-1 [*h* ≤ 60 ft (18.3 m)] or Fig. 30.6-1 [*h* > 60 ft (18.3 m)] as applicable to the leeward surface. Edge and corner zones shall be arranged as shown in the applicable figures. (*GCp*) shall be determined for appropriate roof angle and effective wind area from the applicable figures” (ASCE7-10/Section 30.9).

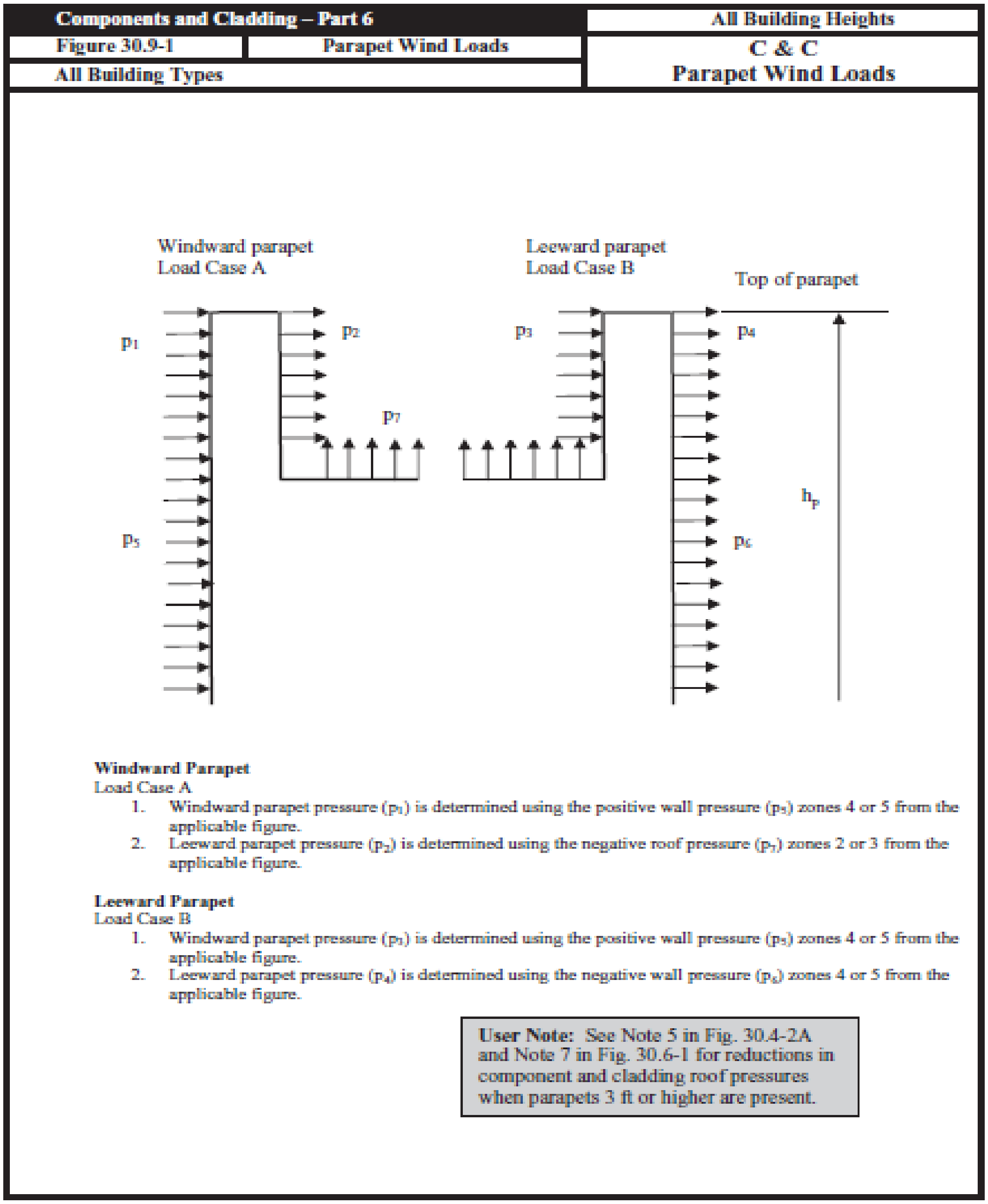

Components and Cladding – Part 6		**All Building Heights**
Figure 30.9-1	**Parapet Wind Loads**	**C & C** **Parapet Wind Loads**
All Building Types		

Windward Parapet
Load Case A

1. Windward parapet pressure (p_1) is determined using the positive wall pressure (p_5) zones 4 or 5 from the applicable figure.
2. Leeward parapet pressure (p_2) is determined using the negative roof pressure (p_7) zones 2 or 3 from the applicable figure.

Leeward Parapet
Load Case B

1. Windward parapet pressure (p_3) is determined using the positive wall pressure (p_5) zones 4 or 5 from the applicable figure.
2. Leeward parapet pressure (p_4) is determined using the negative wall pressure (p_6) zones 4 or 5 from the applicable figure.

User Note: See Note 5 in Fig. 30.4-2A and Note 7 in Fig. 30.6-1 for reductions in component and cladding roof pressures when parapets 3 ft or higher are present.

Figure 2.7: ASCE7-10 parapet wind loads

2.3.3 National Building Code of Canada (NBCC)

The current building code used in Canada is the 2010 edition of the NBCC, which is issued by the NRCC, and incorporates specifications to satisfy the local needs of all the provinces. The NBCC releases revisions approximately every five years. The NBCC 2010 is composed of two volumes:

1. **Volume (1),** including Division A and Division C,
2. **Volume (2),** including Division B and the Structural Commentary.

There are two approaches in the NBCC that can be used for calculating wind loads on a roof: static and dynamic. The static approach is appropriate to calculate the design wind loads for roof claddings, whereas the dynamic approach, although included in the code, is not applicable to the cladding design. Several parameters must be determined in order to use the static approach, some of which are directly affected by the aerodynamics of the considered building, and the other parameters are determined by its location. These parameters are then used in the design equation to calculate the external/internal wind pressures acting on the roof. The NBCC 2010 provides figures and charts for the computed load distribution based on the type of roof.

The external, internal and net wind pressures are determined from the following equations:

External pressure: $$P_e = I_w q C_e C_g C_p \tag{2.3}$$

Internal pressure: $$P_i = I_w q C_e C_{gi} C_{pi} \tag{2.4}$$

Net pressure: $$P = P_e - P_i \tag{2.5}$$

where:

I_w = importance factor for wind load (Table 4.1.1.1),

q = reference velocity pressure (Table C-1),

C_e = exposure factor (Sentence “5” in 4.1.7.1),

C_g = external gust factor (Sentence “6” in 4.1.7.1),

C_{gi} = internal gust factor (Sentence “6” in 4.1.7.1),

C_p = external pressure coefficient, averaged over the area of the surface considered, and

C_{pi} = internal pressure coefficient (Structural Commentary I – Clause 30).

In the NBCC 2010 there are no specifications for wind load design regarding components and cladding elements for parapets.

2.4 Wind Performance of Metal Edge

Wind tunnels are commonly used in order to determine the wind pressure on scale models of buildings. Although roof edge pressures can be found through wind tunnel testing, it is difficult to measure the pressure acting on the roof metal edges due to the scaling of the metal flashings. Therefore, field studies are favoured in order to get accurate measurements on the wind-induced pressures to which metal edges are subjected. When conducting field studies, it is important to take into consideration factors such as cost, time constraints on gathering data and the limited amount of data gathered.

2.4.1 Texas Tech University Experiments

Jiang (1995) conducted several field tests at the Texas Tech Wind Engineering Research Field Laboratory (WERFL), located on the university campus in Lubbock, Texas (Figure 2.8). The WERFL building is 3,300-ft (1,000 m) above sea level, and the terrain around the building is flat and open with a 160-ft (48.8 m) meteorological tower. The test building is a full-size steel frame building with dimensions of 30 x 45 x 13-ft (9.1 x 13.7 x 4.0 m). It is not anchored to the ground, but to a rigid frame undercarriage with wheels at the corners. It can rotate 360° to the desired angle of attack (Figure 2.10).

Figure 2.8: Wind Engineering Research Field Laboratory (WERFL) test building (https://www.depts.ttu.edu/nwi/facilities/WERFL.php.)

Jiang (1995) installed and instrumented several metal edge flashing configurations (Figure 2.9) on the WERFL full-scale building to determine the wind pressure distribution over the different metal flashing surfaces. The flashings were installed on different locations around the roof edge of the building according to the layout in Figure 2.10. Jiang (1995) used two types of metal flashing (cleated and un-cleated) on both roof edge zones. The pressure on the metal flashings was recorded at different angles of attack; windward, leeward, parallel and quartering. Several pressure taps were installed on each of the configurations in order to quantify the profile of the external pressure coefficients, as well as two internal pressure taps installed underneath the metal flashing to verify that the internal pressure coefficients were the same. The quality-controlled data runs from the pressure taps were used to calculate the pressure coefficient. Mean values were identified as a stable descriptor of the pressure coefficient.

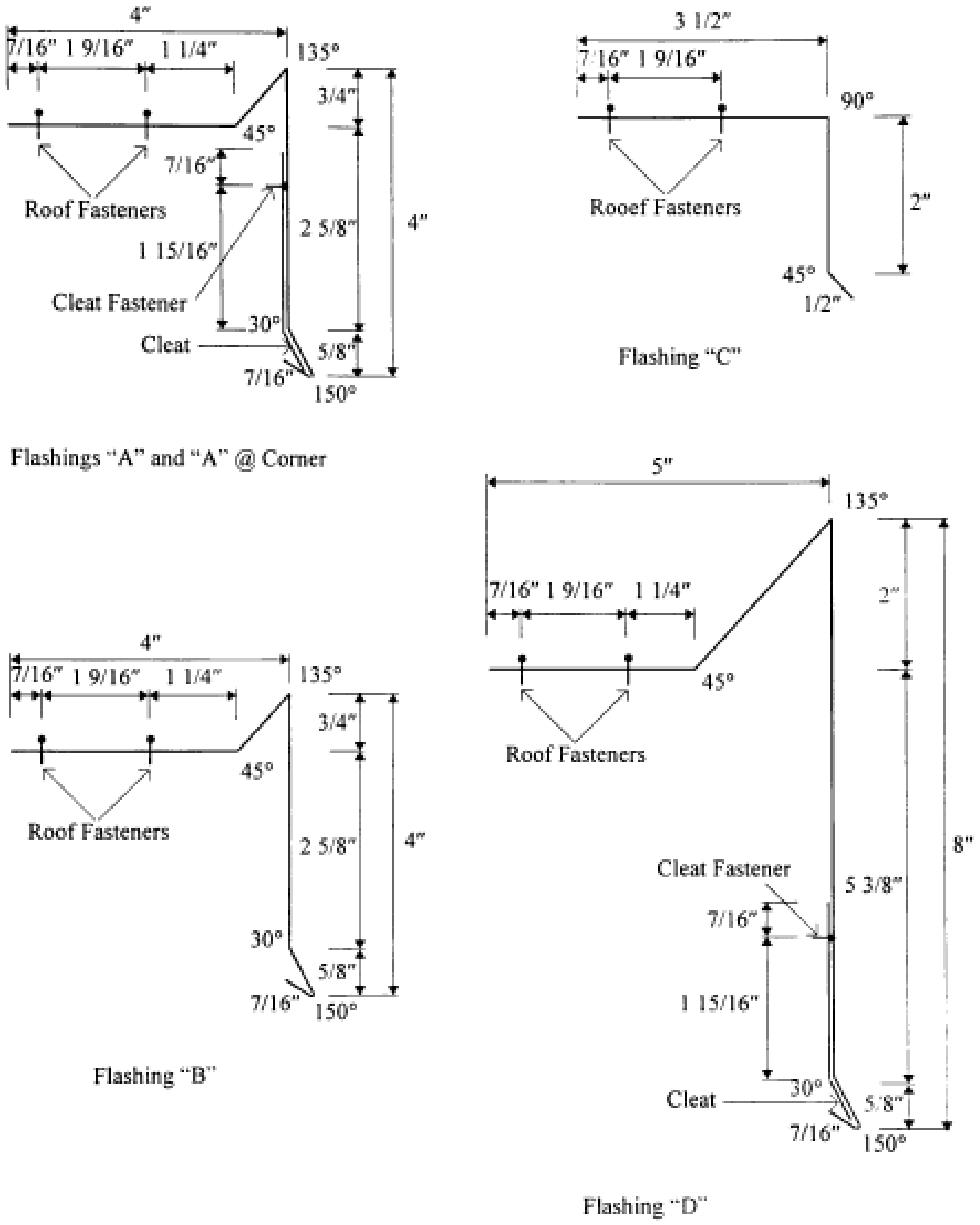

Flashings "A" and "A" @ Corner

Flashing "C"

Flashing "B"

Flashing "D"

Figure 2.9: Dimensions of the metal edge flashings (Jiang, 1995)

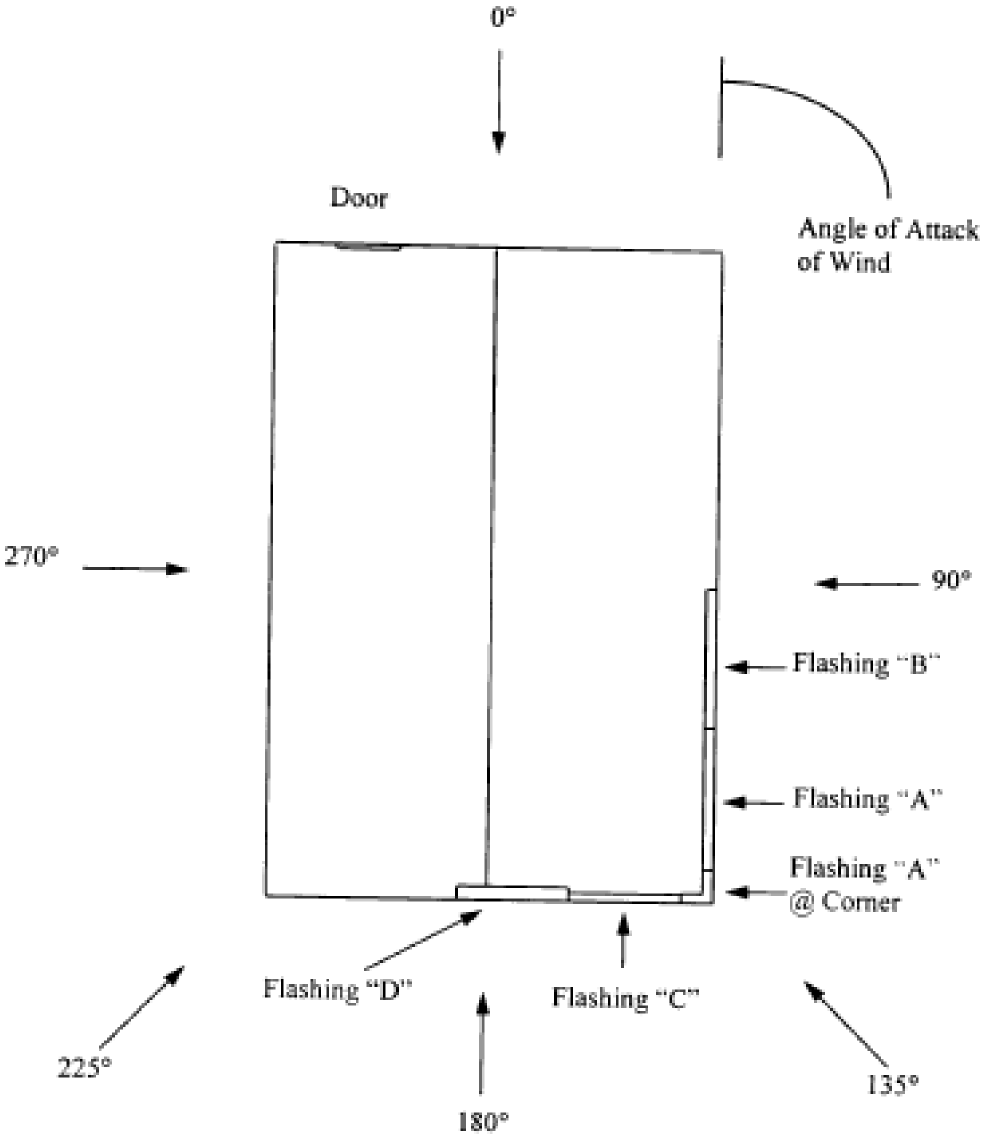

Figure 2.10: Flashing locations on the WERFL (Jiang, 1995)

At the end of the data collection, Jiang (1995) was able to produce distribution graphs of the mean pressure coefficient on each of the metal flashing surfaces for each wind angle of attack: windward, leeward, parallel and quartering (Figure 2.11)..

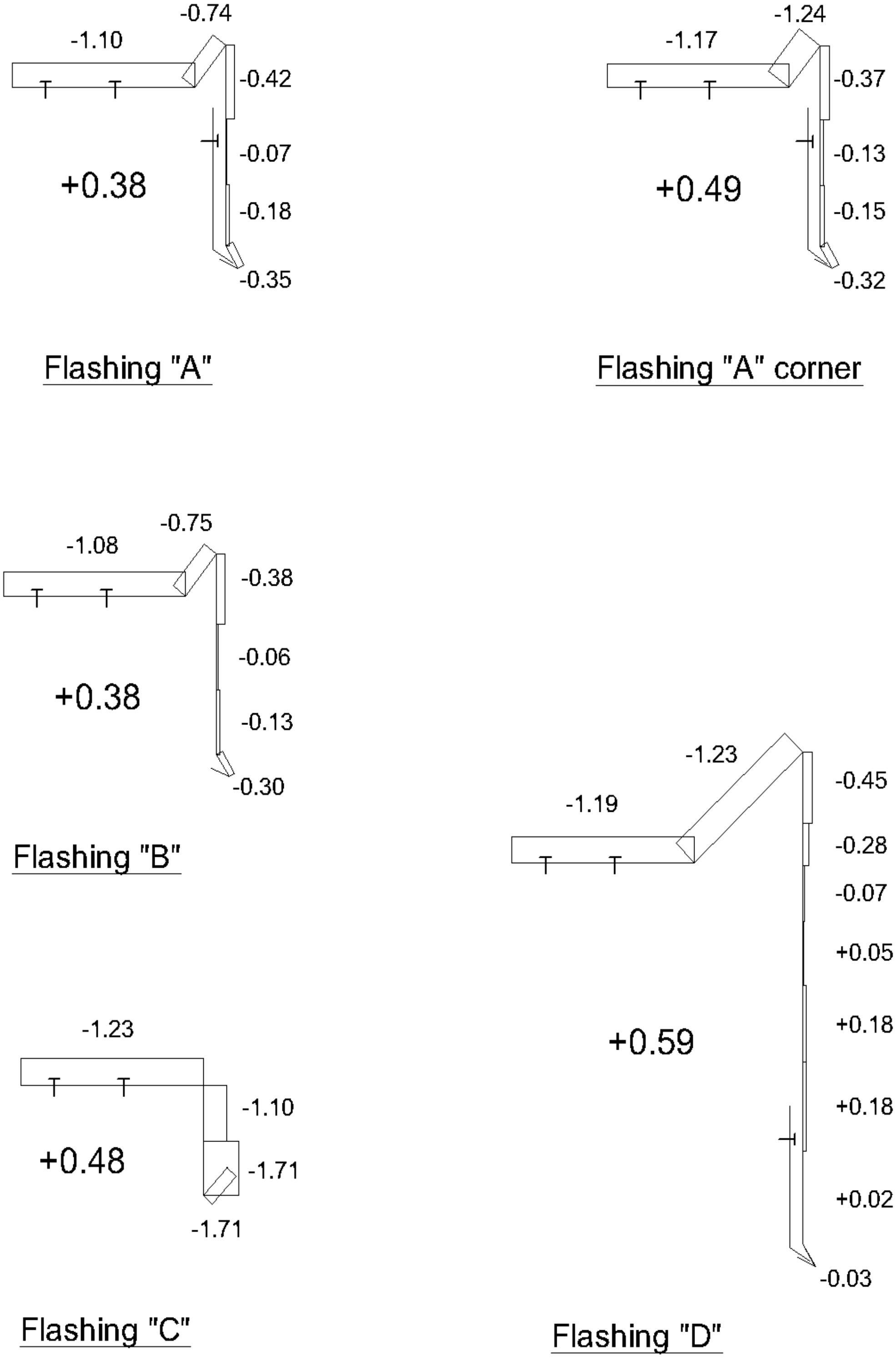

Flashing "A"

Flashing "A" corner

Flashing "B"

Flashing "C"

Flashing "D"

Figure 2.11: Mean pressure coefficients on the flashings along the windward direction (Jiang, 1995)

A similar study conducted by McDonald et al. (1997) at WERFL used a metal edge flashing “A” installed at the corner of the WERFL building and extended along the eaves of the building (Figure 2.10). The geometry of the metal flashing used by McDonald et al. (1997) can be seen in Figure 2.12(a), and the location of the installed pressure taps is illustrated in Figure 2.12(b). Pressure tap #1 was installed on the plywood panel on the roof, pressure taps #2 to #5 were on the front vertical face of the flashing, and pressure taps #6 and #7 were installed between the flashing and the edge wall, as shown in Figure 2.12(b).

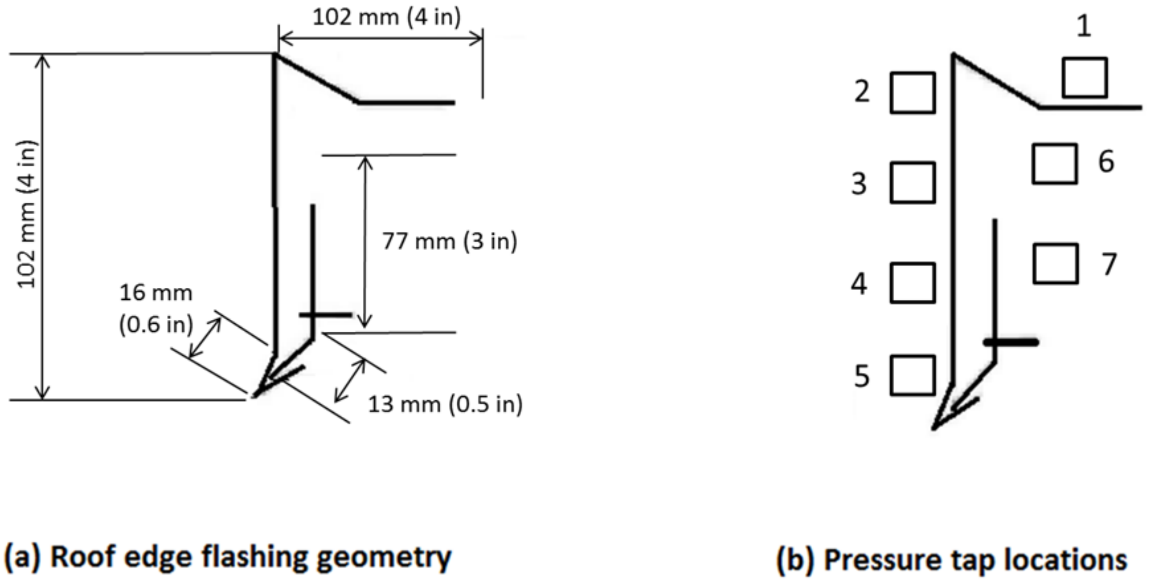

(a) Roof edge flashing geometry **(b) Pressure tap locations**

Figure 2.12: Roof edge flashing in field investigation conducted by McDonald et al. (1997)

Wind pressure data was collected in 15-min runs and sampled at 30 Hz. The collected data was represented in terms of pressure coefficients. Table 2.1 shows the mean, maximum, minimum and root mean square (RMS) of the pressure coefficients computed from the pressure tap data.

Table 2.1: Pressure coefficients at installed pressure taps (McDonald et al., 1997)

Tap	Mean	Maximum	Minimum	RMS
1	-0.92	0.04	-3.67	0.339
2	-0.32	0.55	-1.71	0.178
3	-0.06	1.07	-1.47	0.215
4	-0.14	1.15	-1.70	0.255
5	-0.27	0.85	-1.88	0.224
6	0.37	1.71	-0.59	0.266
7	0.37	1.72	-0.59	0.269

Table 2.1 shows that the vertical face of the flashing was mainly under negative pressure or suction, with the highest suction value of -3.67 recorded at the top (pressure tap #1). The data tabulated in Table 2.1 was calculated with a mean wind speed of 12.8 m/s and a mean wind direction of 74° (windward direction). The study showed that the windward wind angle of attack corresponds to the worst case of negative pressures (external) on the flashing.

2.4.2 Concordia University Study

Stathopoulos et al. (1999) conducted a full-scale experiment in a low-rise building located in the Loyola campus of Concordia University, Montreal (Figure 2.13). In this study, the wind-induced pressure along the roof parapet was evaluated to investigate its effect on the flat roof. No metal edges were installed on the roof parapets.

Figure 2.13: Field site at Concordia University (Stathopoulos et al., 1999)

The building dimensions are 3.3 x 3.7 x 2.6 m, with a low-slope roof with dimensions of 4.0 by 3.2 m. The building was equipped with retractable panels on the corners, each with 12 pressure taps. The study investigated three cases: (i) no parapets, (ii) 0.10 m wide and 0.25 m high parapet installed in the corner, and (iii) 0.10 m wide and 0.50 m high parapet installed in the corner. The terrains around the building are of two types, suburban and open country, each one surrounding two corners of the building. The strongest winds came from the open country terrain, in the South and West directions. A 3-cup anemometer and a wind vane were used to measure the wind speed and direction, with a minimum wind speed requirement to start the data collection of 5.5 m/s. The data collection at the field site used 12 channels with a maximum sampling rate of 1 Hz, run times of 15-min, and 900 samples. Pressure coefficients were calculated using the mean pressure and the 15-min mean wind velocity, and Stathopoulos et al. (1999) presented the pressure coefficients as average values corresponding to a 5°-interval of the wind direction.

In the first phase of the experiment, there were no parapets installed on the roof of the building. Figure 2.14 shows the calculated mean pressure coefficients along the roof edge due to wind directions in the range of 35° to 70°. The data shows that the edge pressure taps had the highest suction for a wind direction between 35° and 60°. It can be seen that taps #2, #3, #4 and #8 experienced near identical mean pressure coefficient values at 45° and more negative than tap #1. The pressure taps along the diagonal direction on the roof, pressure taps #5, # 10 and #12, show that the suction the roof experiences decreases as it moves further away from the corner (Figure 2.15).

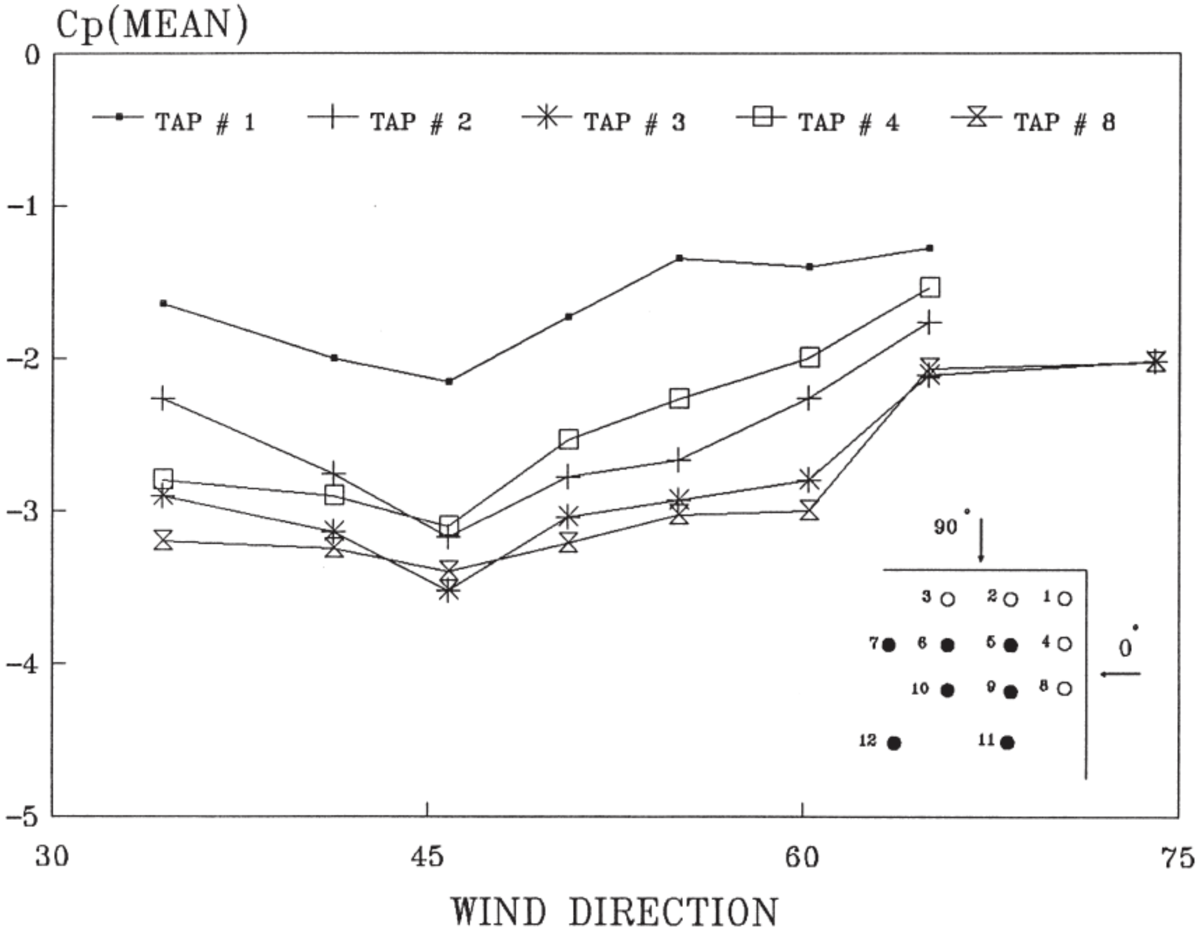

Figure 2.14: Mean pressure coefficients measured along roof edges (Stathopoulos et al., 1999)

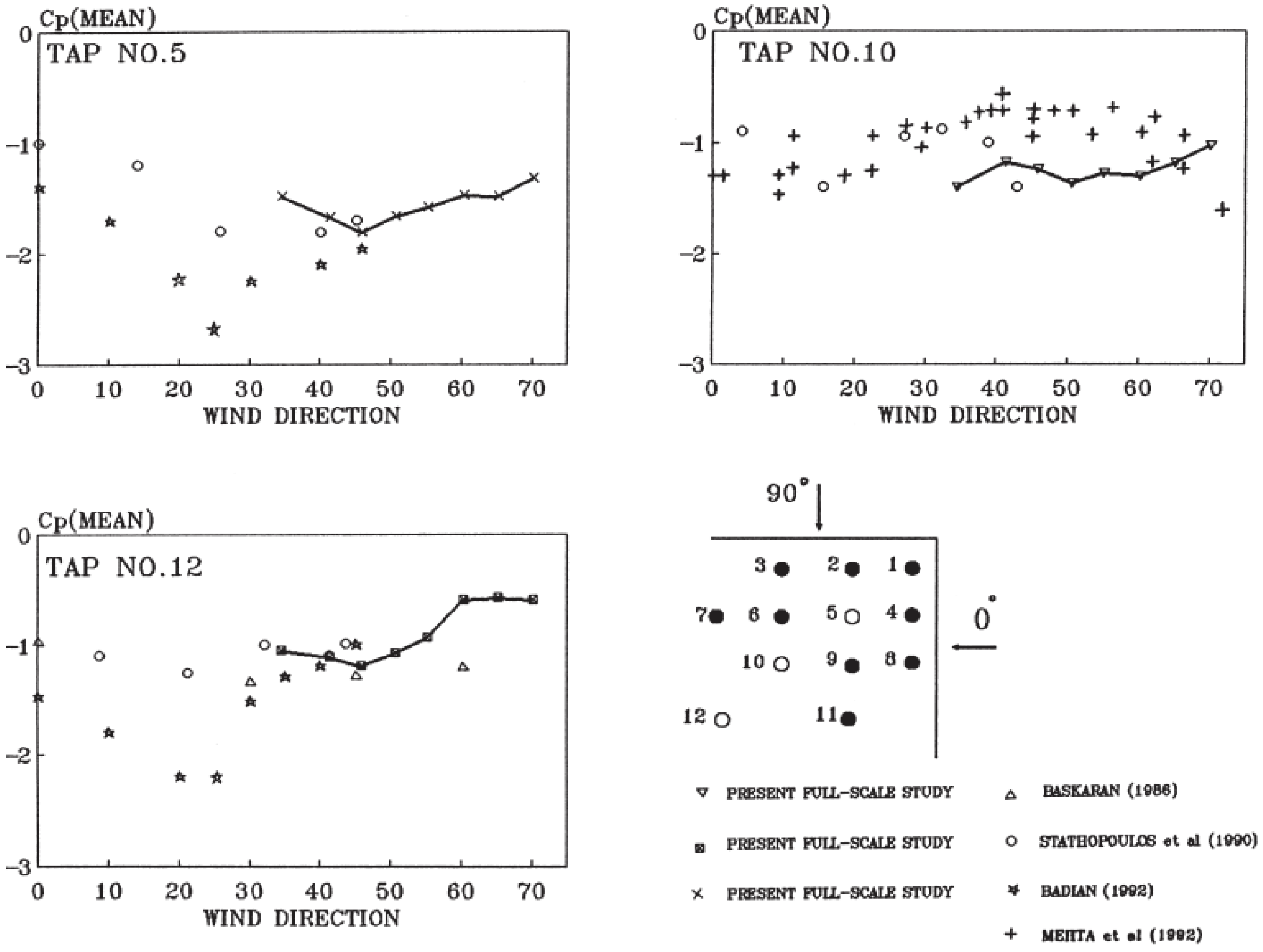

Figure 2.15: Comparison of full-scale results with other studies—flat roof without parapets (Stathopoulos et al., 1999)

The installed parapets covered pressure taps #1, #2, #3, #4, and #8. Tests were completed with two parapets which were 0.25 and 0.5 m high. The effect of parapet height on the pressure coefficients at pressure taps #5, #6, and #7 can be observed in in Figure 2.16, which shows that as the parapet height increases, the pressure coefficient decreases. Similar results were found for pressure taps #9, #10, and #11.

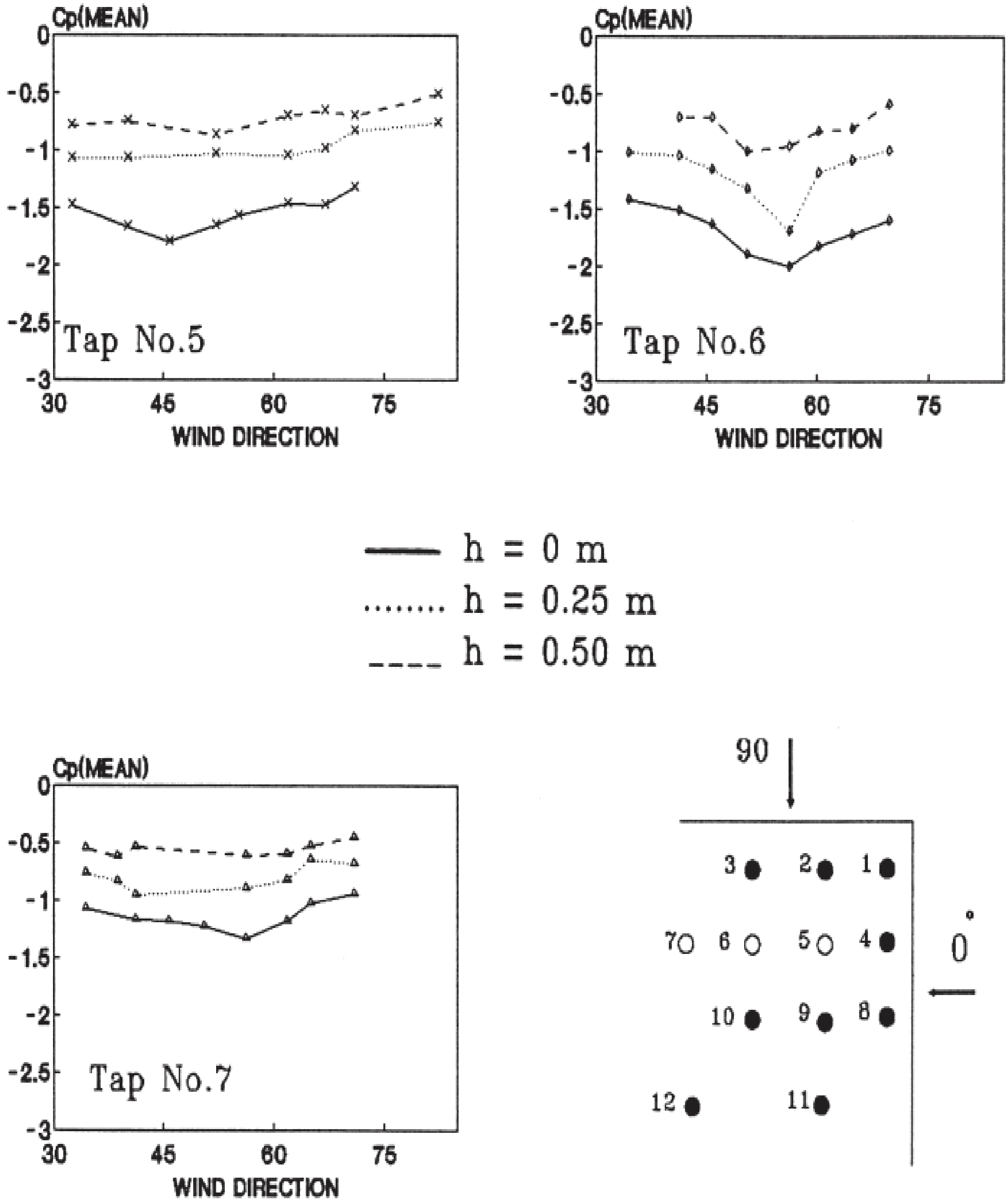

Figure 2.16: Mean pressure coefficients on the corner of the roof, with and without parapets (Stathopoulos et al., 1999)

Bedair (2009) conducted full-scale testing on a low-rise building in order to examine the wind-induced pressure acting on the surface of the parapet, using the same site used by Stathopoulos et al (1999) (Figure 2.13). Field data was collected between the months of May and November for three consecutive years, in which the strongest wind direction in Montreal came from the South-West. The parapet that was installed on site had a height of 0.5 m and a width of 0.16 m and was fixed to the roof by plates. Pressure taps were installed in the interior, exterior, and top of the parapet. Data was collected for wind speeds higher than 5.6 m/s with a sampling rate of 1 Hz.

Figure 2.17 shows the exterior and interior pressure coefficients (maximum and mean values) near the corner for different wind angles of attack. The exterior surface showed peak pressure and suction coefficients of 2.4 at 0° (windward wind) and -2.79 at 90° (parallel wind), respectively, and the interior surface showed peak pressure and suction coefficients of 2 at 180° and -3 at 45°, respectively.

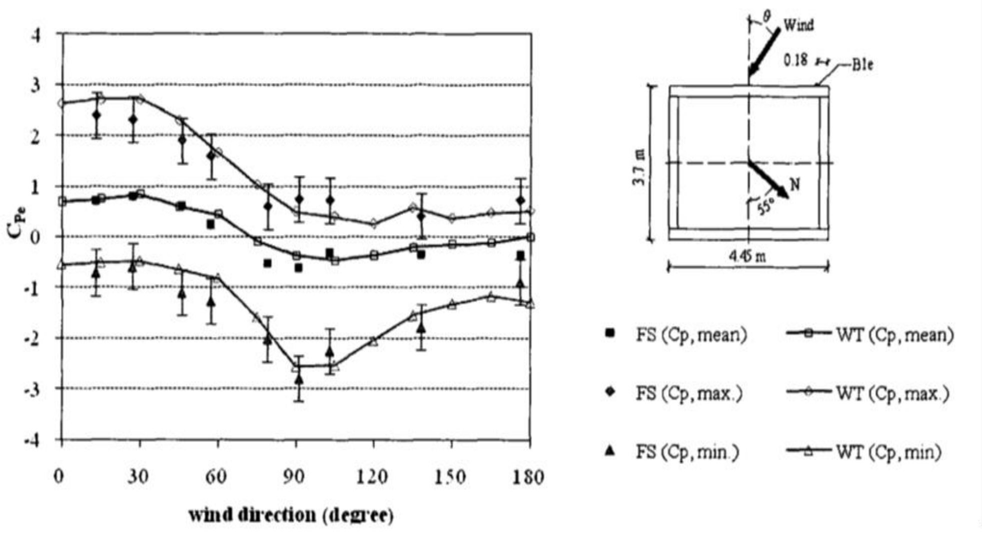

(a) Exterior surface parapet pressure coefficients

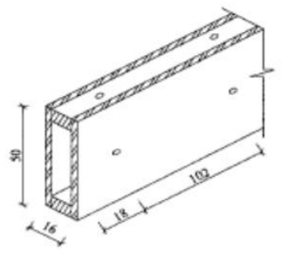

Parapet section

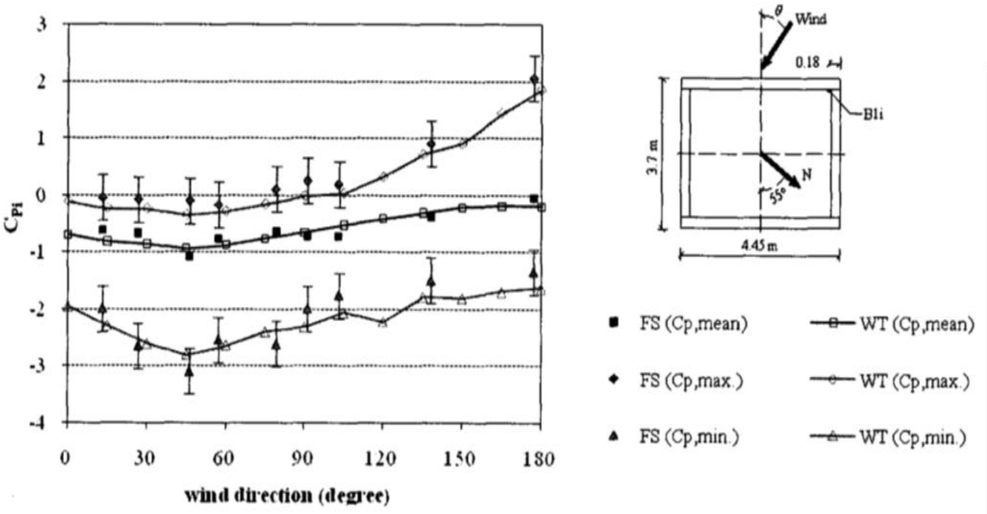

(b) Interior surface parapet pressure coefficients

Figure 2.17: Surface parapet pressure coefficients recorded near the corner (Bedair, 2009)

2.5 Conclusion

Building aerodynamics is complex. When the wind flows over the top of the windward wall (the roof edge), it separates from the leading edge and reattaches at a certain point. The reattachment location varies with building geometry and flow intensity. The region in between the roof edge and the reattachment point is called a separation bubble, as seen in Section 1.2. This region is then characterized by negative pressure, which is more negative at the separation point, and progressively less negative towards the reattachment point. Considerable damage can occur on the roof assembly experiencing pullout forces, which are amplified by the positive internal pressure of the building. This phenomenon happens in every low-rise building roof, regardless of the existence of metal edges or parapets. A parapet depending on its height may reduce the overall suction, by positioning the separation point further from the roof plane, as demonstrated in previous works (Stathopoulos, 1992 and Baskaran, 1986). Nevertheless, if a parapet is a part of the roof, then the flow separation will occur at the parapet itself, which implies that the parapet's top surface will also experience suction. This will be true for parapets with or without metal edge configurations.

The REST project has conducted an experimental pilot study to investigate the forces acting on the metal edges. The study showed that the top face of the metal edges experience negative pressure (suction) and the front leg of the coping is subjected to a net outward pressure. The studies done at Texas Tech also showed that metal flashings installed on the roof edge experience negative pressure. Although the studies at Concordia University did not include metal edges, it was observed that a roof with and without parapets was subjected to negative pressure; however, current building codes in North America do not account for this. Since pre-existing studies are limited in number, further experimentation should be conducted under multiple variant situations in order to justify the improvement of existing codes.

Chapter 3: Field Experimental Site

3.1 Introduction

This chapter presents the details of the field experimental site, located at the Canada Post building near the International Airport in Vancouver, Canada. Three different roof edge configurations, as tested by Alassafin (2013), were installed at the field site on the windward side of the building. These configurations were instrumented to measure the wind pressure. This chapter also describes the data acquisition from the field site and the methodology used for analysis.

3.2 Canada Post Building

A requirement from a preliminary study done by Baskaran et al. (2011) to evaluate the performance of the roof edge suggested that the field site must be located in a windy region with historical weather records showing hourly wind speeds of at least 30 mph (48 kph).

The Canada Post building in Vancouver, Canada, met this requirement and was thus selected as the site for field monitoring of wind-induced pressure on roof edge systems (Figure 3.1). The building is located in the Richmond area of Vancouver, on the north side of the airport, surrounded by open terrain (Figure 3.2). The building has two roof levels (Figure 3.3), with the lower roof elevated at 38-ft (11.6 m) and upper roof elevated at 58-ft (17.7 m). A 16-ft (4.9 m) tall wind tower was installed on the upper roof level, to record wind data (Figure 3.4).

Figure 3.1: Canada post building in Vancouver, Canada (Courtesy of NRCC)

Figure 3.2: Open terrain in the four directions from Penthouse 6. North (a); East (b); South (c); West (d) (Courtesy of NRCC)

Figure 3.3: Elevations of the lower and upper roofs, and of the wind tower (Courtesy of NRCC)

Figure 3.4: Wind tower installation at the upper roof level (Courtesy of NRCC)

Figure 3.5 shows the overall dimensions of the building: 433-ft (132 m) wide by 1440-ft (439 m) long. The roof edge configurations were installed on Penthouse 6, located on the West side (Figure 3.5). Penthouse 6 is 96-ft (29 m) long by 28-ft (8.5 m) wide (Figure 3.6). The wind data was obtained from the wind tower (Figure 3.4), which revealed that the predominant wind direction ranged from south-west to north-west. Figure 3.7 shows the building orientation and the critical wind direction.

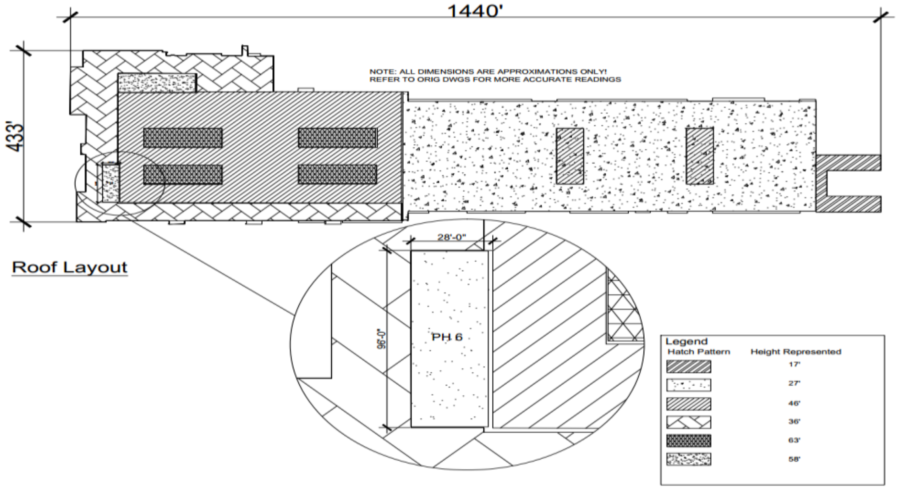

Figure 3.5: Roof layout and Penthouse 6 (PH 6) location

Figure 3.6: Close up of Penthouse 6 (Courtesy of NRCC)

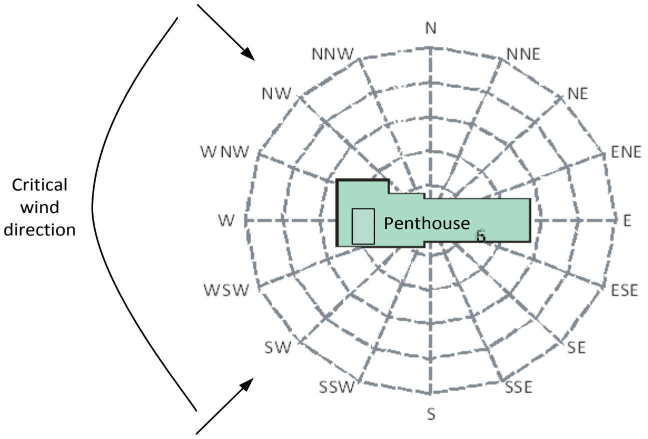

Figure 3.7: Building orientation and critical wind direction

3.3 Roof Edge Configurations

The metal roof edges were placed along the 96-ft (29 m) long segment of Penthouse 6 in order to be exposed to the perpendicular and oblique wind flow conditions (Figure 3.7). The roof edge configurations used were the same as those tested by Alassafin (2013), namely the ACC, CCC and DCC. The three types of edge configurations were designed and installed on the field site by the participating industrial partners. Instrumentations (pressure transducers and wind sensors) were designed, selected, calibrated and installed in collaboration with NRCC.

Figure 3.8: Instrumented edge configurations (Courtesy of NRCC)

The total length of every configuration is 16-ft (4.9 m), consisting of two dummy sections each of 3-ft (0.9 m), and a middle segment of 10-ft (3.0 m) (Figure 3.9). The front, top and back faces are 5-in (101.6 mm), 9.5-in (241.3 mm) and 2.75-in (69.9 mm), respectively.

Windward	P1, P5 and P8
Top	P2, P6 and P9
Leeward	P3
Cleat	P4 and P7

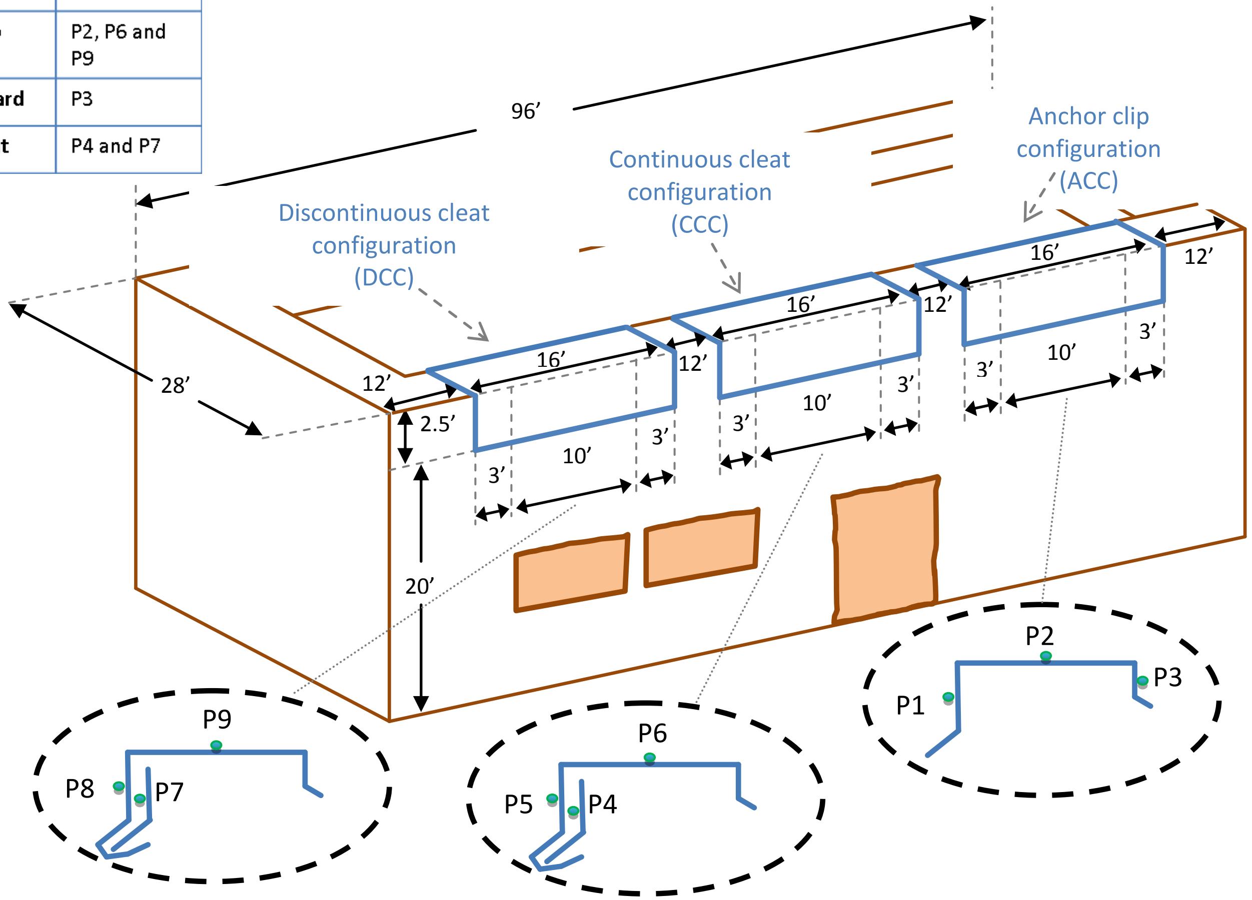

Figure 3.9: Pressure tap locations on the three configurations

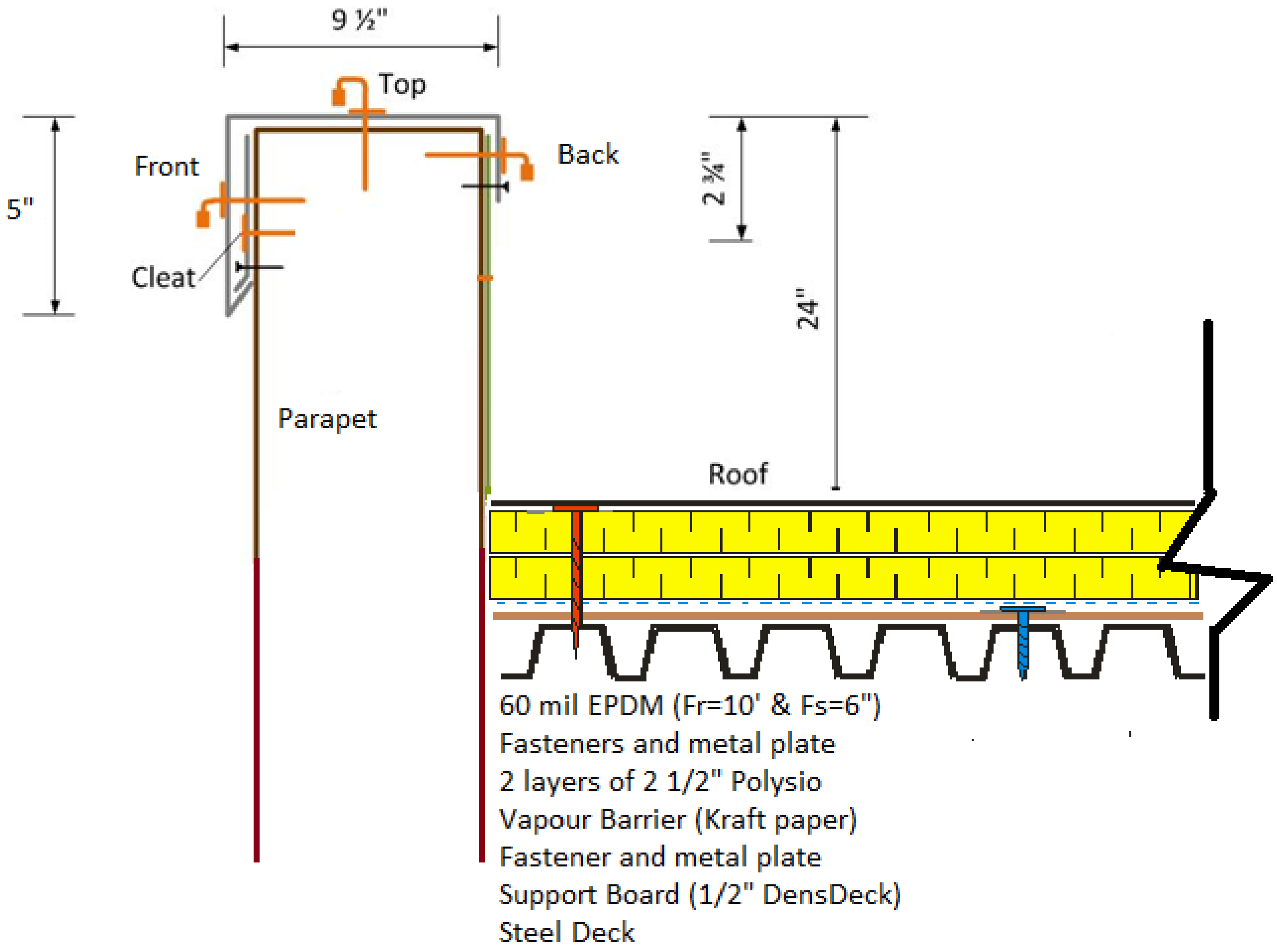

Figure 3.10: Roof edge, pressure tap profile layout, and roof detail

The ACC is built from 24 gauge galvanized steel and has no cleat component, but instead uses anchor clips placed 4-ft (1.22 m) a part (Figure 3.11). The ACC's anchor clips were fastened to the substrate at the top of the parapet, and splice plates with pre-applied adhesive tapes (Figure 3.12) were placed at the joints to secure the coping segment. The coping segments were then clipped to the anchor clips. The ACC was installed on the parapet located on the windward side of Penthouse 6 (Figure 3.8 and Figure 3.9).

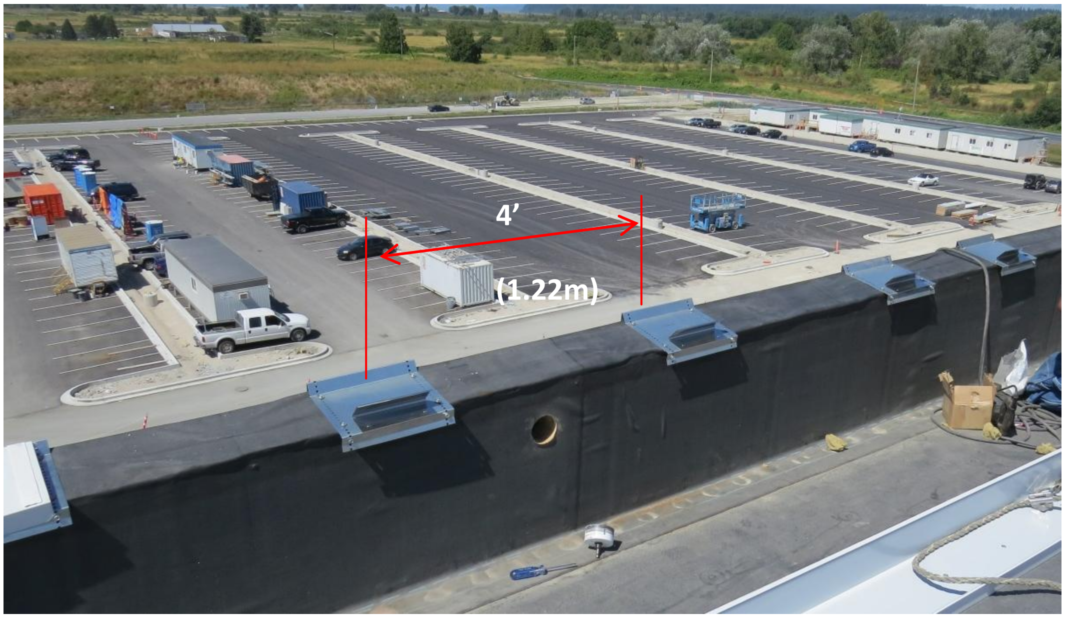

Figure 3.11: Installation of the Anchor Clip Configuration (Courtesy of NRCC)

Figure 3.12: Anchor Clip splice plates with pre-applied adhesive tapes (Courtesy of NRCC)

The CCC comprises of a cleat and a coping, both made of 24 gauge galvanized steel. The cleat of the CCC runs continuously along the length of the edge configuration (Figure 3.13). For the CCC edge system installation, the cleat was first nailed to the parapet using 1½-in (38.1 mm) long galvanized roofing nails at a spacing of 18-in (457.2 mm). The coping was mounted by hooking it onto the cleat at the front face, and then placed over the parapet width. Both ends of the middle segment of the coping were nailed on the top and front where the S-lock joints were located. The dummy segments of the coping were connected to the middle segment by insertion into the S-lock joints (Figure 3.13). The CCC metal edge was installed on the parapet of Penthouse 6, on the windward side (Figure 3.8 and Figure 3.9).

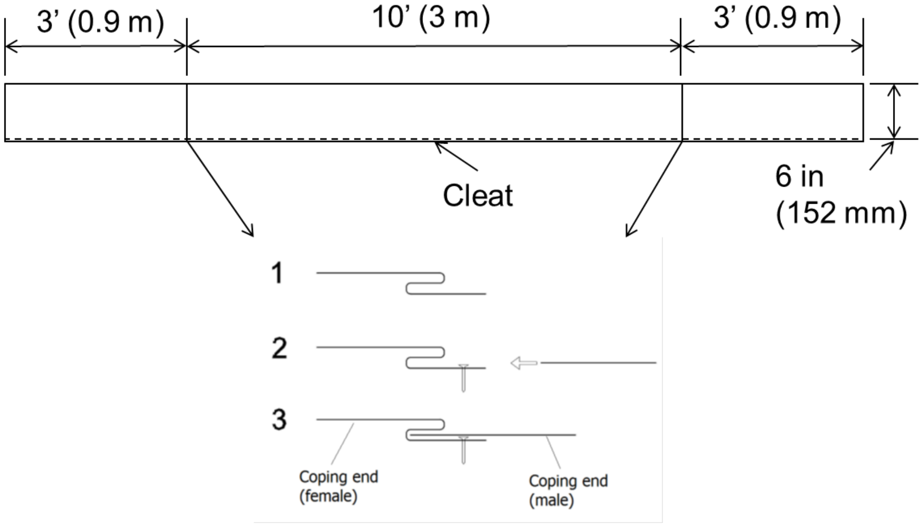

Figure 3.13: Mechanism of S-lock joint on CCC/DCC

Similar to the CCC, the DCC comprises of a cleat and a coping made from 24 gauge galvanized steel. However, the cleat of the DCC does not run continuously, and it is only 40-in (1 m) long, placed at the center of the middle segment. There were two cleats in the dummy segments, each with length of 20-in (0.5 m) (Figure 3.14). For the DCC edge system installation, the cleat was nailed to the parapet using 1½-in (38.1 mm) long galvanized roofing nails at a spacing of 18-in (457.2 mm). Similarly to the CCC, the coping was mounted by hooking it onto the cleat at the front face, and then placing it over the parapet width. The middle segment of the coping was nailed on the top and front at both ends, where the S-lock joints are located. The dummy segments of the coping were also connected to the middle segment by insertion into the S-lock joints (Figure 3.8, Figure 3.9 and Figure 3.13).

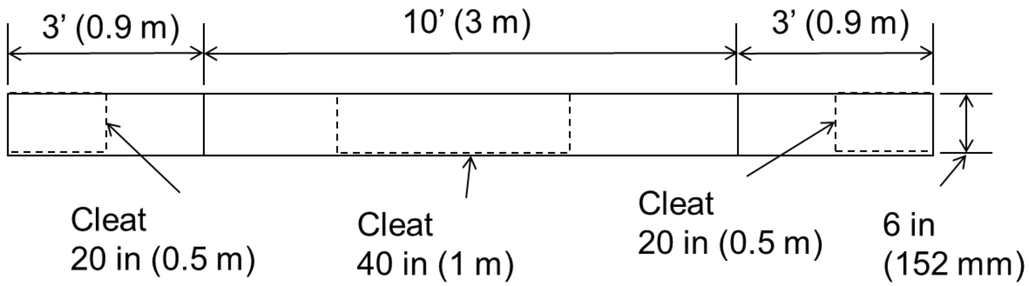

Figure 3.14: DCC cleat location

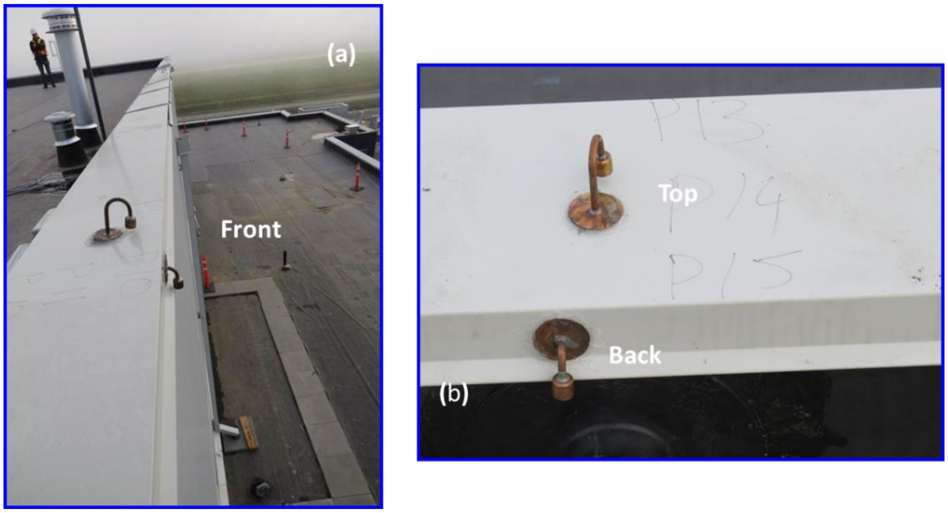

Figure 3.15: Pressure tap locations (Courtesy of NRCC)

3.4 Instrumentation Process

Each roof edge configuration was installed with pressure taps on the coping front, top and back (Figure 3.10 and Figure 3.15) by the NRCC. The pressure taps were inserted after the installation of the metal edges on the parapet, and were located at the center of the middle coping segment. The CCC and DCC were also equipped with pressure taps on the cleat. The pressure taps were manufactured at the NRCC facility in Ottawa and calibrated to ensure accuracy and precise readings. The taps were made from copper with a pipe outer diameter of ¼-in (6.4 mm) and an inner diameter of 1/8-in (3.2 mm), the tip of which included a protecting cover (Figure

3.16). The pressure taps for the coping front, top and back were not designed the same way as the one for the cleat, due to the fact that water should not flow into the pressure taps and affect the readings (Figure 3.10). The pressure taps for each configuration were numbered, with the ACC, CCC and DCC having pressure taps #1 to #3, #4 to #6, and #7 to #9, respectively (Figure 3.9).

For the installation of the pressure taps on the cleat, a hole was first drilled through the cleat and parapet through which the pressure tap was inserted and secured by duct tape (Figure 3.17). To install the pressure taps on the coping front, top and back, a hole was drilled through the coping and parapet (Figure 3.18), and pressure taps were inserted and fixed to the coping faces with epoxy (Figure 3.19).

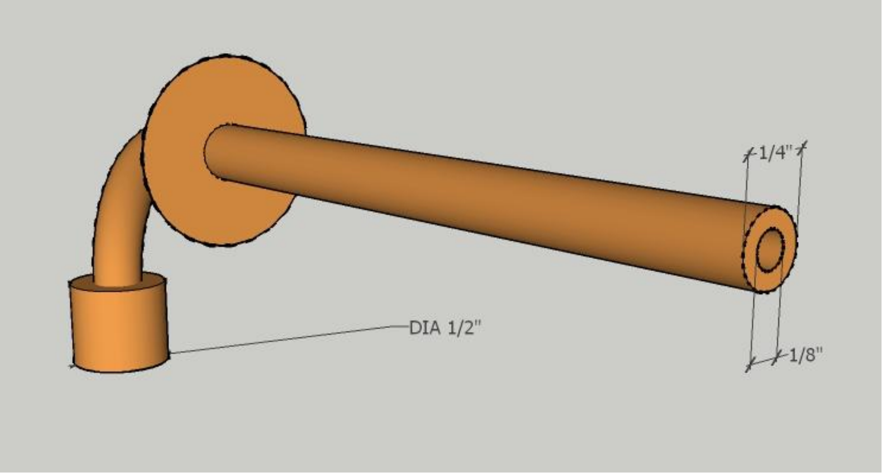

Figure 3.16: 3D model of pressure tap

Figure 3.17: Cleat pressure tap (Courtesy of NRCC)

Figure 3.18: Drilling the hole for the pressure tap on the top face (Courtesy of Laith Hajsaid, University of Ottawa)

Figure 3.19: Applying epoxy to the pressure tap on the top face (Courtesy of Laith Hajsaid, University of Ottawa)

Pressure taps were connected to Setra Model 239 pressure transducers, with nylon tubing of outer diameter of ¼ in (6.4 mm) and inner diameter of 12/64 in (4.8 mm) (Figure 3.20). The nylon tubing ran inside the parapet from the pressure taps to the pressure transducers through the hole in the back of the parapet (Figure 3.21). The pressure transducers, located inside the grey boxes, were installed on the back of the parapet to cope with space limitations inside the parapet (Figure 3.21). The full-scale range of the transducers was ±15 inch water-columns (±78 psf) with 0.14% accuracy. The transducer output range between 4 and 20 milliamps was converted into volts and wired to the junction box. All the pressure transducers were connected to the junction box.

Pressure sensors measure differential pressure. A constant pressure source was required to measure the differential pressures at the roof edges. Previous field studies mainly used two approaches:

1. Use of a pressure vessel below the ground level near the wind tower location (Concordia University study) or
2. Use of a constant pressure tank inside the building, which would not be affected due to changes of the building pressure (Texas Tech University experiments).

The present study uses the latter approach with a copper tank, as seen in Figure 3.22. The pressure in the copper tank was also monitored with an absolute pressure sensor for conformity and was connected to the junction box. The pressure transducers were calibrated to determine their accuracy over the full pressure range as stated in the manufacturer's specifications (Figure 3.23). The trend line in Figure 3.23, illustrating the calibration curve for the pressure transducer on the ACC front leg (P1), shows that the data is linear, with the slope of the trend line representing the sensitivity of the pressure transducer. All data points askew from the trend line represent the transducer inaccuracy (see Appendix A for remainder of calibration curves). The junction box was wired to the VXI system, which converts the electrical analog signal to a digital signal displayed as pressure reading on the computer. The VXI system collected pressure data from the pressure transducers, from the junction box, and determined the sampling rate of the experiment. The computer software runs the VXI system, and the on-site computer recorded all the data for the experiment (Figure 3.24). Pressure, wind speed and wind direction were sampled simultaneously at 100 Hz (100 samples/sec) during the entirety of the study.

Figure 3.20: Pressure transducer inside the grey box (Courtesy of NRCC)

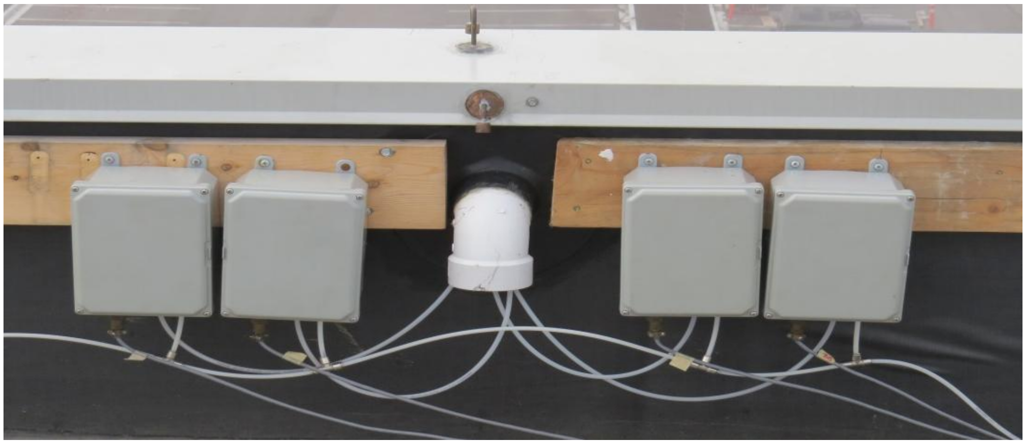

Figure 3.21: Pressure taps connected to the pressure transducers (Courtesy of NRCC)

Figure 3.22: Reference pressure container (Courtesy of NRCC)

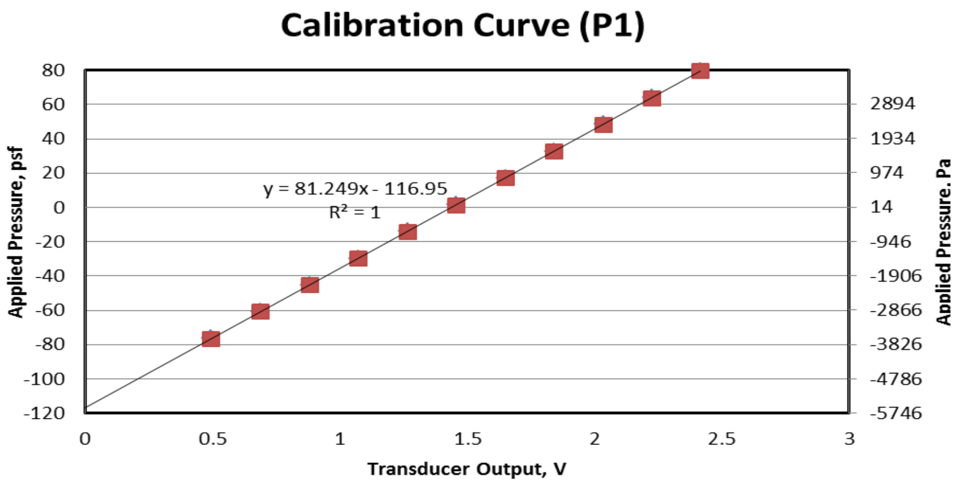

Figure 3.23: Calibration curve for P1

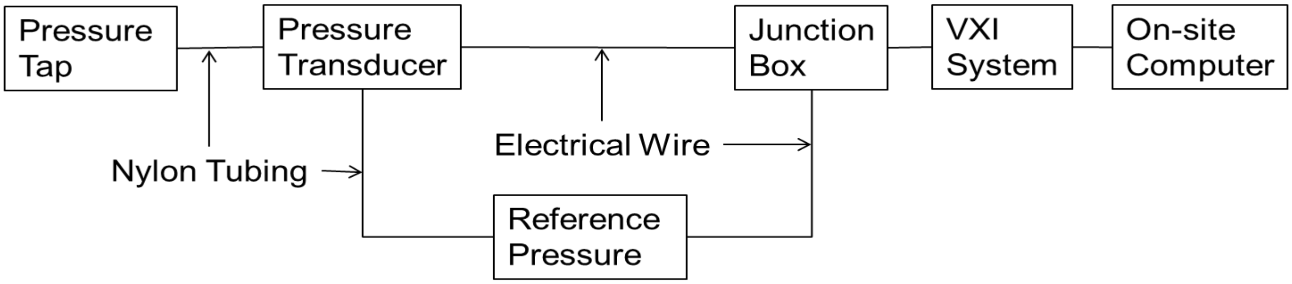

Figure 3.24: Flow diagram of the pressure taps setup and connections

3.5 Data Pre-processing

The data from the pressure taps installed on the roof edge configurations was collected continuously from August 2013 to June 2014. The raw data was pre-processed using a step-by-step procedure as illustrated in Figure 3.25, the results of which are presented and analyzed in Chapter 4.

Not all the collected data was analyzed since it was required to meet two requirements; (i) the daily peak wind speed had to be greater than 30 mph (48 km/h) and (ii) the wind direction had to come between the South-West and North-West (Figure 3.7). As a result, sixteen days of data met the analysis requirements.

The data acquisition collected data at a sampling rate (frequency) of 100 Hz, to ensure no loss of information on the collection of data from field site conditions. Field data, with nonstationary and unpredictable wind conditions, is prone to abrupt changes in pressure, which can be captured only with a sufficiently high sampling rate. Nevertheless, upon examination of the data set, it was observed that a sampling rate of 10 Hz captures the majority of oscillatory behavior of the pressure and wind data. An example is shown in Figure 3.26, which depicts the power spectral density of two minutes of pressure time series collected on the top leg of DCC, centered on the instant of wind speed peak on November 15, 2013. This data is the original data sampled at 100 Hz, and the dashed line shows the data that is ‘observed’, after resampling from 100 Hz to 10 Hz. As there are no significant oscillations beyond 5 Hz, as seen in Figure 3.26, it can be concluded that the Nyquist sampling theorem is essentially respected. In other words, that there is no loss of significant information beyond 10Hz. Moreover, the fact that the maximum peak pressure over one-minute, taken from the original 100-Hz data, was retained during the entire acquisition period ensures that design pressure values, or edge configuration response values, are valid for comparison with previous work and codes of practice with high reliability.

To understand the data pre-processing methodology outlined in Figure 3.25, an example is described for the data collected on November 19, 2013 from the DCC coping front leg as follows:

1. 100 samples were collected per second (6,000 data points per minute), and the minute peak was identified (-8.2 psf in Figure 3.27). This resulted in 1,440 minute peaks per day.
2. Using the 1,440 minute peaks, the peak value for the day and the corresponding time stamp were identified. For pressure tap P8 on the DCC coping front leg, the peak value was a suction of -8.2 psf at 3:18 PM, labelled as “reference time” (Figure 3.28).
3. 30 minutes of raw data (100 samples/second) were extracted before and after the reference time. For the example, 360,000 data points are extracted from 2:48 to 3:48 PM (Figure 3.28).
4. The data was re-sampled at 10 samples per second to reduce the number of data points from 360,000 to 36,000, and consequently the computational requirements. The result was labelled as the daily-hourly data (Figure 3.29).

5. The maximum pressure (positive value), suction (negative pressure), and mean for the daily-hourly data were calculated. For the example given in Figure 3.29, the maximum pressure, suction and mean were found to be 3.9 psf, -8.2 psf, and -0.1 psf, respectively.

The time history plots of pressure, wind speed and direction, and the maximum pressure, suction and mean for the 16 days of collected data can be found in Appendices B, C, and D for the ACC, CCC and DCC, respectively.

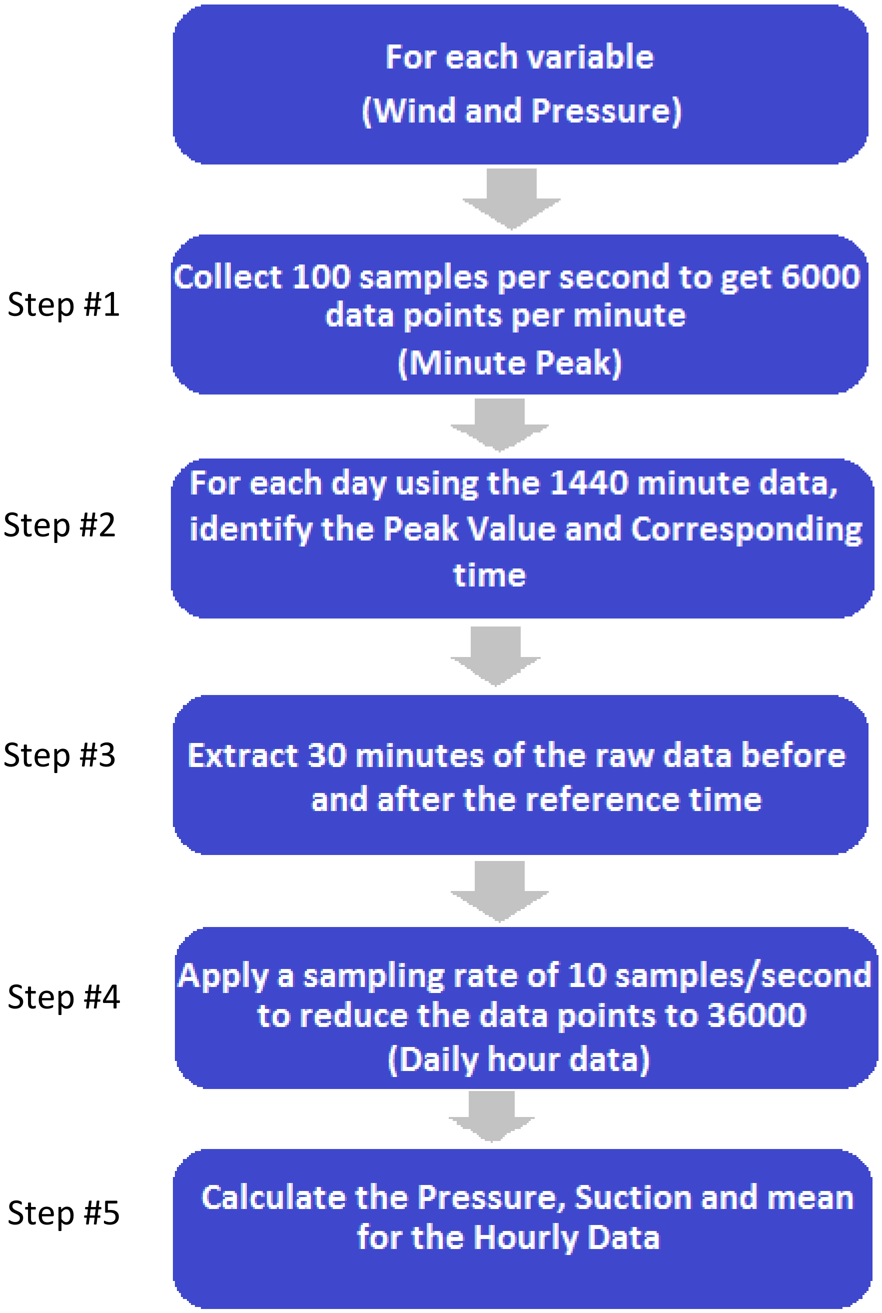

Figure 3.25: Step-by-step data reporting procedure

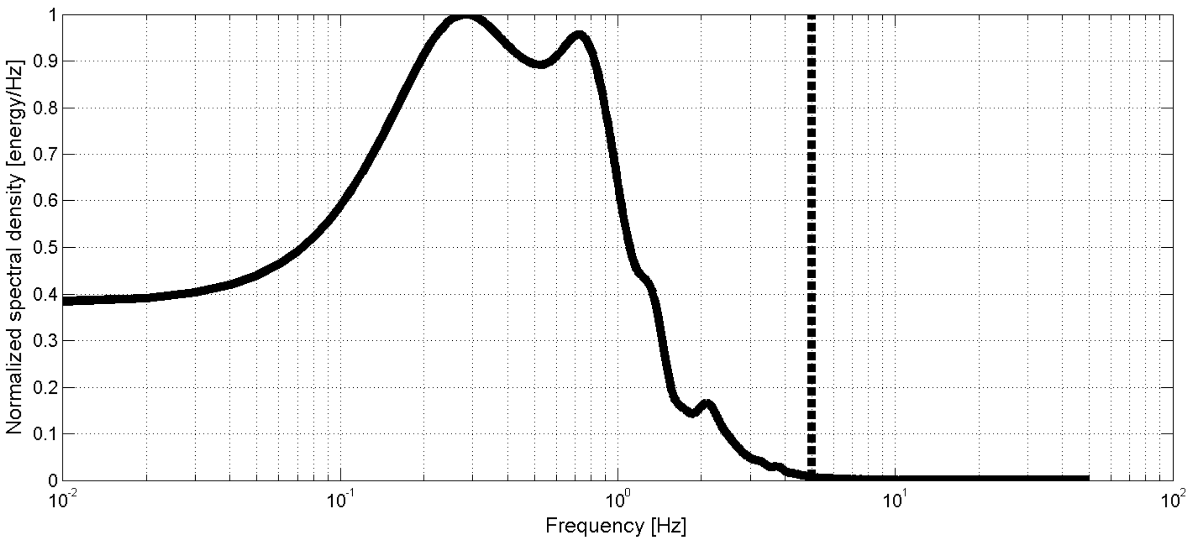

Figure 3.26: Typical power spectral density of two minutes of pressure data sampled at 100 Hz

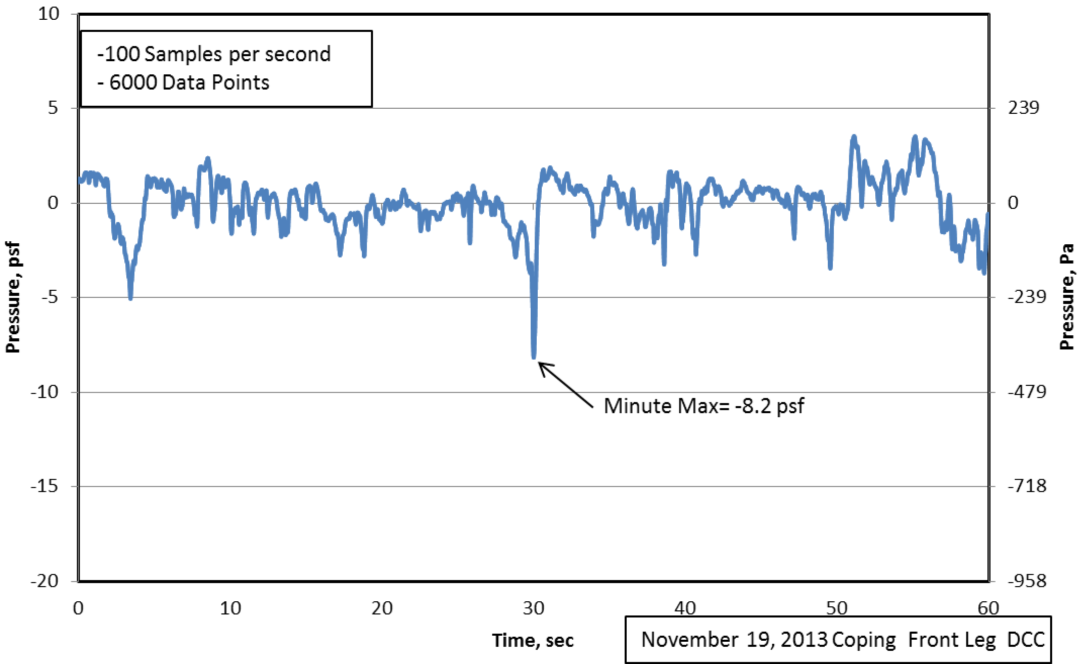

Figure 3.27: Pressure tap raw data during 60 seconds, collected on November 19, 2013 from the DCC coping front leg (Step 1).

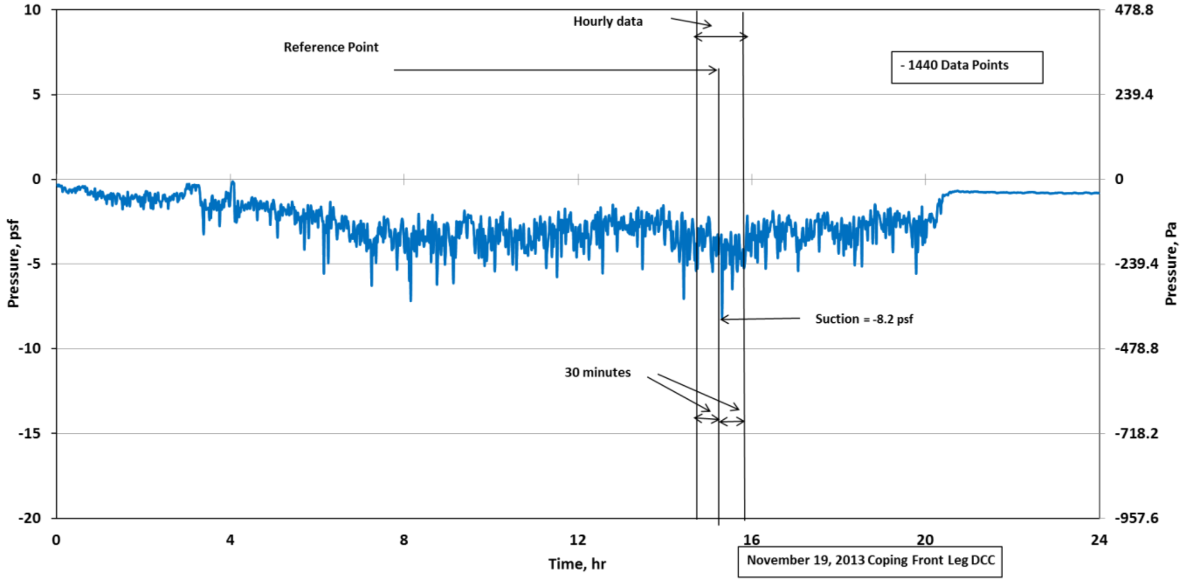

Figure 3.28: Minute maximum pressure data for a 24-hour period for November 19, 2013 from the DCC coping front leg (Step 2 & 3)

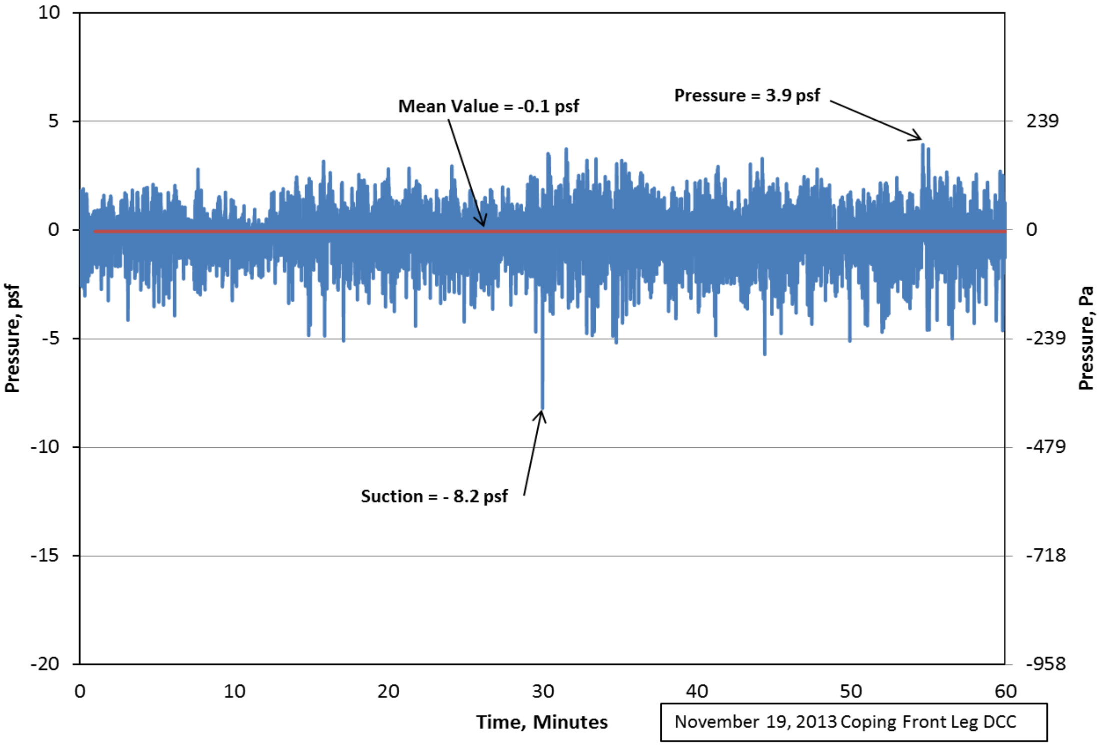

Figure 3.29: Pressure data resampled at 10 Hz (blue), and mean (red) and peak values (positive and negative), for November 19, 2013 (Step 4 & 5)

Chapter 4: Experimental Results and Discussion

4.1 Introduction

This chapter presents the wind pressure data recorded at the field site from August 2013 to June 2014 for the ACC, CCC and DCC edge configurations. The CCC (LW) on the leeward parapet is not considered since it showed significantly lower suction compared to other configurations. Section 4.2 describes the data for the windiest day in the period of time considered. Section 4.3 compares two different data sets of wind pressure illustrating reproducibility, and Section 4.4 observes the effect wind speed has on the various edge configurations. Finally, Section 4.5 compares the edge configurations to each other to see how their responses differ.

4.2 Windiest Day

As discussed in Chapter 3, a total of 16 days between August 6, 2013 and June 30, 2014 had wind that reached speeds of over 30 mph (48 km/h). Table 4.1, Table 4.2 and Table 4.3 show the measured data for ACC, CCC and DCC configurations. The wind speed was measured on top of Penthouse 5 at an elevation of 74 ft. (22.6 m). Due to the requirements of building codes, the speed was automatically corrected to the roof height of 58 ft. (17.7 m) by the data acquisition system using the power law profile (Simiu, 2011). All wind speeds reported in the present thesis are at a roof height of 58 ft. (17.7 m).

The highest recorded wind speed occurred on November 15, 2013. From the minute data of that day (one-hour long), the peak wind speed was recorded as 58 mph (93 kph), and the mean wind speed of the hourly data was 29 mph (47 kph) (Figure 4.1). Every hour of pressure data centered on the daily peak wind speed instant is labeled with a particular wind direction. For this, a compass rose was divided into 16 direction ranges, from which the directions of interest (i.e., cornering and perpendicular winds with respect to the building orientation) are shown in Figure 4.2. The numerical values of the direction increase clockwise, starting at 0° (North) to 270° (West). Each direction has an amplitude range of 22.5° as illustrated in Figure 4.2. For instance, winds coming from the west (perpendicular winds according to the building orientation) have an angle of attack of 270°±11.25°. The windiest day had a wind direction of WNW (Figure 4.3).

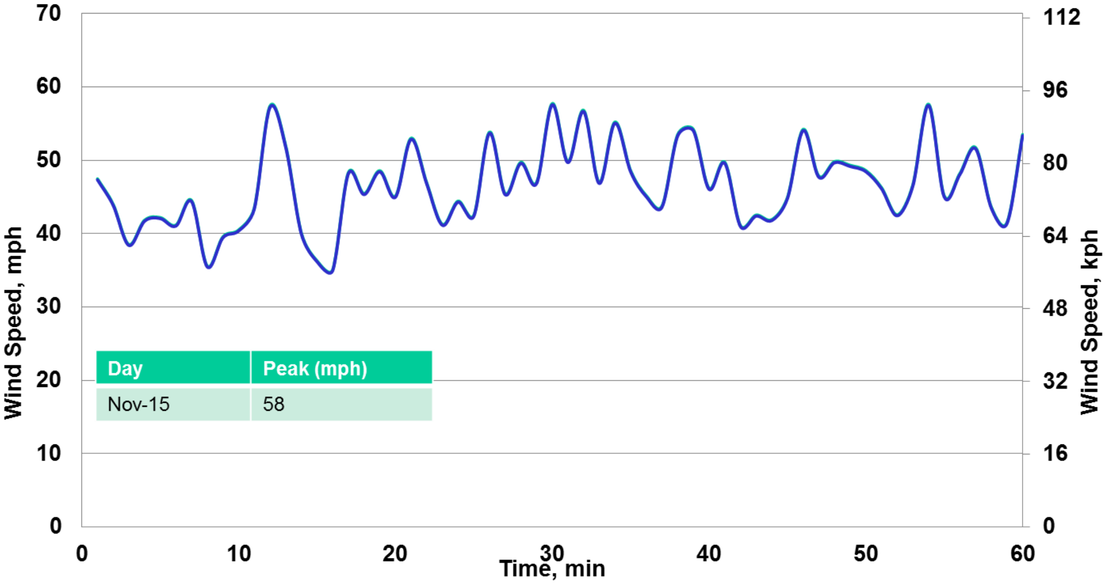

Day	Peak (mph)
Nov-15	58

Figure 4.1: Wind speed on November 15, 2013

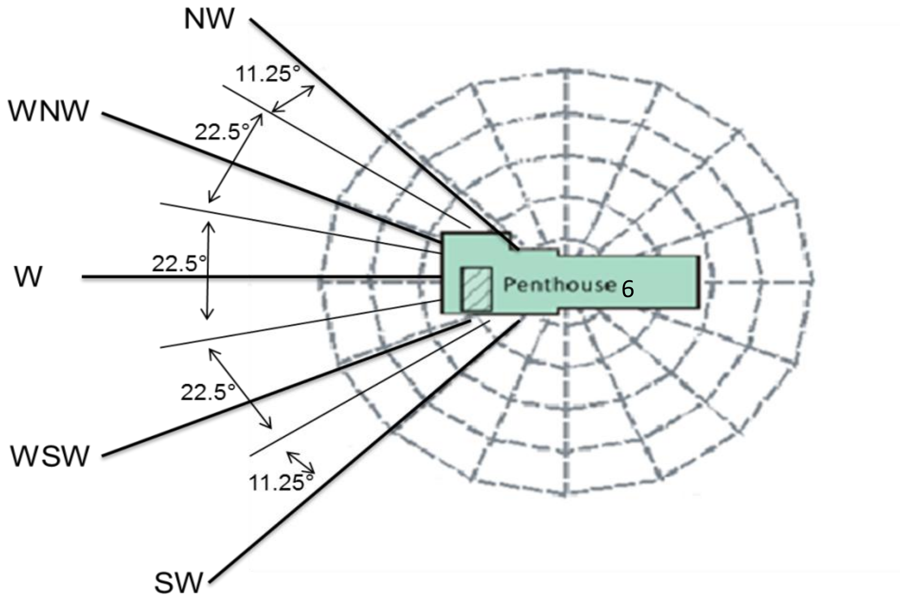

Figure 4.2: Different wind directions with an amplitude range of 22.5°

Table 4.1: Measured wind performance - ACC configuration

Date	Wind		Wind Performance, psf		
	Speed ,mph Peak/Mean	Direction	Coping Front Leg (P1)	Coping Top Leg (P2)	Coping Back Leg (P3)
			Suction/Mean/Pressure	Suction/Mean/Pressure	Suction/Mean/Pressure
02-Nov-13	37/14	NW	-3.4/-0.1/1.4	-3.5/-0.5/0	-2.6/-0.5/0.0
14-Nov-13	32/15	WNW	-2.6/0.2/1.9	-4.9/-0.8/0.0	-3.5/-0.7/0.0
15-Nov-13	58/29	WNW	-7.0/0.4/5.9	-13.6/-2.2/0.0	-8.7/-1.9/0.1
16-Nov-13	49/28	WNW	-6.8/0.2/4.8	-11.0/-2.1/0.0	-7.5/-1.3/0.0
19-Nov-13	48/25	W	-5.7/0.4/4.0	-10.1/-1.7/0.0	-6.5/-1.5/0.1
01-Dec-13	42/19	WNW	-5.0/0.0/3.0	-7.5/-1.3/0.0	-6.1/-1.1/0.0
02-Dec-13	43/17	W	-5.1/0.0/3.6	-8.0/-1.2/0.0	-5.8/-1.1/0.0
18-Dec-13	50/23	W	-5.7/0.3/4.0	-10.1/-1.5/0.0	-6.0/-1.3/0.0
23-Dec-13	36/17	WNW	-3.5/0.0/1.6	-4.5/-0.8/0.0	-2.9/-0.7/0.0
20-Feb-14	42/22	W	-6.2/0.5/3.5	-7.3/-1.3/0.0	-5.4/-1.2/0.0
21-Feb-14	34/16	WSW	-8.3/0.2/3.5	-8.0/-1.8/0.0	-5.7/-1.3/0.0
17-Apr-14	49/25	W	-6.8/0.2/4.2	-12.2/-1.9/0.0	-7.4/-1.8/0.0
21-Apr-14	30/15	W	-2.9/-0.2/1.4	-5.0/-0.7/0.0	-2.7/-0.8/0.0
22-Apr-14	32/15	W	-5.0/0.1/1.7	-4.9/-0.8/0.0	-3.6/-0.8/0.0
09-Jun-14	46/21	W	-5.1/0.3/3.4	-8.1/-1.3/0.0	-6.1/-1.1/0.0
20-Jun-14	32/13	WSW	-1.8/0.2/1.6	-2.7/-0.4/0.9	-1.8/-0.5/0.0

1 psf = 47.9 N/m^2; 1 mph = 0.447 m/s

Table 4.2: Measured wind performance - CCC configuration

Date	Wind		Wind Performance, psf		
	Speed ,mph Peak/Mean	Direction	Cleat (P4)	Coping Front Leg (P5)	Coping Top Leg (P6)
			Suction/Mean/Pressure	Suction/Mean/Pressure	Suction/Mean/Pressure
02-Nov-13	37/14	NW	-1.4/-0.4/0.0	-2.7/-0.2/0.8	-4.0/-0.7/0.0
14-Nov-13	32/15	WNW	-1.4/-0.2/0.4	-2.9/-0.1/1.5	-5.3/-0.8/0.0
15-Nov-13	58/29	WNW	-4.2/-0.8/1.1	-7.5/-0.3/5.7	-11.1/-2.3/0.0
16-Nov-13	49/28	WNW	-3.0/-0.8/0.7	-8.0/-0.3/3.1	-8.1/-1.8/0.0
19-Nov-13	48/25	W	-2.8/-0.5/0.6	-6.4/-0.2/2.5	-9.3/-1.4/0.0
01-Dec-13	42/19	WNW	-2.2/-0.5/0.4	-4.7/-0.2/2.3	-7.9/-1.3/0.0
02-Dec-13	43/17	W	-2.3/-0.5/0.4	-4.5/0.0/1.8	-6.2/-1.2/0.0
18-Dec-13	50/23	W	-3.5/-0.4/0.6	-7.7/-0.2/2.4	-8.4/-1.5/0.0
23-Dec-13	36/17	WNW	-1.4/-0.3/0.3	-3.8/-0.2/1.2	-4.8/-0.5/1.2
20-Feb-14	42/22	W	-2.1/-0.4/0.5	-4.4/-0.1/2.1	-8.9/-1.3/0.0
21-Feb-14	34/16	WSW	-2.9/-0.7/0.5	-4.9/-0.4/2.3	-7.9/-1.5/0.0
17-Apr-14	49/25	W	-3.6/-1.2/0.0	-5.3/-0.3/3.5	-8.0/-2.1/0.0
21-Apr-14	30/15	W	-1.5/-0.3/0.2	-3.4/-0.2/1.4	-3.2/-0.9/0.0
22-Apr-14	32/15	W	-1.4/-0.3/0.2	-3.0/-0.2/1.1	-3.7/-0.8/0.0
09-Jun-14	46/21	W	-2.4/-0.3/0.6	-4.8/-0.2/2.6	N/A/N/A/N/A
20-Jun-14	32/13	WSW	-1.0/-0.2/0.2	-1.9/-0.1/0.9	N/A/N/A/N/A

1 psf = 47.9 N/m^2; 1 mph = 0.447 m/s

Table 4.3: Measured wind performance - DCC configuration

Date	Wind		Wind Performance, psf		
	Speed ,mph Peak/Mean	Direction	Cleat (P7)	Coping Front Leg (P8)	Coping Top Leg (P9)
			Suction/Mean/Pressure	Suction/Mean/Pressure	Suction/Mean/Pressure
02-Nov-13	37/14	NW	-1.1/-0.1/1.1	-2.9/-0.1/1.8	-3.3/-0.8/0.0
14-Nov-13	32/15	WNW	-1.4/0.0/0.8	-3.4/0.1/1.6	-4.7/-0.8/0.0
15-Nov-13	58/29	WNW	-3.1/-0.1/3.6	-7.9/0.4/5.8	-15.5/-2.4/0.0
16-Nov-13	49/28	WNW	-2.4/0.0/3.5	-6.4/0.3/5.6	-10.3/-2.3/0.0
19-Nov-13	48/25	W	-2.6/0.0/3.4	-8.2/-0.1/3.9	-9.2/-1.9/0.0
01-Dec-13	42/19	WNW	-2.2/-0.1/2.2	-4.3/0.1/2.8	-7.3/-1.5/0.0
02-Dec-13	43/17	W	-2.0/-0.1/1.8	-4.8/-0.1/1.9	-8.8/-1.2/0.0
18-Dec-13	50/23	W	-2.6/-0.1/2.0	-6.4/0.2/3.7	-8.4/-1.4/0.0
23-Dec-13	36/17	WNW	-1.3/-0.1/0.7	-3.3/0.1/1.6	-5.7/-0.9/0.0
20-Feb-14	42/22	W	-2.0/-0.2/1.8	-4.8/0.0/2.2	-6.8/-1.3/0.0
21-Feb-14	34/16	WSW	-2.5/-0.2/1.7	-6.4/-0.3/2.5	-8.9/-2.0/0.0
17-Apr-14	49/25	W	-3.6/-0.3/2.9	-8.1/0.0/4.0	-12.6/-2.4/0.0
21-Apr-14	30/15	W	-1.4/-0.1/0.7	-3.2/0.0/1.7	-4.2/-0.8/0.0
22-Apr-14	32/15	W	-1.5/-0.1/1.2	-3.7/-0.1/1.7	-4.6/-0.8/0.1
09-Jun-14	46/21	W	-2.0/-0.1/1.9	-5.5/0.1/3.1	-8.1/-1.4/0.1
20-Jun-14	32/13	WSW	-0.9/-0.1/0.6	-2.0/0.0/1.2	-2.9/-0.6/0.0

1 psf = 47.9 N/m^2; 1 mph = 0.447 m/s

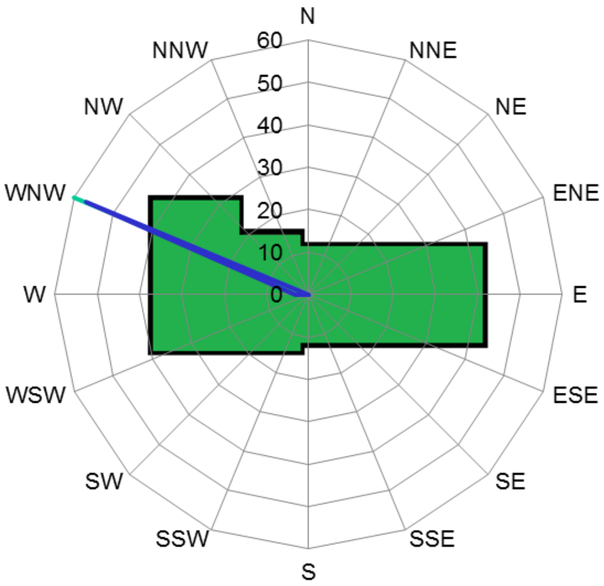

Figure 4.3: Wind direction for the analyzed hour of November 15, 2013

The pressure data recorded on the ACC was chosen to exemplify the coping performance on the windiest day since it showed air pressure acting on all three faces of the edge. The wind-induced pressure distributions on the front, top and back faces of the ACC are shown in Figure 4.4, Figure 4.5 and Figure 4.6, respectively. As discussed in Section 3.5, the presented data represent the maximum measured pressure/suction for each minute. At the front face (Figure 4.4), wind induces both pressure (positive) and suction (negative), whereas the other two faces are subjected to only suction (Figure 4.5 and Figure 4.6). The minimum value for the day can be labelled as peak, with the peak values for the front, top and back legs being -7.0 psf (-335 Pa), -13.5 psf (-646 Pa) and -8.7 psf (-417 Pa), respectively. A peak pressure of +5.9 psf (283 Pa) was also measured on the front leg of ACC metal edge (Figure 4.4).

The range of suction fluctuation is another observation of interest. For the front and back faces of the ACC edge, the suction measured during the representing hour ranged from -4 to -8 psf (-192 to -383 Pa). This is significantly different in the case of the top face, which experienced higher fluctuations ranging from -4 to -12 psf (-192 to -575 Pa). The difference between the two clearly shows that the outward pull force is higher at the top surface, due to wind flow separation from the leading edge. This will be further discussed in Section 4.5.1.

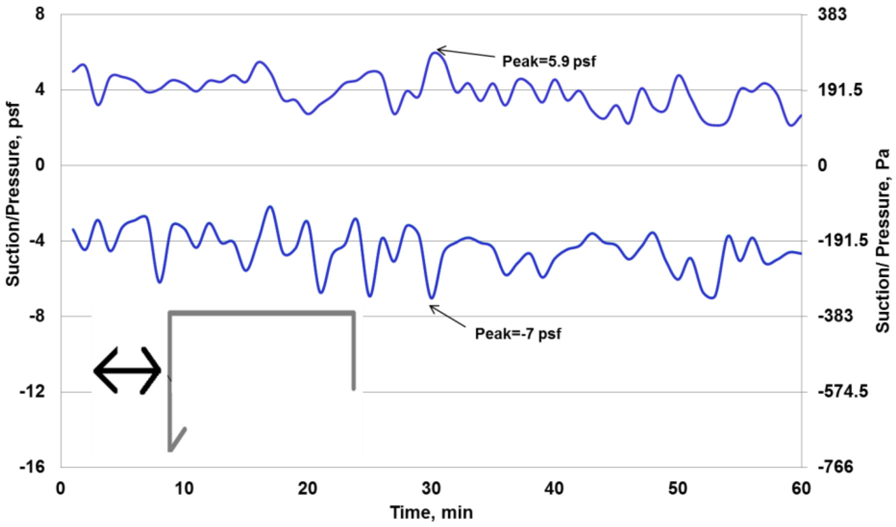

Figure 4.4: Suction on the ACC coping front leg on November 15, 2013

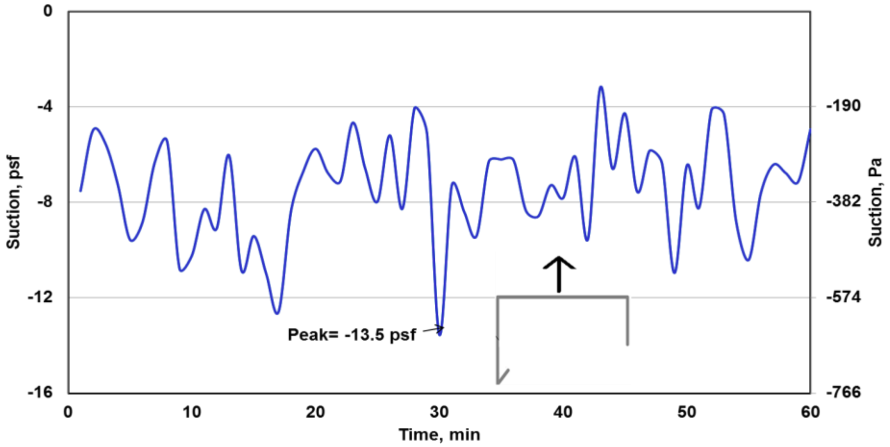

Figure 4.5: Suction on the ACC coping top on November 15, 2013

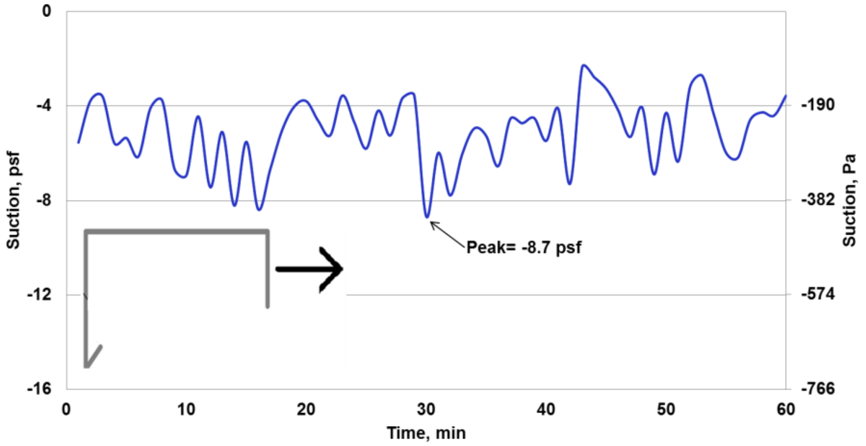

Figure 4.6: Suction on the ACC coping back leg on November 15, 2013

4.3 Reproducibility of Measured Data

Since wind occurred at various speeds and directions over the recorded days, the field data was analyzed to ensure that the suction acting on the coping was reproducible. Two criteria for reproducibility of the data were established to compare the pressure/suction recorded on two different days; (i) the peak wind speeds could only differ by a maximum of 3 mph (4 kph), and (ii) the wind direction had to have the same angle of attack during the peak wind-speed hour. Based on these criteria, two sets of wind pressure/suction measurements were analyzed to determine if the recorded data was reproducible.

4.3.1 First Set of Measured Data

The first set of data compares the days of November 19, 2013 and December 18, 2013, which met the first criteria by having similar peak wind speeds of 49 and 50 mph (79 and 81 kph), respectively. . The hourly wind speed data of these two days are shown in Figure 4.7. The mean wind speed for November 19 and December 18 were 25 and 23 mph (40 and 37 kph), respectively, and wind was directed West in both days (Figure 4.8).

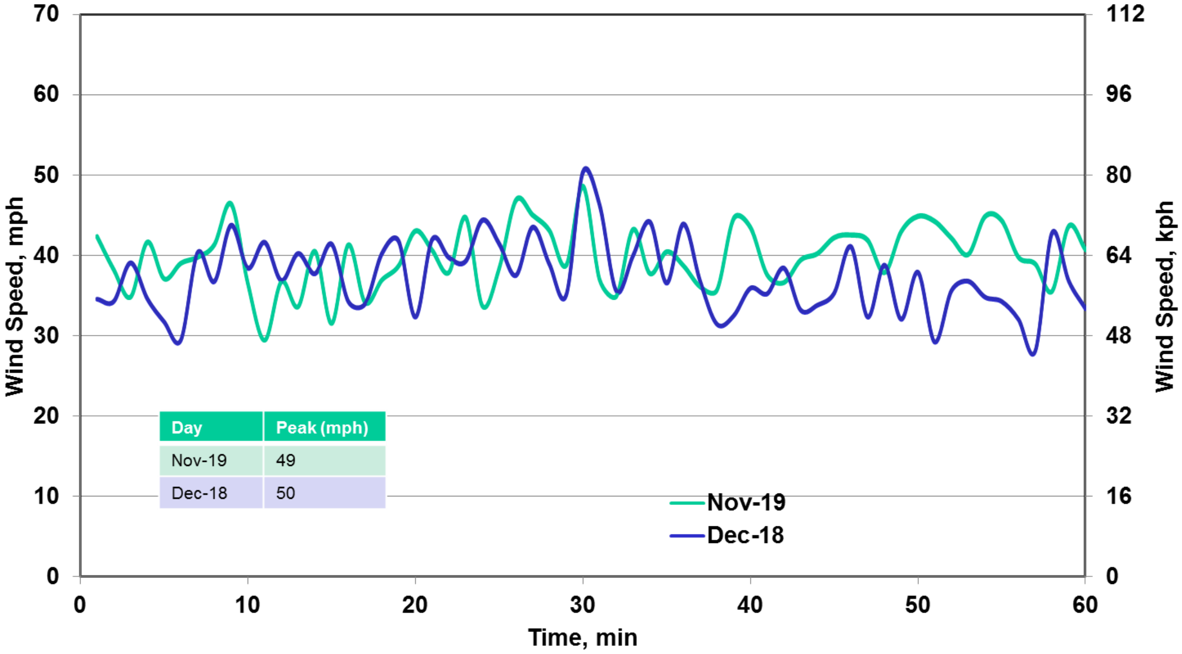

Figure 4.7: Wind speed hourly data of November 19 and December 18, 2013

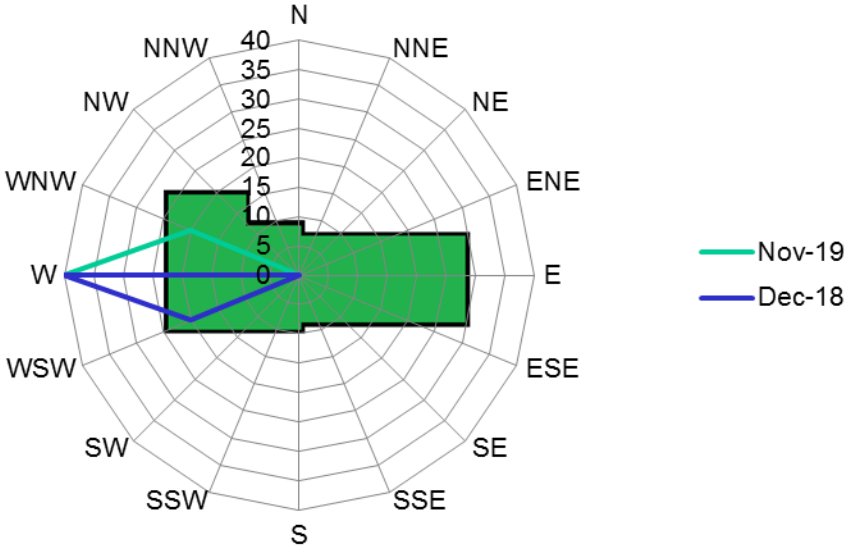

Figure 4.8: Wind direction on November 19 and December 18, 2013

4.3.1.1 Wind Performance of ACC

Figure 4.9, Figure 4.10 and Figure 4.11 illustrate the suction recorded on the ACC coping front, top and back legs, respectively. The front leg hourly suction during the two days showed similar peak values of -6 psf (-287 Pa) and mean pressure of 0.4 and 0.3 psf (19 and 14 Pa) for the two days. The hourly suction acting on the top of the configuration had the same peak value of -10 psf (-479 Pa) for both days, and the mean suction value of the data set was -1.7 and -1.5 psf (-81 and -72 Pa) (Figure 4.10). The peak suction values recorded on the back face of the ACC differed by merely 1 psf, with a value of -7 psf (-335 Pa) for November 19, 2013, and a value of -6 psf (-287 Pa) for December 18, 2013. The difference between the means for both days was also small, with values of -1.5 psf (-72 Pa) and -1.3 psf (-62 Pa), respectively.

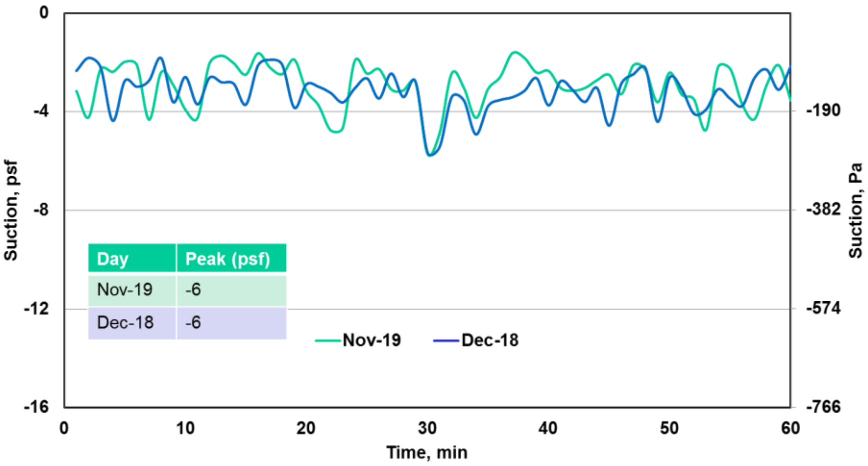

Figure 4.9: Suction on the ACC coping front leg for November 19 and December 18, 2013

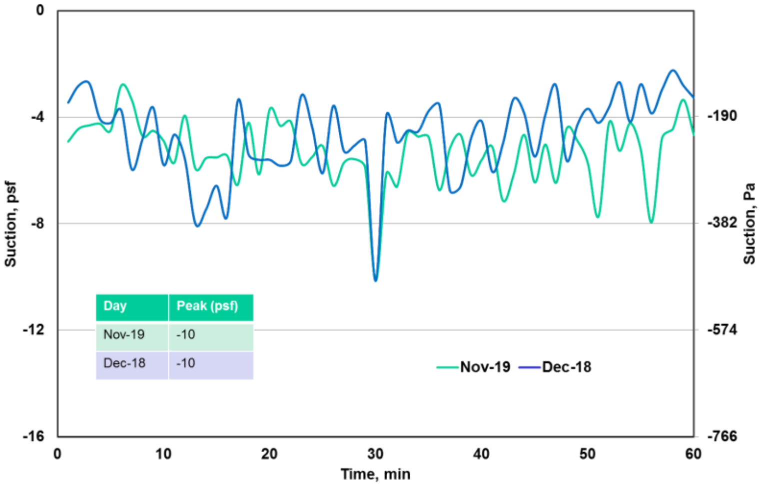

Figure 4.10: Suction on the ACC coping top for November 19 and December 18, 2013

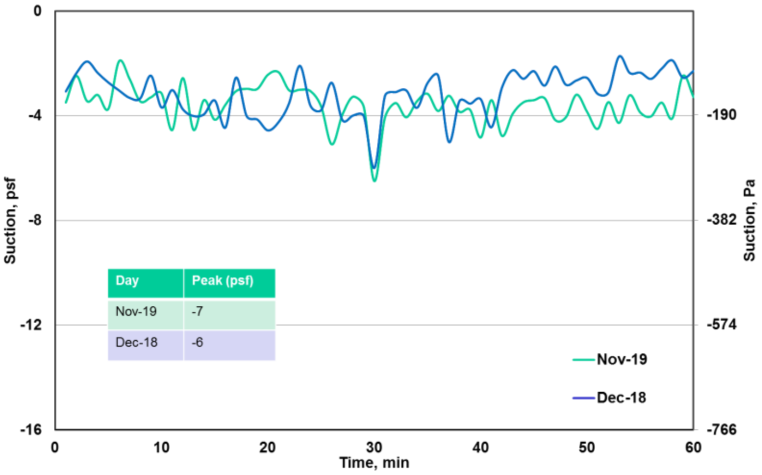

Figure 4.11: Suction on the ACC coping back leg, for November 19 and December 18

4.3.1.2 Wind Performance of CCC

Similar to the previous section, this section compares the suction pressure data acting on the CCC on November 19, 2013 and December 18, 2013. The peak suction acting on the cleat was slightly different on each day, with a value of -3 psf (-144 Pa) and -4 psf (-192 Pa) for November 19 and December 18, 2013, respectively (Figure 4.12). The mean suction values for both days was -0.5 and -0.4 psf (-24 and -19 Pa), respectively. The pressure acting on the front leg of the coping reveals a difference in peak suction with values of -6 psf (-287 Pa) and -8 psf (-383 Pa) for November 19 and December 18, 2013, respectively (Figure 4.13). The peak values recorded on the front leg of the coping were double in magnitude to those measured on the cleat; however, the mean suction values were the same value of -0.2 psf (-10 Pa) for both days. Although Figure 4.14 shows that there is only a slight difference in the peak suction pressure for both days with values of -9 psf (-431 Pa) and -8 psf (-383 Pa) respectively, the variation of the suction pressure over the recorded hour led to a difference in the mean value for the two days, with -1.4 psf (-67 Pa) and -1.5 psf (-72 Pa), respectively. The hourly data measured on the back leg of the CCC is not included here due to failure of the corresponding pressure tap.

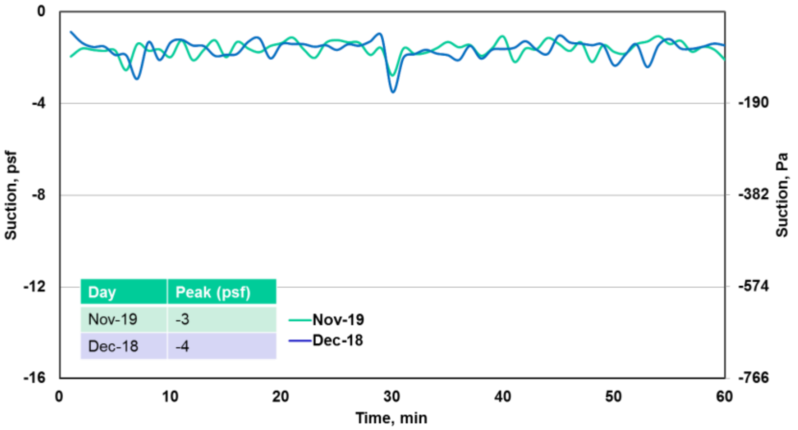

Figure 4.12: Suction on the CCC cleat for November 19 and December 18, 2013

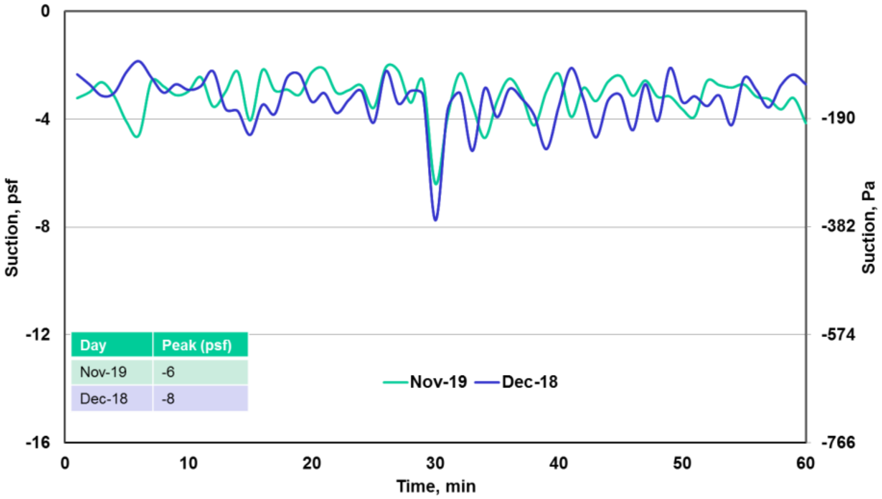

Figure 4.13: Suction on the CCC coping front leg for November 19 and December 18, 2013

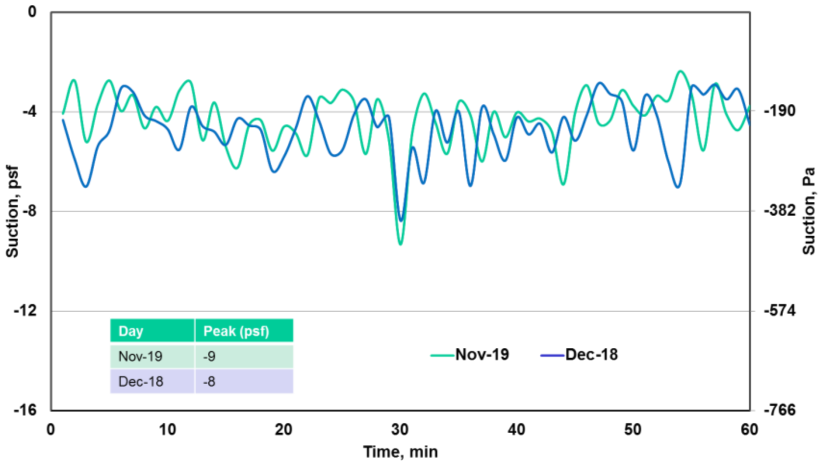

Figure 4.14: Suction on the CCC coping top leg for November 19 and December 18, 2013

4.3.1.3 Wind Performance of DCC

The comparison of the suction pressure data acting on the DCC on November 19, 2013 and December 18, 2013, is established in Figure 4.15, Figure 4.16 and Figure 4.17. The peak suction values acting on the cleat were -3 psf (-144 Pa) for both days; however, the mean values differ, with 0 psf (0 Pa) and -0.1 psf (-5 Pa) for each of the days, respectively (Figure 4.15). The peak suction pressure on the front leg of the coping showed a larger difference in both days, with values of -8 psf (-383 Pa) and -6 psf (-287 Pa), respectively (Figure 4.16). However, the difference in mean values between the two data sets, are -0.1 psf (-5 Pa) and -0.2 psf (-10 Pa) for each day, respectively. Similar to the pressure data recorded on the CCC, the peak suction acting on the DCC front leg was double in magnitude to that measured on the cleat. A minor difference in the peak suction values acting on the top leg of the coping had values of -9 psf (-431 Pa) and -8 psf (-383 Pa) (Figure 4.17). Yet, a different fluctuation on the suction pressure of the two days led to a difference in the mean values of -1.9 psf (-91 Pa) and -1.4 psf (-67 Pa), respectively. The pressure acting on the coping back leg of the DCC for those two days is not reported here due to failure of the corresponding pressure tap.

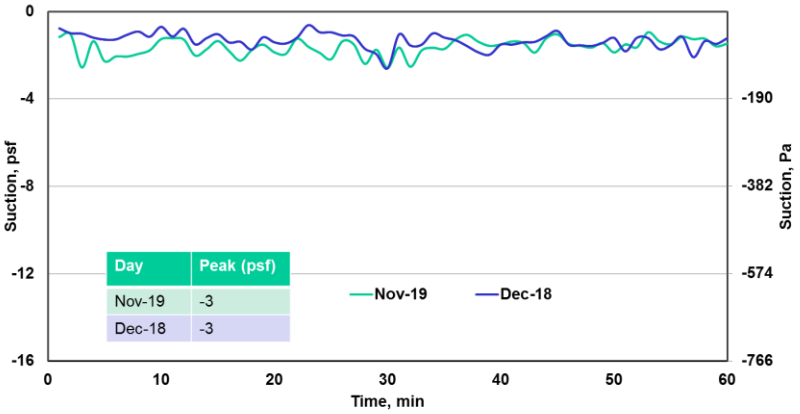

Figure 4.15: Suction on the DCC cleat for November 19 and December 18, 2013

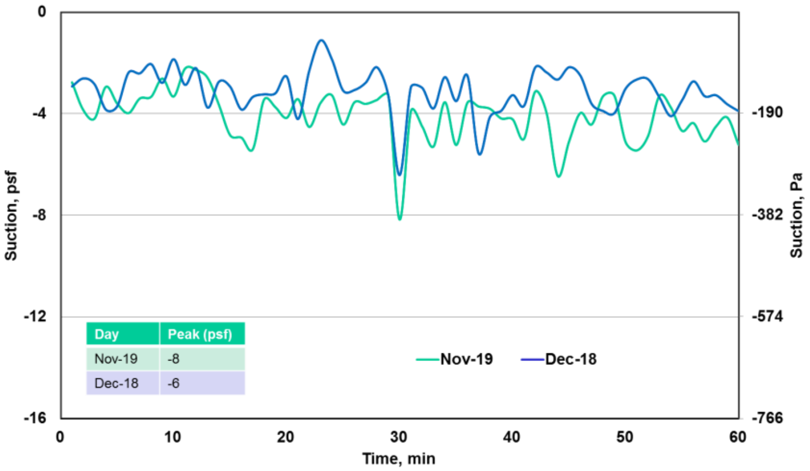

Figure 4.16: Suction on the DCC coping front leg for November 19 and December 18, 2013

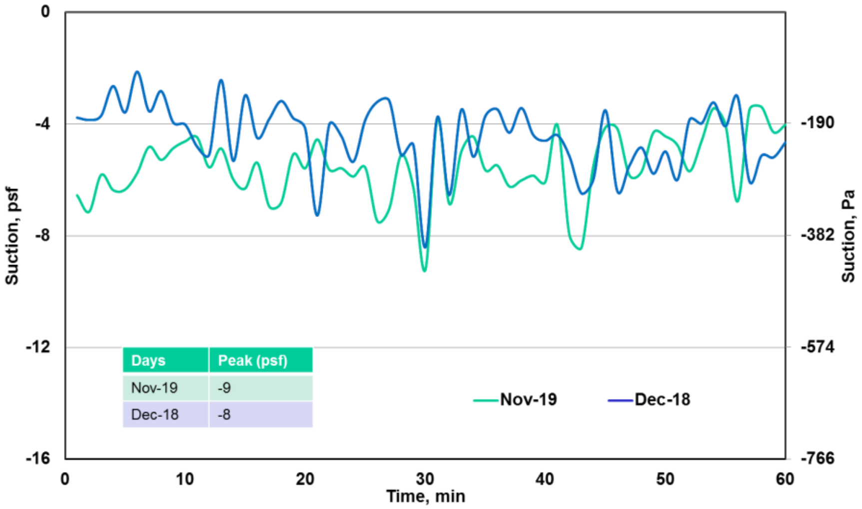

Figure 4.17: Suction on the DCC coping top for November 19 and December 18, 2013

4.3.2 **Second Set of Measured Data**

Similar to the previous section, pressure data that was recorded on two separate days and met the criteria presented in Section 4.3 was compared to examine its reproducibility. The days selected were December 2, 2013 and February 20, 2014, since both days showed comparable peak wind speeds of 43 and 42 mph (69 and 68 kph), respectively (Figure 4.18), and had westward wind directions (Figure 4.19). Compared to the first set of data (Figure 4.7), the second set of data showed a larger variation in the wind speed over the hour (Figure 4.18), implying a difference in the mean wind speed of 17 and 22 mph (27 and 35 kph) for December 2, 2013 and February 20, 2014 respectively.

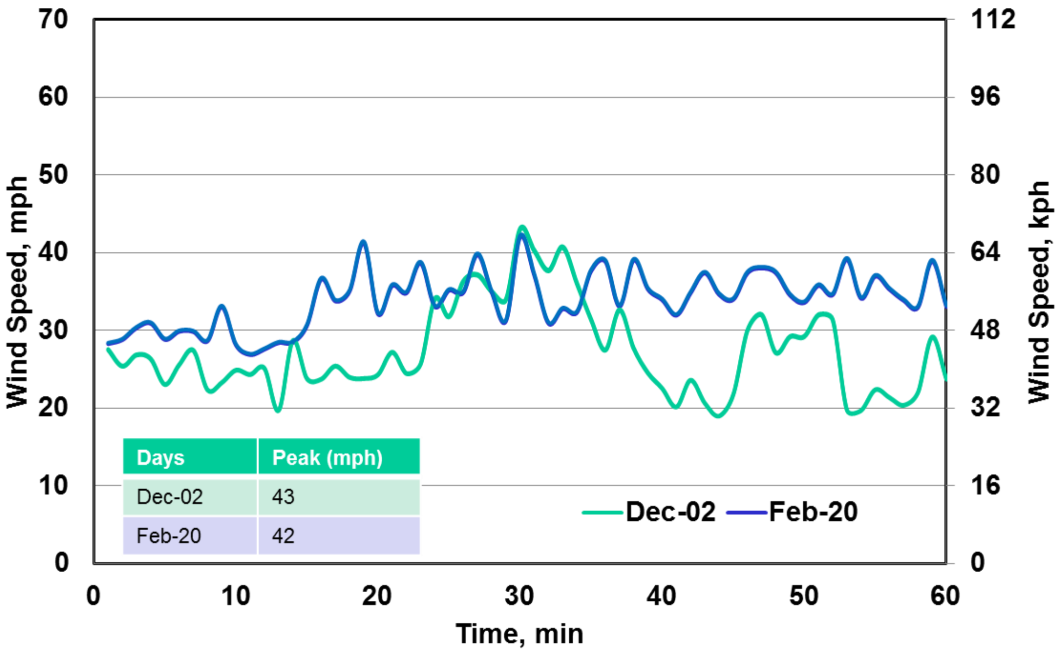

Days	Peak (mph)
Dec-02	43
Feb-20	42

Figure 4.18: Wind speed hourly data on December 2, 2013 and February 20, 2014

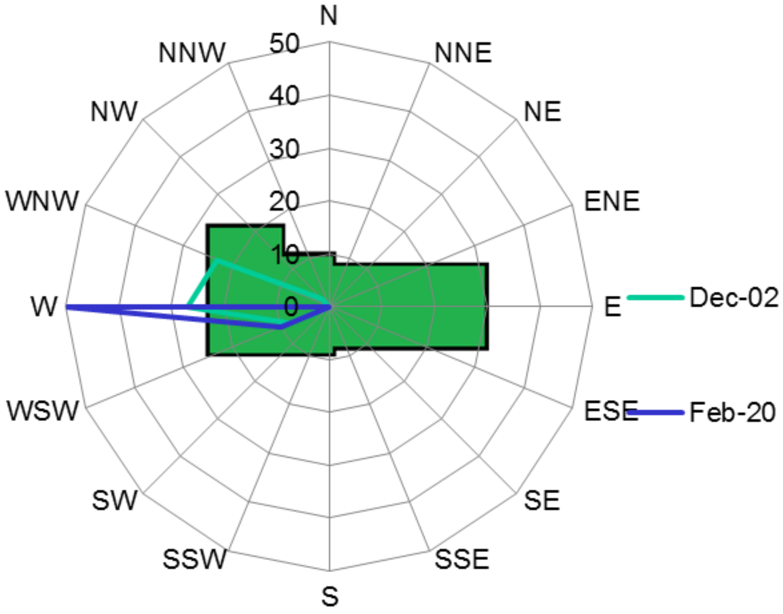

Figure 4.19: Wind direction for December 2, 2013 and February 20, 2014

4.3.2.1 Wind Performance of ACC

Similar to Section 4.3.1.1, this section compares the pressure data recorded on the ACC metal edge on December 2, 2013, and February 20, 2014. The peak suction values for all legs showed small variance, with the front leg being subjected to -5 psf (-239 Pa) and -6 psf (-287 Pa), the coping top experiencing -8 psf (-383 Pa) and -7 psf (-335 Pa) , and the coping back leg experiencing -6 psf (-287 Pa) and -5 psf (-239 Pa), respectively (Figure 4.20). The highest peak value occurred on the top face of the ACC metal edge, and the mean suction values over the hourly peak data for December 2, 2013 and February 20, 2014 were fairly similar on each face of the coping, with 0 psf (0 Pa) and -0.5 psf (-24 Pa) acting on the front face, -1.2 psf (-57 Pa) and -1.3 psf (-62 Pa) acting on the top face, and -1.1 psf (-53 Pa) and -1.2 psf (-57 Pa) acting on the back face, respectively (Figure 4.20).

4.3.2.2 Wind Performance of CCC

When observing the pressure data on the CCC, it was found that the cleat peak and mean suction values for both days were very similar, with a peak of -2 psf (-96 Pa) and a mean of -0.5 and -0.4 psf (-24 and -19 Pa) (Figure 4.21). The peak suction values on the CCC front face were -4 psf (-192 Pa) and mean of 0 psf (0 Pa) and -0.1 psf (-5 Pa) for December 2, 2013 and February 20, 2014, respectively. Peak suction measured on the CCC top face was the highest at -6 psf (-287 Pa) and -9 psf (-431 Pa) for each of the days, respectively. However, the mean values of the suction acting on the CCC top face were closer in magnitude, with values of -1.2 psf (-57 Pa) and -1.3 psf (-62 Pa), respectively.

4.3.2.3 Wind Performance of DCC

Pressure data for DCC was similar to that presented for the CCC configuration (Figure 4.22). The peak and mean values of the pressure measured on December 2, 2013 and February 20, 2014 were quite close for both days, and cleat values were the same with a peak suction of -2 psf (-96 Pa) and a close mean value of -0.1 and -0.2 psf (-5 and -10 Pa). A higher peak value of -5 psf (-240 Pa) was observed on the DCC front leg, with mean values of -0.1 psf (-96 Pa) and 0 psf (0 Pa) for each day, respectively. The top leg face showed a similar peak suction of -9 psf (-431 Pa) and -7 psf (-335 Pa) for both days to that observed on the top face of the CCC. The mean values of the suction acting on the top face were the similar on both days at -1.2 and -1.3 psf (-57 and -62 Pa).

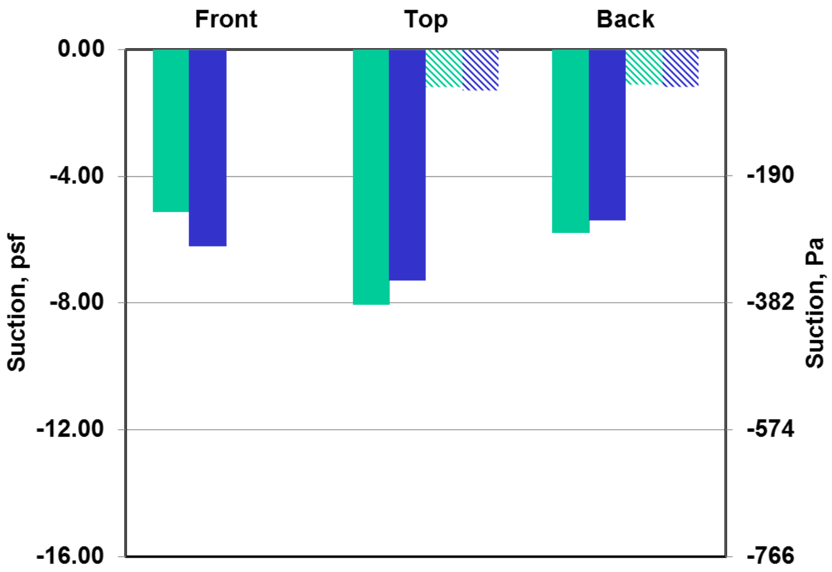

Figure 4.20: Peak (solid colour) and mean (dashed) values of the suction acting on ACC on December 2, 2103, and February 20, 2014

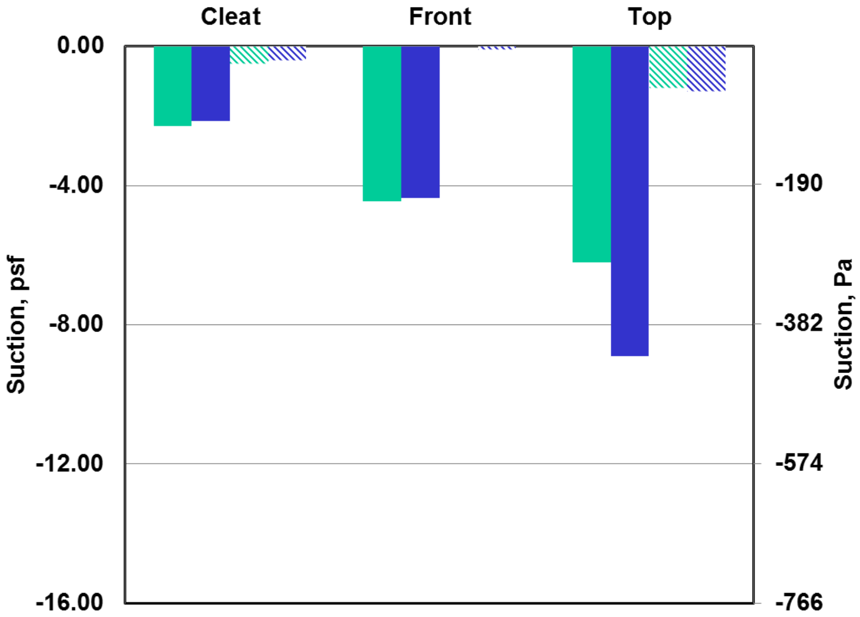

Figure 4.21: Peak (solid colour) and mean (dashed) values of the suction acting on CCC on December 2, 2013, and February 20, 2014

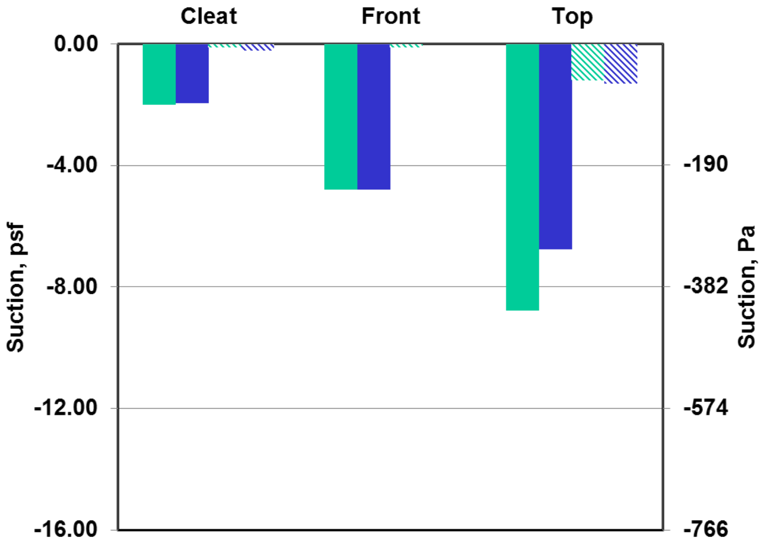

Figure 4.22: Peak (solid colour) and mean (dashed) values of the suction acting on DCC on December 2, 2013, and February 20, 2014

Based on the comparative analysis presented in Section 4.3, the two sets of pressure data show reproducibility. Although the peak suction exhibits differences between the two sets of data, the mean suction for each of the coping faces is very similar. It is observed that the suction is lower in the second data set due to lower wind speeds. The DCC cleat experiences a similar suction pressure to that of the CCC cleat, as shown in Figure 4.12, Figure 4.15, Figure 4.21 and Figure 4.22.

4.4 Effect of Wind Speed

This section examines the effect that wind speed has on the pressure measured on each edge configuration. To isolate the effect of wind speed, only data from days with a West-North-West wind direction (Figure 4.3) was analyzed, resulting in five days of total data collected in the allotted time span.

When observing the effect of wind speed on the ACC, it can be seen that suction on each leg of the configuration increased as wind speed increased, although the rate of suction increase is greater on the top face of the ACC (Figure 4.23). Both the front and back legs of the ACC experienced a similar suction increase as the wind speed increases.

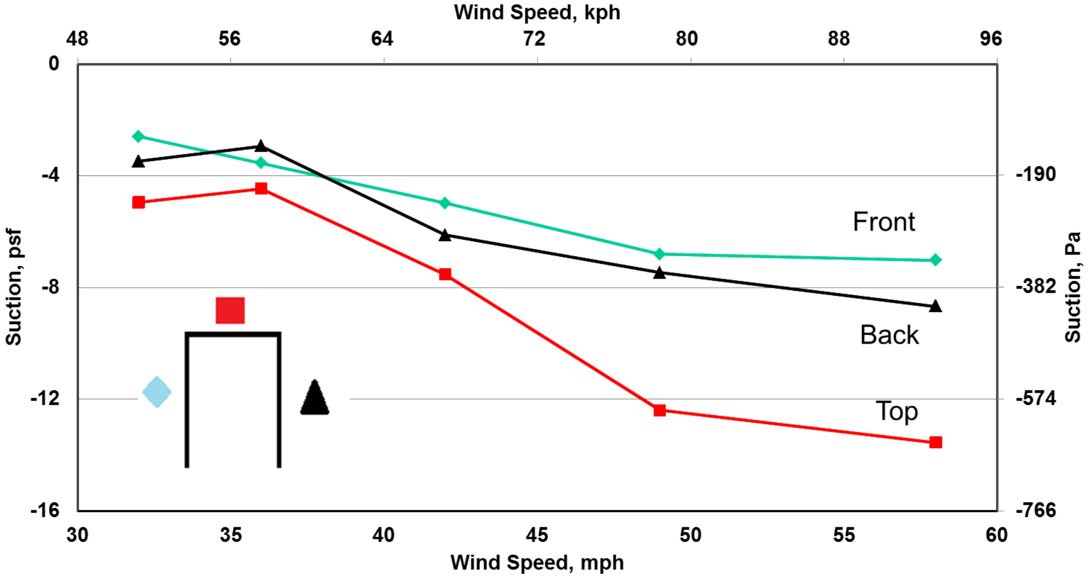

Figure 4.23: Effect of wind speed on ACC under WNW wind direction

The suction measured on the CCC also increases with the wind speed; however, this increase was not as significant as that observed on the ACC (Figure 4.24). The cleat and front legs showed a similar trend, with the suction remaining constant at wind speeds higher than 49 mph. This is most likely due to the cleat extending through the entire configuration. Similar to the ACC, the top face of the CCC experienced the highest suction compared to the other coping legs.

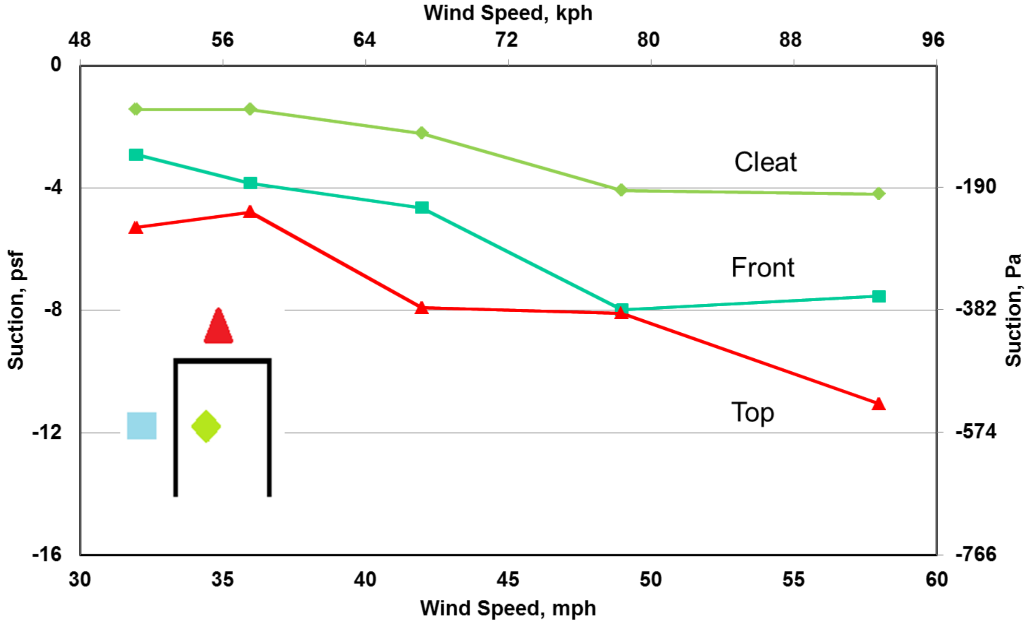

Figure 4.24: Effect of wind speed on CCC under WNW wind direction

The cleat and the coping front leg of the DCC showed a similar trend to the CCC (Figure 4.25). At high wind speeds, the DCC cleat experienced lower suction than the CCC cleat, since the DCC cleat was only placed at mid-span of the edge. The coping top leg suction showed a similar trend to that observed for the ACC.

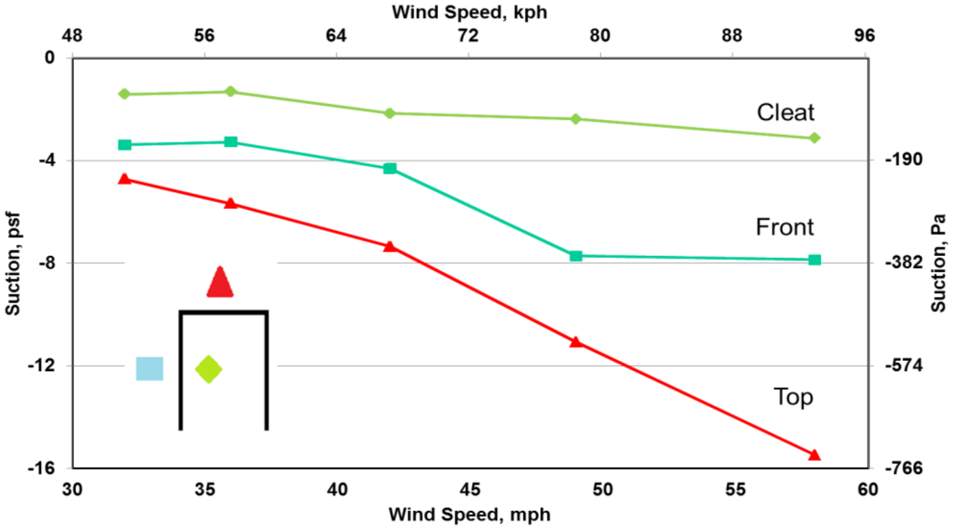

Figure 4.25: Effect of wind speed on DCC under WNW wind direction

4.5 Comparison of Edge Configurations

This section presents a comparison of the suction acting on the different edge configurations installed on the field site. Section 4.5.1 compares the three edge configurations from data recorded on the day with the highest wind speed (November 15, 2013). Section 4.5.2 compares the edge configurations with pressure data recorded with wind blowing in a Westward direction, and Section 4.5.3 compares the edge configurations with pressure data recorded with wind blowing in the West North West direction.

4.5.1 Comparison of Windiest Day

In order to compare the three configurations, the pressure data measured on November 15, 2013 was used since it recorded the highest wind speed. During this day, the wind was blowing from the West North West direction (Figure 4.3).

The minute suction data acting on the front leg for the three configurations was plotted and showed that the peak suction values are very close to each other, with the ACC having a peak suction of -7 psf (-335 Pa), and the CCC and DCC having a peak value of -8 psf (-383 Pa) (Figure 4.26). The mean suction values of the hour data are very close as well, with ACC and DCC having the same value, -0.4 psf (-19 Pa), and the CCC having -0.3 psf (-14 Pa). The edge configuration does not have an impact on the suction acting on the front leg of the corresponding coping (Figure 4.26).

Suction was recorded on the top face of each the configuration copings, with a peak suction value of -11 psf (-527 Pa) acting on the CCC, much less than the -14 psf (-670 Pa) and -15 psf (-718 Pa) acting on the ACC and DCC, respectively (Figure 4.27). Although the hourly-data variation of the suction was different for the three configurations (Figure 4.27), the mean suction values of the ACC, CCC and DCC were close, with a values of -2.2 psf (-105 Pa), -2.3 psf (-110 Pa) and -2.4 psf (-115 Pa), respectively.

Lastly, the suction acting on the cleat for the CCC and DCC configurations was compared (Figure 4.28), both of which displayed close peak suction values of -4 psf (-192 Pa) and -3 psf (-144 Pa), respectively, and mean values of -0.8 psf (-38 Pa) and -0.1 psf (-5 Pa), respectively. In addition, suction fluctuation through the hour was found to be similar for both configurations.

As mentioned in Section 4.3, the range of suction fluctuation observed on the front leg of all configurations was different than that measured on the top face of the tested configurations; however, the range of suction acting on either the front leg or top face was found to be similar among all three configurations. The front face of each configuration experienced similar suction during the representing hour, ranging from -2 psf to -8 psf (-96 to -383 Pa). Nevertheless, the top face was subjected to considerably higher fluctuations, ranging from -4 to -12 psf (-192 to -575 Pa). A comparison of negative pressure acting on the same face for all configurations revealed a similar range, suggesting that different design configurations of roof edges do not affect the wind-induced loads acting on them.

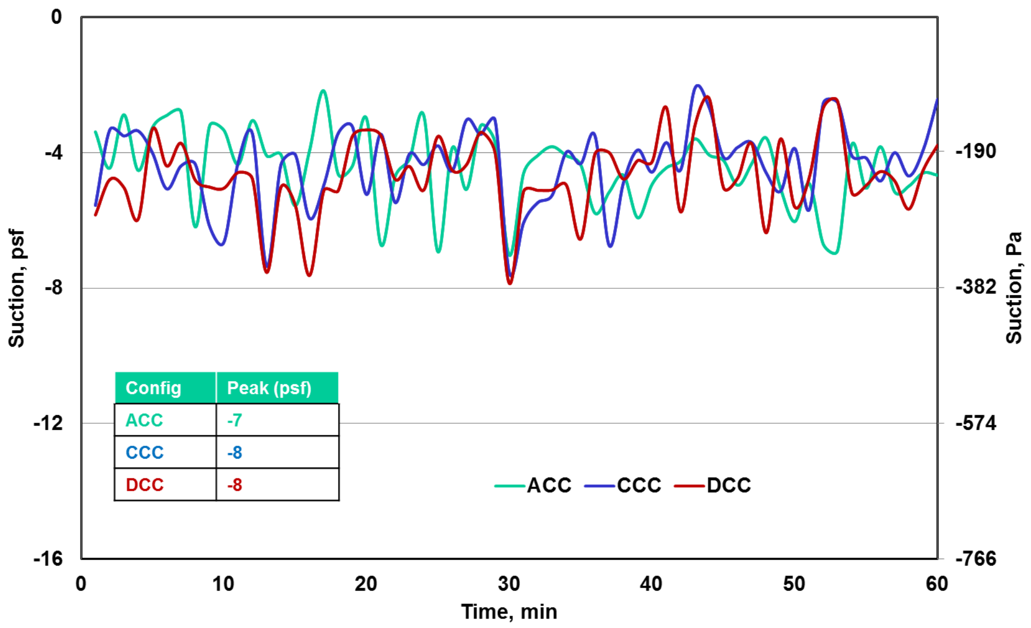

Config	Peak (psf)
ACC	-7
CCC	-8
DCC	-8

Figure 4.26: Configuration comparison of front leg suction on November 15, 2013

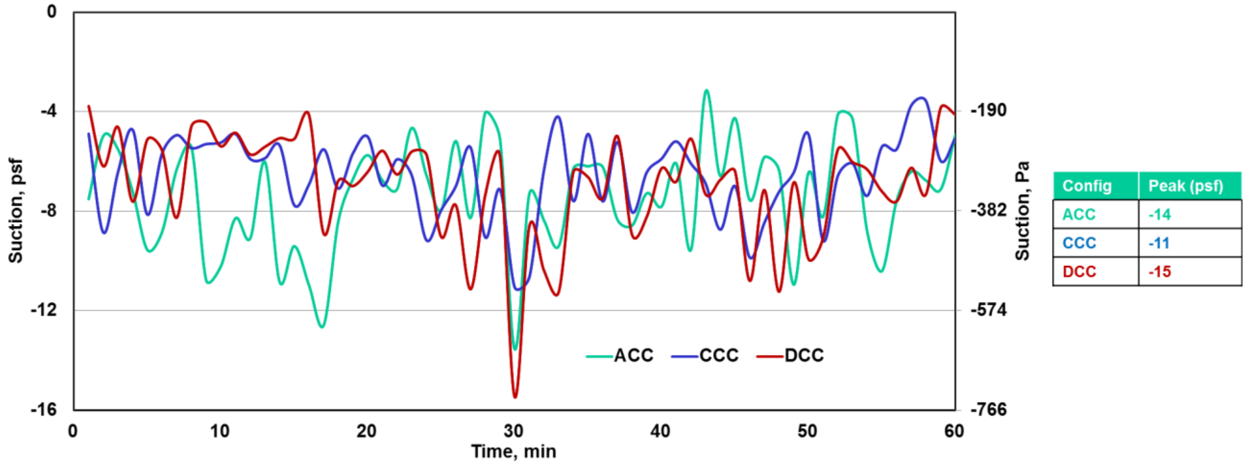

Config	Peak (psf)
ACC	-14
CCC	-11
DCC	-15

Figure 4.27: Configuration comparison of top leg suction on November 15, 2013

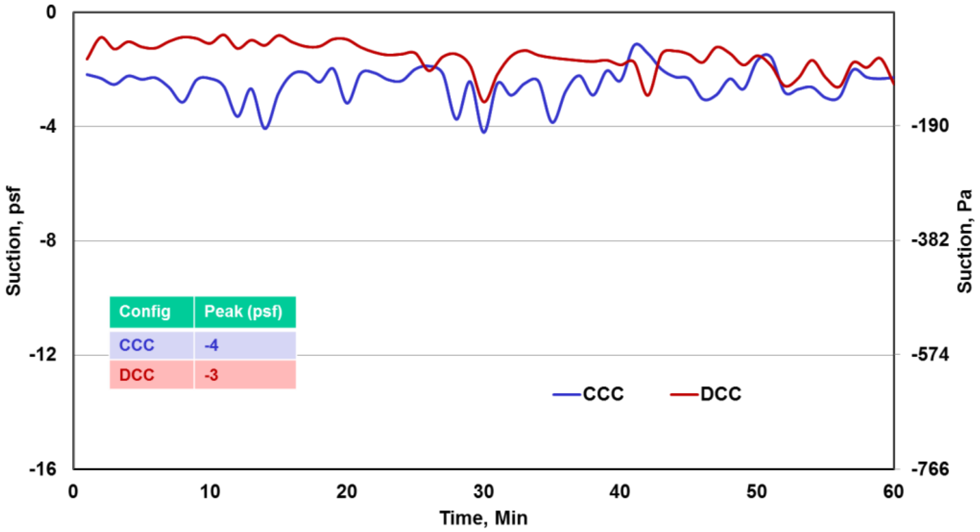

Config	Peak (psf)
CCC	-4
DCC	-3

Figure 4.28: Configuration comparison of cleat suction on Nov 15, 2013

4.5.2 Comparison for West Wind

In this section, the edge configurations are compared with data measured when the wind blew from the West direction, consisting of a total of eight days. Figure 4.29 shows the peak suction acting on the coping front leg for each configuration and each day, with the data arranged from the day with the lowest wind speed (30 mph on April 21, 2014) to the day with the highest wind speed (50 mph on December 18, 2013). It can be seen here that suction increases as peak wind speed increases. November 19, 2013 and April 17, 2014 were two days with identical peak wind speeds but different peak suction values acting on the ACC and CCC, while the peak suction value acting on the DCC were the same for both days.

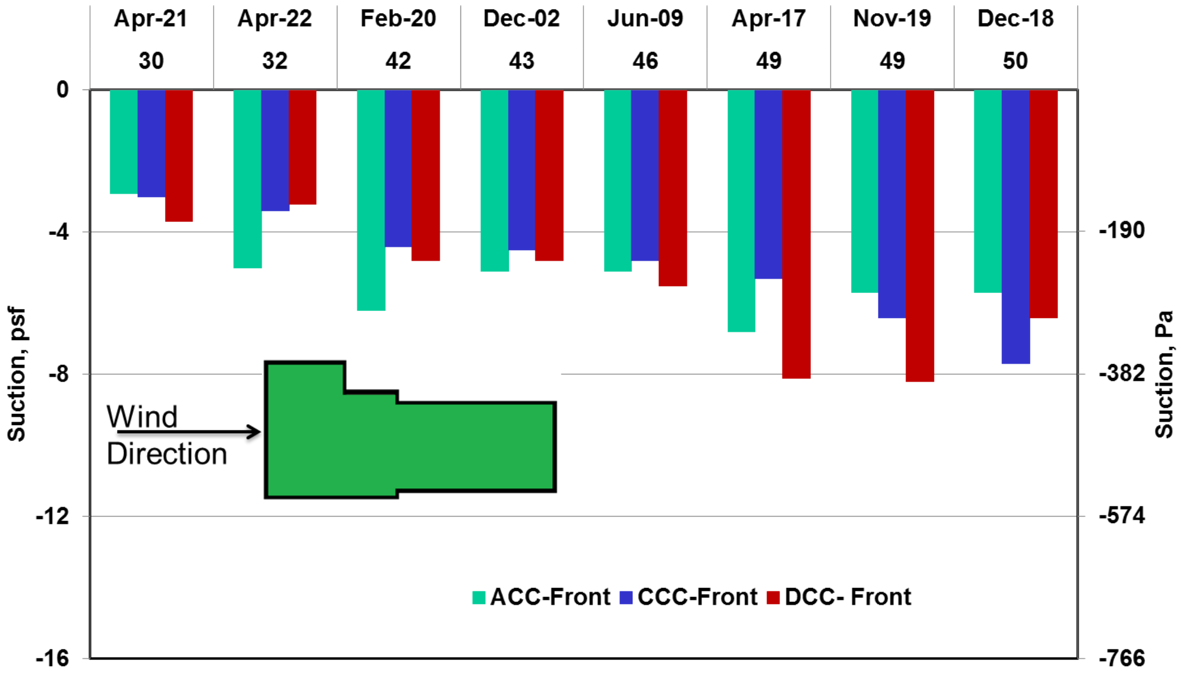

Figure 4.29: Configuration comparison of front leg suction for West wind

The cleat of the CCC and DCC metal edges also experienced positive pressure during the recording period. Positive pressure acted on the inner side of the front leg of the metal edge, and negative pressure on the outer side, resulting in the front leg being subjected to a net outward pressure (Figure 4.30).

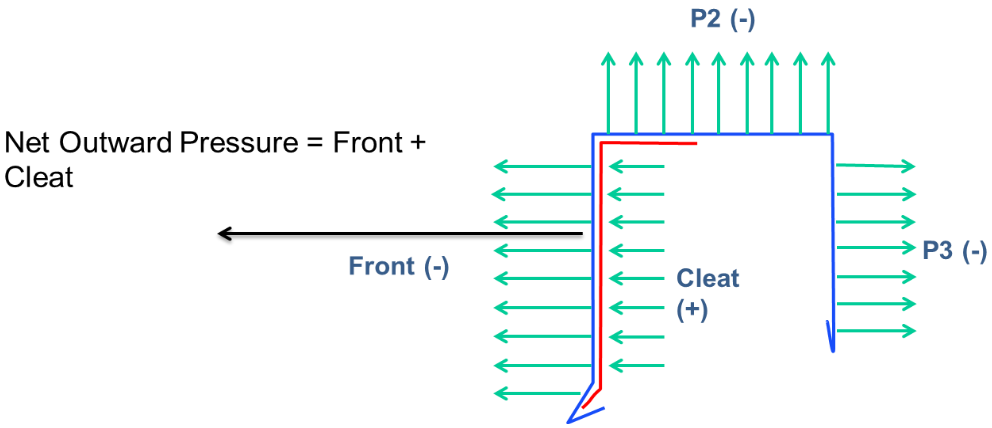

Figure 4.30: Front net outward pressure

A comparison of the net outward suction pressure acting on the front for the CCC and DCC shows that the net suction acting on the DCC is consistently greater than the one acting on the CCC (Figure 4.31). It is also noted that the rate of suction increase with wind speed is greater for the DCC metal edge than the CCC one.

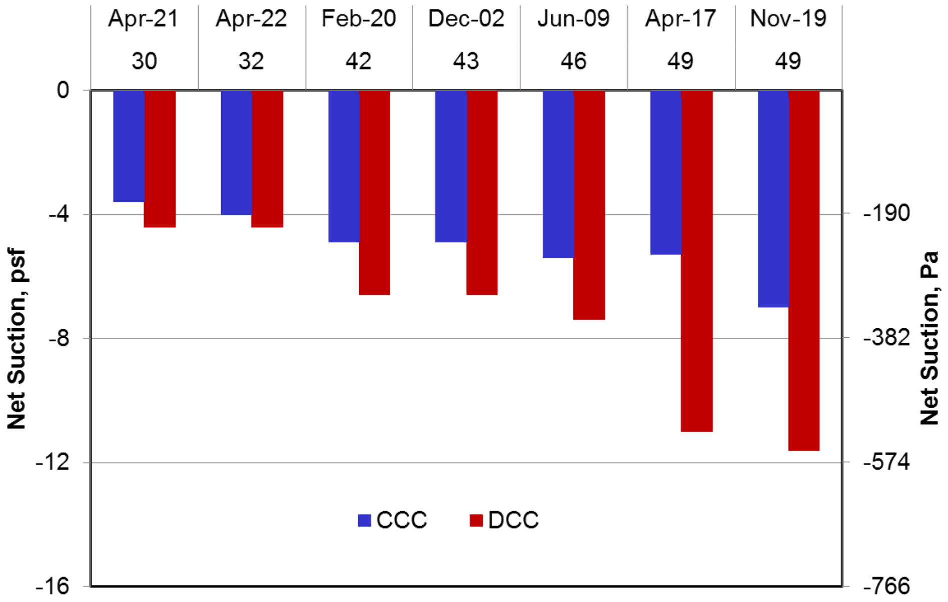

Figure 4.31: Configuration comparison of net outward suction pressure for West wind

Comparing the top face suction for West wind shows that similar to previous findings, suction acting on the top face increases as wind speed increases (Figure 4.32). The suction values recorded on April 17, 2014 and November 19, 2013, both with the same wind speed, showed very different peak suction results. The suction recorded on the DCC on April 17, 2014 had the highest value among all the configurations, and a similar observation was noted for the suction acting on the coping front leg (Figure 4.29). On November 19, 2013, the ACC experienced the highest peak suction on the coping top face. The CCC peak suction value is similar between both days.

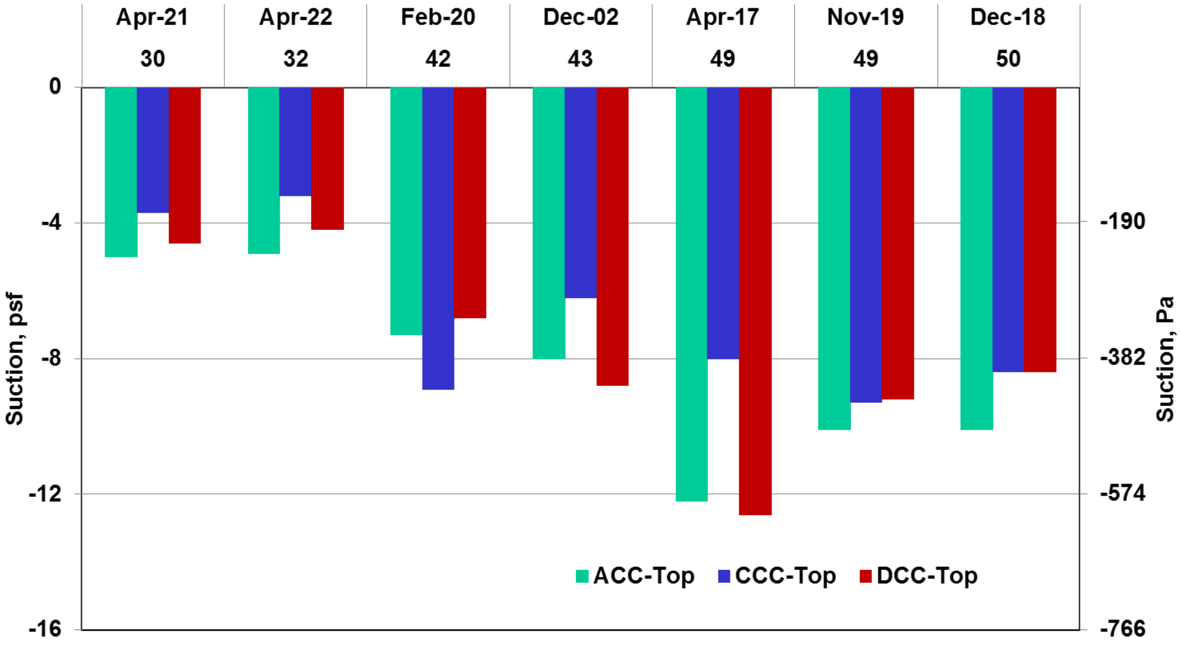

Figure 4.32: Configuration comparison of top face suction for West wind

4.5.3 Comparison for West North West Wind

In this section, the configurations are compared with data taken during days on which the wind was coming from the West North West direction. It was found that the pressure increased as the wind speed increased for all three configurations, with the rate of pressure increase being similar for all the configurations and the CCC experiencing the lowest pressure (Figure 4.33). In addition, it was observed with the positive pressure that, as wind speed increased, suction acting on the front face of the coping also increased (Figure 4.34). At higher wind speeds (greater than 50 mph), this increase leveled off for all configurations. The net outward pressure acting on the front face of the CCC and DCC edges was plotted against wind speed in Figure 4.35. Since the net outward suction is the combination of the positive pressure and suction acting on the front face, it increased with the wind speed. Although the CCC and DCC showed similar trends, the CCC metal edge experienced a lower net outward pressure than the DCC for the same wind speed.

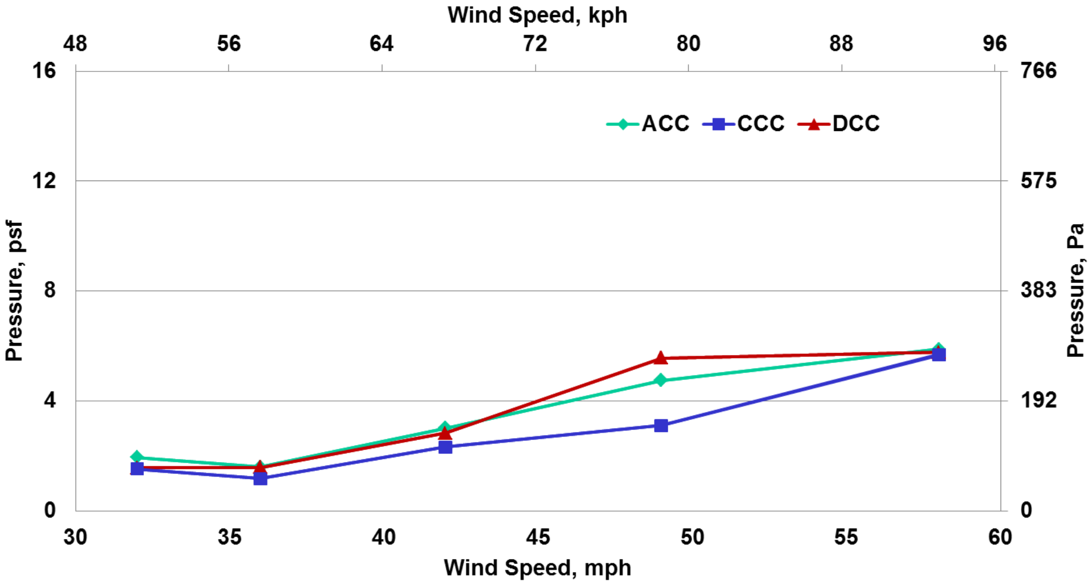

Figure 4.33: Configuration comparison for front leg pressure for West-North-West wind

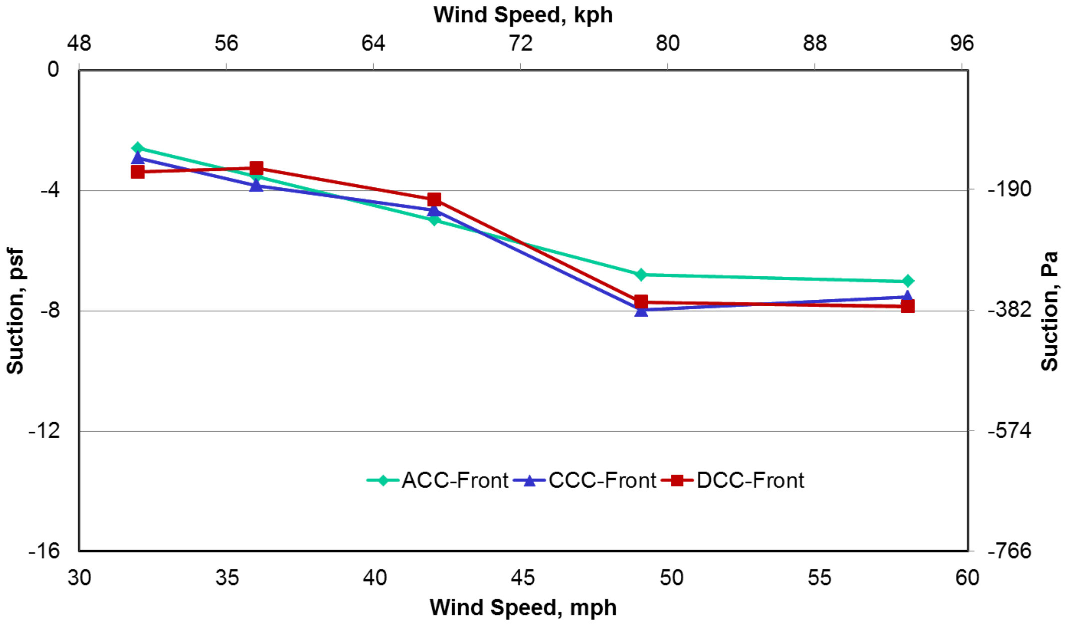

Figure 4.34: Configuration comparison of front leg suction for West-North-West wind

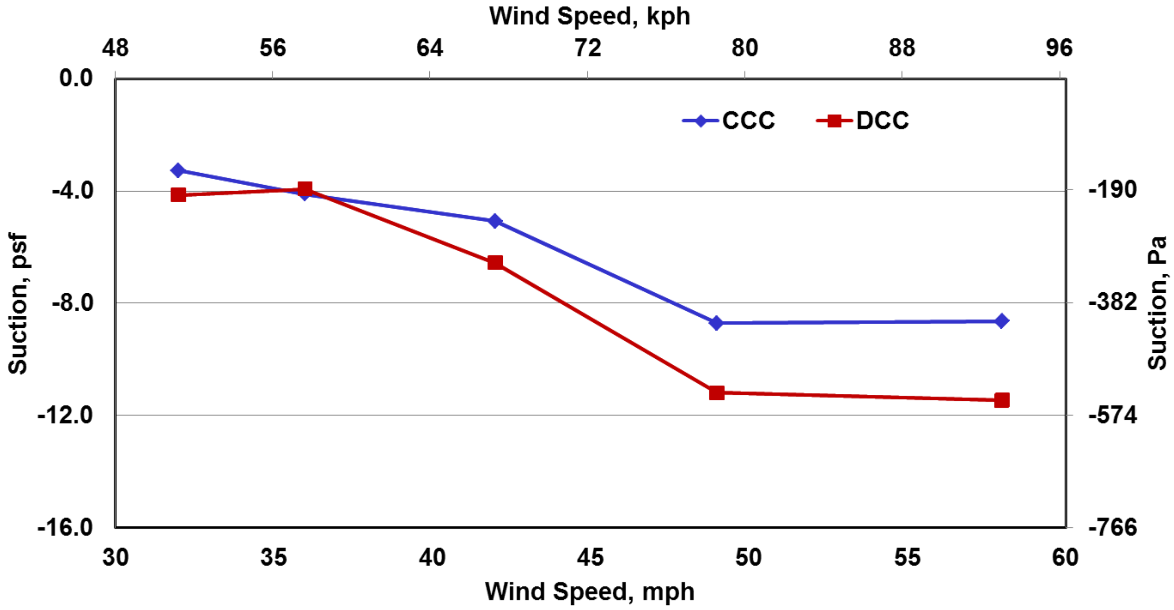

Figure 4.35: Front net outward suction pressure for CCC and DCC

The suction acting on the top of the coping increases with speed for all configurations: however, both the ACC and DCC coping top face experienced a higher suction than the CCC (Figure 4.36).

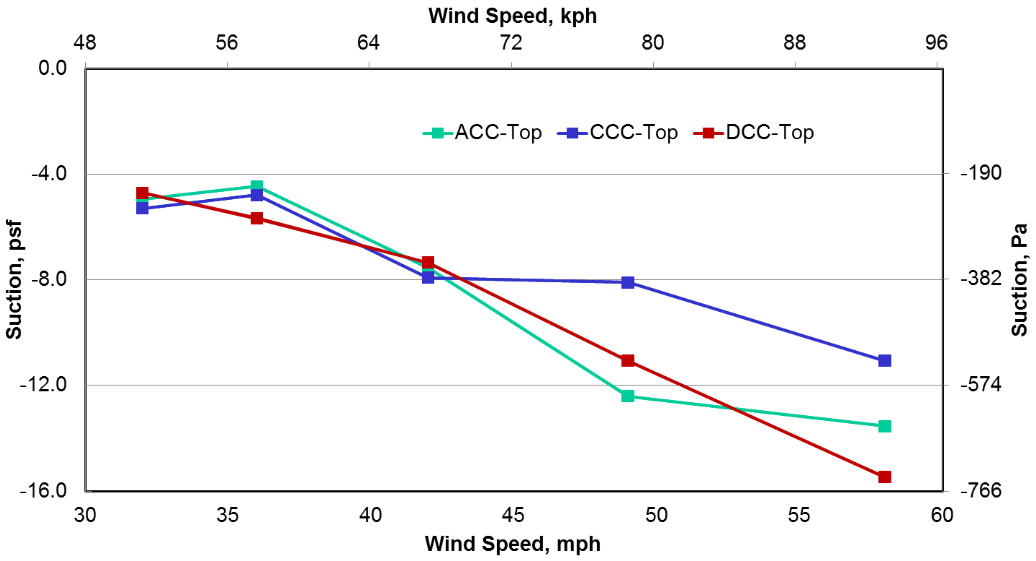

Figure 4.36: Configuration comparison of top face suction for West-North-West wind

4.6 Discussion of Results

By comparing two different sets of data obtained from days with nearly the same peak wind speed and wind direction, it is shown that the pressure data measured is reproducible. Although the peak suction exhibited a few differences, the mean suction for all three faces of the coping was found to be quite similar. It is also observed that the suction is lower in the second data set due to the lower wind speeds. In addition, the DCC cleat experienced similar suction pressures to the CCC cleat.

From the results presented in this chapter, it can be observed that negative pressure or suction acted on each face of the edge configurations, with the top face exhibiting the highest values. Furthermore, although positive pressure is also recorded on the front leg of the coping, the net pressure to which the front face is subjected is negative or outward. These findings show different type of wind-induced loads than what the current wind guidelines state.

Regarding the configuration's sensitivity to wind speed, the results show that the suction acting on all three faces of the coping increases with wind speed for all configurations. The suction acting on the top face of the coping of the CCC was not as high as the DCC or ACC. The combination of the front face suction and the cleat pressure increased the net outward suction acting on the front leg of the CCC and DCC edges. This created a higher pullout force on the fasteners which connected the cleat to the parapet. From this, the coping can disengage from the cleat causing the failure of the roof edge system, resulting in the failure of the entire roof system.

When comparing all configurations, all three showed similar results for the mean suction acting on the front and top faces of the coping. April 17, 2014 and November 13, 2013 exhibited some similarities for the peak suction of the front leg of the coping, but differing results for the top face. However, the net outward suction acting on the coping front leg of the CCC and DCC is very similar for both days, meaning the type of configuration does not affect the magnitude of the wind loads acting on them.

Chapter 5: Data Validation and Codification Comparisons

5.1 Introduction

The results of the field study presented in Chapter 4 highlighted the fact that all faces of the three different edge configurations are subjected to negative pressure or suction, which differs from current industry standard beliefs. This chapter presents comparisons of the data collected at the Canada Post building in Vancouver with previous field studies, namely the Texas Tech and Concordia studies (summarized in Chapter 2). Furthermore, the field results of this study are compared with calculations done according to two current building codes in North America: the NBCC and the ASCE codes, and the ES-1 standard. Finally, a proposal for code modification based on the field observations presented in this thesis is considered at the end of this chapter.

5.2 Texas Tech Comparison

As seen in Section 2.4.1, there were two studies done on the WERFL facility at Texas Tech. These studies are the most common in the relevant literature that investigate wind loads on cladding systems along the roof edge.

A few geometrical differences lie between the Texas Tech WERFL and the Canada Post building in Vancouver. Although the WERFL is a rectangular building with a standard roof edge (Figure 2.8), the Canada Post building consisted of two roofing levels, and the test site of this work is located on the upper roof level of Penthouse 6, with a parapet installed on the roof edge (Figure 3.2). The difference in height between the two buildings is also significant, 13-ft (4.0 m) vs. 58-ft (17.8 m) for the WERFL and the Canada Post building, respectively. The length of the Vancouver site is over double than the WERFL's length, with 98-ft (29.9 m) compared to 45-ft (13.7 m). The only similarity in the dimensions of the two buildings is the width, which is 28-ft (8.5 m) for the Canada Post building and 30-ft (9.1 m) for the WERFL testing facility.

The study conducted by Jiang (1995) looked at four configurations, as discussed in Chapter 2; however, only two configurations, flashing types A and B, are examined here in more detail to compare to the edge configurations used in the present study. Likewise, the data collected by

McDonald et al. (1997) on flashing type A is also used here for comparison purposes. Table 5.1 lists the lengths of each of the edge components for the configurations that have a cleat. Table 5.2 lists the lengths of each of the edge components for configurations that do not have a cleat.

Table 5.1: Dimensions of edge components with cleats in Texas Tech and present study

	Texas Tech Jiang (1995) Flashing A	**Texas Tech McDonald et al (1997)** Flashing A	**Present study** CCC
Front	4 in (101.6 mm)	4 in (101.6 mm)	5 in (127 mm)
Top	4 in (101.6 mm)	4 in (101.6 mm)	9 ½ in (241 mm)
Cleat	3 in (76.2 mm)	3 in (76.2 mm)	5 in (127 mm)

Table 5.2: Dimensions of edge components without cleat in Texas Tech and present study

	Texas Tech Jiang (1995) Flashing B	**Present study** ACC
Front	4 in (101.6 mm)	5 in (127 mm)
Top	4 in (101.6 mm)	9 ½ in (241 mm)

Jiang (1995) presented the mean wind pressure distribution in terms of pressure coefficients on all the metal flashings in his study (Figure 2.12), whereas McDonald et al. (1997) provided the pressure coefficient values for one run of the mean, peak maximum and minimum. In order to compare these studies to the present study results, the pressure measurements collected from the Canada Post building must be converted into pressure coefficient. The pressure coefficients are a dimensionless form of measured pressure. The pressure coefficients are calculated as follows:

$$C_p = \frac{P}{1/2\,\rho V^2} \tag{5.1}$$

where:

C_p is the non-dimensional pressure coefficient,

P is the measured pressure at a particular pressure tap, psf (Pa),

ρ is the mass air density, slug/ft^3 (kg/m^3), and

V is the reference wind speed at the height of the building, ft/sec (m/sec).

The CCC data from November 19, 2013 is used as an example of this conversion. First, the mean wind speed was calculated from the average raw daily hourly data, presented in Appendix B. The average raw data corresponding to the 15 minutes centered at the peak wind speed (Figure 5.1) was used, to correlate with the 15-min wind speed averages used in the Texas Tech studies. The time compression changed the mean wind speed to 26 mph (42 kph). The 15-min averages of the pressure were also obtained for the CCC front and top legs, since the Texas Tech studies had pressure taps on the front and top legs of the metal flashings. The raw data in Appendix B was used to solve for the pressure coefficients for the leggings of the configurations that were being compared. Similar to the wind speed, the mean pressure of the leggings was altered because of the reduction in the time considered (1 hour to 15 minutes). The mean pressure acting on of the front leg and top face was -0.2 psf (-9.6 Pa) and -1.4 psf (-67 Pa), respectively (Figure 5.2 and Figure 5.3).

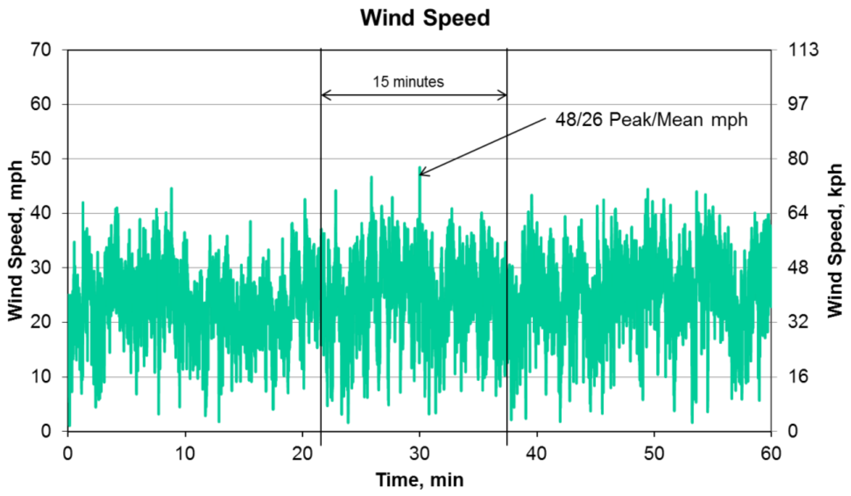

Figure 5.1: November 19, 2013 15-min average wind speed

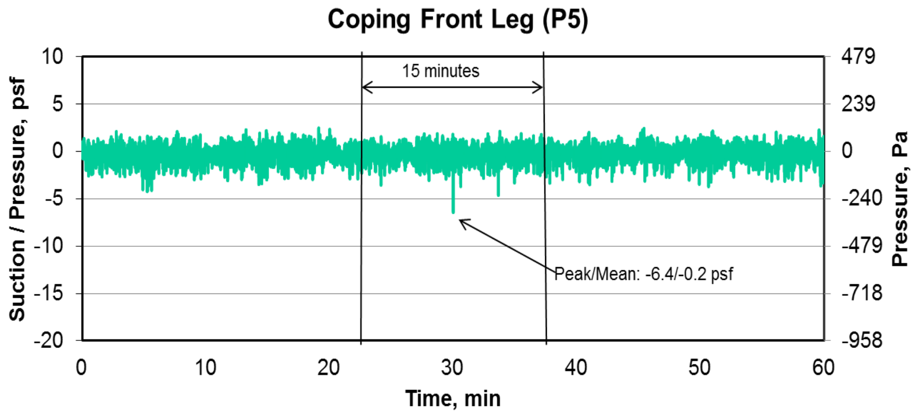

Figure 5.2: November 19, 2013 15-min CCC pressure on front leg

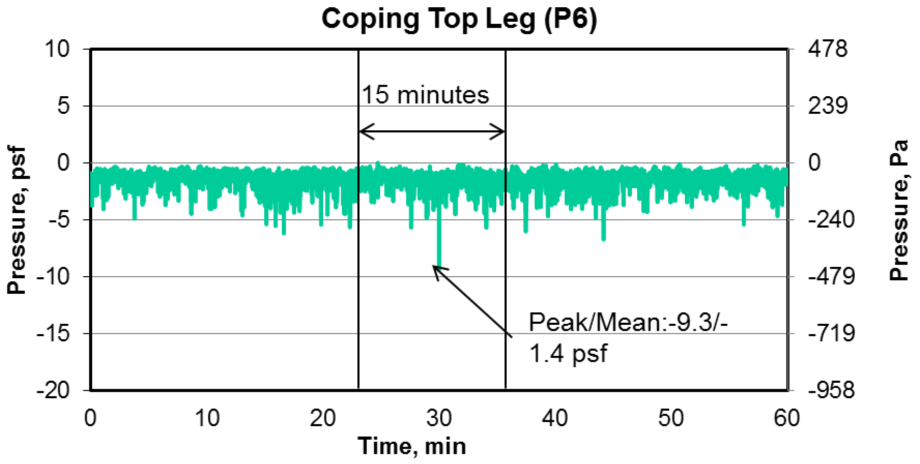

Figure 5.3: November 19, 2013 15-min CCC pressure on top face

The pressure coefficients for the front and top legs of the CCC were calculated using the mean pressure values, shown in Figure 5.2 and Figure 5.3, respectively, using a mass air density of 1.225 Kg/m^3. With Eq. 5.1, the pressure coefficient for the front face of the CCC C_{pf} was calculated as follows:

$$P_f = -0.2 \text{ psf} = -10 \text{ Pa}$$

$$1/2\,\rho V^2 = 82 \text{ Pa}$$

$$C_{pf} = -0.12$$

The pressure coefficient for the top face of the CCC C_{pT} was calculated as follows:

$$P_T = -1.4 \text{ psf} = -67 \text{ Pa}$$

$$1/2\,\rho V^2 = 82 \text{ Pa}$$

$$C_{pT} = -0.82$$

This process was completed for all the days with wind coming from the West direction. These were eight days for the present study that wind is carrying from the west (see Figure 4.29). However, when 15 min mean wind speed is less than 18 mph, April 21, 22 and June 09 are excluded for the comparison. The five data runs that Jiang (1995) used for each flashing in the study had an average mean wind speed above 18 mph (29 kph) (Figure 5.4). The highest suction coefficient was found to occur on February 20, 2014, with a value -0.16 for the CCC front leg and -1.20 for the CCC top face. These values were compared to the mid-section pressure taps of the metal flashings with cleats listed in Table 5.1.

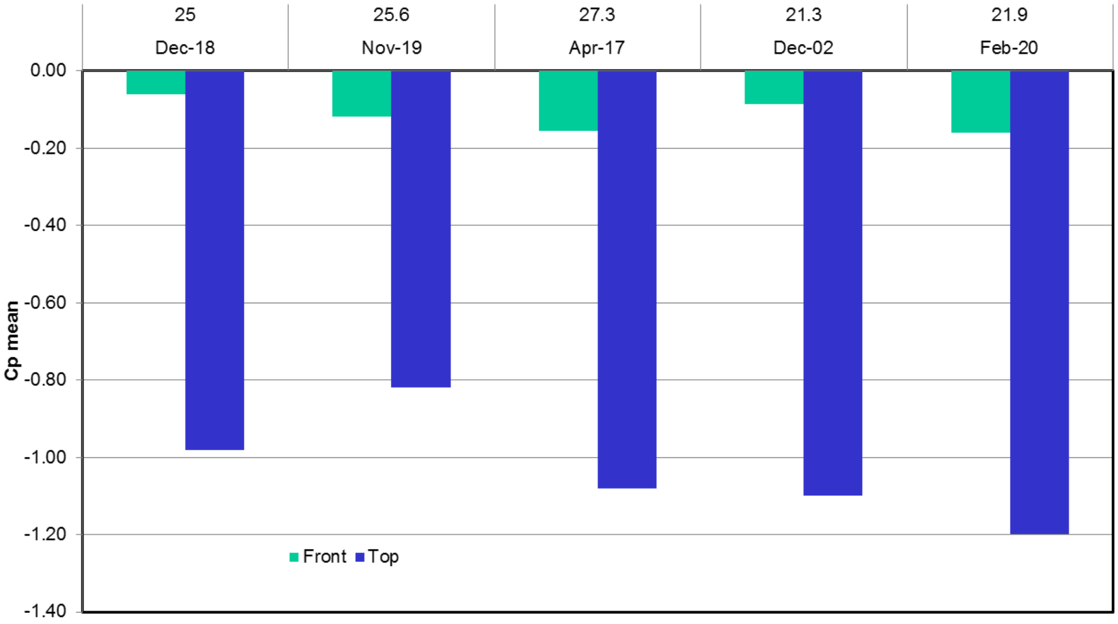

Figure 5.4: Pressure coefficients for CCC front and top faces

Jiang's (1995) comparison of pressure coefficients between flashing "A" and CCC for the metal edge shows that the front legs of the two configurations experience similar suction, with flashing "A" having a value of -0.18 and the CCC having a value of -0.16 (Figure 5.5). Although the edge configurations of the present study have more than twice the width of flashing type "A" top leg, both configurations encounter similar suction on the top face, with flashing "A" having a value of -1.1 and the CCC having a value of -1.2.

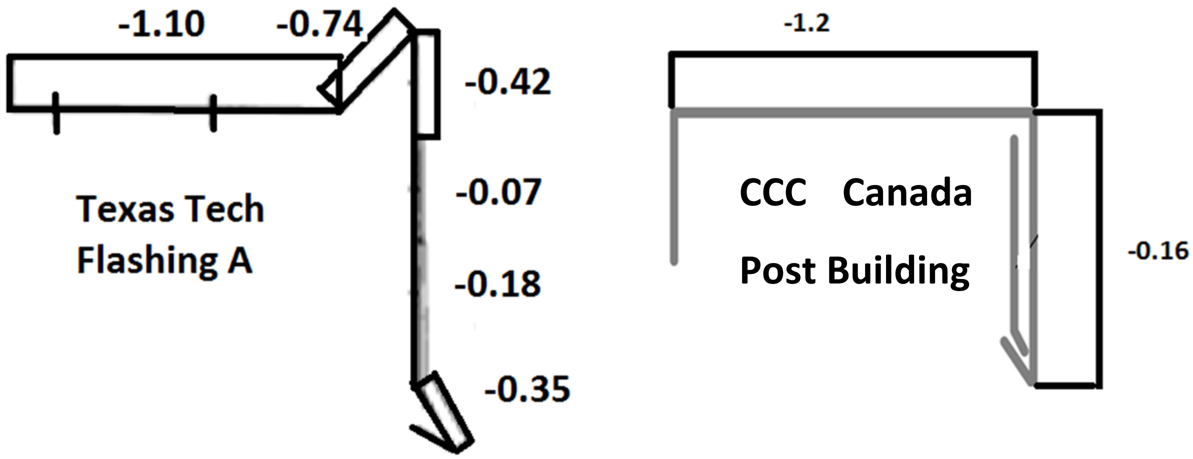

Figure 5.5: Jiang (1995) flashing A vs CCC pressure coefficients

The only data run which was provided by the study conducted by McDonald et al. (1997) was of mean wind speed of 12.8 m/s (28.6 mph), and the wind angle of attack was 74° (windward direction). McDonald's comparison of pressure coefficient profiles for flashing "A" and CCC metal edge shows that the pressure coefficients on the front face are similar in both studies, with McDonald et al. (1997) flashing "A" having a value of -0.14, and the CCC having a value of -0.16 (Figure 5.6). However, a difference between both profiles is observed for the pressure coefficient on the top face, with flashing "A" having a value of -0.92, and the CCC having a value of -1.2.

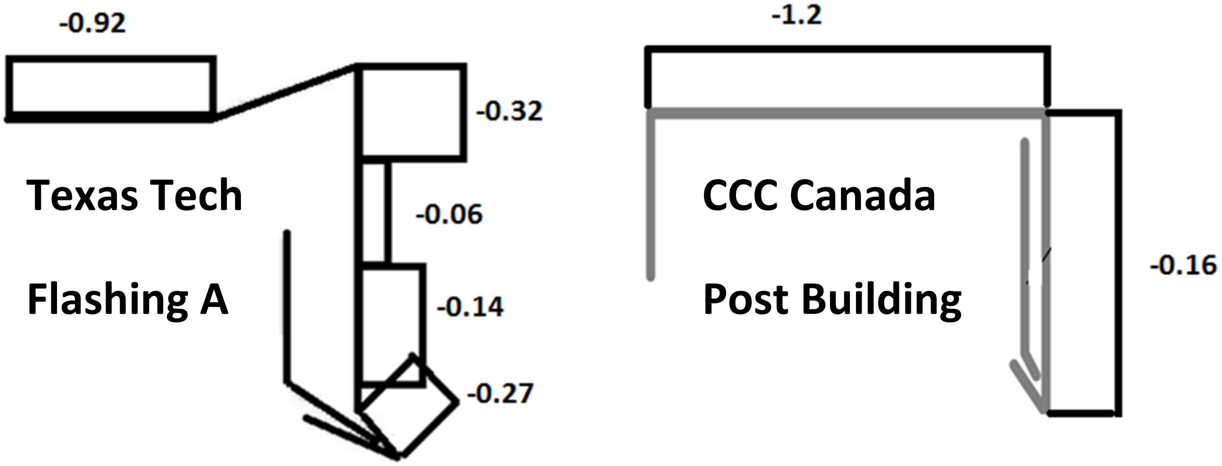

Figure 5.6: McDonald et al (1997) flashing A vs CCC pressure coefficients

The comparison between edge configurations without a cleat was done between flashing “B” from Jiang (1995) and the ACC used in this study (Table 5.2). Pressure coefficients were calculated for the ACC edge in the same manner as the CCC edge and for the same days, as shown in Figure 5.7. The pressure coefficients corresponding to December 2, 2013 (0.25 for the front face and -1.18 for the top face) were compared to the pressure coefficients reported by Jiang (1995).

Figure 5.8 illustrates the pressure coefficient profiles for flashing “B” in Jiang (1995) and ACC in this study. As can be seen in the figure, the top face of both configurations experience quite close suction with a value of -1.08 in Jiang (1995) versus -1.18 in this thesis. However, where flashing “B” experienced a suction of -0.13 on the front face, the ACC edge had a pressure coefficient of 0.25 on the front leg of the configuration. This is likely due to the ACC location on the parapet of Penthouse 6 which hangs a few millimetres out from the parapet, compared to flashing “B” which sits close to the roof edge. In the former, the space between the parapet and the metal edge had increased wind flow, causing less suction on the front leg of the coping.

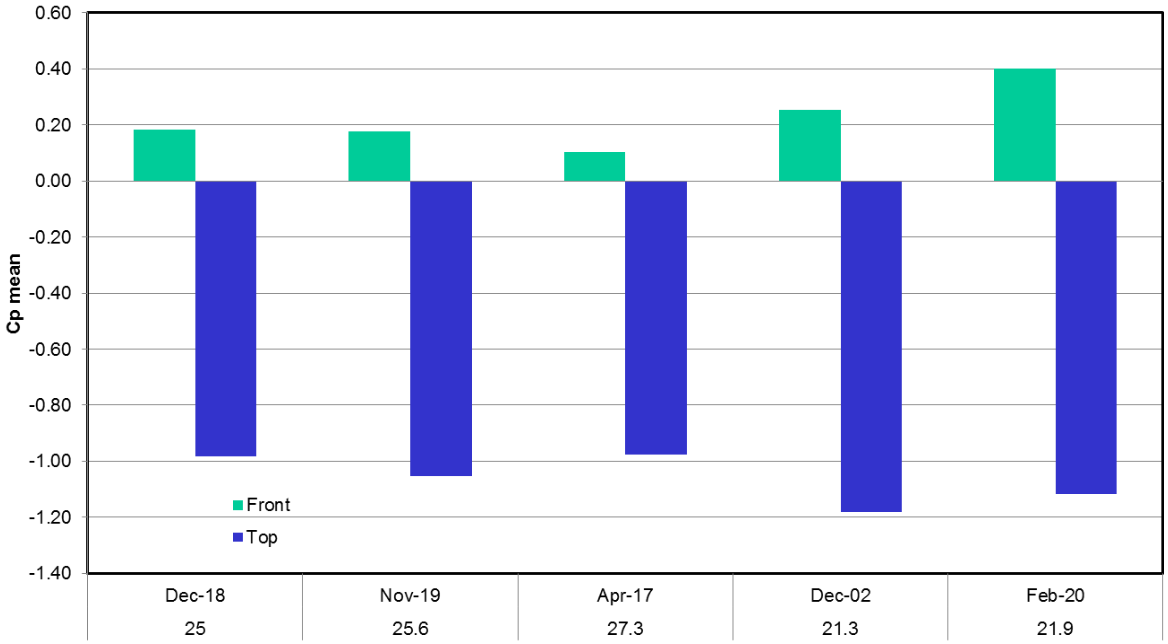

Figure 5.7: Pressure coefficients for ACC front and top faces

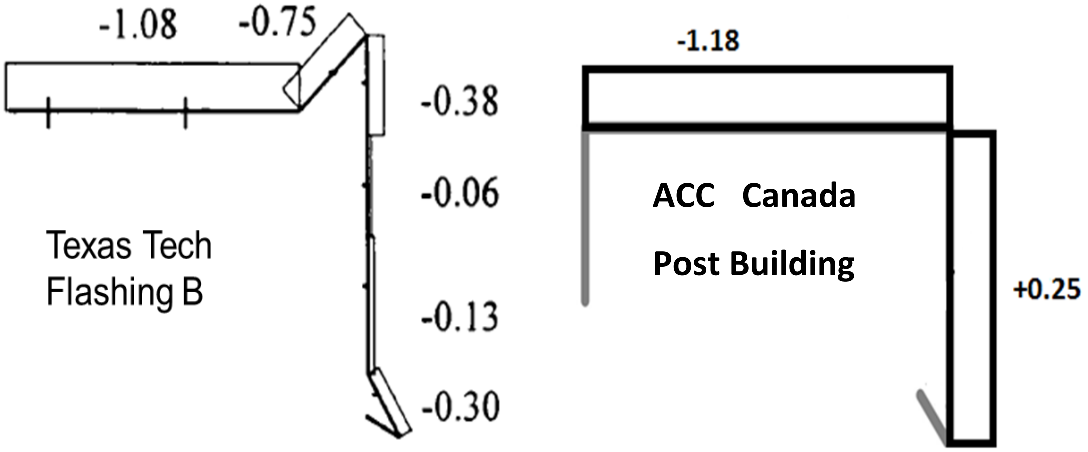

Figure 5.8: Jiang (1995) Flashing B vs ACC pressure coefficients

5.3 Concordia Comparison

In this section the results obtained in the study conducted by Bedair (2009) at Concordia University in Montreal, summarized in Section 2.4.2, are compared to the results obtained in the present study. It should be noted that the study done by Bedair (2009) observed the effect of wind on roof parapets and reported pressure coefficients on parapets without metal flashings. The comparison between the two studies is accomplished with the goal of investigating the effect of metal edges on wind-induced loads acting on a parapet.

The parapet dimensions used by Bedair (2009) were 0.5-ft (0.16 m) in width and 1.6-ft (0.5 m) in height, similar to the parapet dimensions of Penthouse 6 in the Canada Post building of 9.5-in (0.24 m) in width and 2-ft (0.61 m) in height. Therefore, the parapet dimensions are not considerably different between the two field studies.

As stated in Section 2.4.2, Bedair (2009) installed pressure taps on the front and back faces (exterior and interior, respectively) of the parapet (Figure 2.18). However, the peak suction coefficient obtained by Bedair (2009) could not be used for this comparison since the corresponding wind direction was parallel to the parapet. In contrast, the data collected in this study corresponds to windward wind (±45°). Therefore, the pressure coefficients reported by Bedair (2009) that are within the angle of attack range of 0° to 45° are used for comparison purposes. These pressure coefficients were calculated with a wind speed average over 10 minutes. Consequently, the pressure coefficients resulting from the present study results were calculated with the 10-minute wind speed average, following a similar process to that used in Section 5.2 (Figure 5.1, Figure 5.2 and Figure 5.3). The peak pressure coefficients were calculated using this wind speed average for all of the configurations and all the days. Of all the days, February 21, 2014 showed the highest peak suction coefficients on the configuration front legs with values of -13.42, -7.92 and -9.12 for the ACC, CCC and DCC, respectively. The peak suction coefficient found on the exterior face of the Concordia site was -1.1 at an angle of attack of 45°. The peak values resulting from this study were very high compared to Bedair's (2009) observations. The interior face of the parapet showed a peak suction coefficient of -3 at an angle of attack of 45° (Figure 2.18). Only the back leg of the ACC could be compared to this value, with a corresponding peak suction coefficient of -9.22, still showing a significant difference between these two values.

The higher suction coefficients obtained from the data collected in this study may be a result of the Canada Post building being taller than the Concordia's field site. The building geometry is also an important factor to take into consideration, since the Canada Post building has a lower roof (38-ft high), affecting the wind flow around the building.

5.4 Comparison of the measured data with ASCE Specifications

Measured data from the present study has been compared with the current ASCE 7-10 specifications. Note that there is no specify provisions in the ASCE for the wind load design of roof edge metals. However, as presented in Section 2.3.2, there are design procedures and coefficients listed for parapet design. Using those procedures and equations, numerical calculations are shown in Appendix E by assuming the following parameters:

- Wind directionality factor K_d = 1.0 for components and cladding (Table 26.6-1 of ASCE 7-10), since the calculated pressure is not used in conjunction to other load combinations (eg dead and live loads). When used with other load combinations, K_d = 0.85;

- Velocity pressure exposure coefficient K_z = 1.13, for open exposure at the building height of 60-ft (Table 30.3-1 of ASCE 7-10);
- Topographic factor K_{zt} = 1.0 (Section 26.8.2. of ASCE 7-10);
- Interior pressure coefficient = ±0.55 (Table 26.11-1 of ASCE 7-10) for a partially enclosed building, since there are some openings in Penthouse 6 of the Canada Post building;
- External pressure coefficient for the windward side of the parapet can be found in Figure 30.4-2A of the ASCE 7-10, which is for enclosed and partially-enclosed buildings; and,
- Effective wind area = 1-ft^2 (0.09 m^2). Although the pressure taps at the field site cover less area than this area, 1-ft^2 (0.09 m^2), this is the lowest value given by Figure 30.4-2A of ASCE 7-10.

Velocity pressures are determined at the roof height of the experiment site and for different wind conditions of 30, 40, 50, 60, 70, 80 and 90 mph (48.3, 64.4, 80.5, 96.6, 112.7, 128.7 and 144.8 kph). Calculated velocity pressures are also shown in Appendix E.

The measured data are converted to a 50-year return period to have comparable data set with the values calculated according to ASCE 7-10. The 50-year period conversion equation for the wind load pressure is given by Peterka and Shahid (1998) as:

$$P_{50} = \frac{P_d}{0.36 + 0.1\ln(12)} \tag{5.2}$$

where:

P_{50} is the 50-year wind pressure, kPa (psf), and

P_d is the present wind pressure, kPa (psf).

Figure 5.9 plots the measured wind pressure and suctions acting on the front face of the three edge configurations, shown as CCC –P, DCC-P and ACC-P for pressures and CCC-S, DCC-S and ACC-S for suctions. The design pressure obtained from ASCE 7-10 is shown as ASCE-P. The ASCE only specifies pressure on the windward face of the parapet, while measured field data of all configurations experienced both pressure and suction. The following observations are noted from the comparison:

- Irrespective of the configurations, a maximum of 10 psf (479 Pa) pressures was measured, whereas the suction was doubled.
- Irrespective of the wind speed, the measured pressures are lower than ASCE specifications.

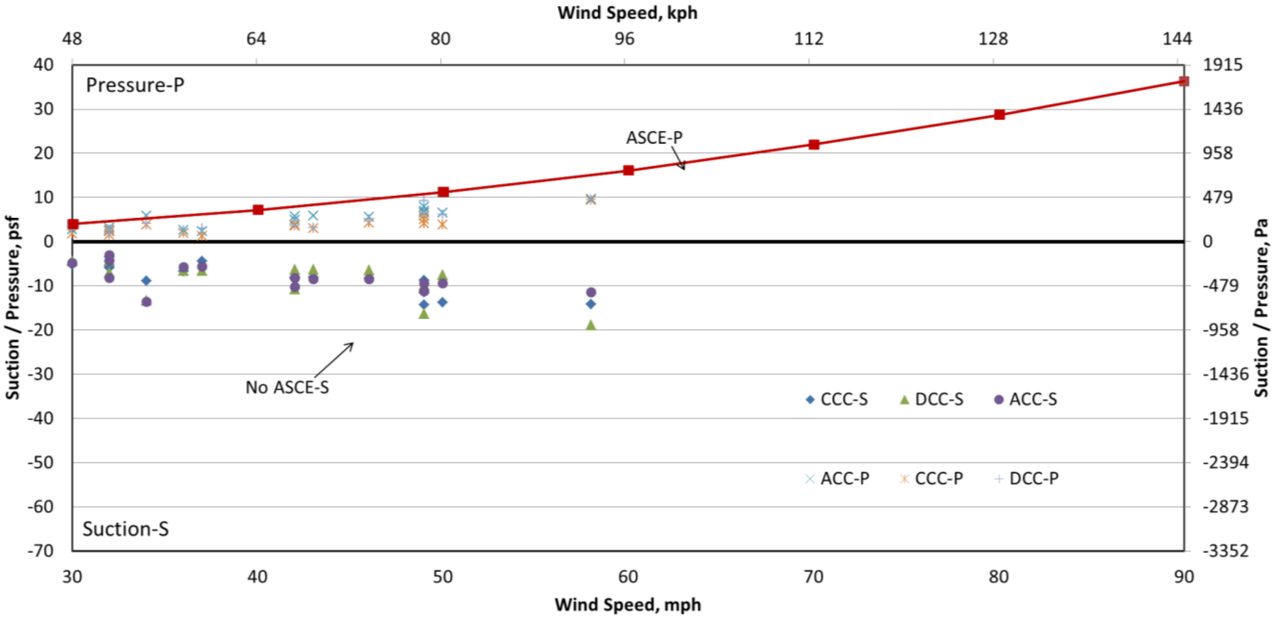

Figure 5.9: Comparison of the ASCE Windward Parapet specification to the measured data on front legs (FL) for all configurations

Following a similar process, the measured suctions acting on the top surface of the edge configurations are compared with the ASCE. It is noted that no specific provisions exist in the ASCE 7-10 standard for roof edge metal design. Moreover, there is no design loads specified for the top surface of a parapet. Because of this, the measured suction acting on the top surface of the edges is compared in Figure 5.10 to the ASCE roof pressure data. The field data presented in Figure 5.10 has been converted to a 50-year return period according to Eq. 5.2. The findings show that the top face of the edge configurations experiences suction, whereas ASCE 7-10 does not specify any wind load acting on the top of the parapet. It is important that the ASCE 7-10 be revised to account for these pressures. The following observations are also noted from the comparison:

- All configurations show increase of suction as the wind speed increases. However, there are no defined differences among the three configurations.
- Irrespective of the wind speed, the measured suctions on the top face of the edges are lower than the ASCE specifications for roof pressure.
- Irrespective of the wind speed, the measured pressure on the top face of all configurations is always negative (i.e., suction or puling upwards).

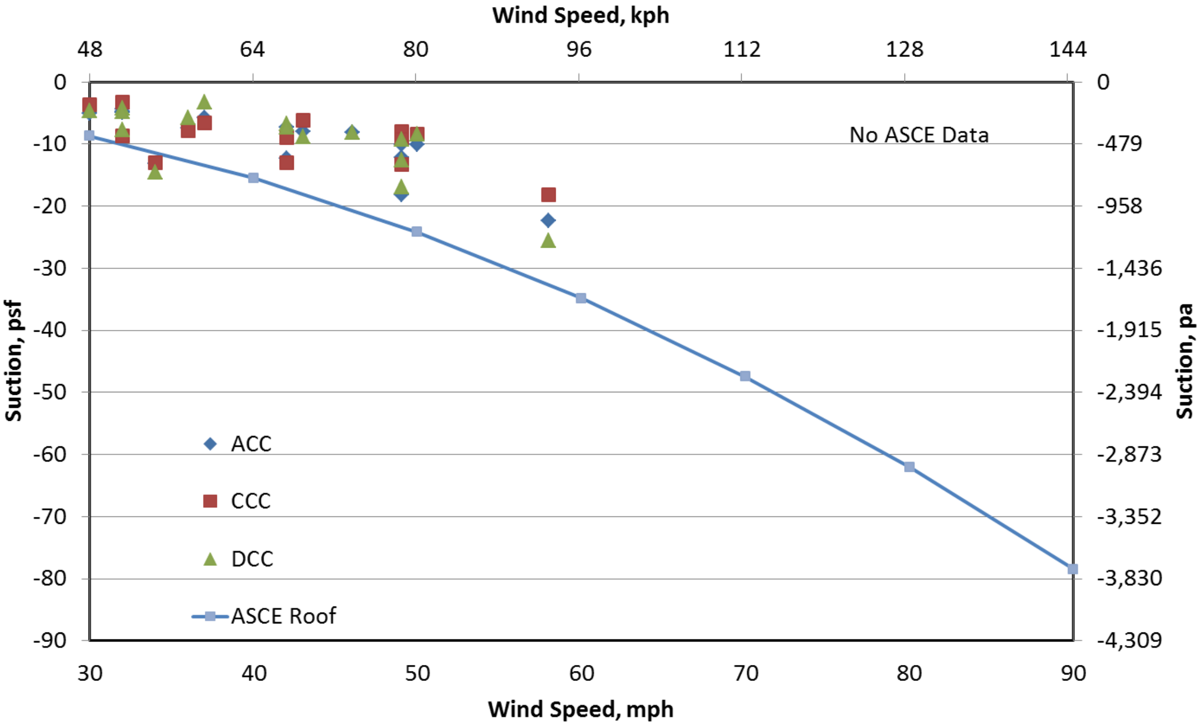

Figure 5.10: Comparison of the ASCE Roof specification to the measured data on the top legs (TL) for all configurations

5.5 ES-1 Standard Comparison

The pressure data collected during this study is compared here to the edge system wind design load as given in Section 4.2 of the ES-1 standard. The ES-1 standard, as stated in Section 2.3.1, is the only existing standard for design and testing of metal roofs edges. In order to compare with the present study results, the roof edge design pressure, *P*, is calculated according to the following equation:

$$P = 2.0 \times q_{fz} \times GC_p \times I \tag{5.3}$$

where:

2.0 = Design safety actor (ES-1, 2011);

q_{fz} = Field of roof pressure at height *z* in feet (ES-1, 2011);

GC_p = External pressure coefficient (Table 2 in ES-1, 2011); and,

I = Importance factor (Table A1 in ES-1, 2011).

The parameters of the present field study are used to calculate the roof edge design pressure according to Eq. 5.3. First, the wind load parameters of the Canada Post building are determined to calculate the field of roof pressure, q_{fz}. The building height, *z*, is 60 ft (18.3 m). The wind speed considered ranges from 30-90 mph (48-144 kph). Since the building is located near an airport, it is surrounded by open terrain; therefore, the applicable exposure category is C. The occupancy category for the Canada Post building, according to Table A1 from the ES-1 standard, is Category II with an importance factor I = 1.0.

The ES-1 standard calculates the field of roof pressure q_{fz} for components and cladding from Eq. 6-22 ($z \leq 60$ ft) or Eq. 6-23 ($z > 60$ ft) of the ASCE 7-05 standard, i.e.,

$$q_{fz} = q_h \times \left(GC_{p,roof} - GC_{pi} \right) \tag{5.4}$$

where:

q_h = velocity pressure evaluated at mean roof height *h*;

$GC_{p,roof}$ = external pressure coefficient for the field of roof. For *h* = 60 ft, $GC_{p,roof}$ = -1.0 from Figure 6-11B of the ASCE 7-05 standard;

GC_{pi} = internal pressure coefficient. This value is ±0.55 for a partially enclosed building (Figure 6-5 in ASCE 7-05) like the Canada Post building field site. GC_{pi} = +0.55 is used for worst case pressure.

Therefore, the field of roof pressure q_{fz} for the field site of this study is given by:

$$q_{fz} = q_h \times (-1.0 - 0.55) = -1.55 \times q_h \tag{5.5}$$

The velocity pressure evaluated at mean roof height q_h is the same as in Section 5.4 and the procedures, equations and numerical calculations are shown in Appendix E.

Using Eqs. 5.5 and 2.2a, the velocity pressure at mean roof height q_h and the field of roof pressure q_{fz} for wind speeds ranging from 30 to 90 mph (48-144 kph) are tabulated in Table 5.3.

Table 5.3: Field of roof pressure q_{fz} according to ES-1 for recorded wind speed range

Wind speed V, mph (kph)	**Field of roof pressure q_{fz}, psf (kPa)**
30	-4.0 (-0.19)
40	-7.2 (-0.34)
50	-11.2 (-0.53)
60	-16.1 (-0.77)
70	-22.0 (-1.05)
80	-28.7 (-1.37)
90	-36.3 (-1.74)

The external pressure coefficient GC_p for partially enclosed buildings to be used in Eq. 5.3 is taken from Table C-A2 in the ES-1 standard. These values are reproduced here in Table 5.4:

Table 5.4: External pressure coefficient GC_p for partially enclosed buildings with $z \leq 60$ ft

Type of loading	**Edge location**	**GC_p**
Horizontal (acting outward)	Perimeter	-0.95
	Corner	-1.13
Vertical (acting upward)	Perimeter	-1.52
	Corner	-2.16

Finally, the roof edge design pressure P is calculated from Eq. 5.3. In order to have comparable data with the pressure data measured in the field, design safety factor of 2.0 is not used in the equation. The resulting values corresponding to wind speeds ranging from 30 to 90 mph (48 to 114 kph) are listed in Table 5.5.

Table 5.5: Horizontal and vertical roof edge design pressures P according to ES-1

Wind speed V, mph (kph)	Horizontal, psf (kPa)		Vertical, psf (kPa)	
	Perimeter	Corner	Perimeter	Corner
30	-3.8 (-0.18)	-6.1 (-0.29)	-4.6 (-0.22)	-8.7 (-0.42)
40	-6.8 (-0.33)	-10.9 (-0.52)	-8.1 (-0.39)	-15.5 (-0.74)
50	-10.6 (-0.51)	-17.0 (-0.81)	-12.7 (-0.61)	-24.2 (-1.16)
60	-15.3 (-0.73)	-24.5 (-1.17)	-18.2 (-0.87)	-34.9 (-1.67)
70	-20.9 (-1.00)	-33.4 (-1.60)	-24.8(-1.19)	-47.5 (-2.27)
80	-27.3 (-1.31)	-43.6 (-2.09)	-32.4 (-1.55)	-62.0 (-2.97)
90	-34.5 (-1.65)	-55.2 (-2.64)	-41.0 (-1.96)	-78.4 (-3.75)

Figure 5.11 shows the pressure data recorded on the top leg of all configurations after being converted to a 50-year return period according to Eq. 5.2. Also shown in the figure are the vertical design pressures calculated according to the ES-1 standard for edges located in the corner. It is noted that the suction values calculated according to ES-1 are slightly higher than those recorded in the field. Figure 5.12 displays the pressure and suction recorded on the site, after conversion to a 50-year return period, with the ES-1 horizontal pressure acting on the edge front. It is seen in the figure that the ES-1 horizontal design pressure is negative (i.e. acting outwards) and similar in nature and magnitude to that measured in the field.

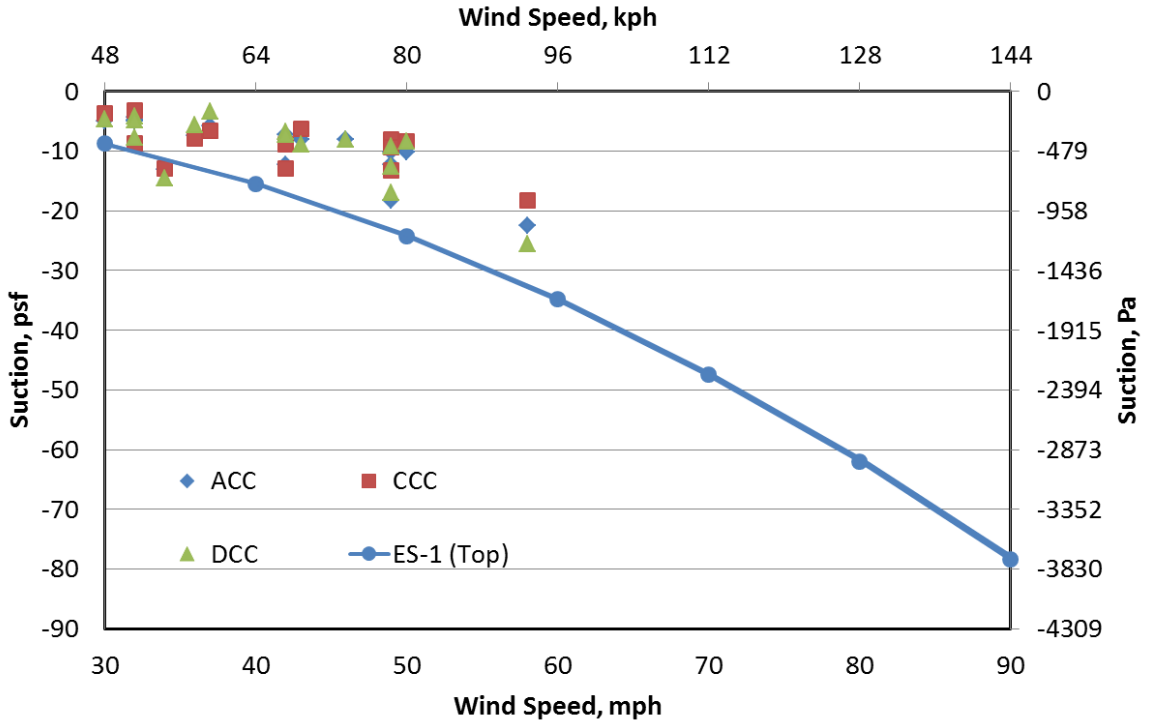

Figure 5.11: Field suction results on the top leg vs ES-1 vertical pressure on corner edge

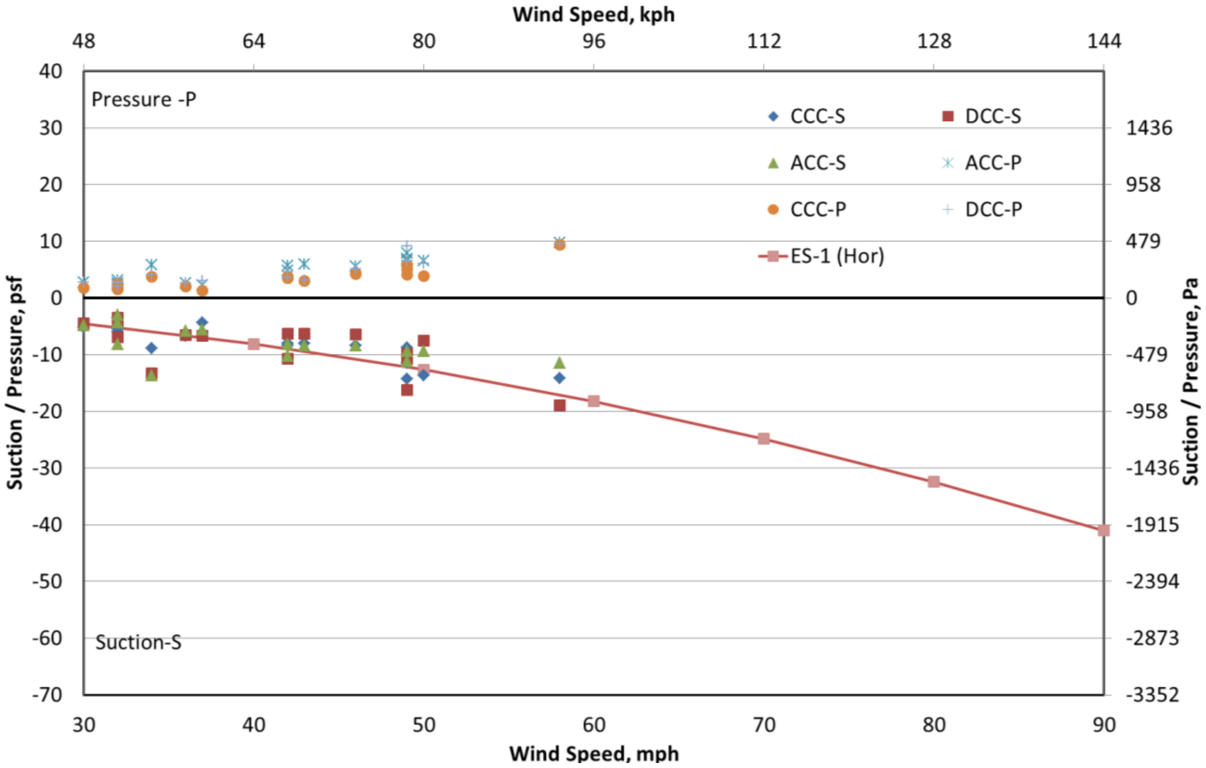

Figure 5.12: Field suction results on the front (FL) and back legs (BL) of all configurations compared to the ES-1 horizontal pressure and to the ASCE07-10 front-leg pressure

5.6 Comparison with the NBCC

In order to compare these findings with the NBCC (2010), the NBCC was used to calculate the wind loads along the roof edge of the Canada Post building, using the Wind-RCI. The Wind–RCI calculator, originally based on the NBCC (2005) and published by Baskaran and Smith (2005), is an online tool that implements the NBCC six-step procedure for calculating wind loads on claddings and roof coverings (Baskaran et al., 2008). In 2010, Wind-RCI was updated with the latest NBCC (2010). To use Wind-RCI, the user provides information regarding the building location, geometry, exposure, openings and the importance category of the building. Appendix F shows snapshots of the different screens used to calculate the wind loads for the Canada Post building, and they are described in the following:

1. Screen 1: Building location. The building is in the province of British Columbia, city of Vancouver Region, Richmond. This information is used to get the 50-year wind speed.
2. Screen 2: Building geometry. This is a low-rise building with a height of 60-ft (17.8 m), width of 28-ft (8.5 m) and length of 98-ft (29.9 m).
3. Screen 3: Building exposure. The building is in open terrain.
4. Screen 4: Building openings. Category 1 was chosen since the building has little openings.
5. Screen 5: Importance category. Since the building is a postal building, it has a normal importance.

Based on the inputted information, Wind-RCI creates a report with the summary of the data. It shows the calculated values in a table with the wind loads on the different roof zones, i.e., roof edge and corner (see Appendix F).

The calculations were done for a low-rise building with a height less than 60-ft (20 m).The wind load for the corner was determined as -61 psf (-2.9 kPa), the wind load for the edge was -40 psf (-1.9 kPa), and the wind load for the field roof was -27 psf (-1.3 kPa). Calculations were also done for a high-rise building with a height greater than 60-ft (20 m) to have the option of using the parapet in the calculations. The snapshot of the report made by Wind-RCI can be found in Appendix F. The report states that for a 70-ft (21.3 m) tall building with the same dimensions as the Canada Post building, the wind load for the corner is -55 psf (-2.6 kPa), for the edge is -41 psf (-2.0 kPa), and for the roof field is -27 psf (-1.3 kPa). In order to compare the field results recorded at the Canada Post building to the wind loads calculated by the Wind-RCI, the pressure must therefore be converted to a 50-year return pressure as well (Eq. 5.2).

Since the present study results are from metal flashings on a parapet, it is difficult to compare these results to the Wind-RCI calculations, since the NBCC (2010) does not provide the option of having a parapet on a low-rise building with a height less than 60-ft (20 m). However, the converted results are compared to the corner of the roof, since that represents the worst case scenario. After converting the results from Chapter 4 into the 50-year return period, the top face of DCC on November 15, 2013 had the highest value of -25.5 psf (-1.22 KPa). The other configurations highest recorded values were both from the top face, with ACC having a value of -22.4 psf (-1.07 KPa) and CCC having a value of -18.2 psf (-0.87 KPa). Figure 5.13 illustrates the highest wind pressures calculated from the NBCC (2010) for both building heights (low rise and high rise) and the highest values for the configurations in the present study. As it can be seen from the figure, the suction acting on the top face of all configurations is approximately more than half of the roof corner value for a high-rise building calculated according to Wind-RCI.

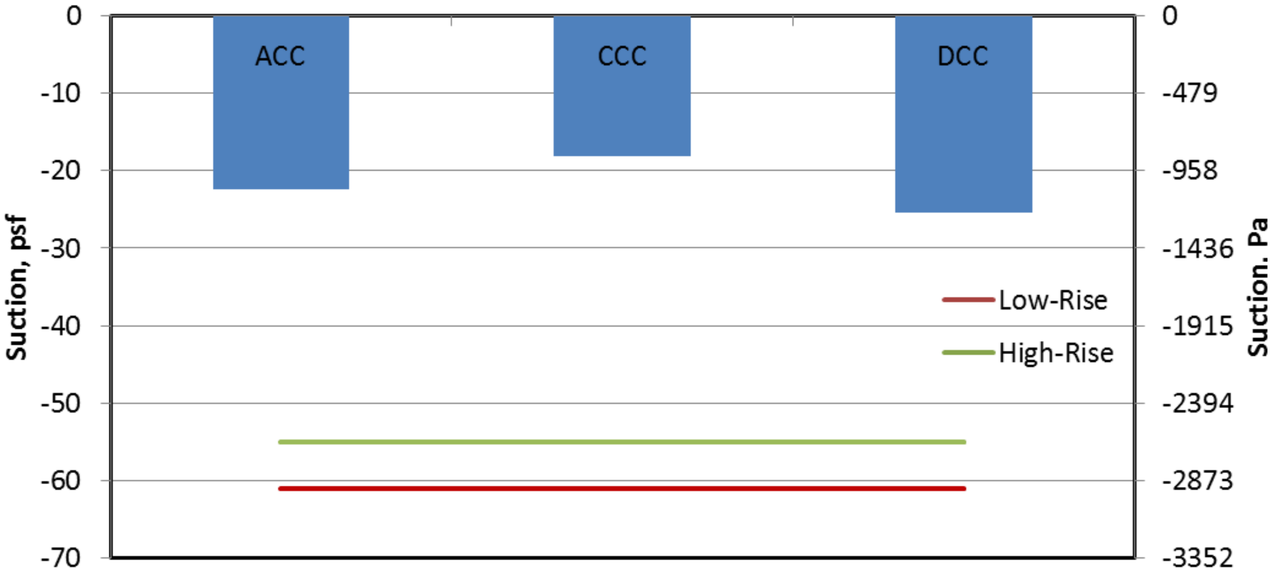

Figure 5.13: Comparison of NBCC (2010) with measured wind pressures

As of now, there are no specifications for wind loads acting on metal flashings on parapets by the NBCC (2010), which should be taken into account (Figure 5.13). It is clearly seen through the Wind-RCI that the NBCC (2010) does not take into account wind loads on parapets, regardless of whether or not they have metal flashing. The NBCC (2010) only considers wind loads acting on the roof (not on the parapet) of tall buildings with parapets, with heights above 60-ft (20 m).

5.7 Codification Proposal

Based on the findings in the present study, the NBCC and ASCE building codes can be updated for the 2020 edition, since they do not adequately account for the actual wind loads acting on the metal edges of a building. The results presented in Chapter 4 have shown that the front and top faces of the metal edge experience negative pressure along their surfaces, further validated in this chapter with investigations conducted by Jiang (1995) and McDonald et al. (1997). The prescription of wind loads acting on metal edges on roof parapets should be modified so that metal edges are designed for negative pressure or suction on all faces of the edge, as proposed in Figure 5.14. The highest suction observed for all configurations consistently acts on the top face of the metal edge. Furthermore, the values for this suction are of lower magnitude than those observed in roofs by Stathopoulos et al. (1999). This was also observed when comparing the suctions measured on the top surface of all configurations against the prescribed ASCE roof suction. The suggested change to the codes is therefore simple; for conservatism, the design wind loads prescribed for the roof should be applied to all the faces of the metal edges. A formal code change proposal for the NBCC (2020) is included in Appendix G

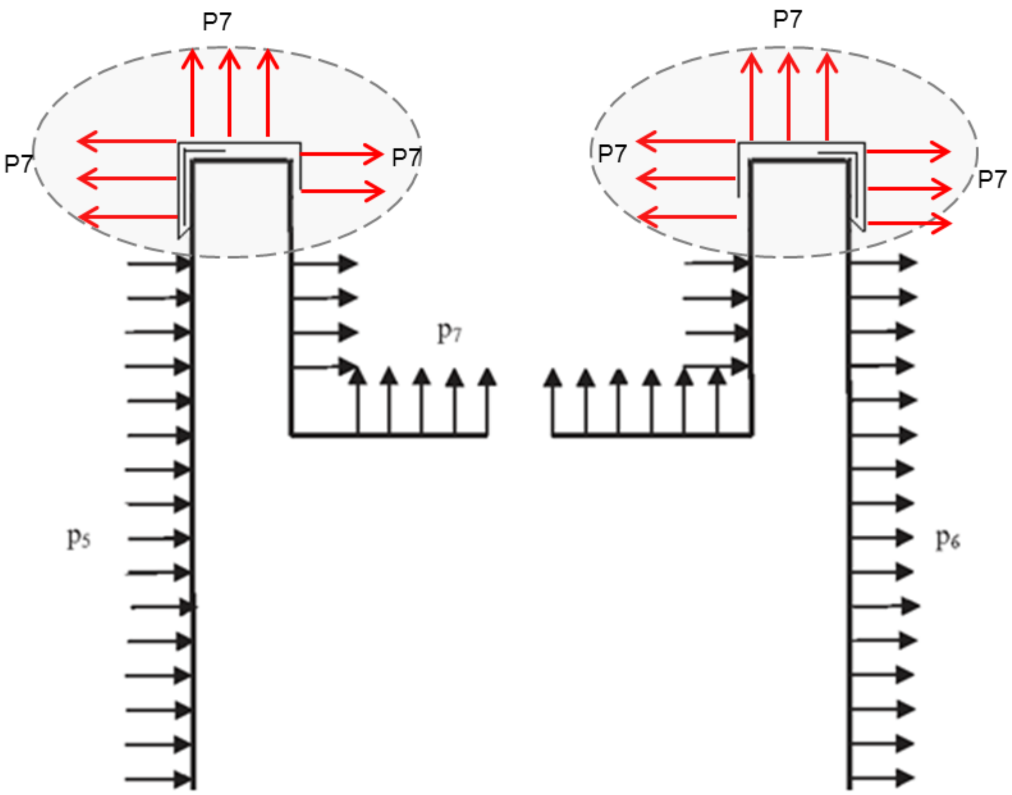

Figure 5.14: Proposed change to building codes

5.8 Summary

This chapter has presented comparisons of the field data recorded at the Canada Post building with the field studies conducted at Texas Tech and Concordia universities as well as with calculations according to the building codes in Canada and the U.S.

Two field studies at Texas Tech, which observed wind-induced loads on metal edge flashings along the roof edge, were compared with the present study. The Canada Post building had metal edge flashings on parapets, which affects the wind flow along the roof edge. The metal flashing in the present study was compared to similar flashings tested by Jiang (1995) and McDonald et al. (1997). The CCC edge was compared to flashings with cleats and showed a similar suction coefficient on the top and front faces to that reported in the Texas Tech studies, whereas the ACC was compared to flashings without cleats and showed that the top face was similar to flashing "B" in the Texas Tech studies. However, the ACC front leg experienced pressure instead of suction as reported by Jiang (1995), most likely due to the design of the ACC, which sits a few millimetres further away from the parapet (Chapter 3). Moreover, the building height and geometry in the studies being compared are different from each other.

The Concordia studies investigated the wind loads acting on the corner of a roof edge with parapets and the pressure experienced on the parapets. The difference in dimensions between the Loyola field site and the Canada Post building is likely the reason the results are vastly different. The peak suction coefficients of the Canada Post field study were much larger than the peak suction coefficients reported by Bedair (2009).

At present, the ASCE 7-10 specifies wind pressure and suction acting on the front and back of a parapet, respectively. ASCE 7-10 has no specific provisions for the wind load design of roof edge metal. However, the findings from the field study showed that the front face of all edge configurations experienced suction and the ASCE 7-10 does not specify any negative wind pressure on the front face of the parapet. Furthermore, the ASCE 7-10 showed no pressure or suction on the top face of the parapet, and the field data showed that top face of the edge configurations experienced suction and it was usually the highest wind-induced load on the metal edges.

The ES-1 standard specifies procedures for the wind design and testing of roof metal edges. By comparing ES-1 design specifications to the measured pressure data in the field site, it is observed that the design wind pressures calculated according to the ES-1 standard are similar in nature and magnitude to those recorded on the top and front legs of the metal edges installed in the field. Both sets of pressure are negative (i.e., acting outward from the edge). Whereas the field suction values acting on the front leg of the edges were of similar magnitude to those calculated by ES-1, the field suction values of the top surface of the edges were slightly lower than those calculated by the ES-1.

The comparison of the field study results with the NBCC (2010) highlights the lack of specifications or wind design guidelines in the Canadian building code for metal edges on parapets in low-rise buildings.

Chapter 6: Conclusions and Future Recommendations

6.1 Conclusions

The present study documented the analysis of in-situ wind-induced loads acting on roof edge systems. The field experiment measured wind-induced loads on a number of commonly used roof edge systems. A complete comparison of the wind-induced loads acting along the roof edge was presented. The study also included a detailed review of the current code load provisions for roof edges and parapets. The following summarizes the contributions of the current thesis:

1. The study presented the results of wind-induced pressure acting on the ACC, CCC and DCC configurations. The investigation revealed that all three faces of the edge configuration experience negative pressure or suction, with the top face being subjected to the highest suction. The front leg of the coping records positive pressure; however, the net pressure acting on the front face is negative. The front legs of the CCC and DCC have a higher net outward suction acting on them from the combination of the front face suction and the cleat pressure. The type of configuration though does not affect the magnitude of the wind loads acting on them.
2. The methodology used to analyze the data is a five-step process that involves: (i) collecting 100 samples per second to get 6,000 data points per minute; (ii) identifying the peak pressure/suction value and corresponding time for each day; (iii) extracting the 30-minute raw data before and after the reference time; (iv) reducing the sampling rate from 100 Hz to 10 Hz to produce the daily-hour data; and, (v) calculating the pressure, suction and mean for the hourly data.
3. The comparison of the present study to the one done at Concordia University to investigate the effect of metal edges on wind-induced loads acting on a parapet showed that there was a large difference between the two studies' peak suction coefficients. This could be a result of the Canada Post building being taller than the Concordia's field site.

4. A comparison of the present study with field studies conducted at Texas Tech was presented. Both studies observed wind-induced loads on metal edge flashings along the roof edge. However, the present study included parapets which affect the wind flow along the roof edge. The CCC edge was compared to flashing with cleats in the Texas Tech study, whereas the ACC was compared to flashings without cleats. The CCC showed a similar suction coefficient on the front and top faces to that of the reported Texas Tech studies. The ACC showed that the top face was similar to the compared flashing, but the front face experienced pressure instead of suction as reported by Jiang (1995).
5. The present study results were compared to the current ASCE code for wind loads on roof edges. The ASCE 7-10 specifies wind pressure and suction acting on the front and back of a parapet, respectively. The present study showed that the front face of all configurations experienced suction. The ASCE 7-10 shows no pressure or suction on the top face of the parapet; however, the field study revealed that the top face on all the edge configurations experienced suction, this being regularly the highest wind-induced load on the metal edges.
6. The comparison of the present study to the NBCC (2010) shows the lack of specifications or wind-design guidelines in the Canadian building code for metal edges on parapets in low-rise buildings.

6.2 Recommendations for Future Research

The following includes possibilities to expand the research contribution to field monitoring of wind-induced loads on metal flashings:

1. In Chapter 3, the range of the angle of wind attack was ±45° from the windward direction. It is recommended that the angle of attack range be increased to investigate wind-induced loads parallel to the metal flashings. This would provide a clearer understanding of the type of wind-induced loads acting on the roof edge configurations.
2. In Chapter 4, it was concluded that the top face of all the configurations experienced suction. For future field monitoring, it is suggested to install a pressure tap on the roof of the building to measure the wind up-lift pressure acting on it, in order to

compare it to the suction acting on the top face of the metal edge and find out which wind-induced load is higher.

3. The Canada Post building was built with a low level roof, whose roof edge was not instrumented with pressure taps. It is recommended that pressure taps are installed on the lower-level roof edge in order to compare wind-induced loads acting on metal flashings located at different heights.
4. The front face of all the configurations experience both positive and negative pressure. For future monitoring, it is advised to install pressure taps along the wall below the roof edge systems, in order to determine when the wind-induced loads go from positive to negative pressure.

References

ASCE7-10. (2010). “Minimum Design Loads for Buildings and Other Structures.” *American Society of Civil Engineers (ASCE),* Reston, VA.

ASCE7-05. (2005). “Minimum Design Loads for Buildings and Other Structures.” *American Society of Civil Engineers (ASCE),* Reston, VA.

Alassafin, W. (2013). “Wind Uplift Resistance of Roof Edge Components.” Master’s Thesis, University of Ottawa, Canada.

Alassafin, W., Baskaran, A., Martín-Pérez, B., and Tanaka, H. (2014). “Testing the wind uplift resistance of roof edge components.” ICBEST 2014, Aachen, Germany, June 9-12, 2014.

ANSI/SPRI/FM 4435/ES-1 (2011). Wind Design Standard for Edge Systems Used with Low Slope Roofing Systems. Single Ply Roofing Industry, Waltham, MA, USA.

Badian L. (1992). “Wind pressures on flat roof edges and corners with and without parapets.” Thesis presented to Concordia University at Montreal, Canada, in partial fulfilment of the requirements for the degree of M.A.Sc.

Baskaran A., (1986). “Wind loads on flat roofs with parapets.” Thesis presented to Concordia University at Montreal, Canada, in partial fulfilment of the requirements for the degree of M. Eng.

Baskaran, A., and Smith, T. L. (2005). “A guide for the wind design of mechanically attached flexible membrane roofs.” *Institute for Research in Construction*, NRCC, Ottawa, ON.

Baskaran, A., Molleti, S. and Roodvoets, D. (2007) “Understanding low-slope roofs under hurricane Charley from field to practice.” *Journal of ASTM International*, 4, (10).

Baskaran, A., Molleti, S., and Yew, H. (2008). “Wind-Roof Calculator on Internet (Wind-RCI)- Feel the Wind on Your Laptop.” *Institute for Research in Construction*, NRCC, Ottawa, ON.

Baskaran, A., W. Alassafin, M. Borzoee, R. Flores-Vera, B. Martín- Pérez and H. Tanaka (2011), “Field Monitoring of Roof Edge Systems - Pilot Study”

Baskaran, A., Hajsaid, L., Martín-Pérez, B., Molleti, S., Singla, A., Tanaka, H. (2013) "Wind Uplift Standard for Roof Edge Systems and Technologies (REST): Progress Report - Year 3."

Baskaran, A., Molleti, S., Ko, S., Van Reenen, D. (2011), "Field monitoring the wind performance of commercial roofs – Part 1: Data from Ottawa Site", 13th International Conference on Wind Engineering, Amsterdam, Netherlands, July.

Bedair, R. (2009). "Comprehensive Study of Wind Loads on Parapets." Ph.D. thesis, Concordia University, Montreal, QC, Canada.

Borzoee, M. (2012). "A pilot study on the Wind Uplift Performance Evaluation of Roof Edge Systems." M.Eng. project, the University of Ottawa, Ottawa, ON, Canada.

CBC News (2012). "Power returning to Toronto in the wake of a storm". http://www.cbc.ca/news/canada/toronto. (November 15, 2012).

CSA A123.21-10 (2010) "Standard Test Method for the Dynamic Wind Uplift Resistance of Mechanically Attached Membrane Roofing System." (www.csashop.ca)

Dabas, M. (2013). "Finite element analysis of wind-uplift resistance of roof edge com-ponents." M.A.Sc. thesis, the University of Ottawa, Ottawa, ON, Canada.

FM Global (2005) "Approval Standard: Class I Roof Covers (FMG 4470)." Norwood, Massachusetts, USA.

Hajsaid, L. (2014). "Laboratory Evaluation of Roof Edge Components Under Simulated Wind Pressure." M.Eng. project, The University of Ottawa, Ottawa, ON, Canada.

Holmes, J.D. (2001). "Wind loadings of structures." Spon Press, Canada.

Jiang, H. (1995). "Wind Effects on Metal Edge Flashings." Master's thesis, Texas Tech University, Lubbock, Texas, USA.

Kopp, G., D. Surry, and C. Mans (2005). "Wind Effects of Parapets on Low Buildings: Part 1. Basic Aerodynamics and Local Loads." *Journal of Wind Engineering and Industrial Aerodynamics* 93.11: 817-841.

Mcdonald, J., P. Sarkar, and H. Gupta (1997). "Wind-induced Loads on Metal Edge Flashings." *Journal of Wind Engineering and Industrial Aerodynamics* **72**: 367-77.

Mehta KC, Levitan ML, Iverson RE, McDonald JR. Roof corner pressures measured in the field on a low building. J Wind Engrg and Ind Aerodyn 1992;41–44:181–92.

Mellott, J.W., and Diamond, T.G., (2015) “*Overcoming Vapor Drive Issues in Cool Roofing*”, Interface, The Journal of RCI, **33**(6): 18-24.

Murty, B. (2010). “Wind Uplift Performance Evaluation of Adhesive Applied Roofing Systems.”Ph.D. thesis, the University of Ottawa, Ottawa, ON, Canada.

National Research Council of Canada (2010) “National Building Code of Canada” NRCC, Ottawa, Canada.

Peterka, J. A., and Shahid, S. (1998). “Design gust wind speeds in the United States.” *J. Struct. Engrg.*, **124**(2), 207–214.

Simiu E, (2011). “Design of Building for Wind: A Guide for ASCE 7-10 Standard User and Designers of Special Structures.” John Wiley and Sons, Hoboken, New Jersey.

SPRI. (2011). “*Wind Design Standard for Edge Systems Used with Low Slope Roofing Systems.”* Waltham, MA, USA.

Stathopoulos T, Baskaran A, Goh PA. Full-scale measurements of wind pressures on flat roof corners. J Wind Engrg and Ind Aerodyn 1990;36:1063–72.

Stathopoulos, T., Marathe, R., Wu, H (1999). “Mean wind pressures on flat roof corners affected by parapets: field and wind tunnel studies.” *Engineering Structures* **21**: 629–638.

Texas Tech University (2015). “Wind Engineering Research Field Laboratory (WERFL)”. https://www.depts.ttu.edu/nwi/facilities/WERFL.php.

Vision Roof Services (2015). http://www.visionroofservices.com/

Appendix A

Calibration Curves for the Pressure Transducers

The calibration curves of the pressure transducers are shown in the following appendix. These figures show that each pressure transducer used in the present study is properly calibrated. The pressure transducers output data is initially in milliamps (mA) and must be is then converted to volts at the junction box. In order to convert the milliamps to volts, the following equation must be used,

$$V = IR$$

Where,

R = the resistance at 120 Ω,and

I = milliamps of the pressure transducer

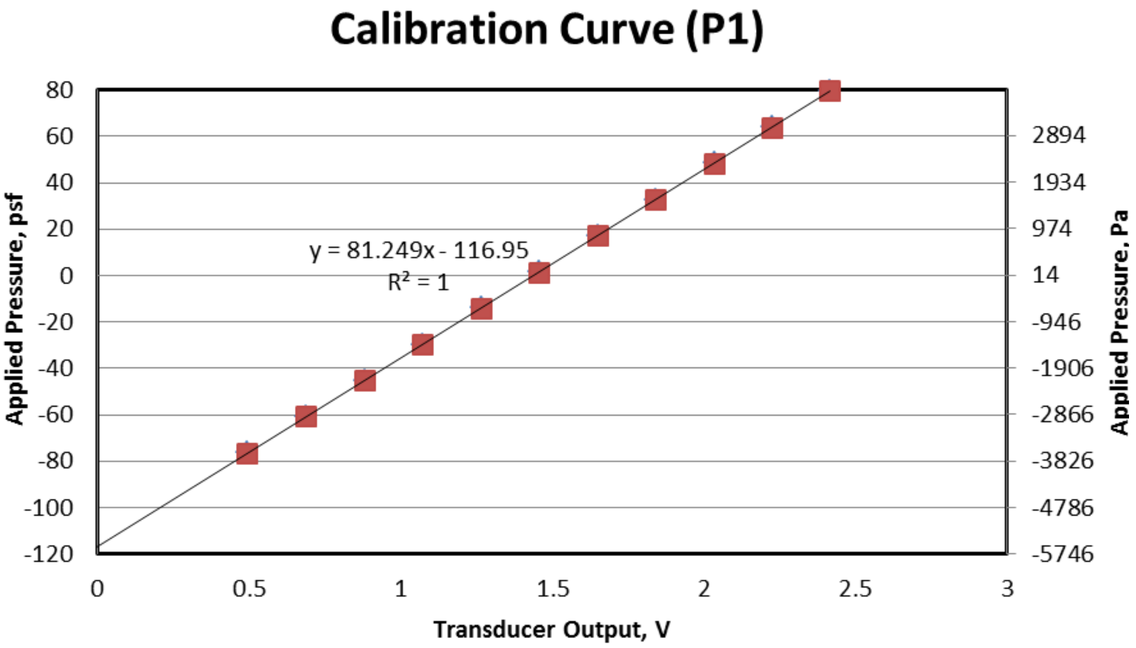

Figure A.1: Calibration curve of pressure transducer, P1

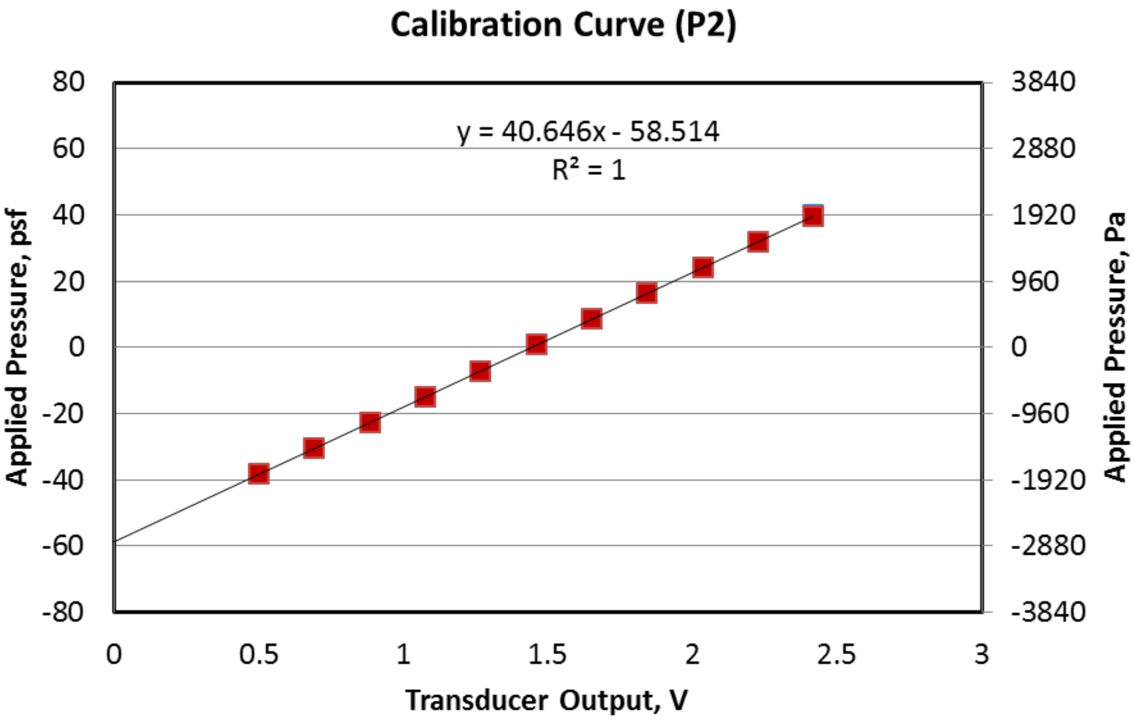

Figure A.2: Calibration curve of pressure transducer, P2

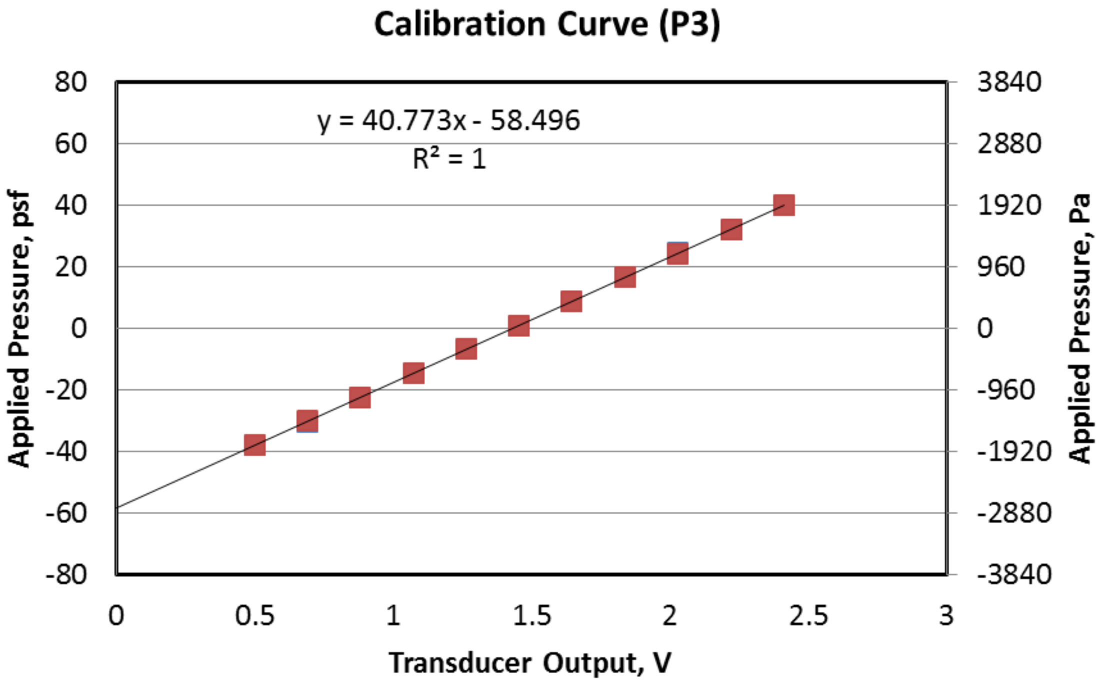

Figure A.3: Calibration curve of pressure transducer, P3

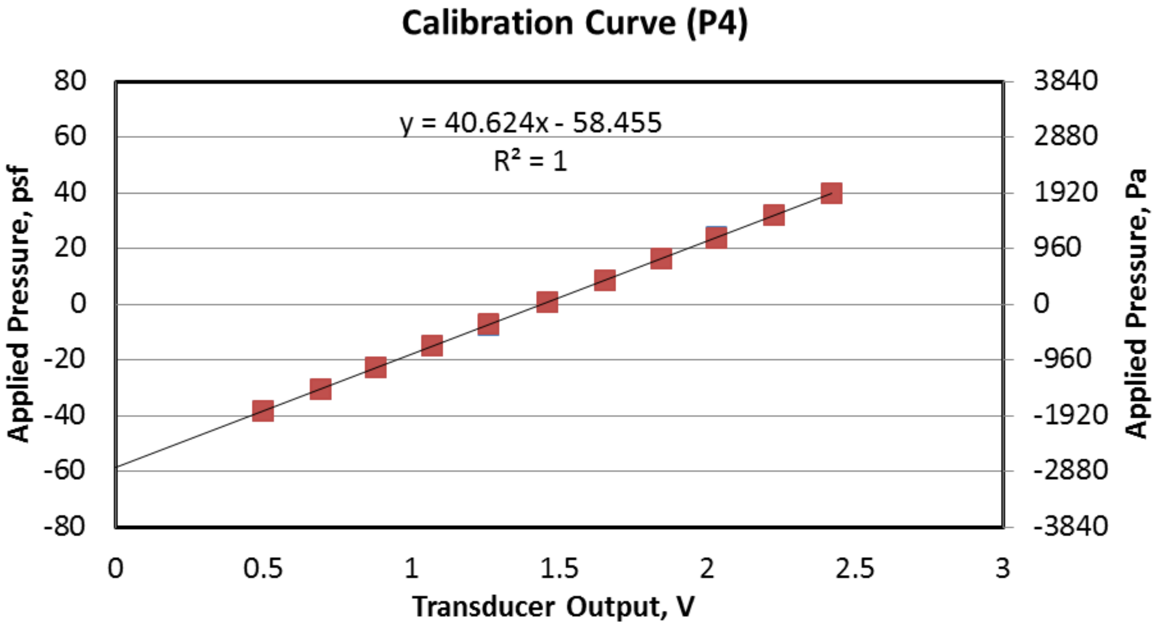

Figure A.4: Calibration curve of pressure transducer, P4

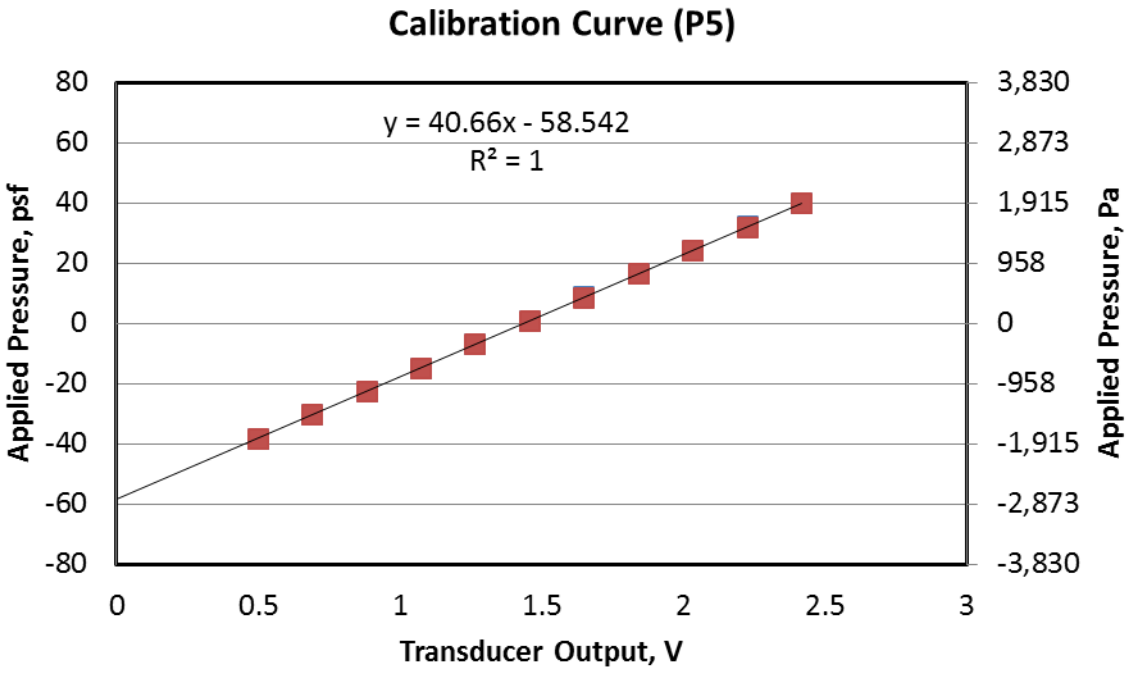

Figure A.5: Calibration curve of pressure transducer, P5

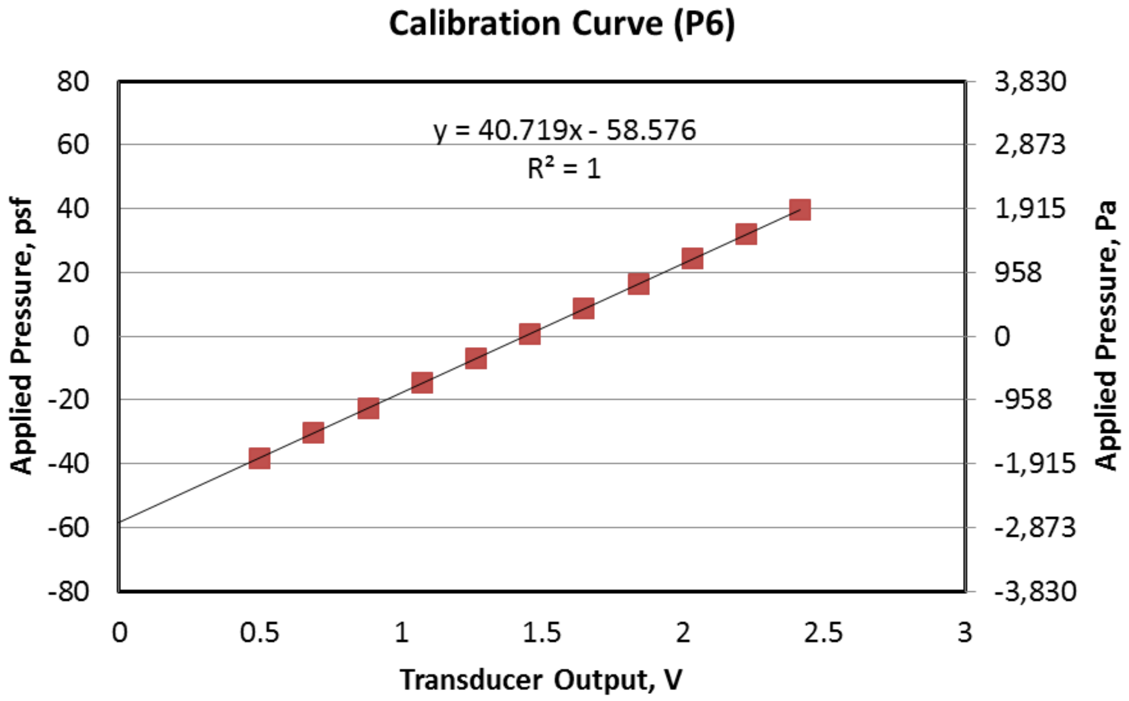

Figure A.6: Calibration curve of pressure transducer, P6

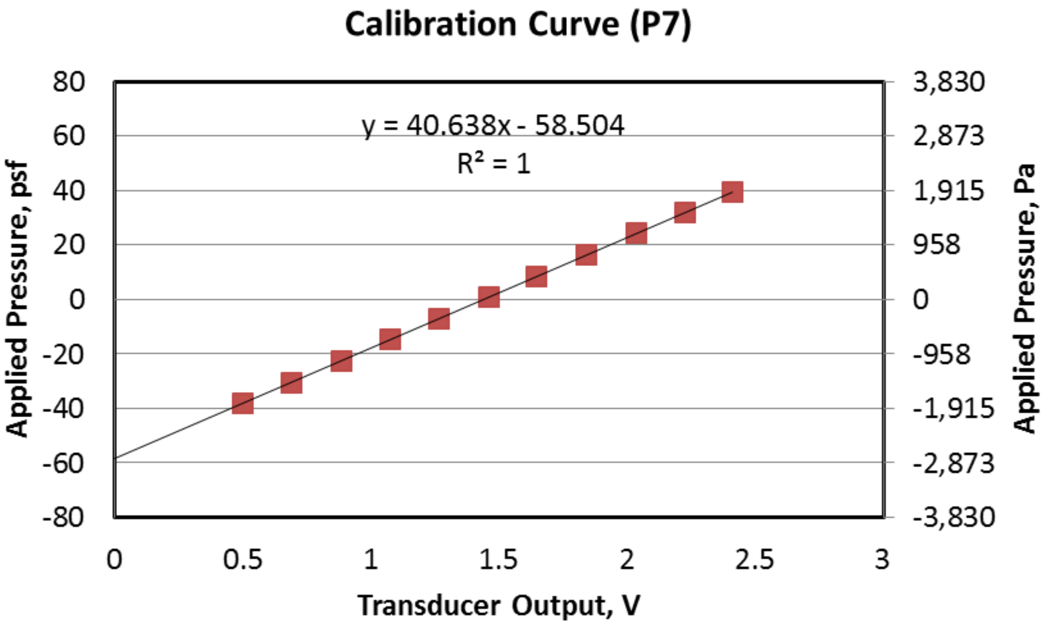

Figure A.7: Calibration curve of pressure transducer, P7

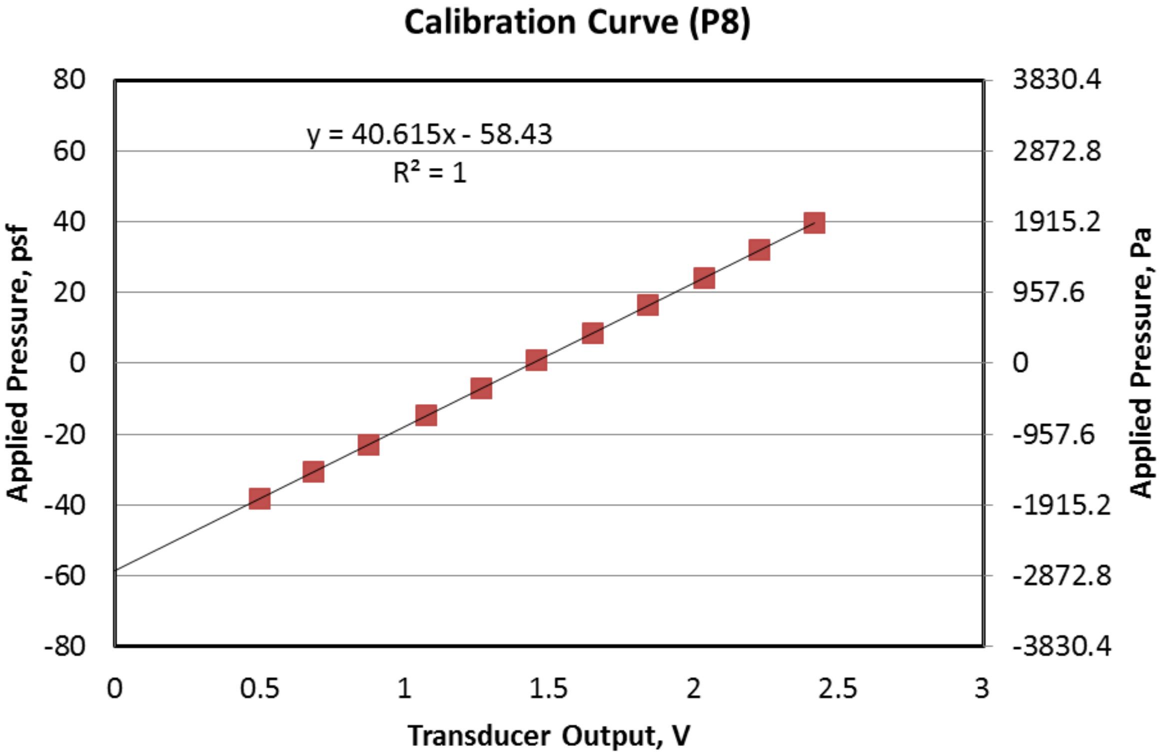

Figure A.8: Calibration curve of pressure transducer, P8

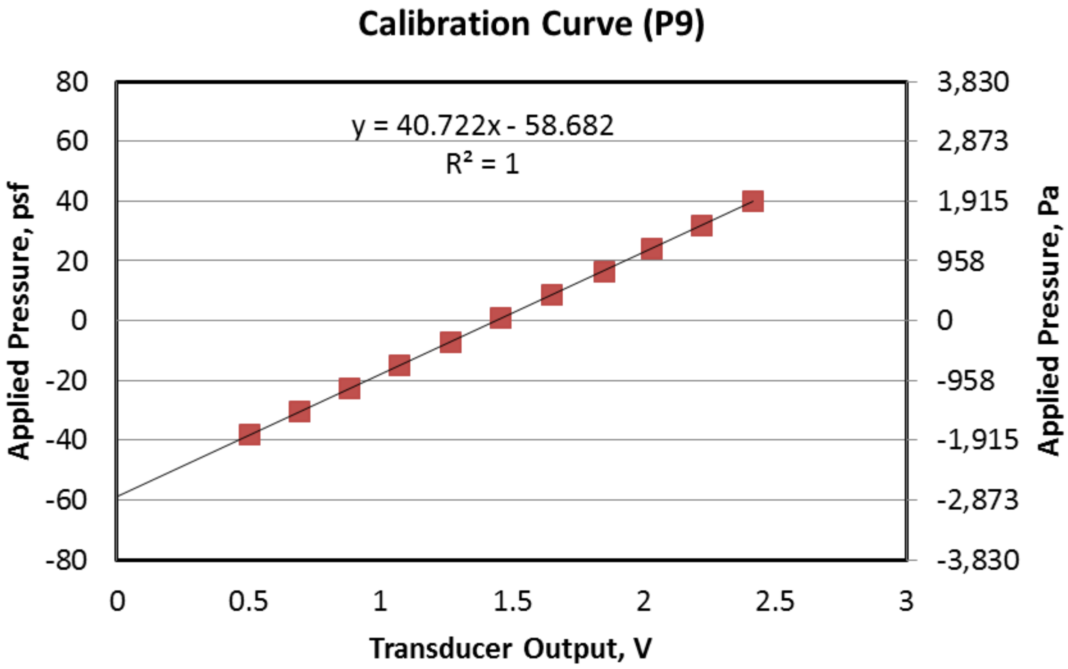

Figure A.9: Calibration curve of pressure transducer, P9

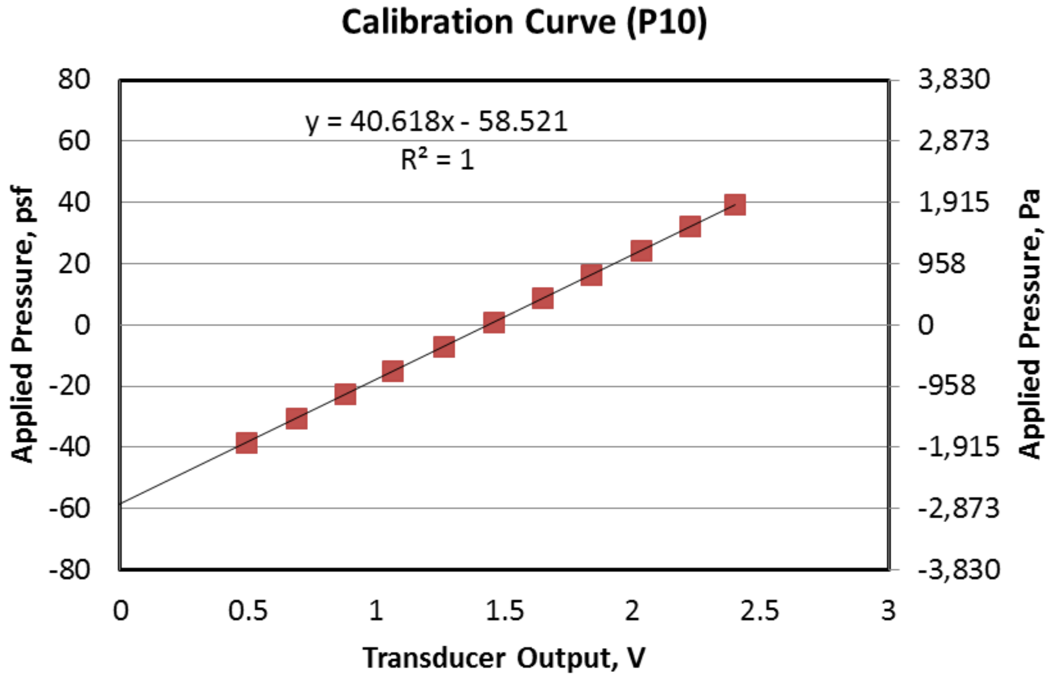

Figure A.10: Calibration curve of pressure transducer, P10

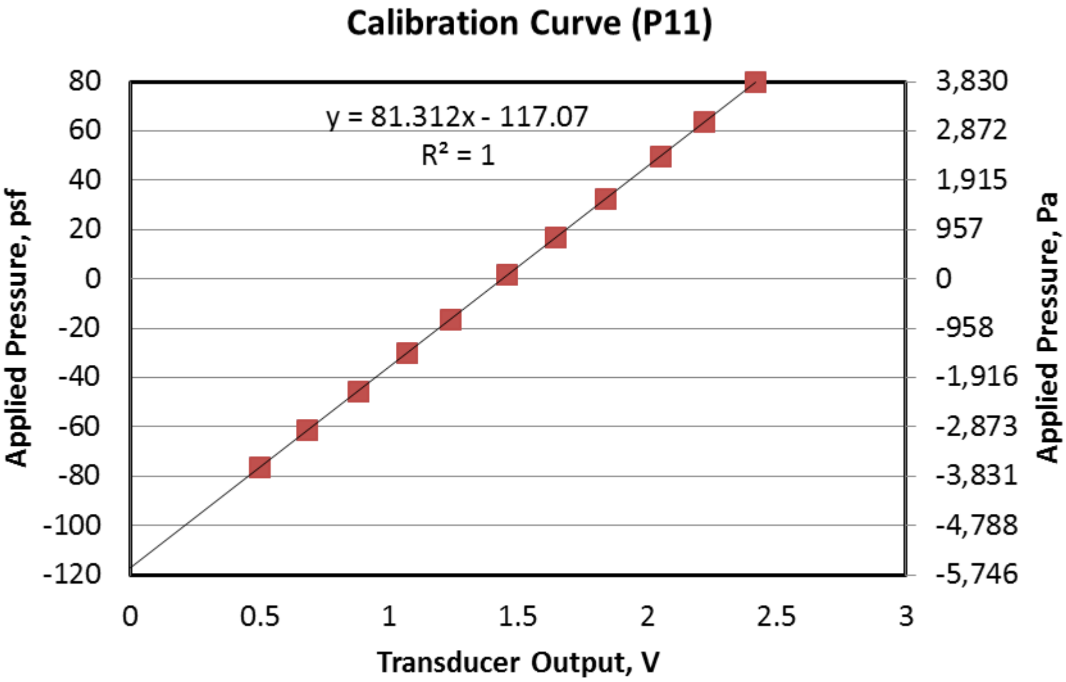

Figure A.11: Calibration curve of pressure transducer, P11

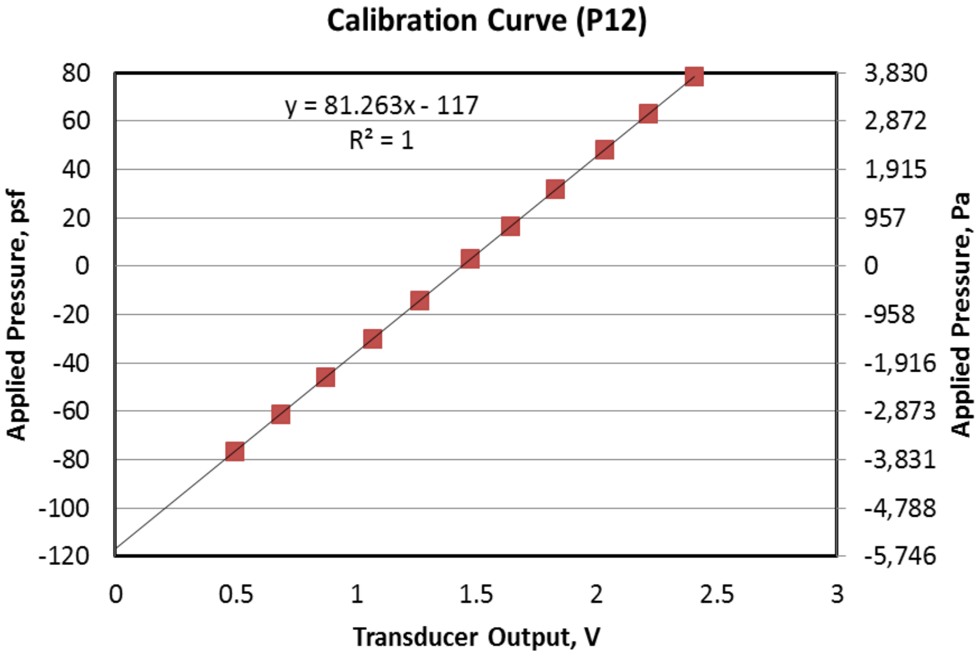

Figure A.12: Calibration curve of pressure transducer,P12

Appendix B

ACC

The following appendix shows all the raw data from the present study for the Anchor Clip Configuration. Each of the 16 recorded days illustrates the hour wind speed and direction for the day and the hourly data for the pressure taps. The table at the bottom of each page shows the peak and mean hourly wind speed. As well as the peak pressure, the mean, and the peak suction of each pressure tap during the hourly data.

NOV 2, 2013

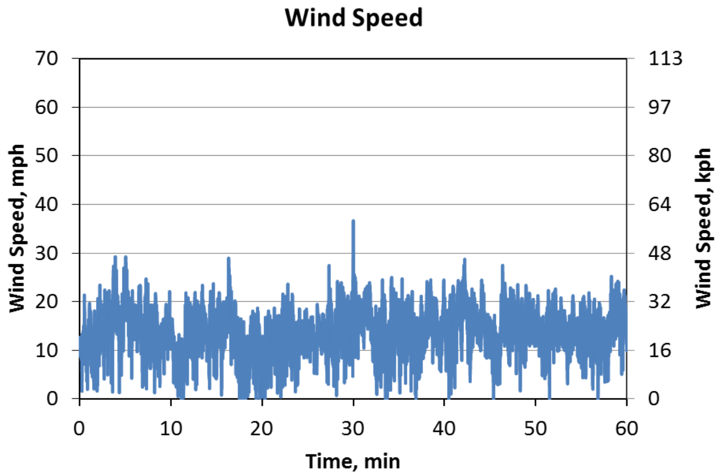

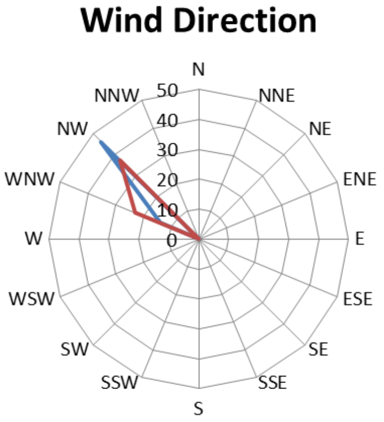

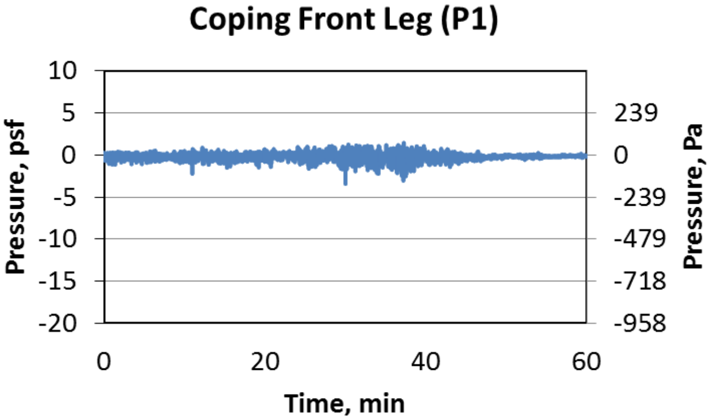

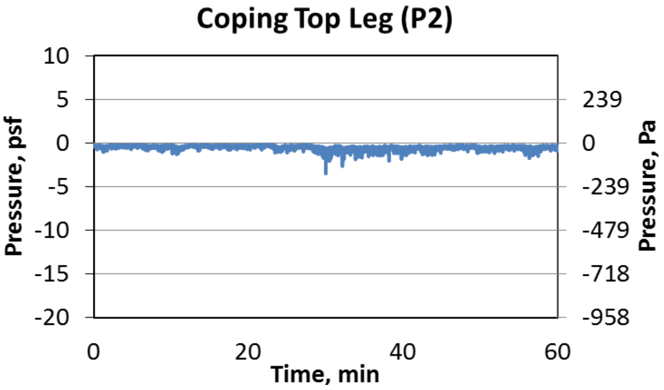

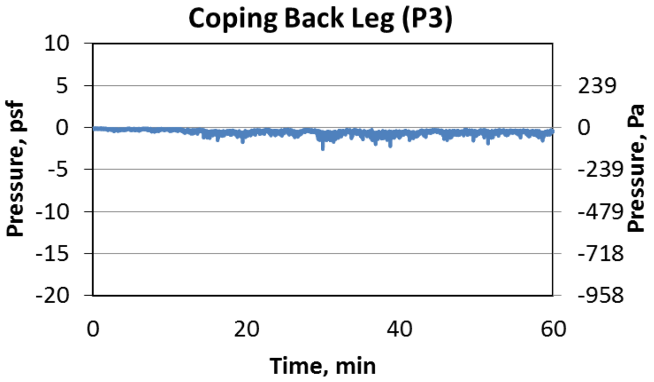

	Wind Speed, mph(kph)		Coping front leg (P1)	Coping Top Leg (P2)	Coping Back Leg (P3)
Peak	36 (59)	Pressure, psf (Pa)	1.4 (68.9)	0.0 (0)	0.0 (0)
Mean	14 (22)	Mean, psf (Pa)	-0.1 (-6.0)	-0.5 (-23.5)	-0.5 (-24.7)
		Suction, psf (Pa)	-3.4 (-163)	-3.5 (-166.1)	-2.6 (-122.9)

NOV 14, 2013

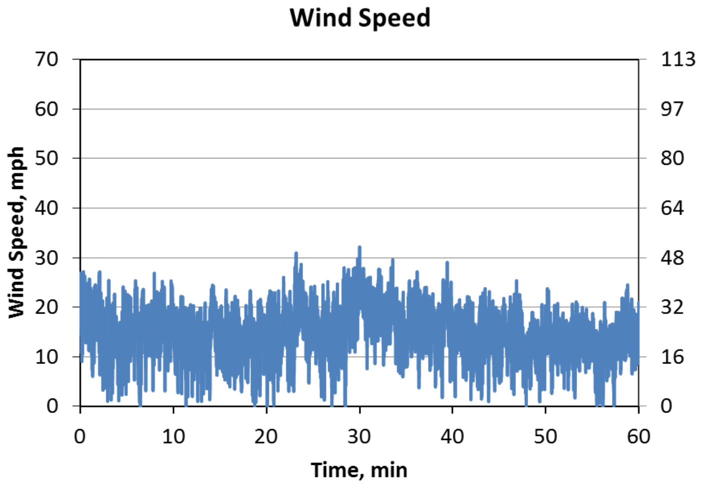

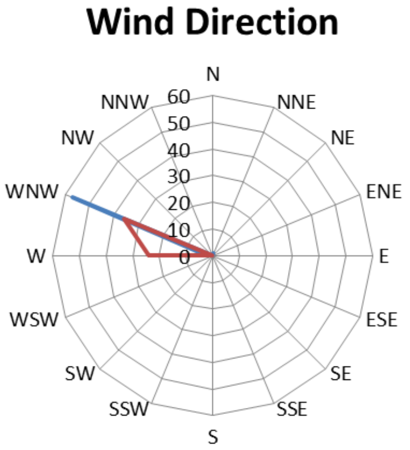

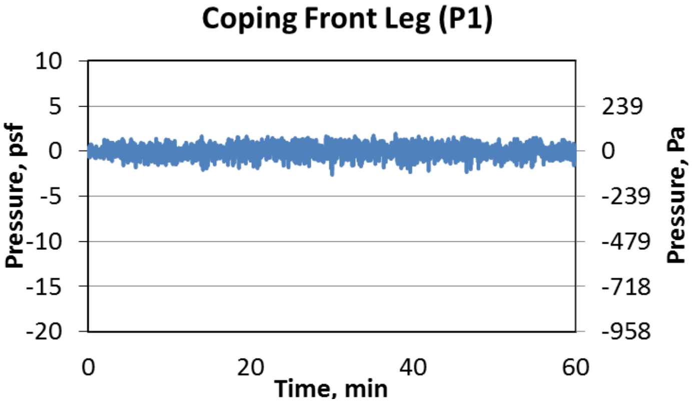

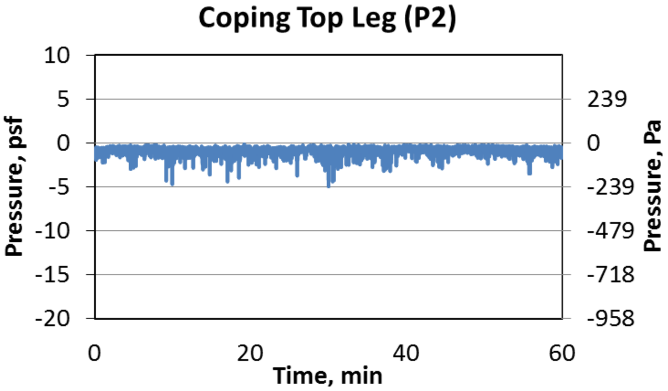

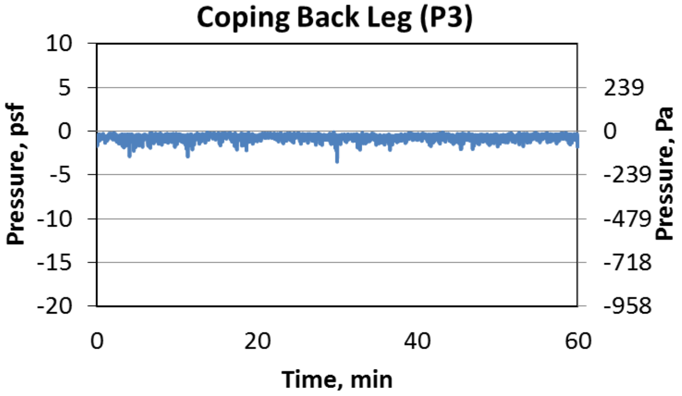

	Wind Speed, mph(kph)		Coping front leg (P1)	Coping Top Leg (P2)	Coping Back Leg (P3)
Peak	32 (52)	Pressure, psf (Pa)	1.9 (93.2)	0.0 (0)	0.0 (0)
Mean	15 (24)	Mean, psf (Pa)	0.2 (8.0)	-0.8 (-38.6)	-0.7 (-32.2)
		Suction, psf (Pa)	-2.6 (-124.5)	-4.9 (-237.0)	-3.5 (166.8)

NOV 15, 2013

Wind Speed

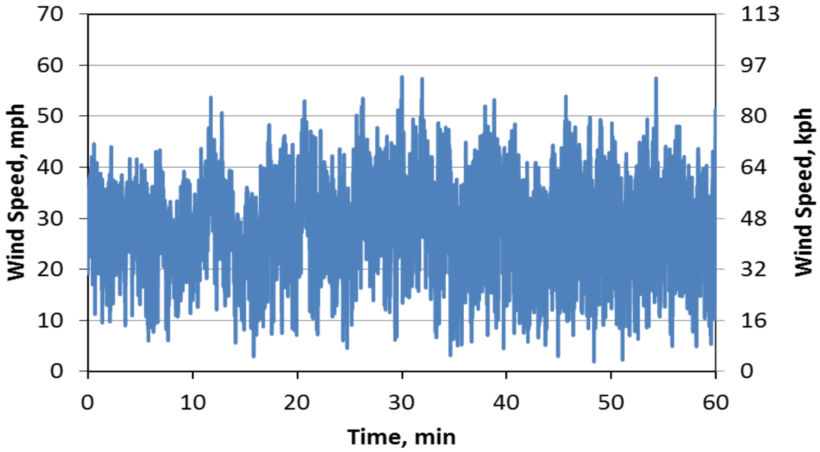

Wind Direction

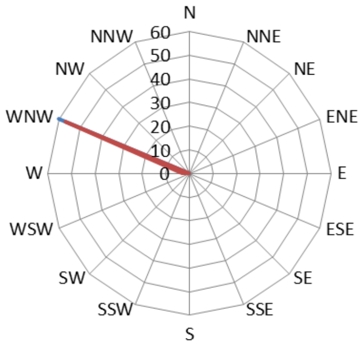

Coping Front Leg (P1)

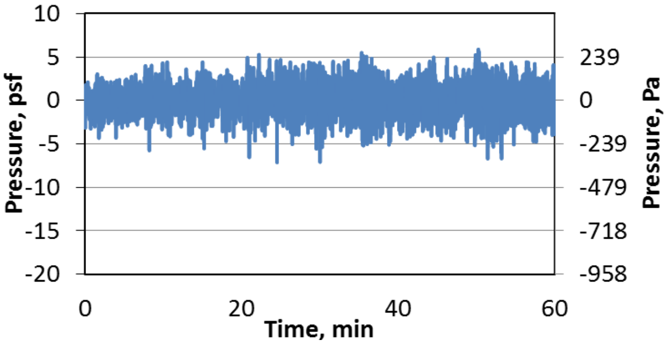

Coping Top Leg (P2)

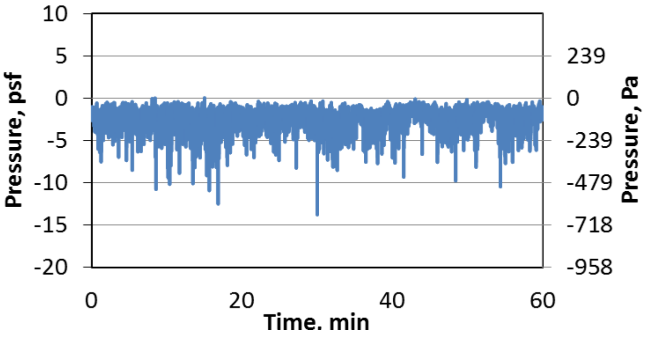

Coping Back Leg (P3)

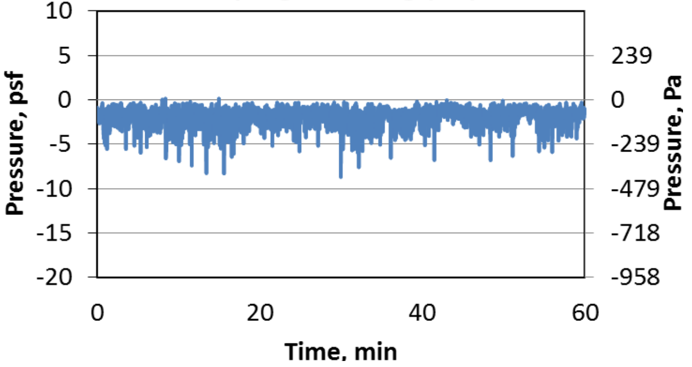

	Wind Speed, mph(kph)		Coping front leg (P1)	Coping Top Leg (P2)	Coping Back Leg (P3)
Peak	58 (93)	Pressure, psf (Pa)	5.9 (281.3)	0.0 (0)	0.1 (6.0)
Mean	29 (47)	Mean, psf (Pa)	0.4 (20.9)	-2.2 (-106.8)	-1.9 (-90.4)
		Suction, psf (Pa)	-7.0 (-336.4)	-13.5 (-648.5)	-8.7 (-415.2)

NOV 16, 2013

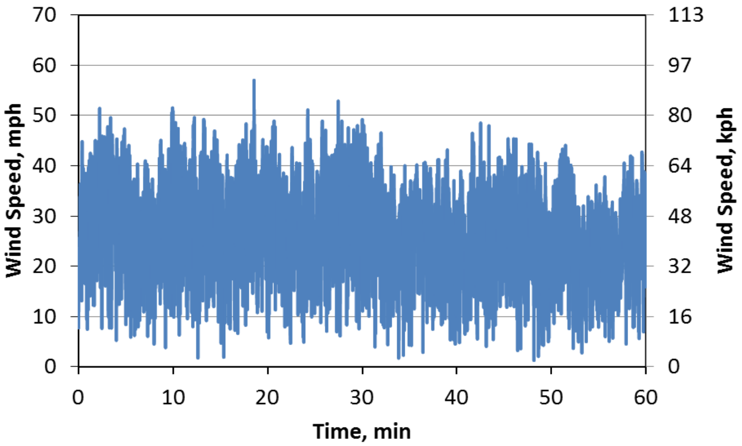

Wind Speed

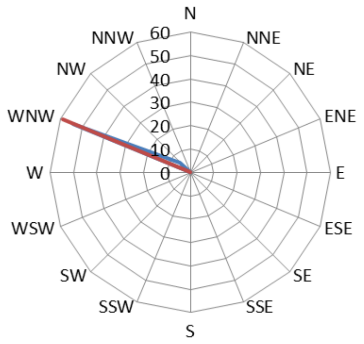

Wind Direction

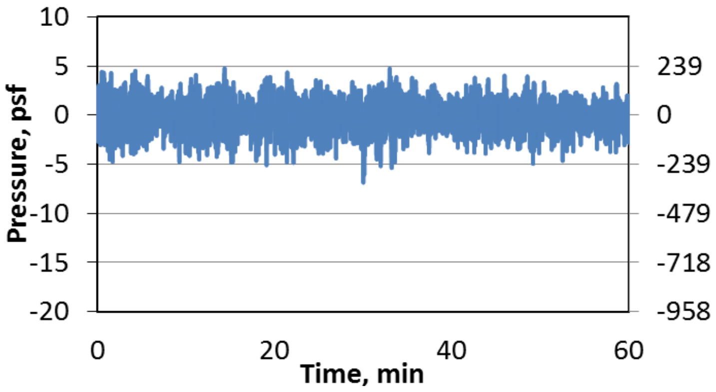

Coping Front Leg (P1)

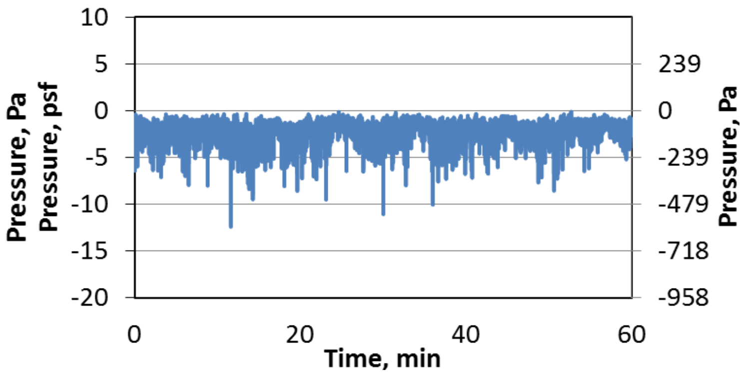

Coping Top Leg (P2)

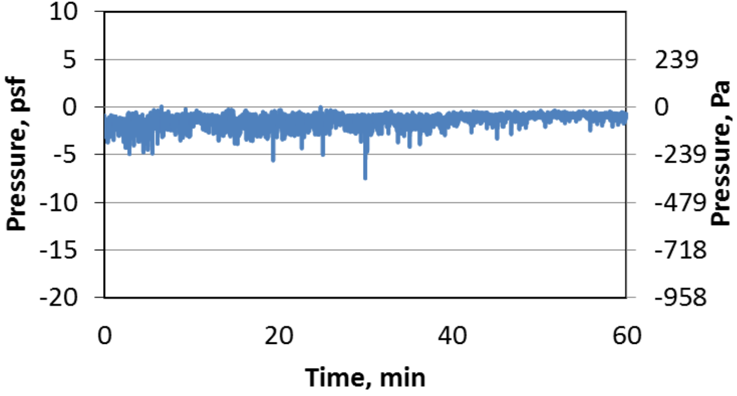

Coping Back Leg (P3)

	Wind Speed, mph(kph)		Coping front leg (P1)	Coping Top Leg (P2)	Coping Back Leg (P3)
Peak	49 (79)	Pressure, psf (Pa)	4.8 (227.6)	0.0 (0)	0.0 (0)
Mean	28 (45)	Mean, psf (Pa)	0.2 (9.0)	-2.1(-100.4)	-1.3 (-64.5)
		Suction, psf (Pa)	-6.8 (-325.9)	-11 (-593.6)	-7.5 (-357.7)

NOV 19, 2013

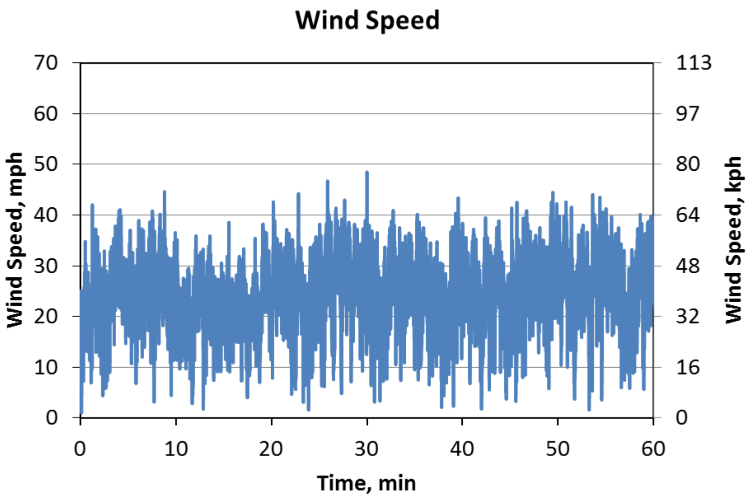

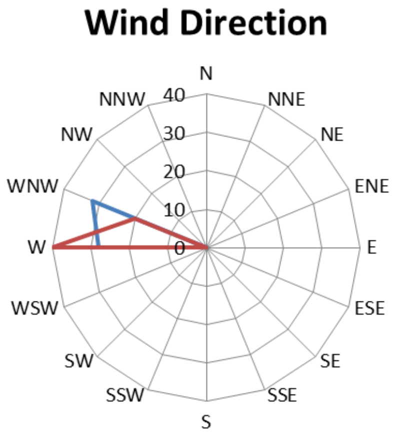

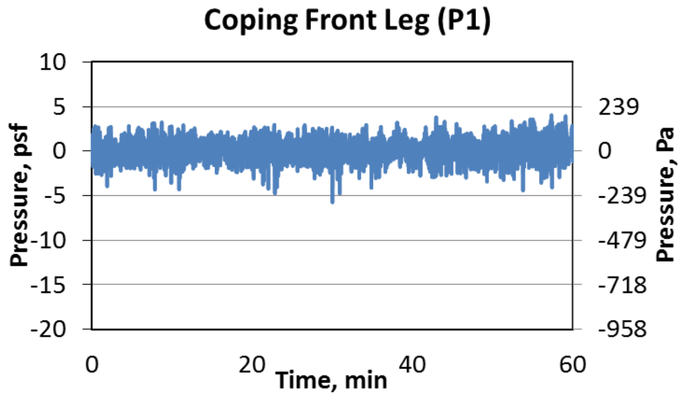

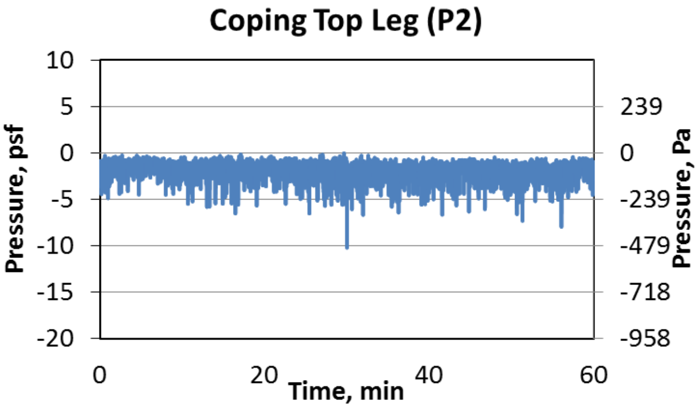

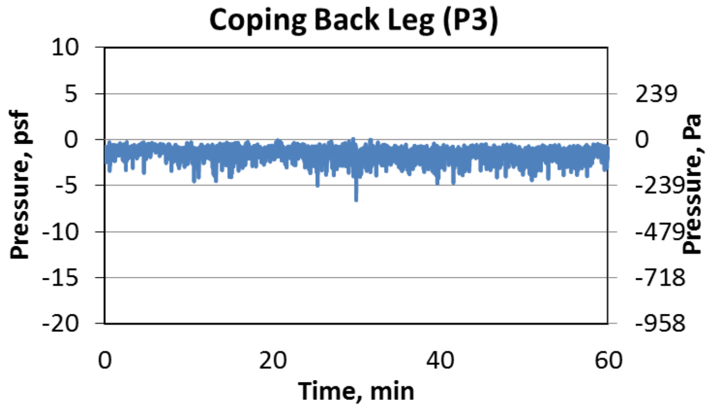

	Wind Speed, mph(kph)		Coping front leg (P1)	Coping Top Leg (P2)	Coping Back Leg (P3)
Peak	49 (79)	Pressure, psf (Pa)	4.0 (193.0)	0.0 (0)	0.1 (3.8)
Mean	25 (40)	Mean, psf (Pa)	0.4 (21.4)	-1.7 (-81.9)	-1.5 (-70.3)
		Suction, psf (Pa)	-5.7 (-273.1)	-10.1 (-484.9)	-6.5 (311.0)

Dec 1, 2013

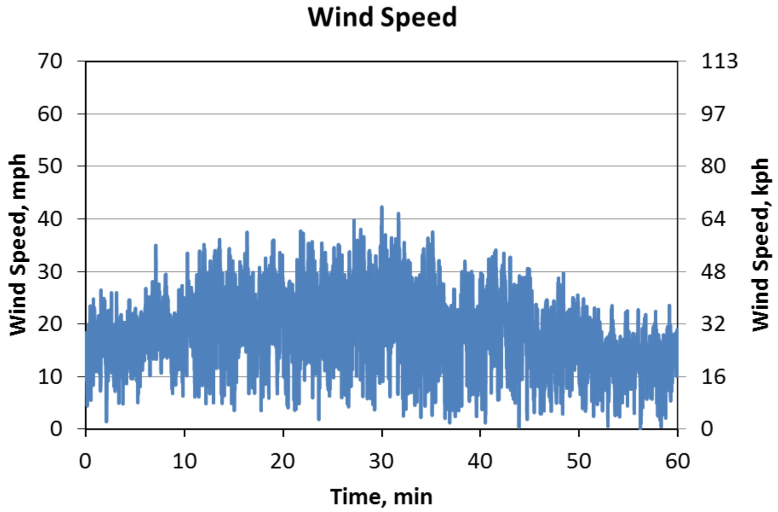
Wind Speed

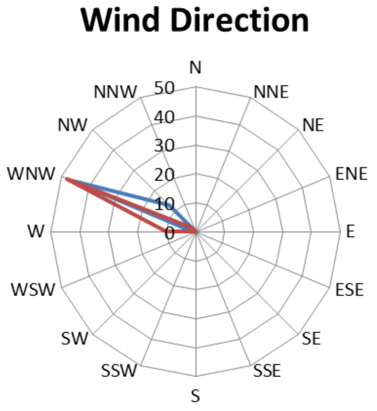
Wind Direction

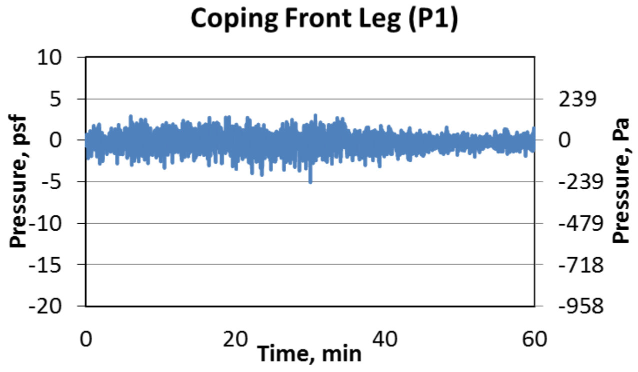
Coping Front Leg (P1)

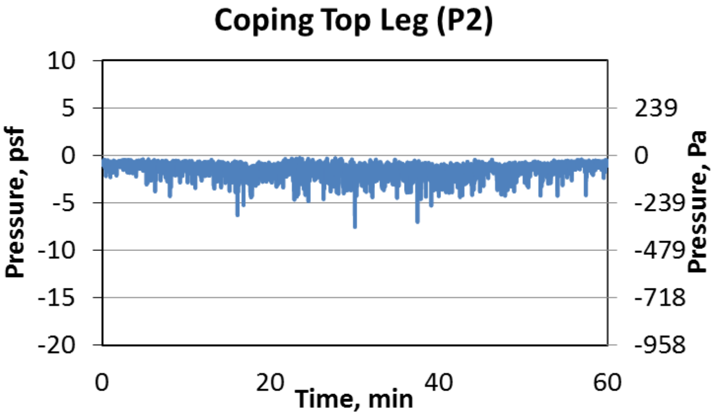
Coping Top Leg (P2)

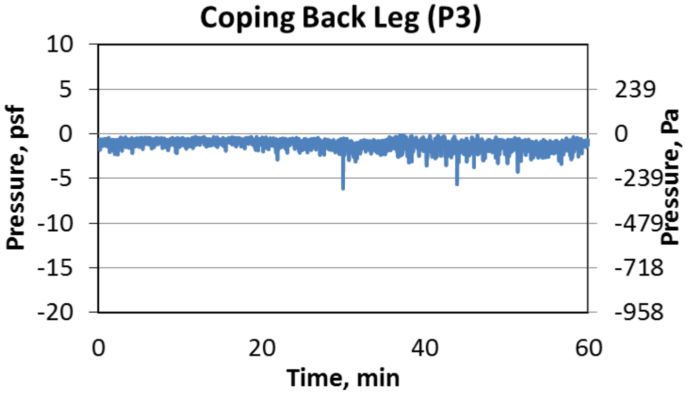
Coping Back Leg (P3)

	Wind Speed, mph(kph)		Coping front leg (P1)	Coping Top Leg (P2)	Coping Back Leg (P3)
Peak	42 (68)	Pressure, psf (Pa)	3.0 (144.1)	0.0 (0)	0.0 (0)
Mean	19 (30)	Mean, psf (Pa)	0.0 (0)	-1.3 (-63.6)	-1.1 (-53.4)
		Suction, psf (Pa)	-5.0 (-238.4)	-7.5 (-360.9)	-6.1 (-293)

Dec 2, 2013

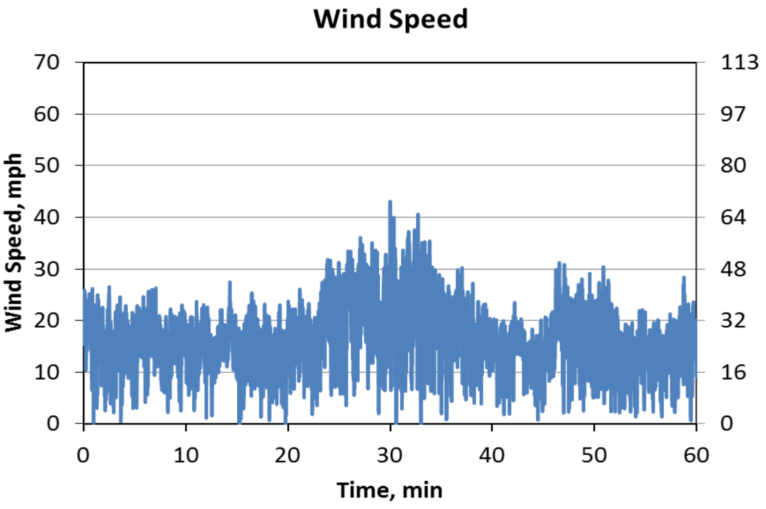
Wind Speed

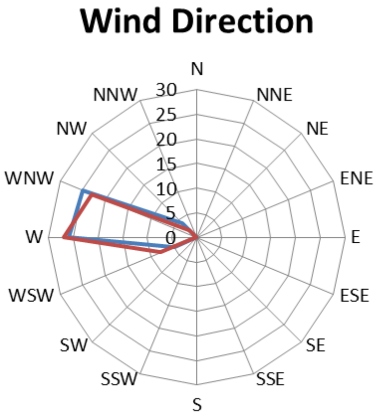
Wind Direction

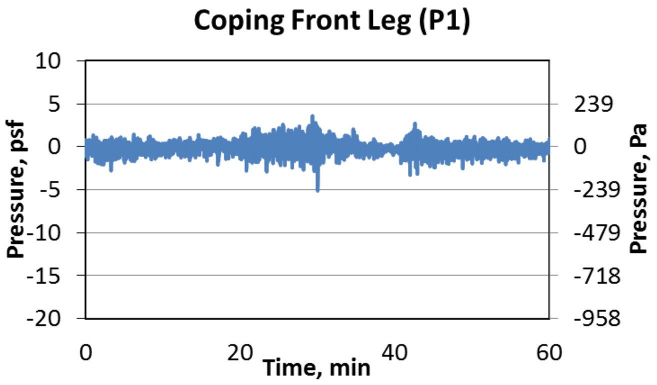
Coping Front Leg (P1)

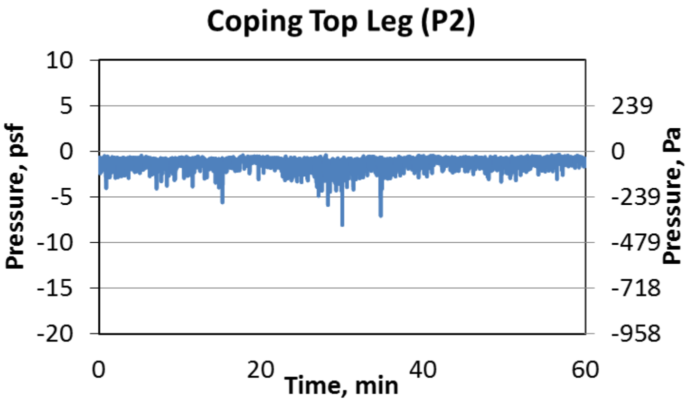
Coping Top Leg (P2)

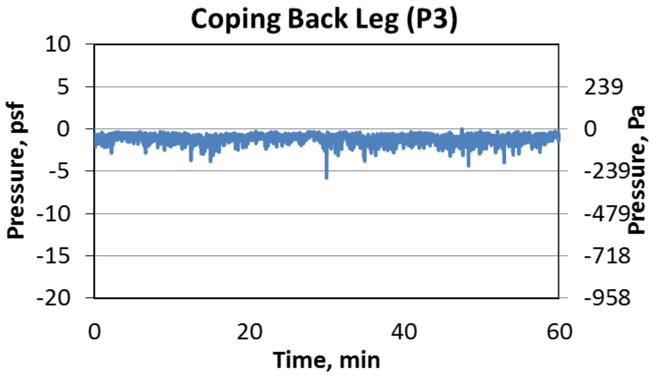
Coping Back Leg (P3)

	Wind Speed, mph(kph)		Coping front leg (P1)	Coping Top Leg (P2)	Coping Back Leg (P3)
Peak	43 (69)	Pressure, psf (Pa)	3.6 (172.6)	0.0 (0)	0.0 (0)
Mean	17 (27)	Mean, psf (Pa)	0.0 (0)	-1.2 (-56.3)	-1.1 (-52.2)
		Suction, psf (Pa)	-5.1 (-244.5)	-8.0 (-384.4)	-5.8 (-276.5)

Dec 18, 2013

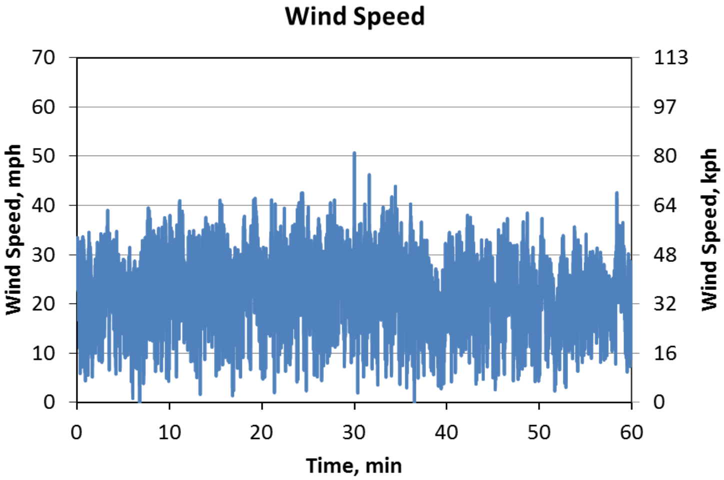

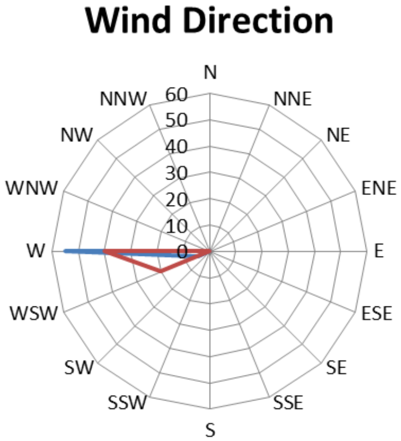

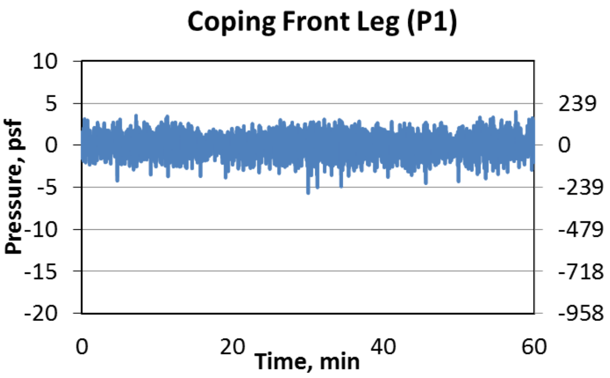

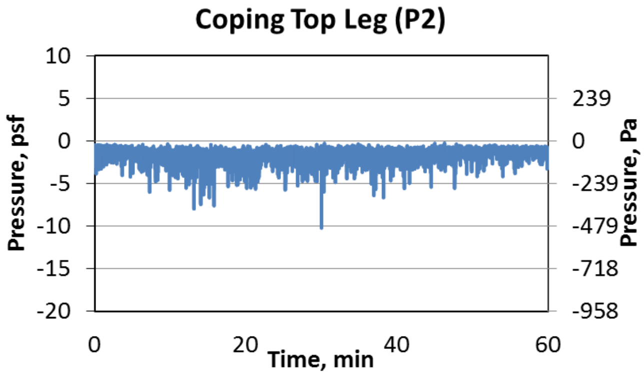

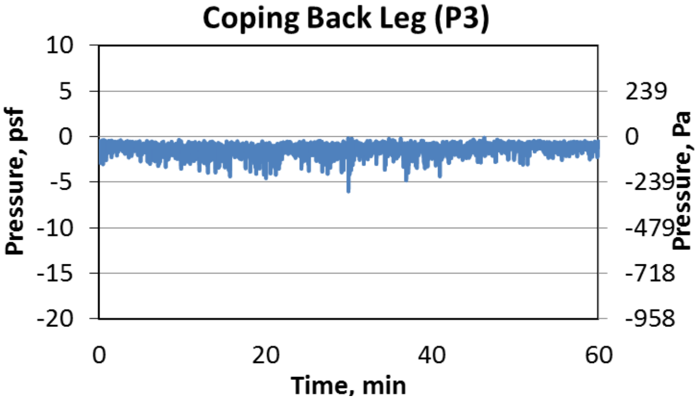

	Wind Speed, mph(kph)		Coping front leg (P1)	Coping Top Leg (P2)	Coping Back Leg (P3)
Peak	50 (81)	Pressure, psf (Pa)	4.0 (190.3)	0.0 (0)	0.0 (0)
Mean	23 (37)	Mean, psf (Pa)	0.3 (15.8)	-1.5 (-72.3)	-1.3 (-62.4)
		Suction, psf (Pa)	-5.7 (-270.6)	-10.1 (-485.6)	-6.0 (-286.8)

Dec 23, 2013

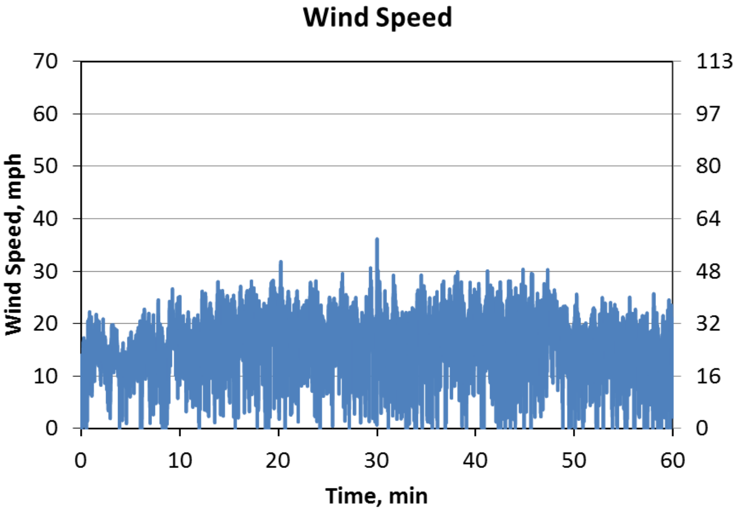
Wind Speed

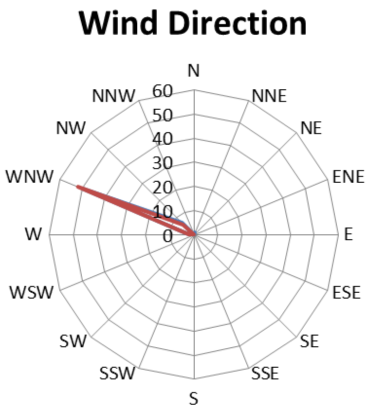
Wind Direction

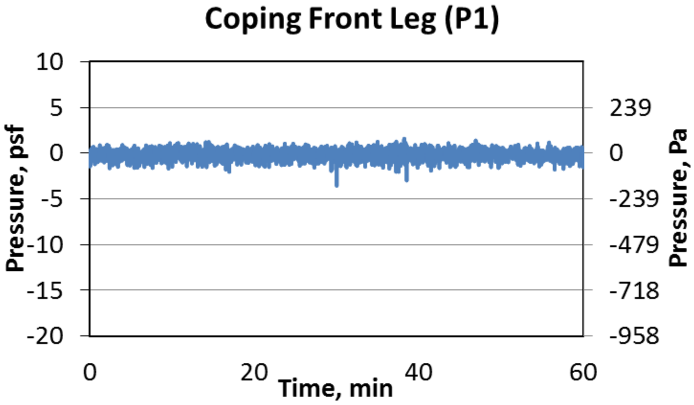
Coping Front Leg (P1)

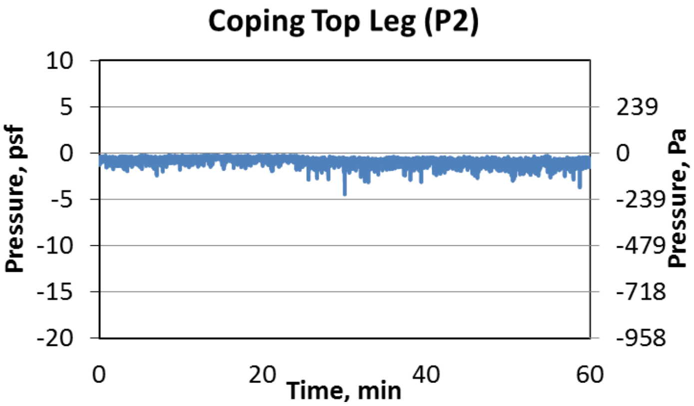
Coping Top Leg (P2)

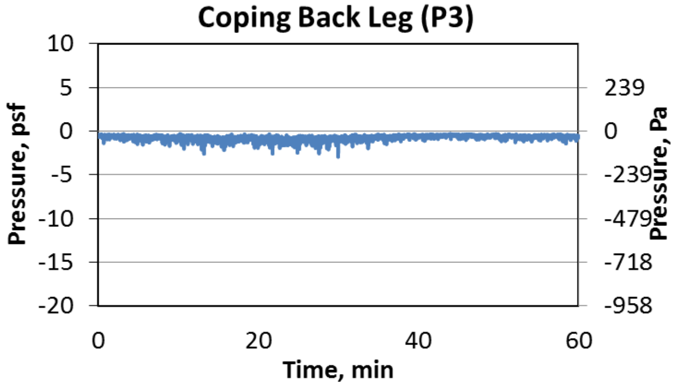
Coping Back Leg (P3)

	Wind Speed, mph(kph)		Coping front leg (P1)	Coping Top Leg (P2)	Coping Back Leg (P3)
Peak	36 (58)	Pressure, psf (Pa)	1.6 (76.5)	0.0 (0)	0.0 (0)
Mean	17 (27)	Mean, psf (Pa)	0.0 (0)	-0.8 (-38.1)	-0.7 (-35.5)
		Suction, psf (Pa)	-3.5 (-169.6)	-4.5 (-213.6)	-2.9 (-140.7)

Feb 20, 2014

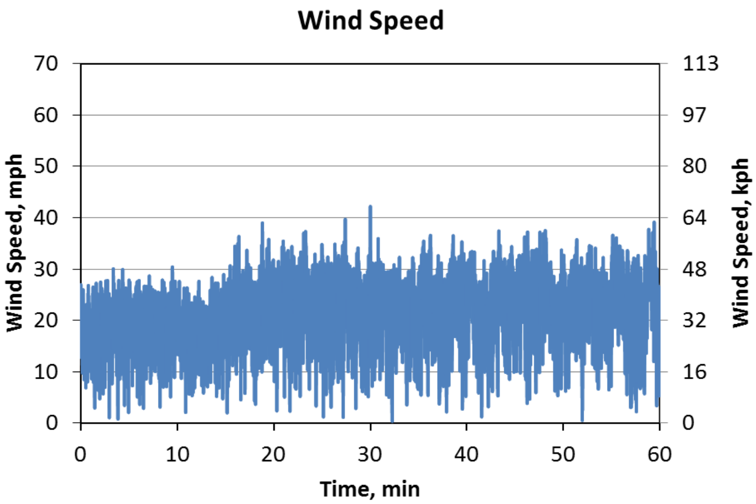
Wind Speed

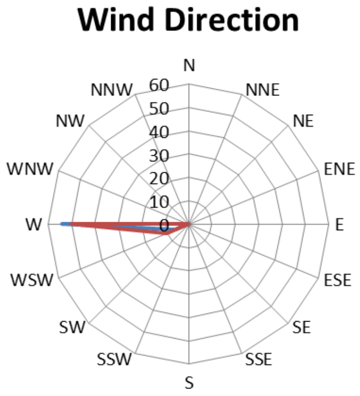
Wind Direction

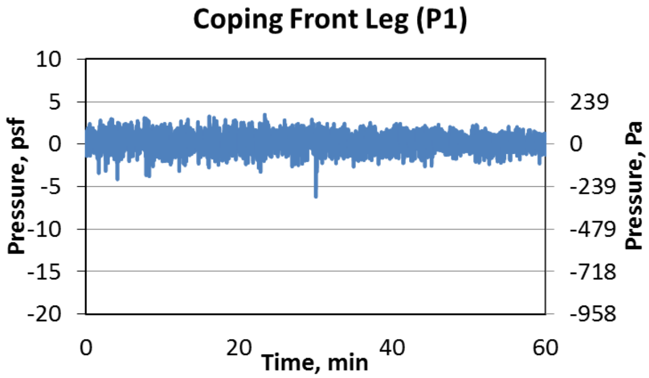
Coping Front Leg (P1)

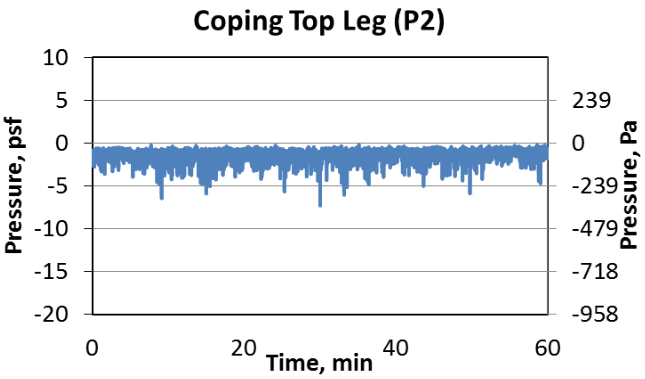
Coping Top Leg (P2)

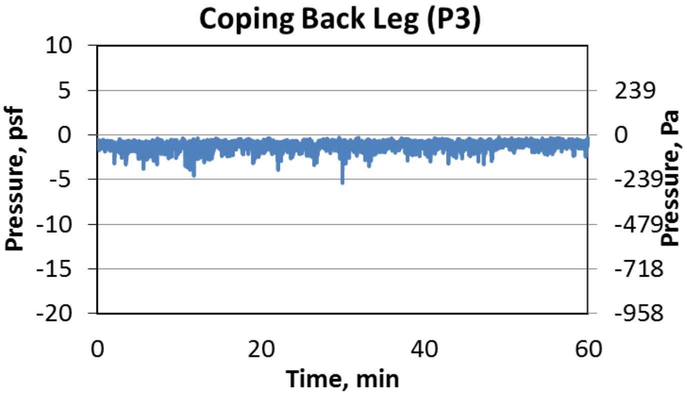
Coping Back Leg (P3)

	Wind Speed, mph(kph)		Coping front leg (P1)	Coping Top Leg (P2)	Coping Back Leg (P3)
Peak	42 (68)	Pressure, psf (Pa)	3.5 (167)	0.0 (0)	0.0 (0)
Mean	22 (35)	Mean, psf (Pa)	0.5 (25.1)	-1.3 (-62.4)	-1.2 (-55.8)
		Suction, psf (Pa)	-6.2 (-296.2)	-7.3 (-348.8)	-5.4 (-257.2)

Feb 21, 2014

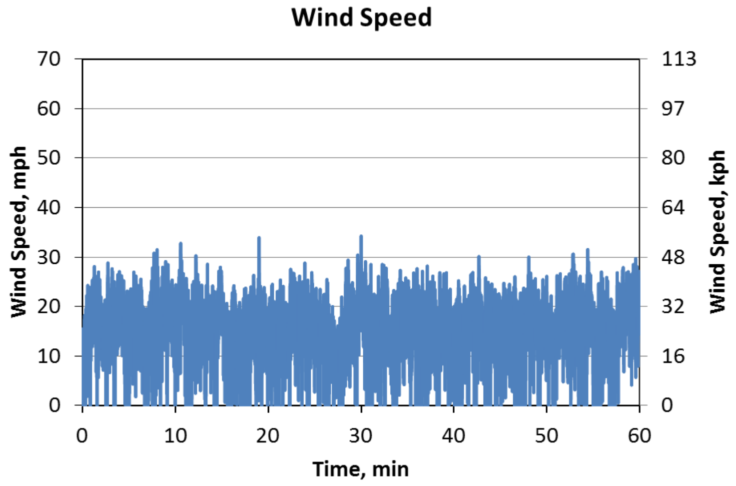

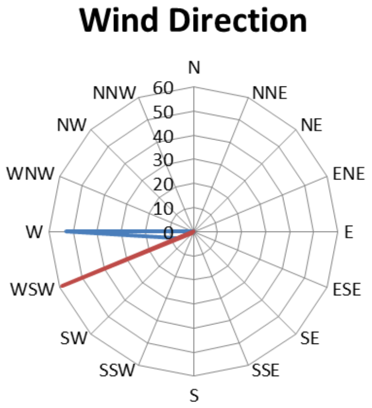

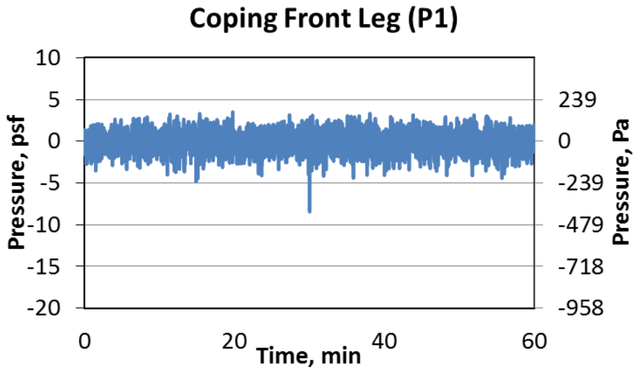

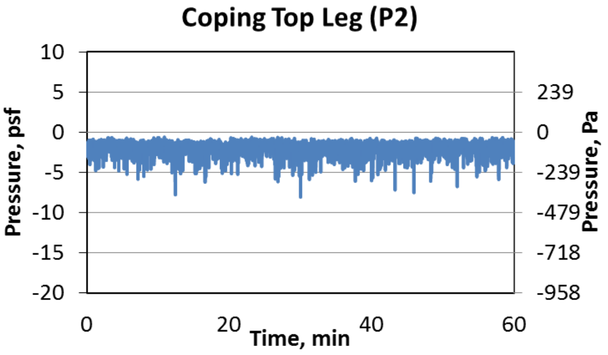

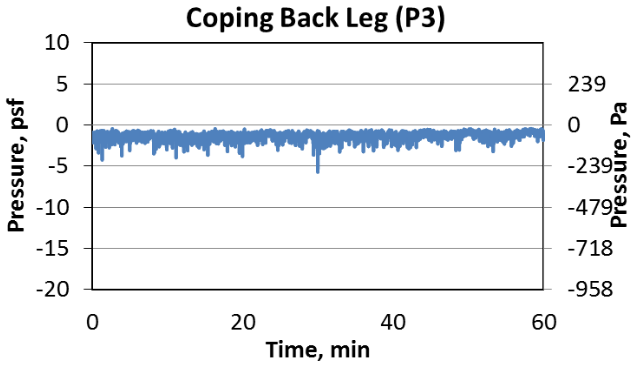

	Wind Speed, mph(kph)		Coping front leg (P1)	Coping Top Leg (P2)	Coping Back Leg (P3)
Peak	34 (55)	Pressure, psf (Pa)	3.5 (167.5)	0.0 (0)	0.0 (0)
Mean	16 (26)	Mean, psf (Pa)	0.2 (10.4)	-1.8 (-88)	-1.3 (-63.2)
		Suction, psf (Pa)	-8.3 (-399.3)	-8.0 (382.6)	-5.7 (-273.3)

April 17, 2014

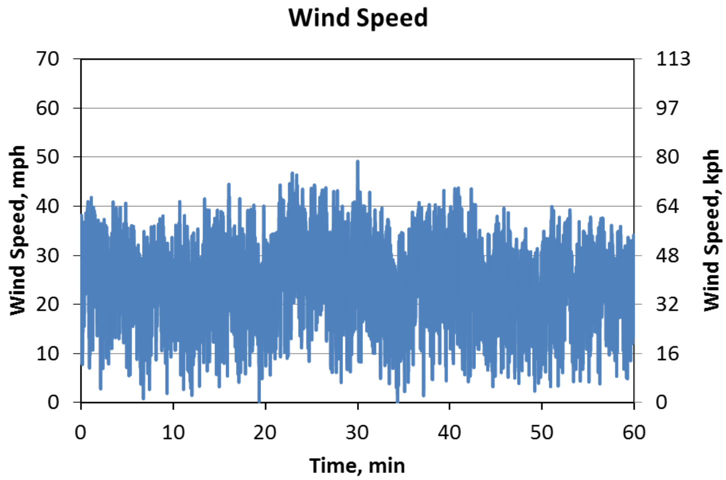

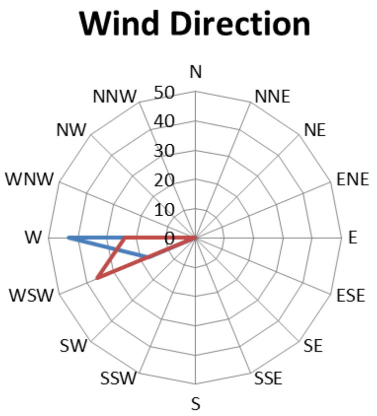

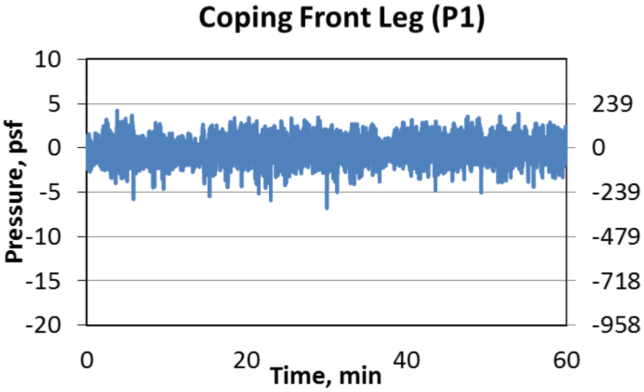

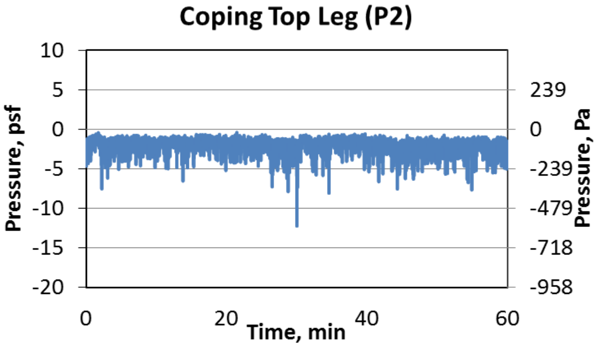

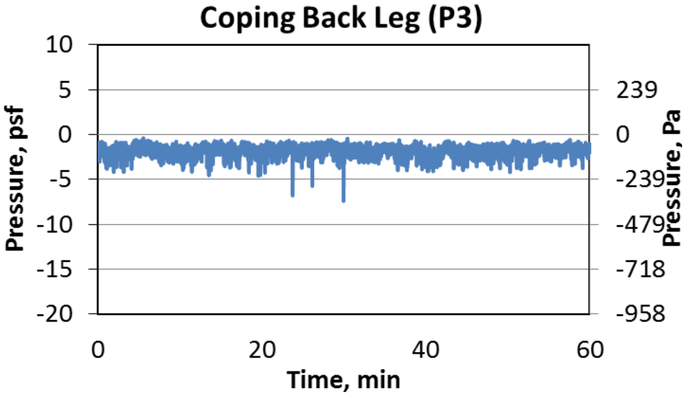

	Wind Speed, mph(kph)		Coping front leg (P1)	Coping Top Leg (P2)	Coping Back Leg (P3)
Peak	49 (79)	Pressure, psf (Pa)	4.2 (202.4)	0.0 (0)	0.0 (0)
Mean	25 (41)	Mean, psf (Pa)	0.2 (7.3)	-1.9 (-90.1)	-1.8 (-86)
		Suction, psf (Pa)	-6.8 (-325.4)	-12.2 (-585.8)	-7.4 (353.5)

April 21, 2014

Wind Speed

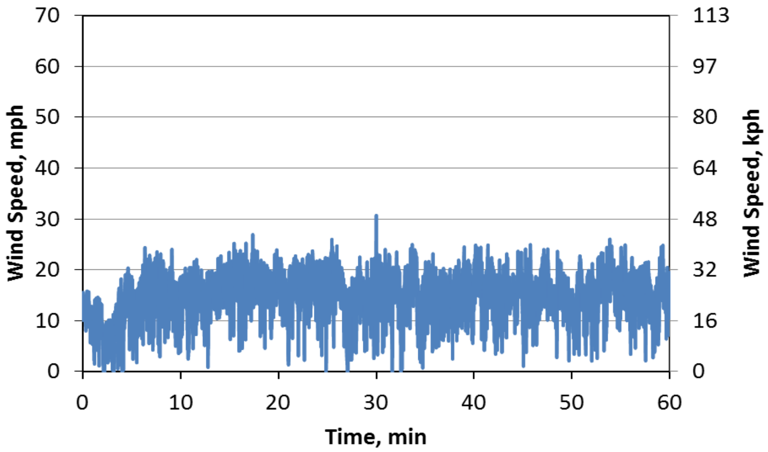

Wind Direction

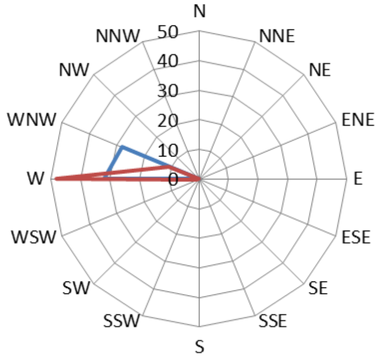

Coping Front Leg (P1)

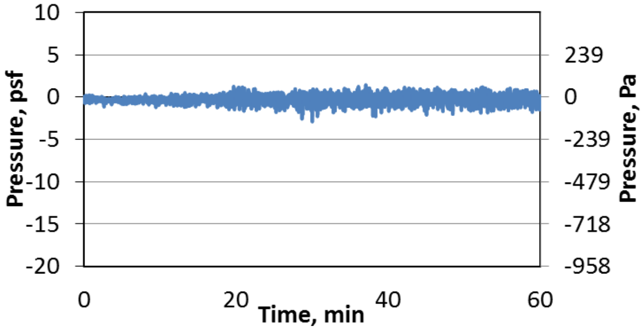

Coping Top Leg (P2)

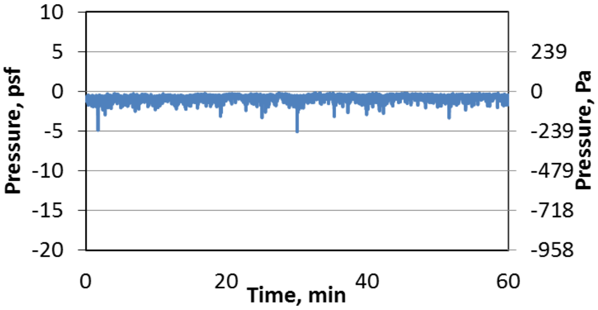

Coping Back Leg (P3)

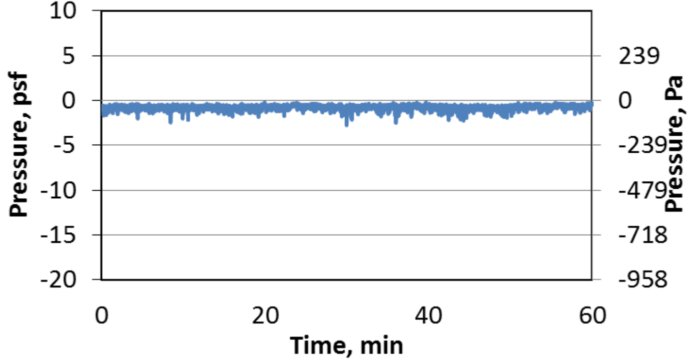

	Wind Speed, mph(kph)		Coping front leg (P1)	Coping Top Leg (P2)	Coping Back Leg (P3)
Peak	30 (49)	Pressure, psf (Pa)	1.4 (68.4)	0.0 (0)	0.0 (0)
Mean	15 (24)	Mean, psf (Pa)	-0.2 (-7.6)	-0.7 (-35.9)	-0.8 (-36.5)
		Suction, psf (Pa)	-2.9 (-138.2)	-5.0 (-240.5)	-2.7 (-131)

April 22, 2014

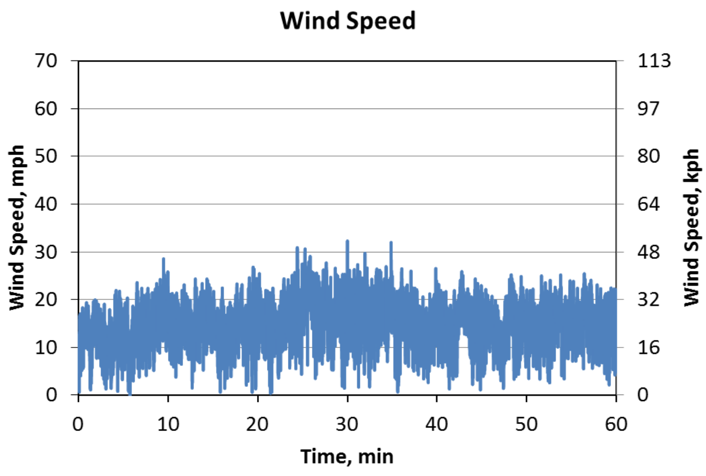
Wind Speed

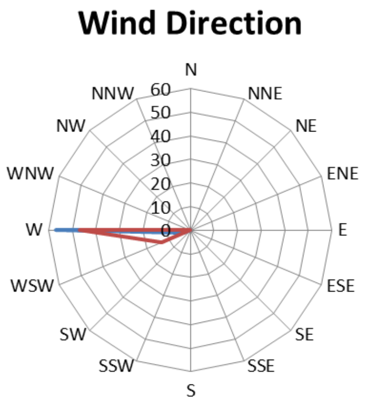
Wind Direction

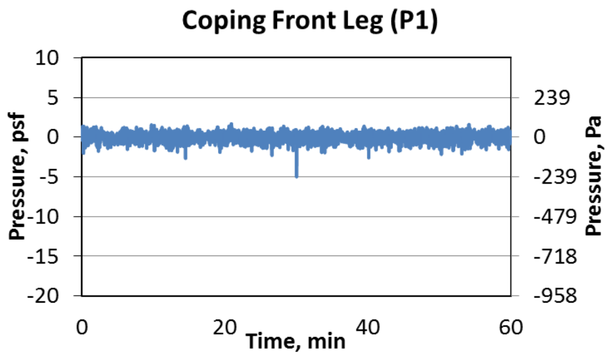
Coping Front Leg (P1)

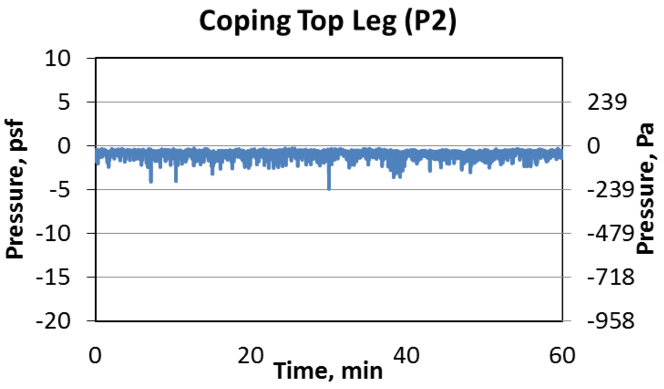
Coping Top Leg (P2)

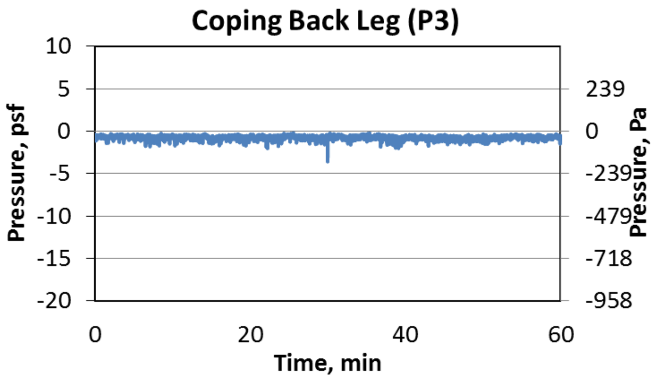
Coping Back Leg (P3)

	Wind Speed, mph(kph)		Coping front leg (P1)	Coping Top Leg (P2)	Coping Back Leg (P3)
Peak	32 (52)	Pressure, psf (Pa)	1.7 (80.8)	0.0 (0)	0.0 (0)
Mean	15 (25)	Mean, psf (Pa)	0.1 (5.8)	-0.8 (-40.6)	-0.8 (-36.4)
		Suction, psf (Pa)	-5.0 (-238.5)	-4.9 (-234.9)	-3.6 (-171)

June 9, 2014

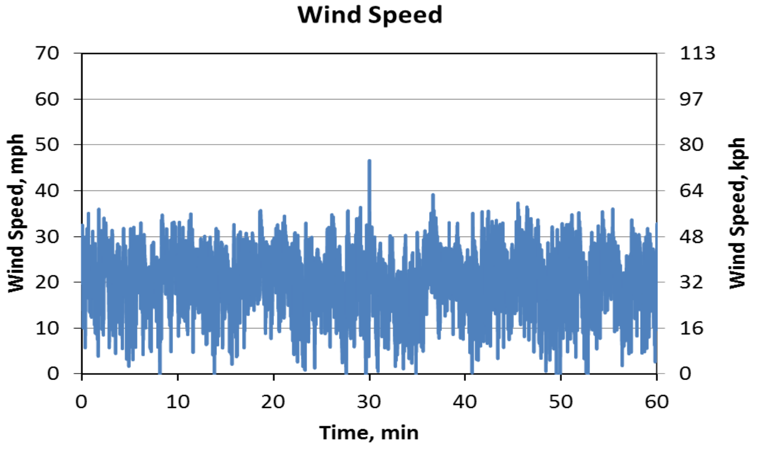

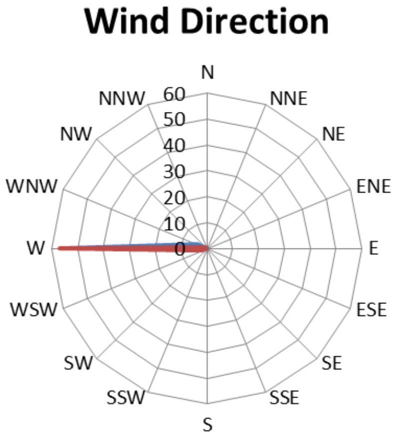

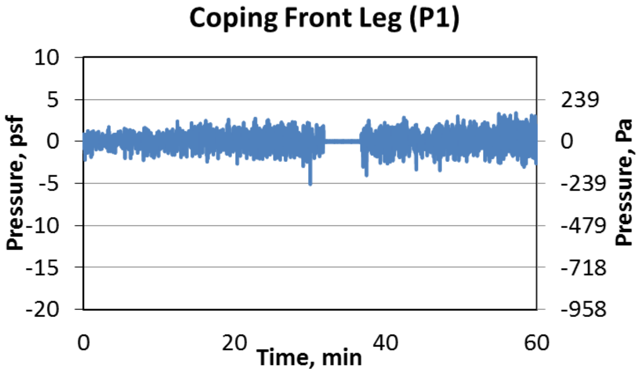

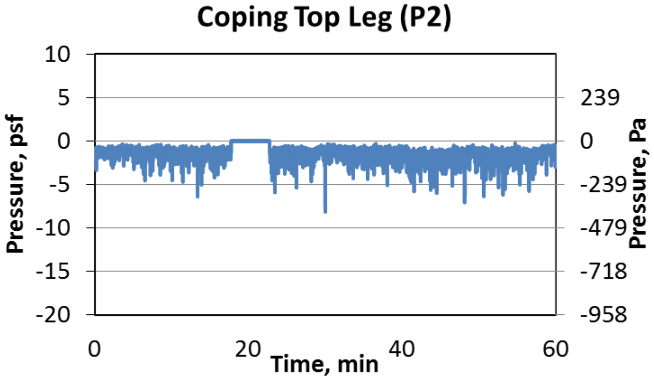

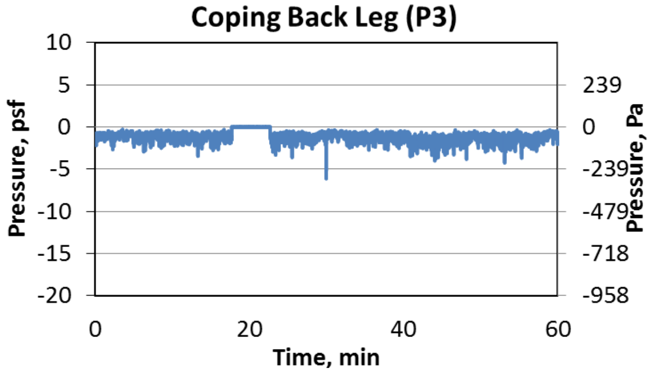

	Wind Speed, mph(kph)		Coping front leg (P1)	Coping Top Leg (P2)	Coping Back Leg (P3)
Peak	46 (74)	Pressure, psf (Pa)	3.4 (162.8)	0.0 (0)	0.0 (0)
Mean	21 (33)	Mean, psf (Pa)	0.3 (16.2)	-1.3 (-62.3)	-1.1 (-54.6)
		Suction, psf (Pa)	-5.1 (-243.7)	-8.1 (-390)	-6.1 (-292.9)

June 20, 2014

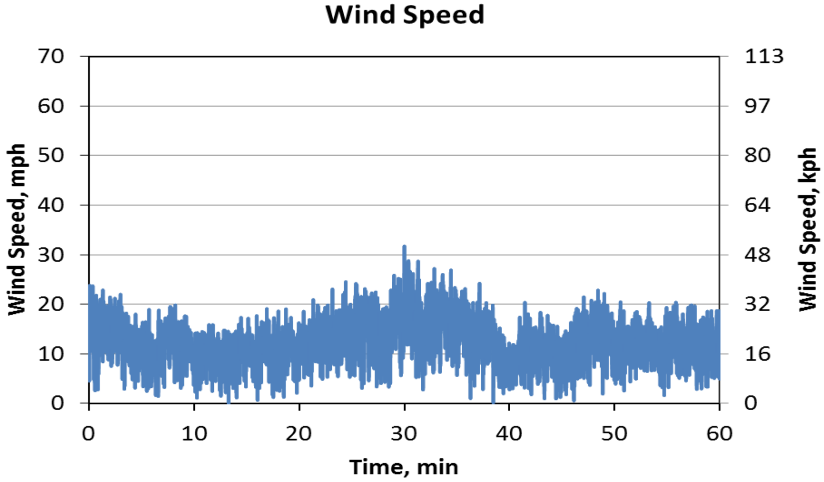

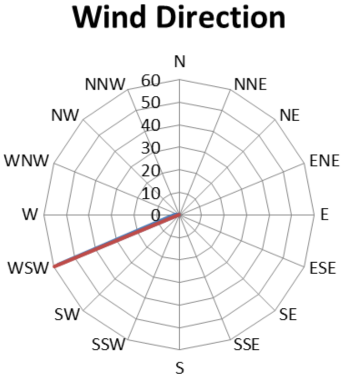

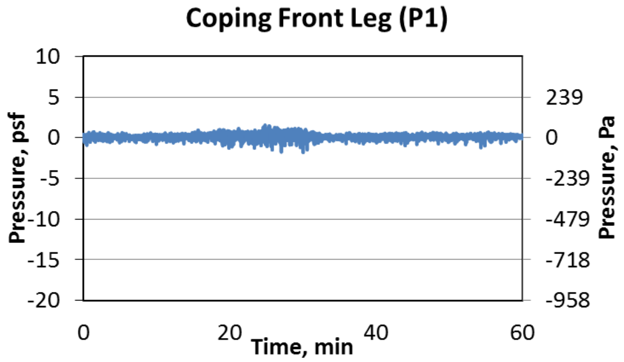

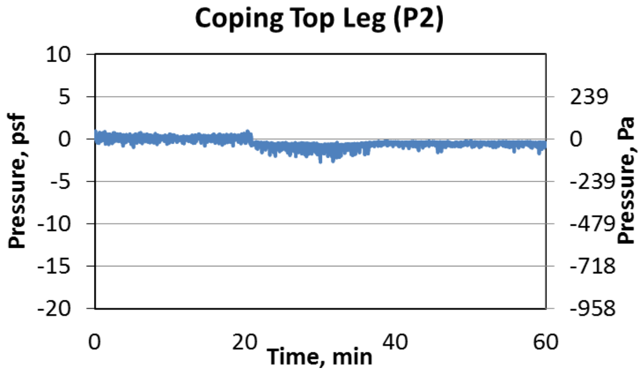

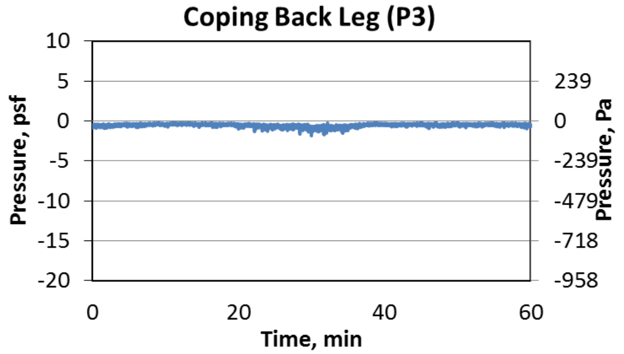

	Wind Speed, mph(kph)		Coping front leg (P1)	Coping Top Leg (P2)	Coping Back Leg (P3)
Peak	32 (51)	Pressure, psf (Pa)	1.6 (74.5)	0.9 (45)	0.0 (0)
Mean	13 (20)	Mean, psf (Pa)	0.2 (8.5)	-0.4 (-17)	-0.5 (-25.1)
		Suction, psf (Pa)	-1.8 (-86.1)	-2.7 (-129.3)	-1.8 (-87.2)

Appendix C

CCC

The following appendix shows all the raw data from the present study for the Continuous Cleat Configuration. Each of the 16 recorded days illustrates the hour wind speed and direction for the day and the hourly data for the pressure taps. The table at the bottom of each page shows the peak and mean hourly wind speed. As well as the peak pressure, the mean, and the peak suction of each pressure tap during the hourly data.

NOV 2, 2013

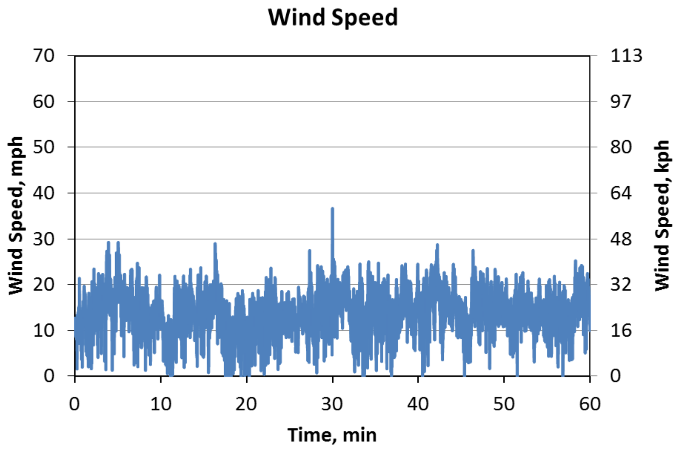

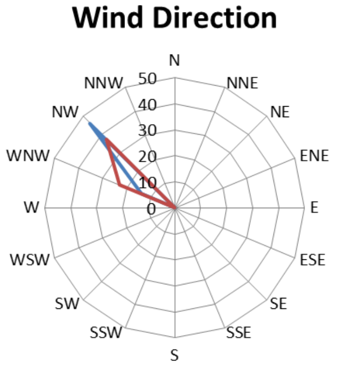

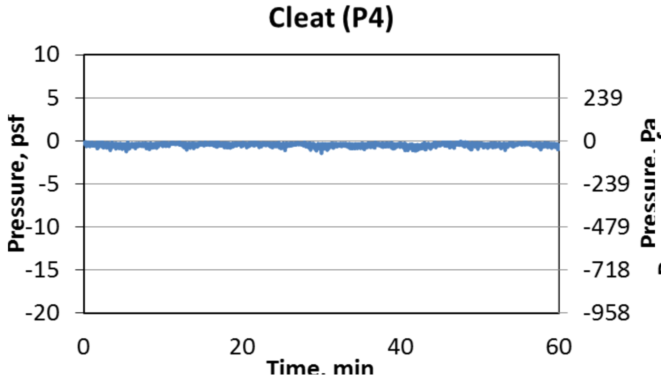

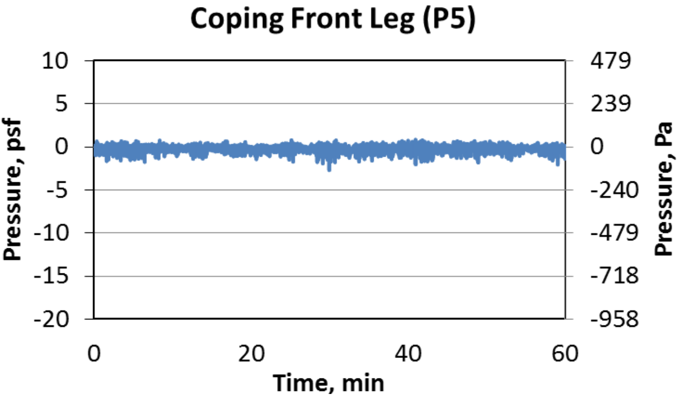

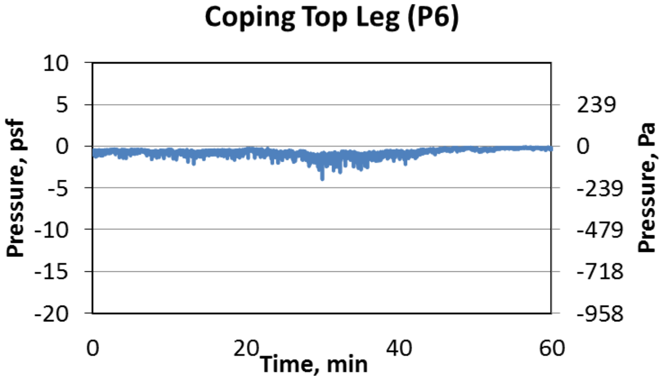

	Wind Speed, mph(kph)		Cleat (P4)	Coping Front Leg (P5)	Coping Top Leg (P6)
Peak	36 (59)	Pressure, psf (Pa)	0.0 (0)	0.8 (39.6)	0.0 (0)
Mean	14 (22)	Mean, psf (Pa)	-0.4 (-21.4)	-0.2 (-10.6)	-0.7 (-33.1)
		Suction, psf (Pa)	-1.4 (-68.7)	-2.7 (-129.3)	-4.0 (-190.7)

NOV 14, 2013

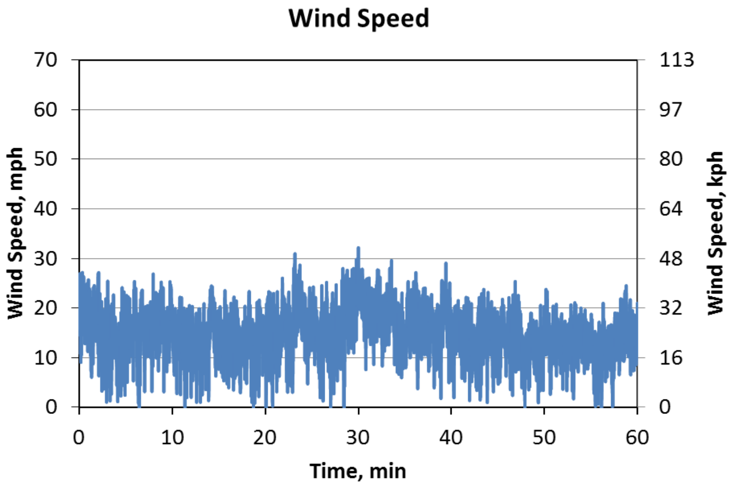
Wind Speed

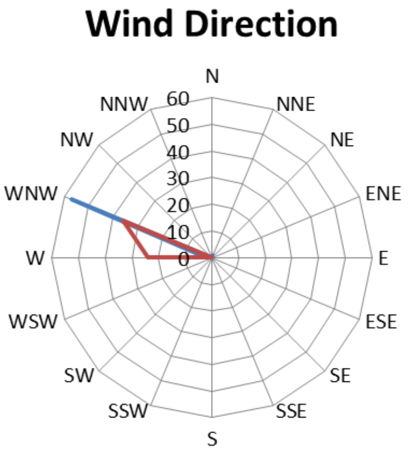
Wind Direction

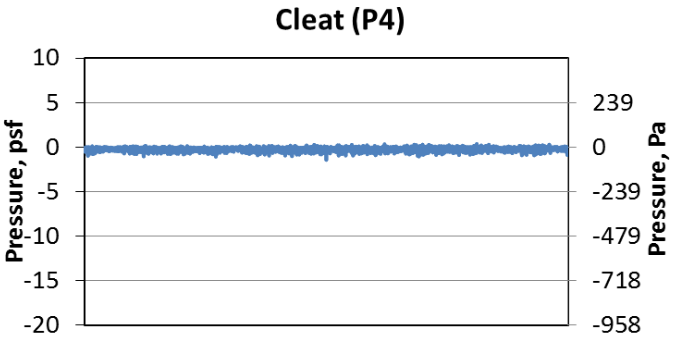
Cleat (P4)

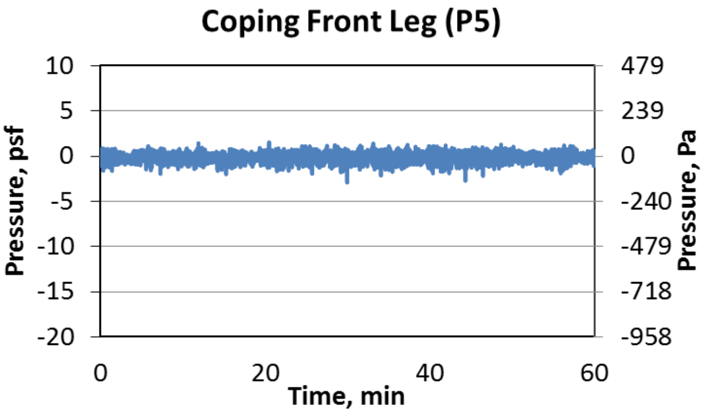
Coping Front Leg (P5)

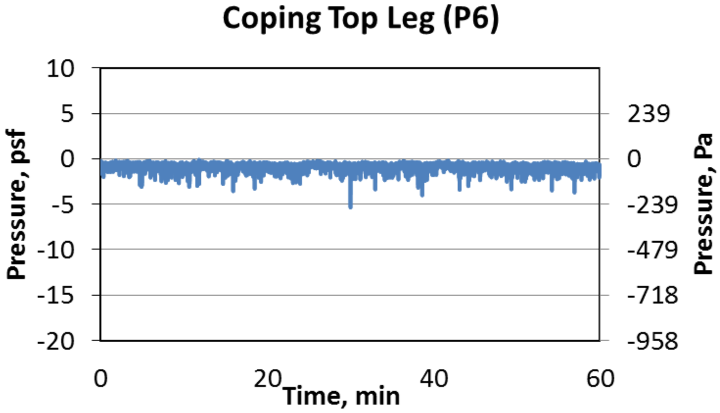
Coping Top Leg (P6)

	Wind Speed, mph(kph)		Cleat (P4)	Coping Front Leg (P5)	Coping Top Leg (P6)
Peak	32 (52)	Pressure, psf (Pa)	0.4 (17.3)	1.5 (73.1)	0.0 (0)
Mean	15 (24)	Mean, psf (Pa)	-0.2 (-11.5)	-0.1 (-3.7)	-0.8 (-39.9)
		Suction, psf (Pa)	-1.4 (-68.5)	-2.9 (-139.5)	-5.3 (-253.4)

NOV 15, 2013

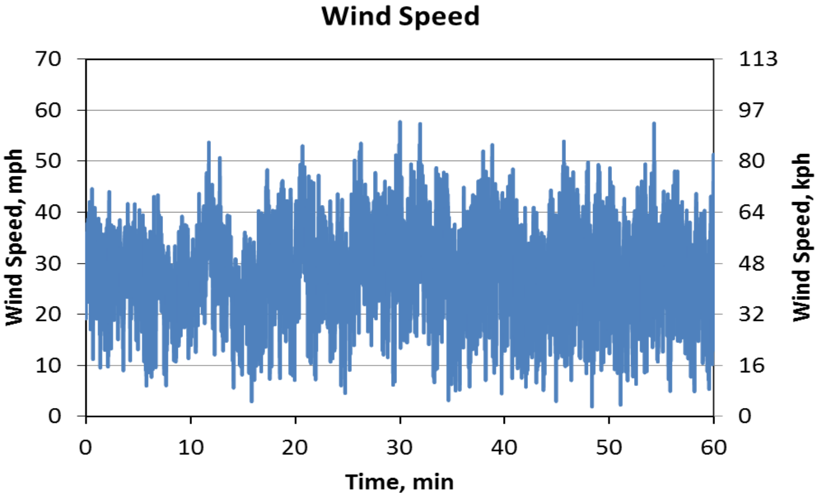
Wind Speed

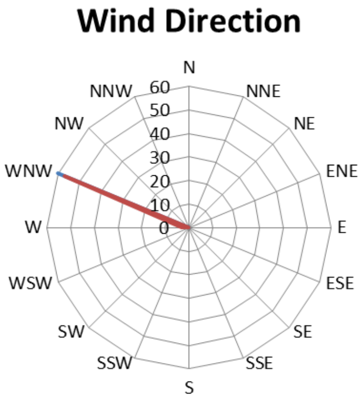
Wind Direction

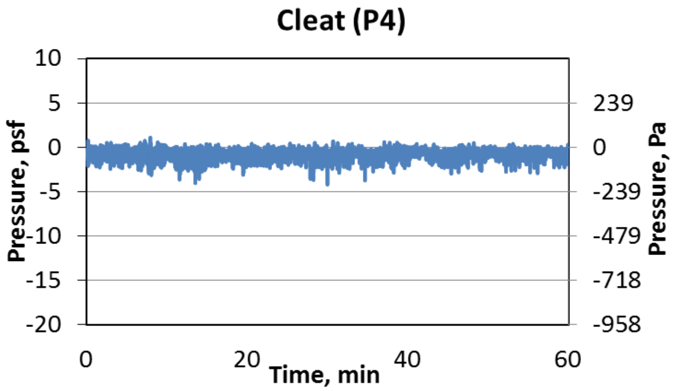
Cleat (P4)

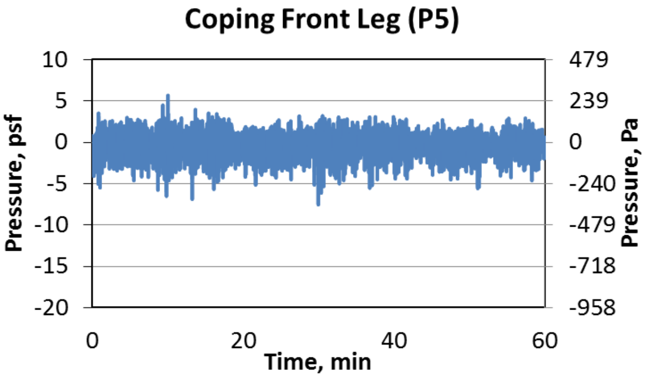
Coping Front Leg (P5)

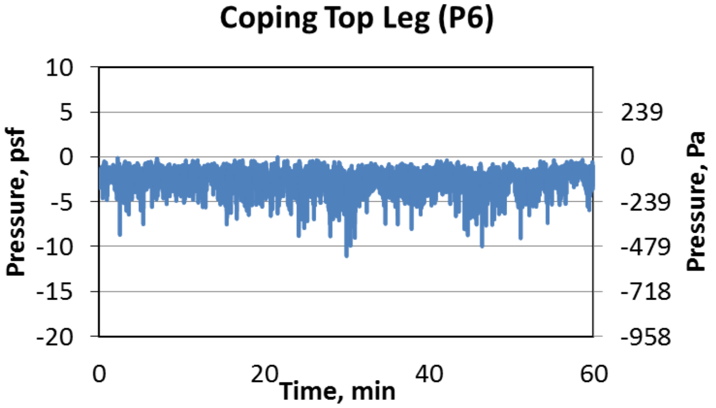
Coping Top Leg (P6)

	Wind Speed, mph(kph)		Cleat (P4)	Coping Front Leg (P5)	Coping Top Leg (P6)
Peak	58 (93)	Pressure, psf (Pa)	1.1 (52.7)	5.7 (271.9)	0.0 (0)
Mean	29 (47)	Mean, psf (Pa)	-0.8 (-39.6)	-0.3 (-14.6)	-2.3 (-110.5)
		Suction, psf (Pa)	-4.2 (-201)	-7.5 (-361)	-11.1 (-529.5)

NOV 16, 2013

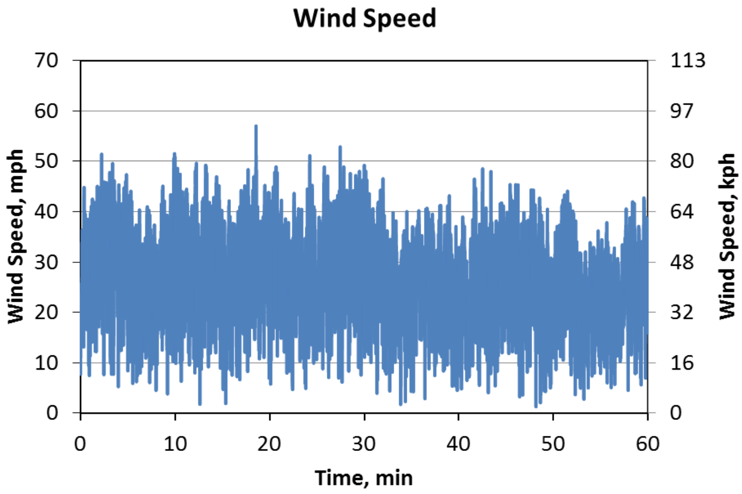

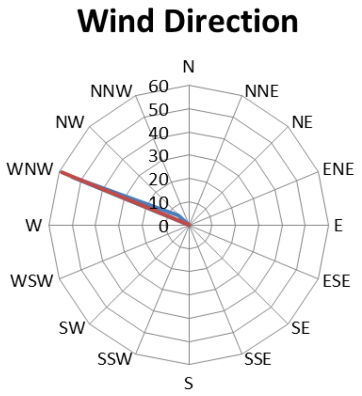

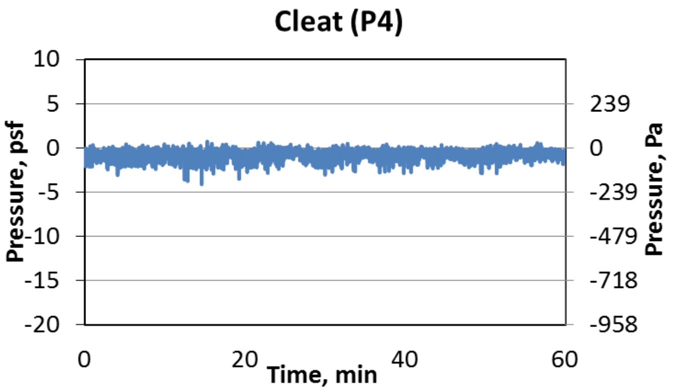

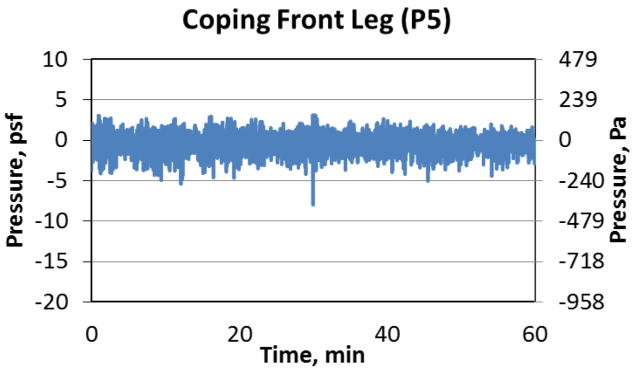

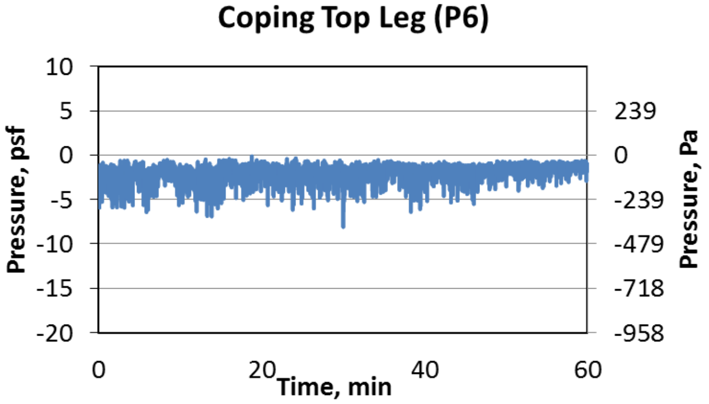

	Wind Speed, mph(kph)		Cleat (P4)	Coping Front Leg (P5)	Coping Top Leg (P6)
Peak	49 (79)	Pressure, psf (Pa)	0.7 (34.7)	3.1 (148.6)	0.0 (0)
Mean	28 (45)	Mean, psf (Pa)	-0.8 (-38.0)	-0.3 (-14.1)	-1.8 (-88.3)
		Suction, psf (Pa)	-3.0 (-195.3)	-8.0 (-382.1)	-8.1 (-387.7)

NOV 19, 2013

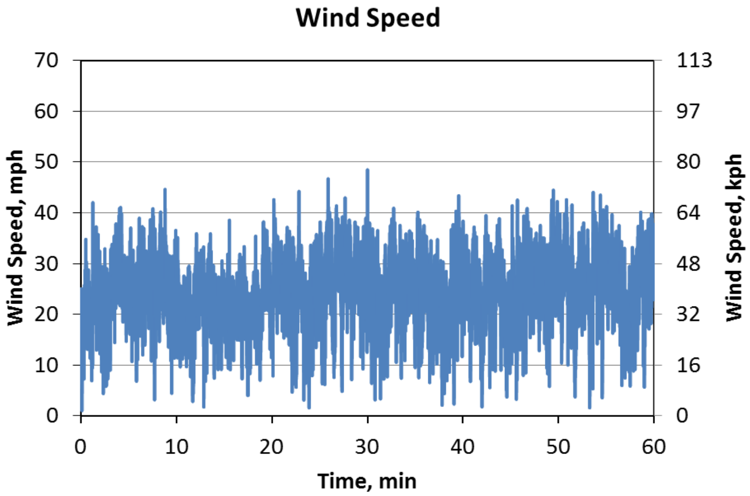

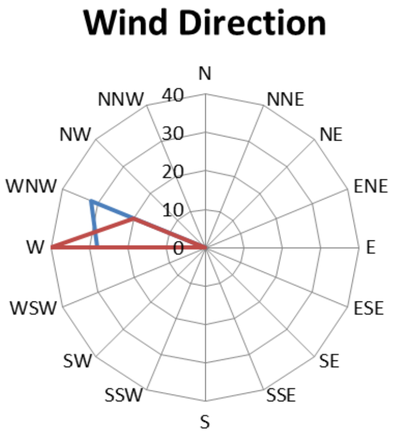

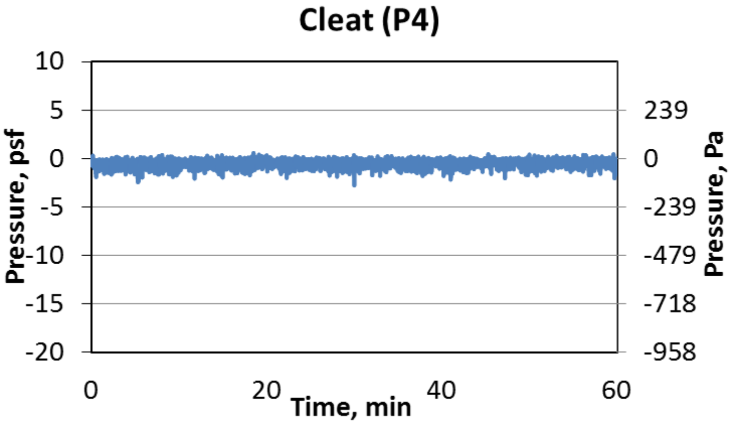

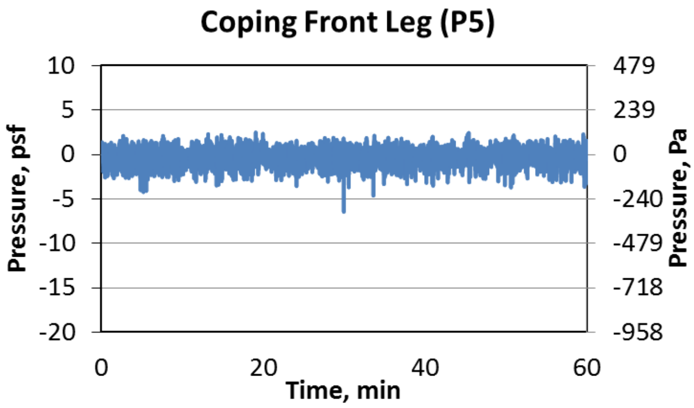

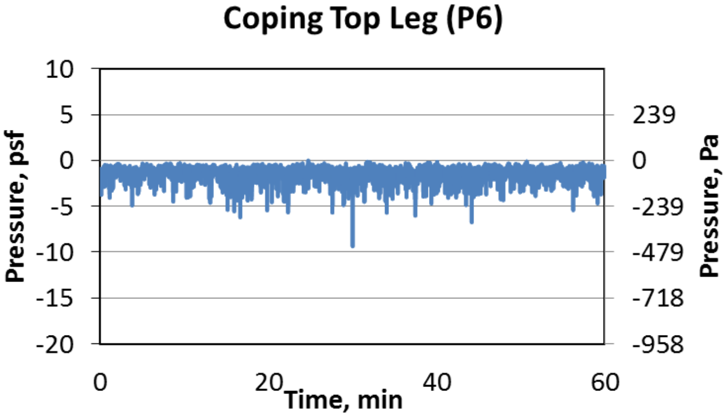

	Wind Speed, mph(kph)		Cleat (P4)	Coping Front Leg (P5)	Coping Top Leg (P6)
Peak	49 (79)	Pressure, psf (Pa)	0.6 (27.8)	2.5 (118.8)	0.0 (0)
Mean	25 (40)	Mean, psf (Pa)	-0.5 (-24.1)	-0.2 (-8.8)	-1.4 (-65.2)
		Suction, psf (Pa)	-2.8 (-132.8)	-6.4 (-306)	-9.3 (-446.3)

Dec 1, 2013

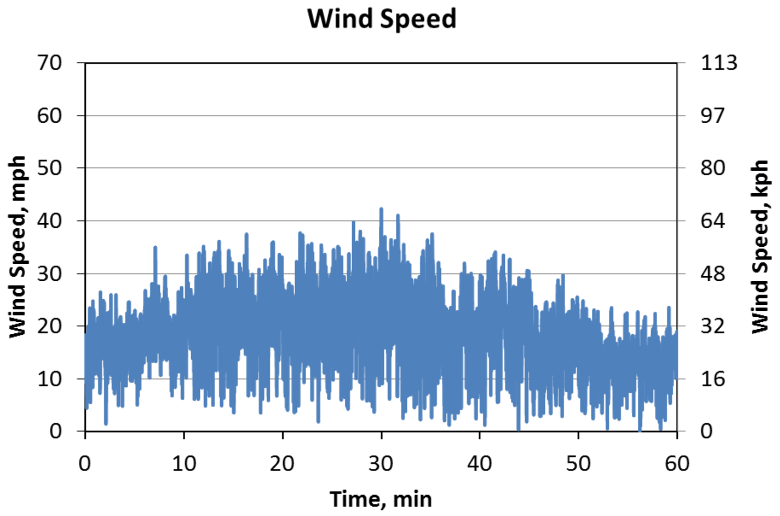

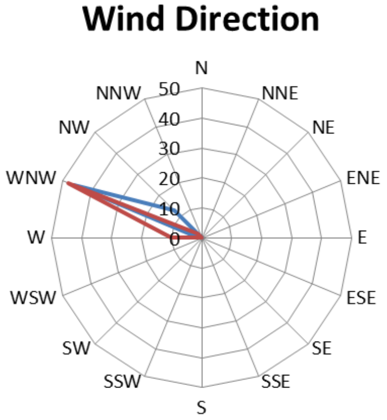

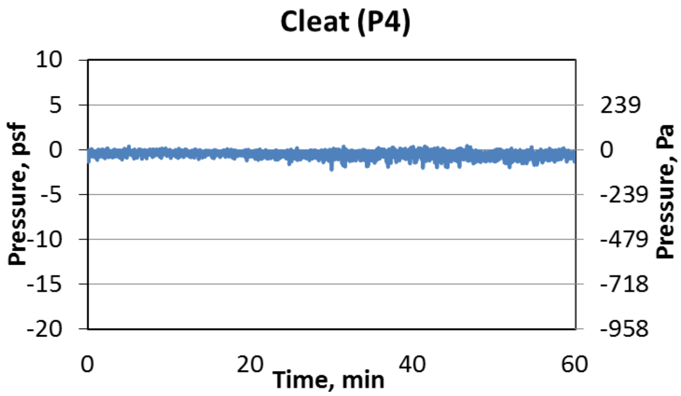

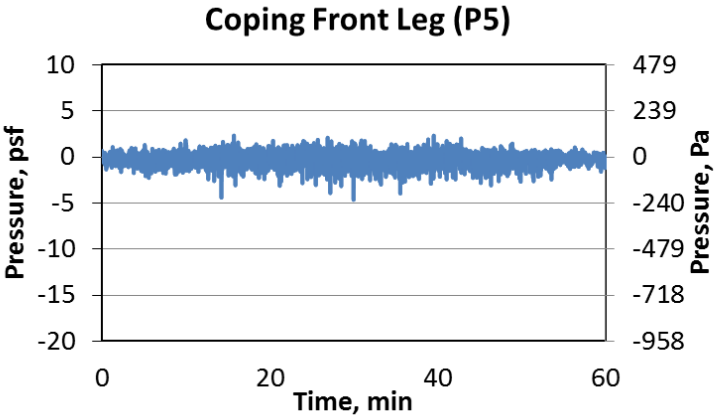

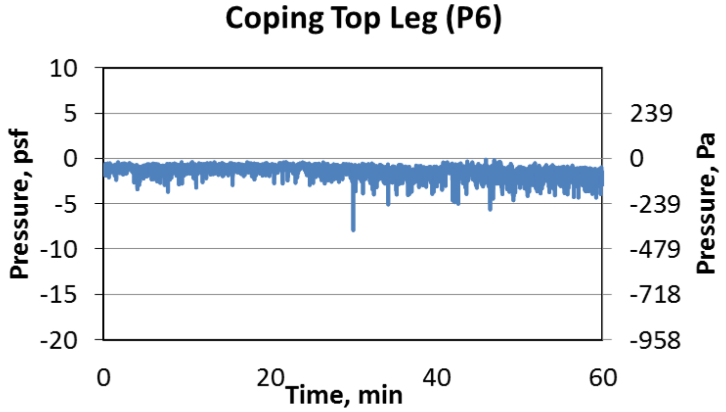

	Wind Speed, mph(kph)		Cleat (P4)	Coping Front Leg (P5)	Coping Top Leg (P6)
Peak	42 (68)	Pressure, psf (Pa)	0.4 (20.7)	2.3 (111.1)	0.0 (0)
Mean	19 (30)	Mean, psf (Pa)	-0.5 (-22.6)	-0.2 (-8.8)	-1.3 (62.2)
		Suction, psf (Pa)	-2.2 (-105.9)	-4.7 (-222.7)	-7.9 (-379.2)

Dec 2, 2013

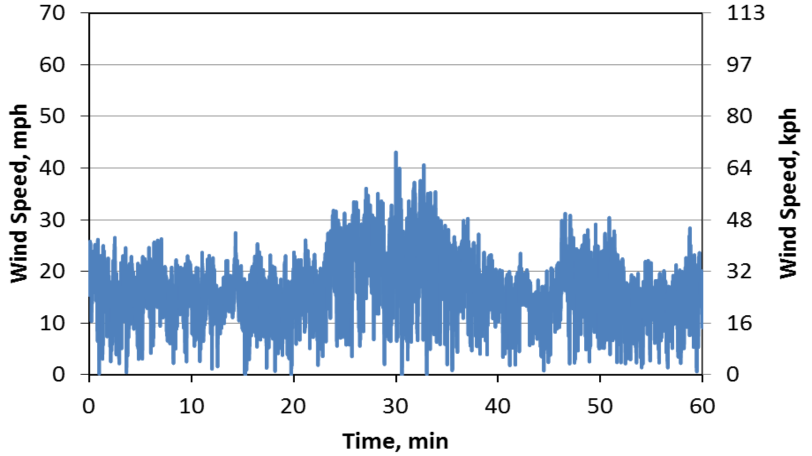
Wind Speed

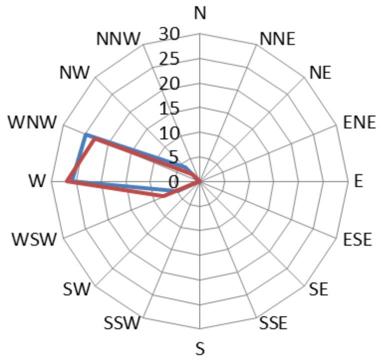
Wind Direction

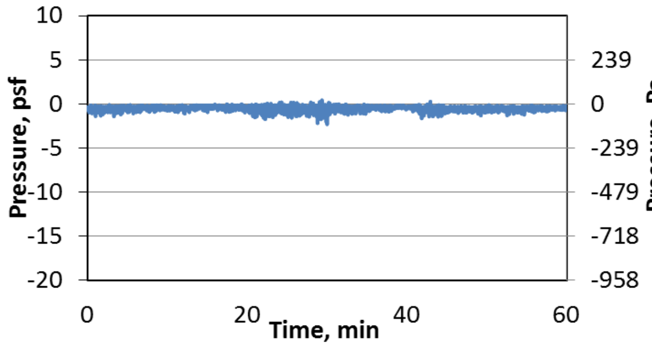
Cleat (P4)

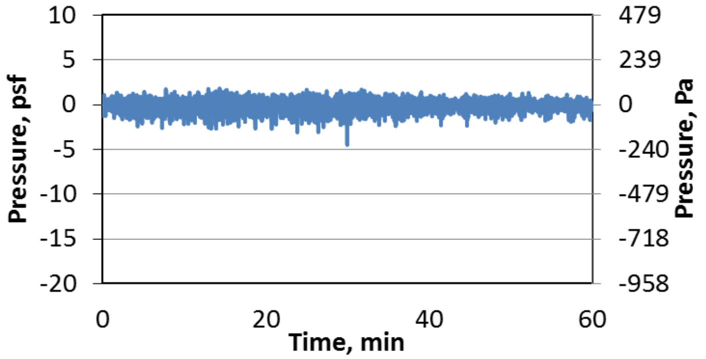
Coping Front Leg (P5)

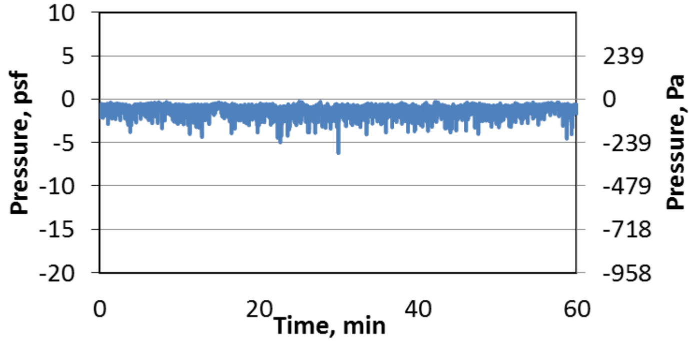
Coping Top Leg (P6)

	Wind Speed, mph(kph)		Cleat (P4)	Coping Front Leg (P5)	Coping Top Leg (P6)
Peak	43 (69)	Pressure, psf (Pa)	0.4 (20.5)	1.8 (86.6)	0.0 (0)
Mean	17 (27)	Mean, psf (Pa)	-0.5 (-24.4)	0.0 (0)	-1.2 (-55.6)
		Suction, psf (Pa)	-2.3 (-110.2)	-4.5 (-213.2)	-6.2 (-297)

Dec 18, 2013

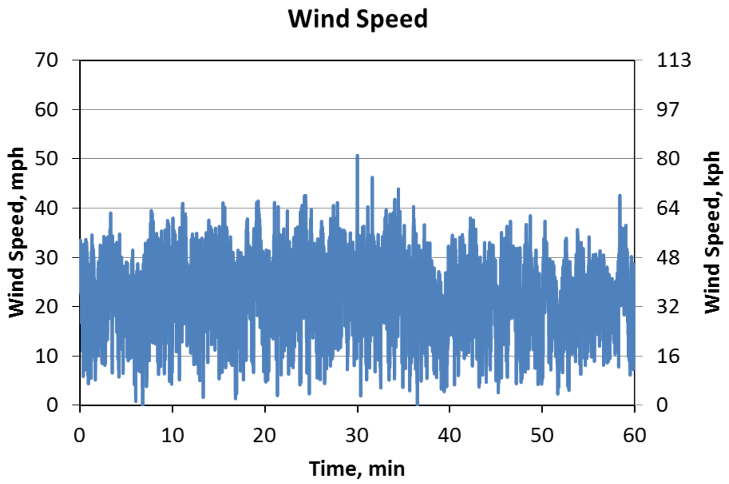

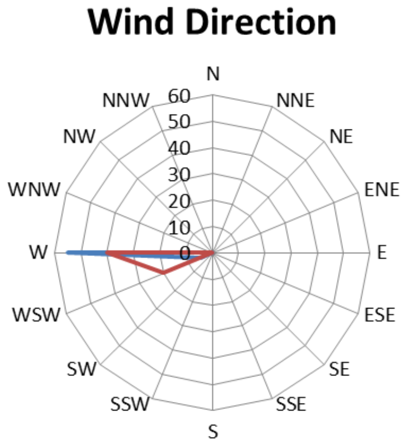

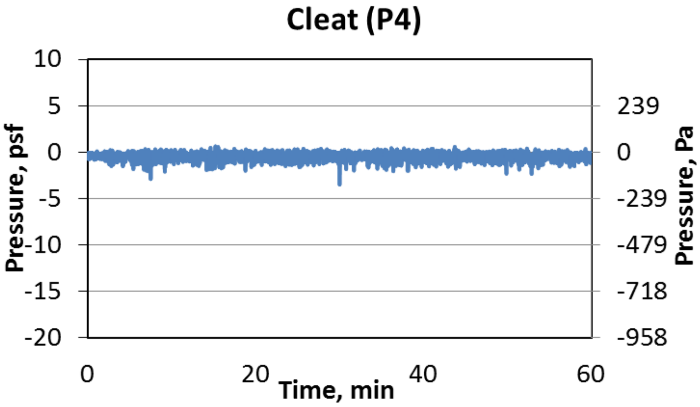

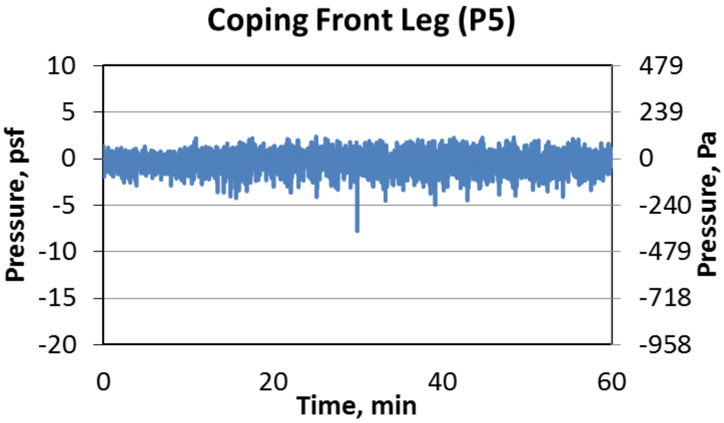

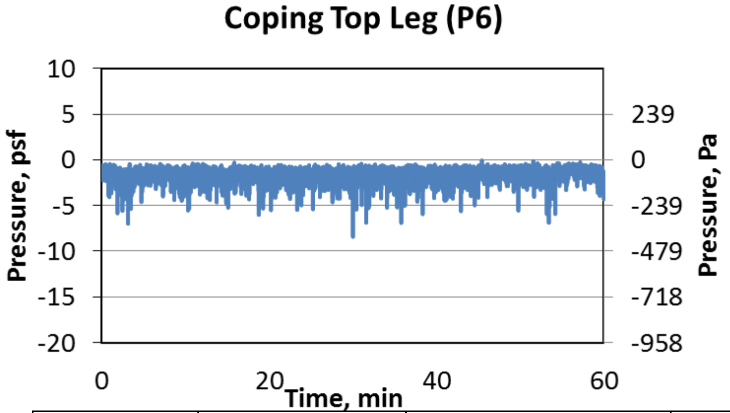

	Wind Speed, mph(kph)		Cleat (P4)	Coping Front Leg (P5)	Coping Top Leg (P6)
Peak	50 (81)	Pressure, psf (Pa)	0.6 (30.4)	2.4 (113.5)	0.0 (0)
Mean	23 (37)	Mean, psf (Pa)	-0.4 (-21.3)	-0.2 (-9.9)	-1.5 (-72.7)
		Suction, psf (Pa)	-3.5 (-167.1)	-7.7 (-370.9)	-8.4 (-400.6)

Dec 23, 2013

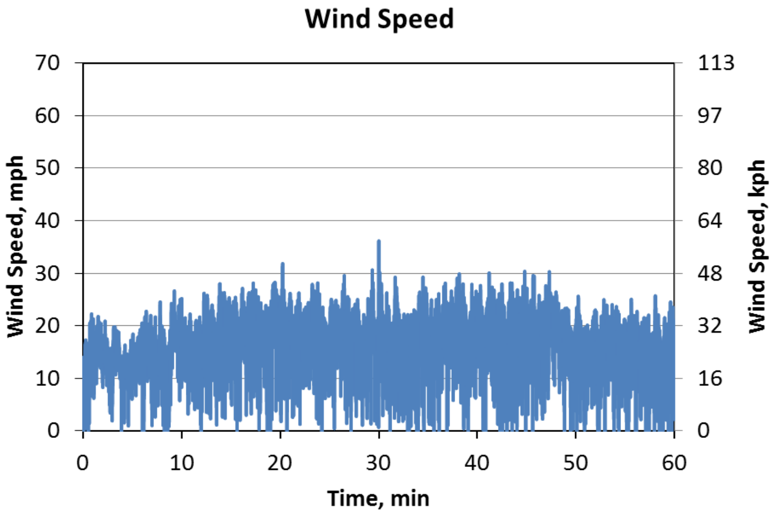

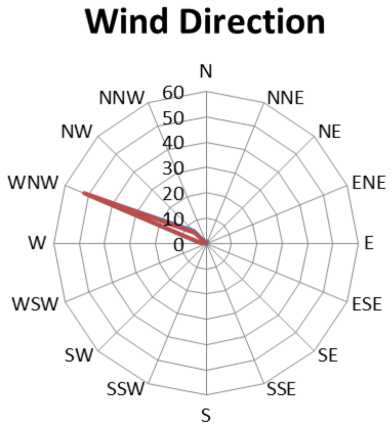

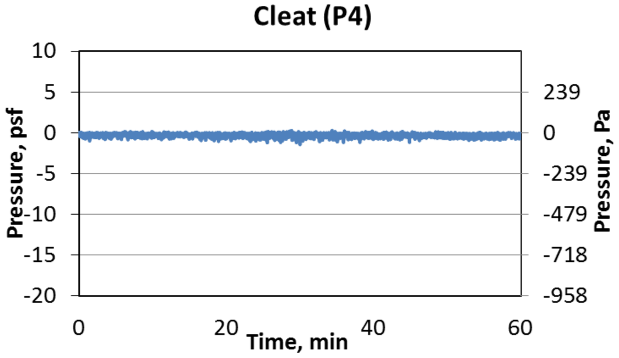

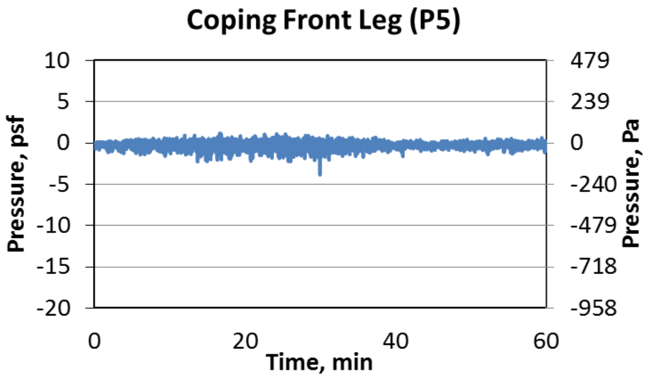

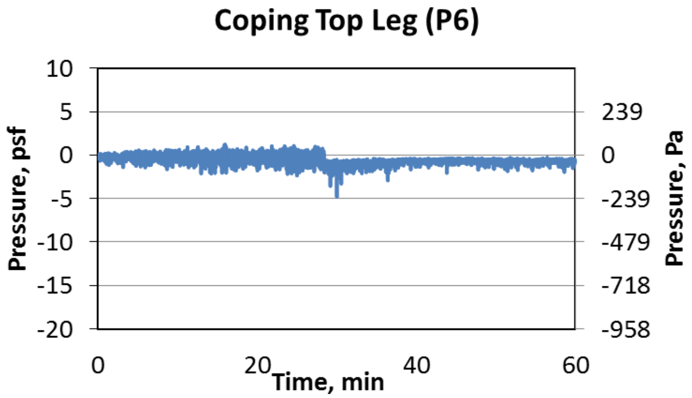

	Wind Speed, mph(kph)		Cleat (P4)	Coping Front Leg (P5)	Coping Top Leg (P6)
Peak	36 (58)	Pressure, psf (Pa)	0.3 (13.4)	1.2 (56.3)	1.2 (57.7)
Mean	17 (27)	Mean, psf (Pa)	-0.3 (-14.5)	-0.2 (-10.6)	-0.5 (-24.3)
		Suction, psf (Pa)	-1.4 (-68.8)	-3.8 (-183.9)	-4.8 (-229)

Feb 20, 2014

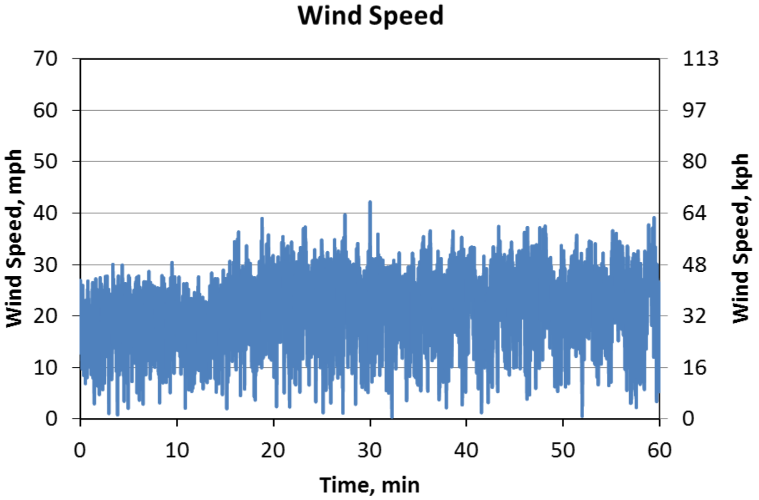

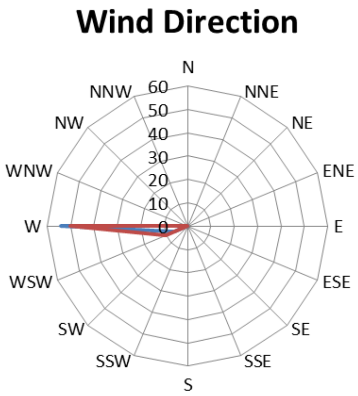

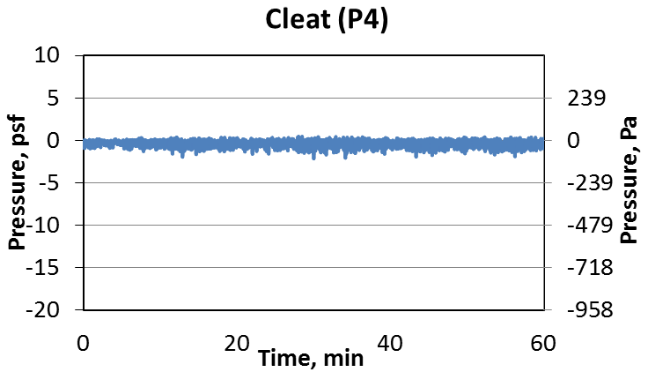

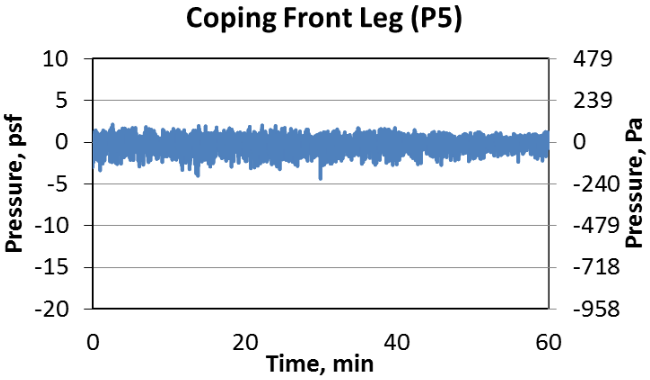

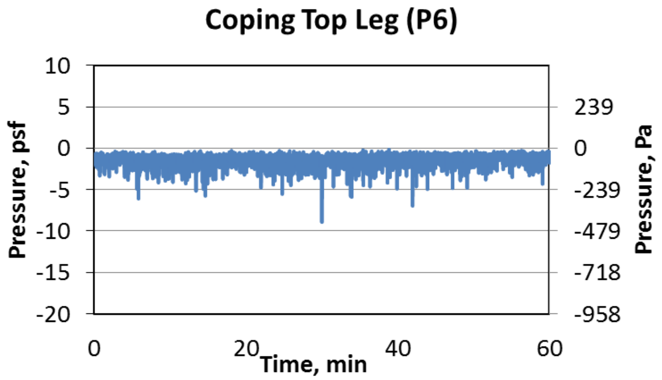

	Wind Speed, mph(kph)		Cleat (P4)	Coping Front Leg (P5)	Coping Top Leg (P6)
Peak	42 (68)	Pressure, psf (Pa)	0.5 (21.8)	2.1 (102.1)	0.0 (0)
Mean	22 (35)	Mean, psf (Pa)	-0.4 (-18.1)	-0.1 (-7.1)	-1.3 (-64.1)
		Suction, psf (Pa)	-2.1 (-102.4)	-4.4 (-209.1)	-8.9 (-425.7)

Feb 21, 2014

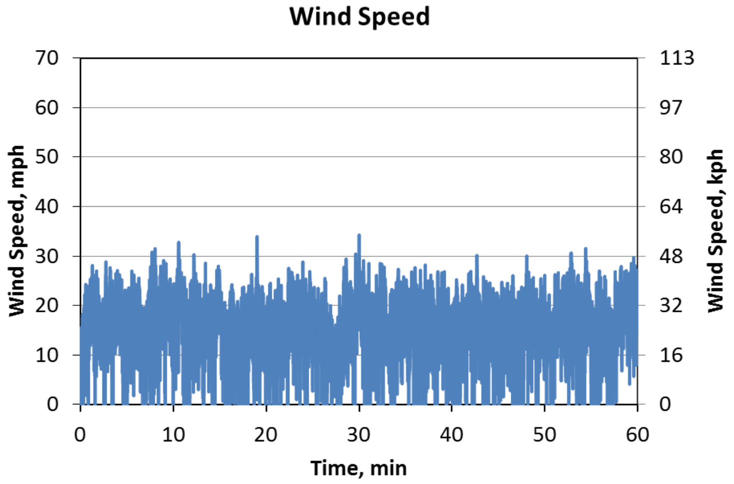

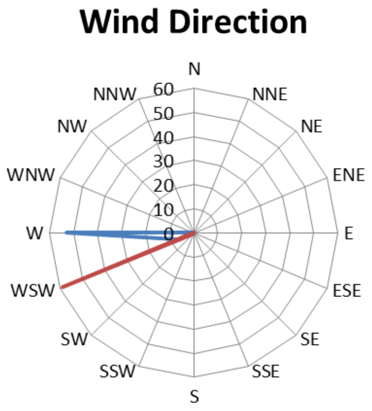

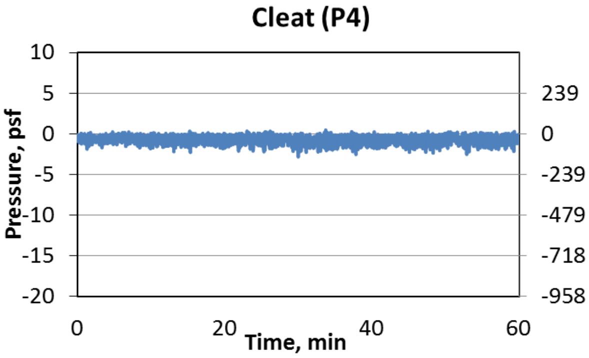

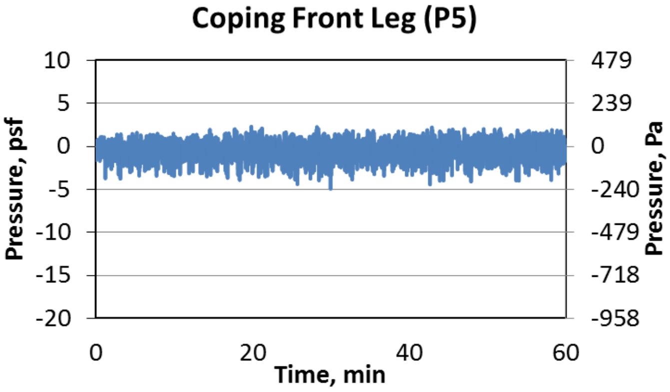

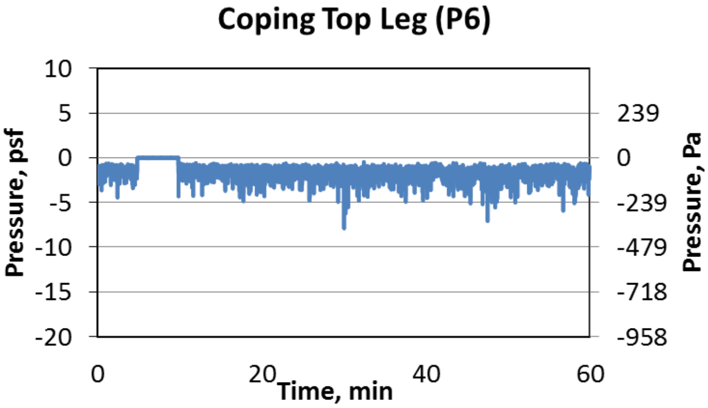

	Wind Speed, mph(kph)		Cleat (P4)	Coping Front Leg (P5)	Coping Top Leg (P6)
Peak	34 (55)	Pressure, psf (Pa)	0.5 (22.3)	2.3 (108.3)	0.0 (0)
Mean	16 (26)	Mean, psf (Pa)	-0.7 (-33)	-0.4 (-19)	-1.5 (-70.1)
		Suction, psf (Pa)	-2.8 (-134.9)	-4.9 (-236.2)	-7.9 (-376.2)

April 17, 2014

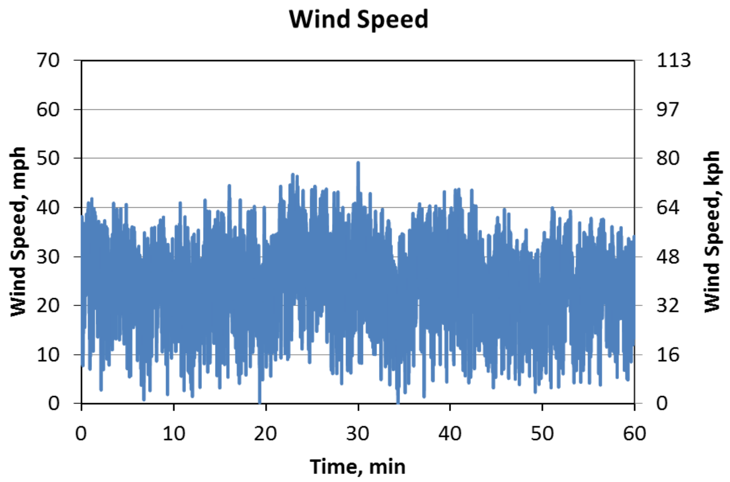

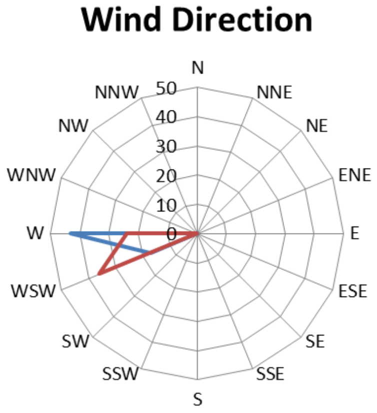

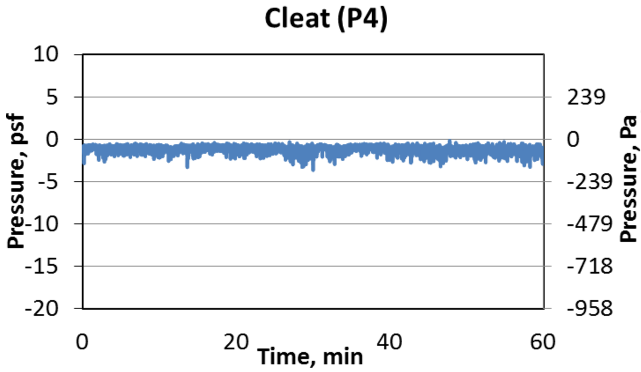

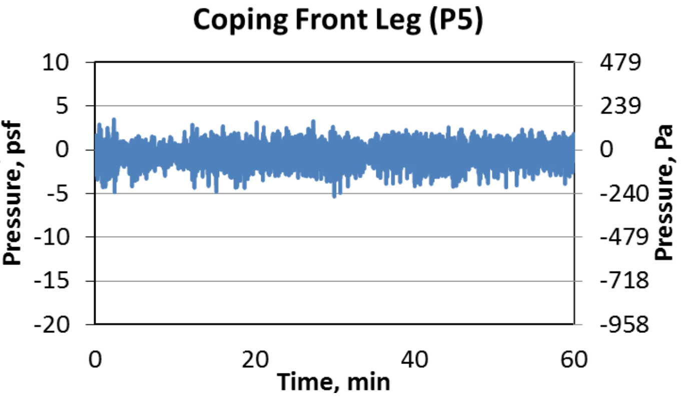

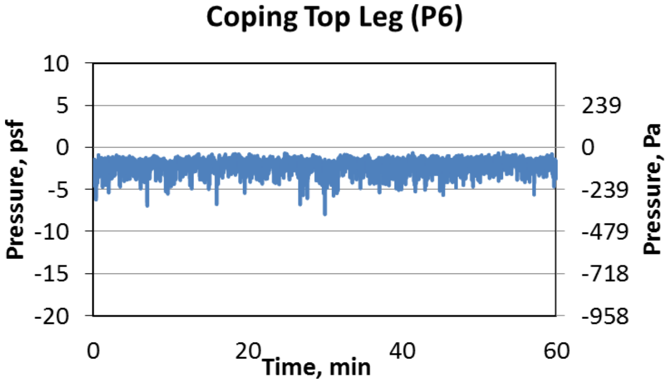

	Wind Speed, mph(kph)		Cleat (P4)	Coping Front Leg (P5)	Coping Top Leg (P6)
Peak	49 (79)	Pressure, psf (Pa)	0.0 (0)	3.5 (166.4)	0.0
Mean	25 (41)	Mean, psf (Pa)	-1.2 (-58.3)	-0.3 (-15.7)	-2.1 (-98.7)
		Suction, psf (Pa)	-3.6 (-174.4)	-5.3 (-255)	-8.0 (-381.1)

April 21, 2014

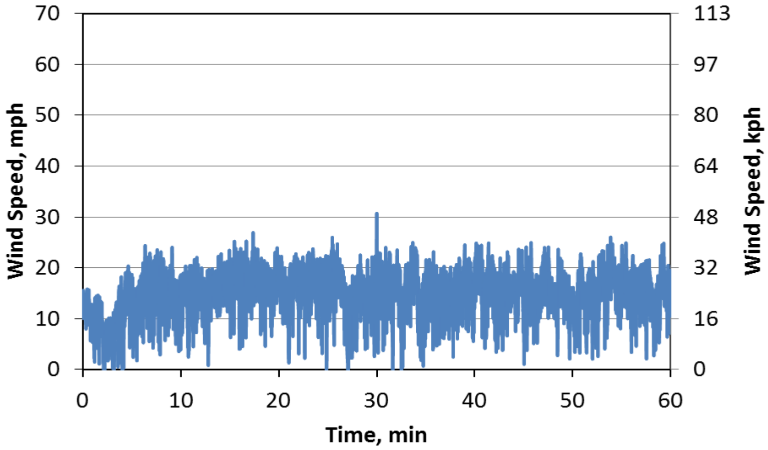

Wind Speed

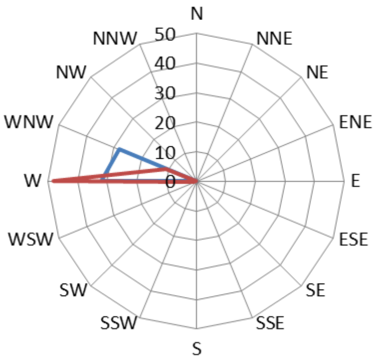

Wind Direction

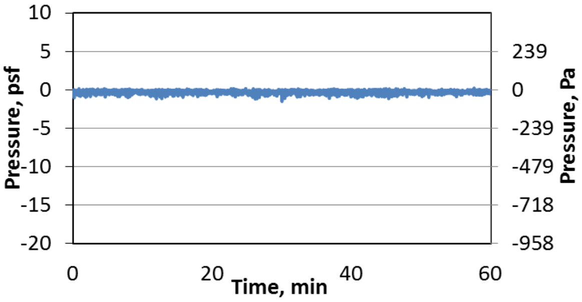

Cleat (P4)

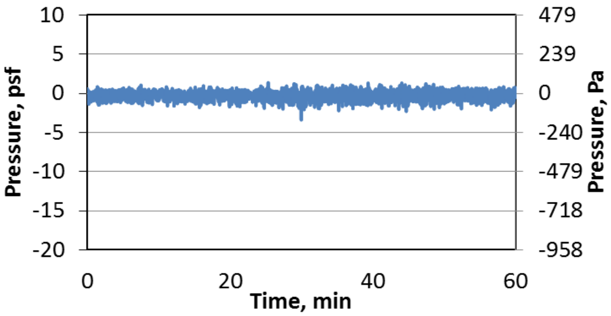

Coping Front Leg (P5)

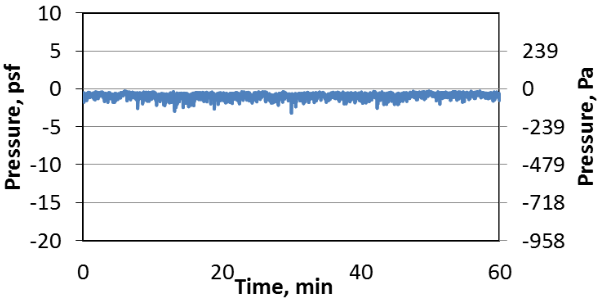

Coping Top Leg (P6)

	Wind Speed, mph(kph)		Cleat (P4)	Coping Front Leg (P5)	Coping Top Leg (P6)
Peak	30 (49)	Pressure, psf (Pa)	0.2 (10.8)	1.4 (64.7)	0.0 (0)
Mean	15 (24)	Mean, psf (Pa)	-0.3 (-14.2)	-0.2 (-9)	-0.9 (-41.9)
		Suction, psf (Pa)	-1.5 (-71.4)	-3.4(-160.7)	-3.2 (-153.2)

April 22, 2014

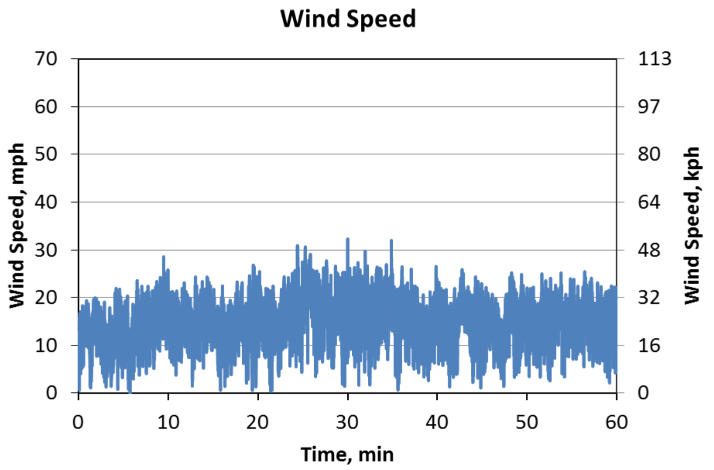
Wind Speed

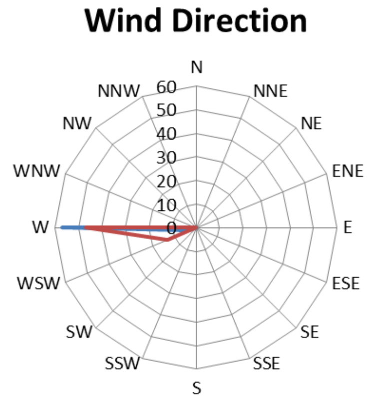
Wind Direction

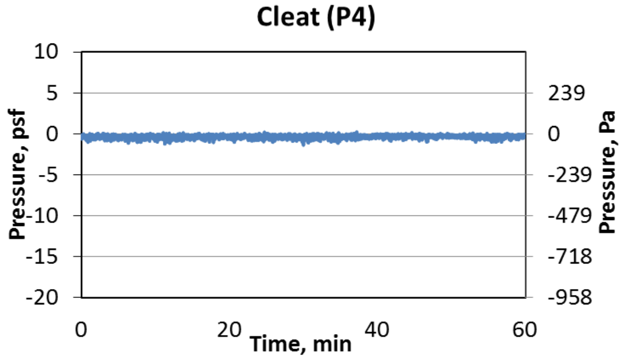
Cleat (P4)

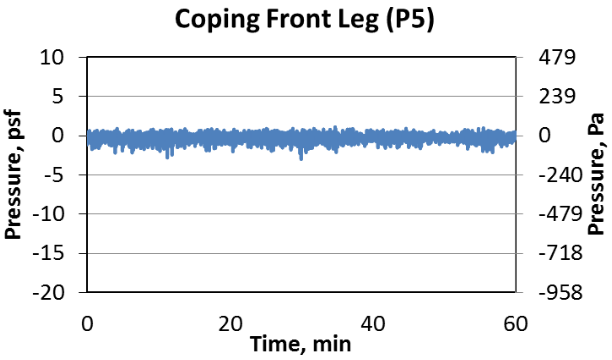
Coping Front Leg (P5)

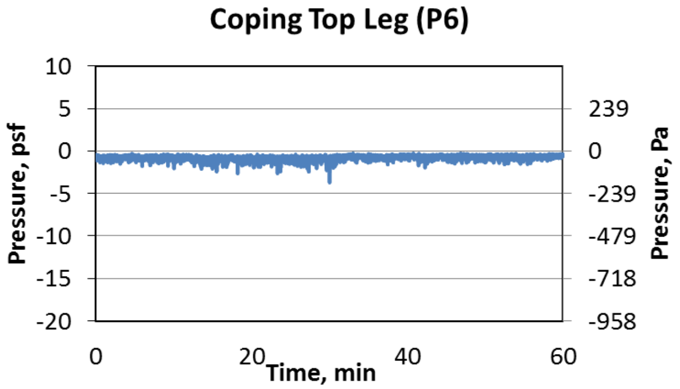
Coping Top Leg (P6)

	Wind Speed, mph(kph)		Cleat (P4)	Coping Front Leg (P5)	Coping Top Leg (P6)
Peak	32 (52)	Pressure, psf (Pa)	0.2 (10.6)	1.1 (53.5)	0.0 (0)
Mean	15 (25)	Mean, psf (Pa)	-0.3 (-16)	-0.2 (-9.6)	-0.8 (-37)
		Suction, psf (Pa)	-1.4 (-65)	-3.0 (-142.5)	-3.7 (-177.1)

June 9, 2014

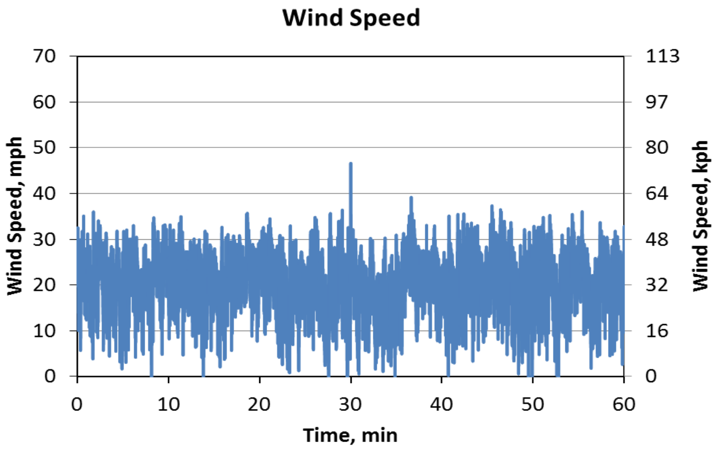
Wind Speed

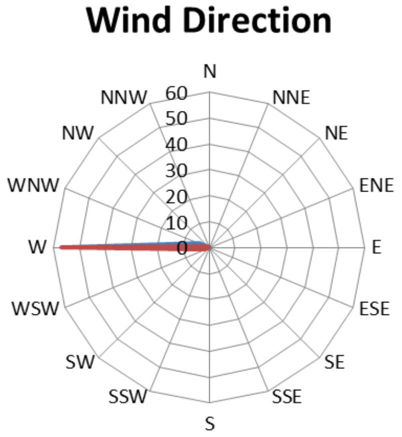
Wind Direction

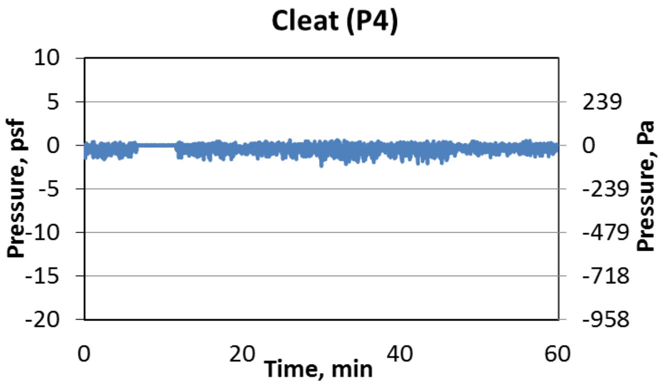
Cleat (P4)

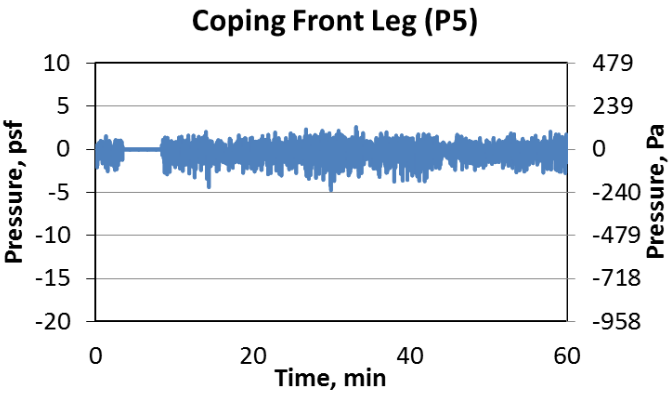
Coping Front Leg (P5)

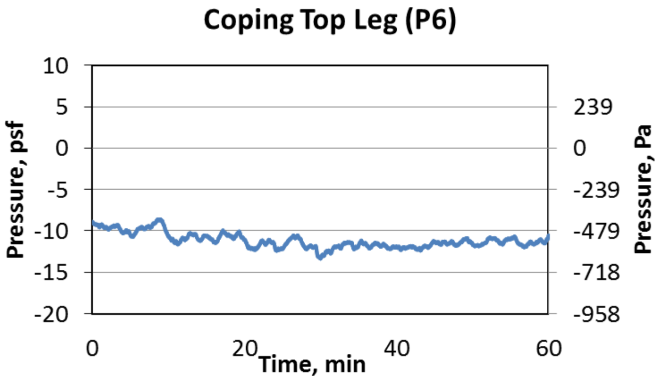
Coping Top Leg (P6)

	Wind Speed, mph(kph)		Cleat (P4)	Coping Front Leg (P5)	Coping Top Leg (P6)
Peak	46 (74)	Pressure, psf (Pa)	0.6 (29.6)	2.6 (124.2)	N/A
Mean	21 (33)	Mean, psf (Pa)	-0.3 (-16.5)	-0.2 (-7.8)	N/A
		Suction, psf (Pa)	-2.4 (-114.1)	-4.8 (-227.4)	N/A

June 20, 2014

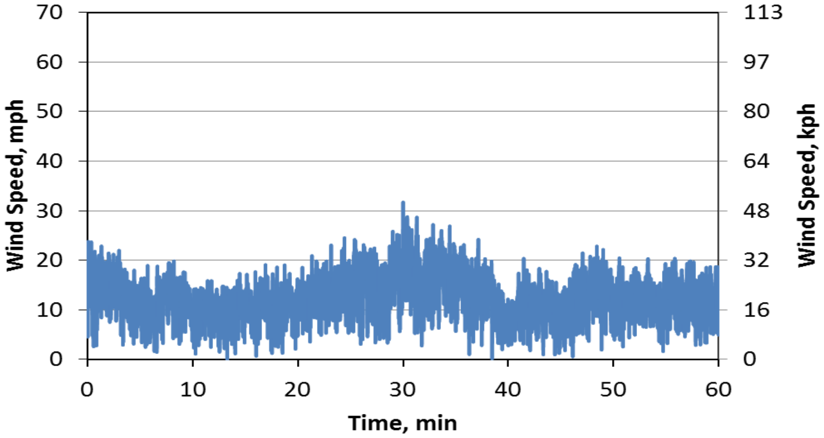

Wind Speed

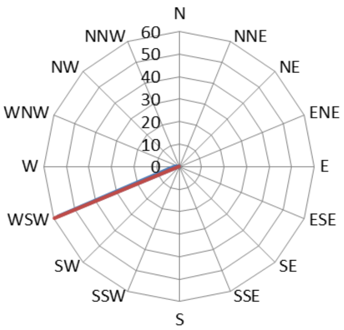

Wind Direction

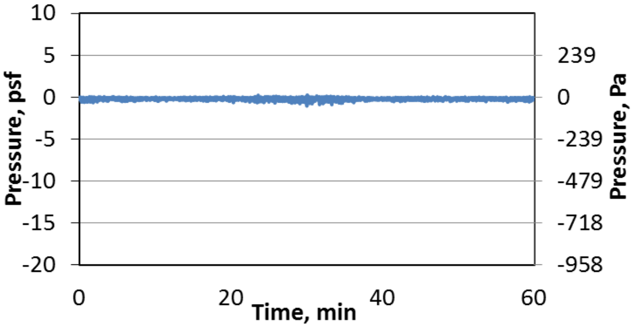

Cleat (P4)

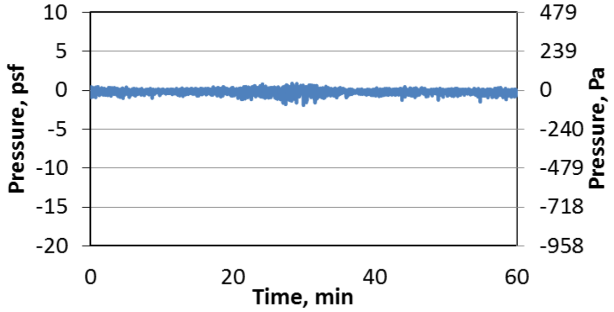

Coping Front Leg (P5)

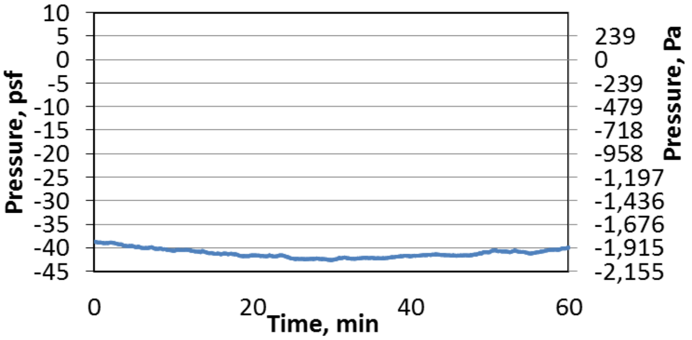

Coping Top Leg (P6)

	Wind Speed, mph(kph)		Cleat (P4)	Coping Front Leg (P5)	Coping Top Leg (P6)
Peak	32 (51)	Pressure, psf (Pa)	0.2 (117)	0.9 (42.1)	N/A
Mean	13 (20)	Mean, psf (Pa)	-0.2 (-9.3)	-0.1 (-6.8)	N/A
		Suction, psf (Pa)	-1.0 (-49.3)	-1.9 (-92.6)	N/A

Appendix D

DCC

The following appendix shows all the raw data from the present study for the Discontinuous Cleat Configuration. Each of the 16 recorded days illustrates the hour wind speed and direction for the day and the hourly data for the pressure taps. The table at the bottom of each page shows the peak and mean hourly wind speed. As well as the peak pressure, the mean, and the peak suction of each pressure tap during the hourly data.

NOV 2, 2013

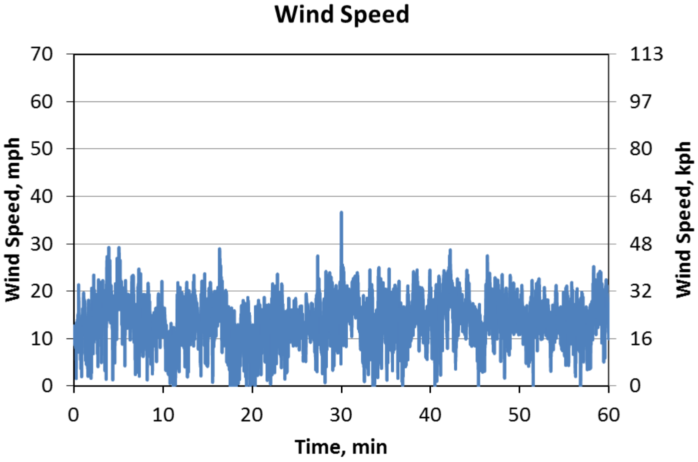
Wind Speed

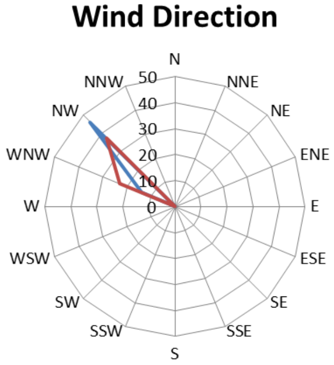
Wind Direction

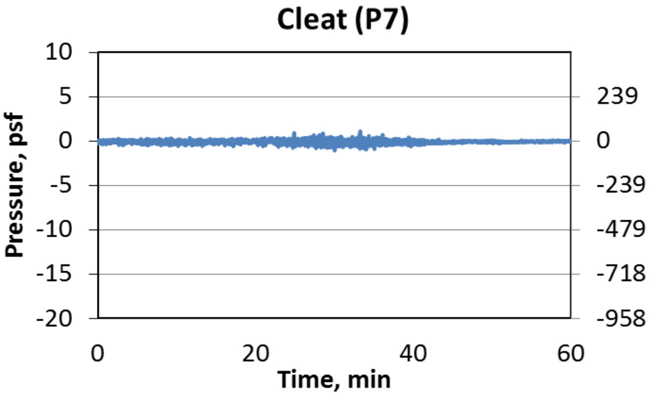
Cleat (P7)

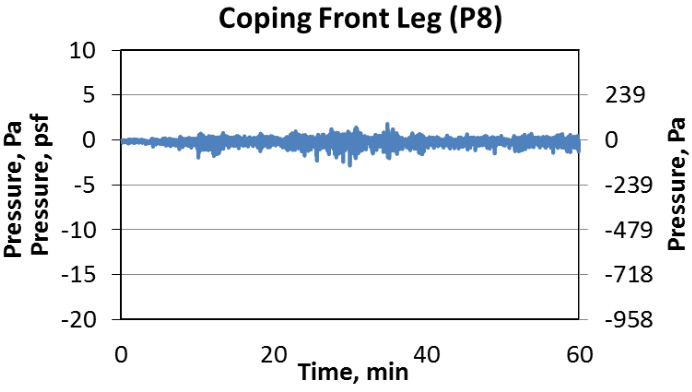
Coping Front Leg (P8)

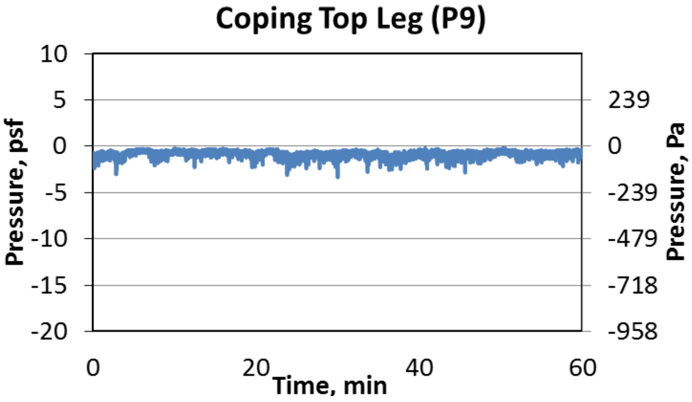
Coping Top Leg (P9)

	Wind Speed, mph(kph)		Cleat (P7)	Coping Front Leg (P8)	Coping Top Leg (P9)
Peak	36 (59)	Pressure, psf (Pa)	1.1 (51.2)	1.8 (85.9)	0.0 (0)
Mean	14 (22)	Mean, psf (Pa)	-0.1 (-4.5)	-0.1 (-4.8)	-0.8 (-38.6)
		Suction, psf (Pa)	-1.1 (-52.2)	-2.9 (-136.5)	-3.3 (-160.1)

NOV 14, 2013

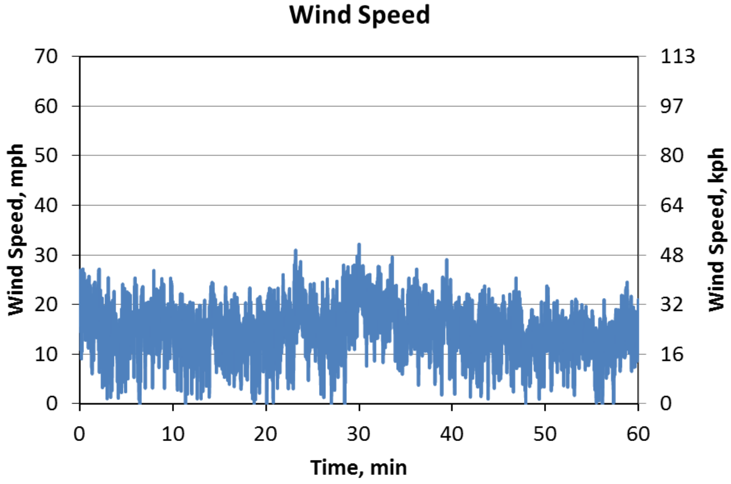

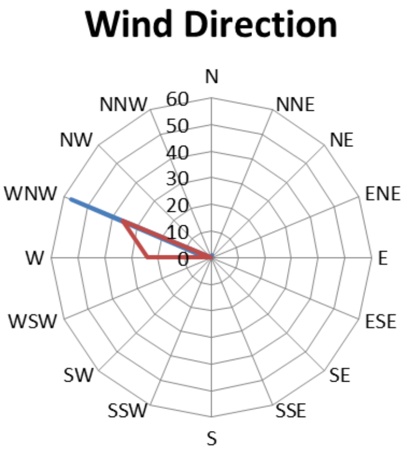

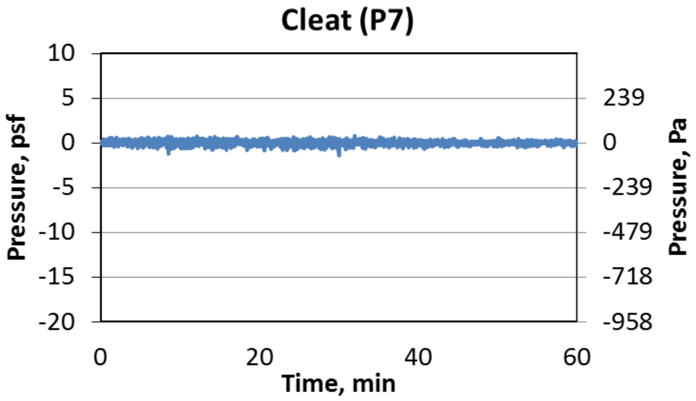

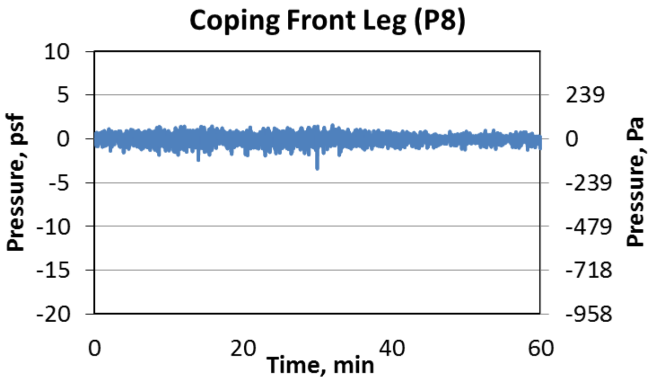

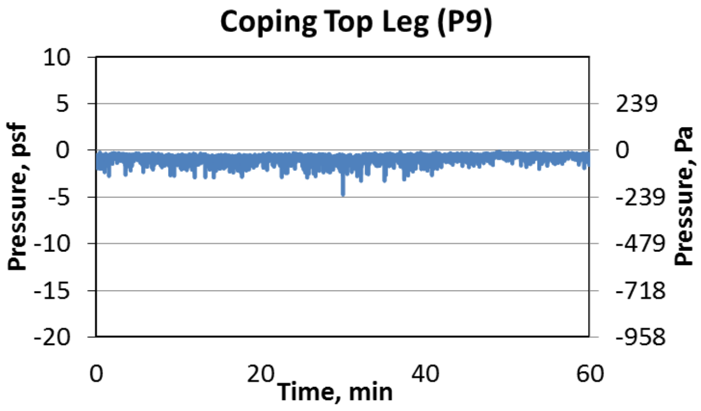

	Wind Speed, mph(kph)		Cleat (P7)	Coping Front Leg (P8)	Coping Top Leg (P9)
Peak	32 (52)	Pressure, psf (Pa)	0.8 (36.7)	1.6 (75.0)	0.0 (0)
Mean	15 (24)	Mean, psf (Pa)	0.0 (0)	0.1 (6.7)	-0.8 (-36.8)
		Suction, psf (Pa)	-1.4 (-67.9)	-3.4 (-162.1)	-4.7 (-225.6)

NOV 15, 2013

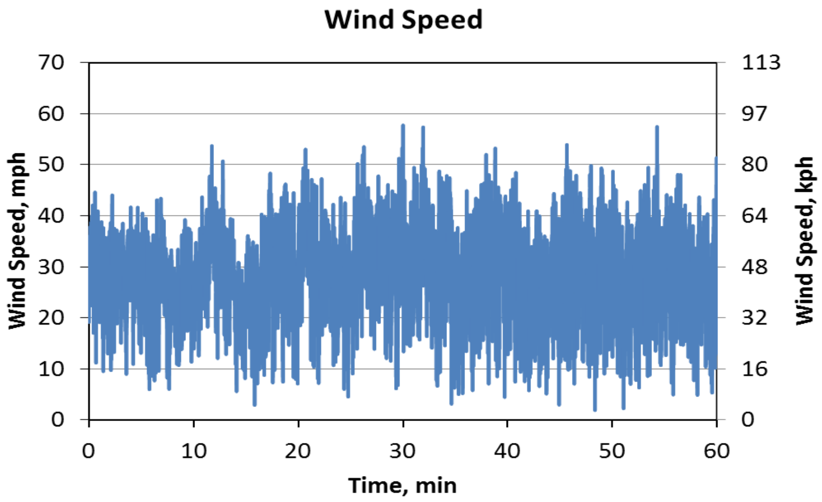

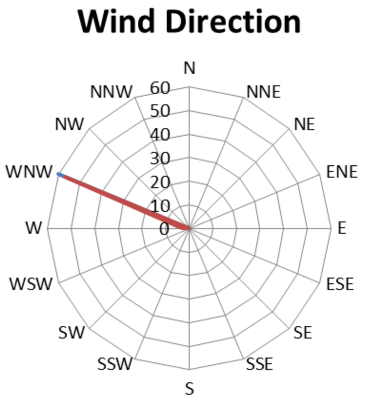

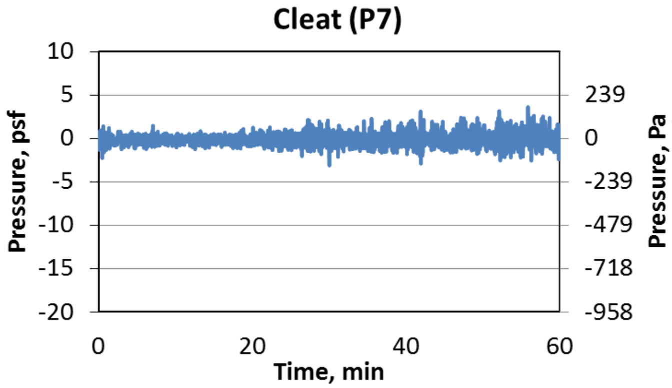

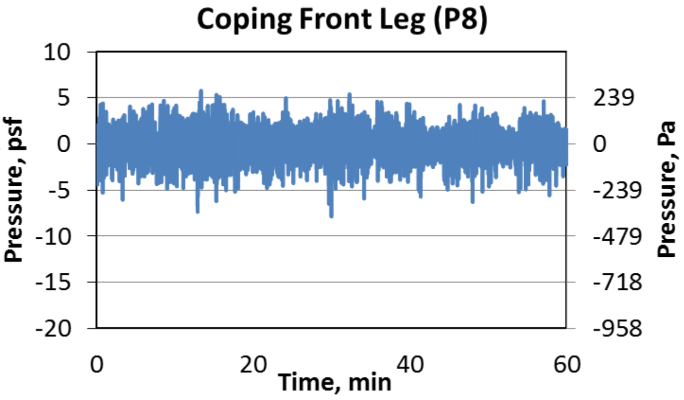

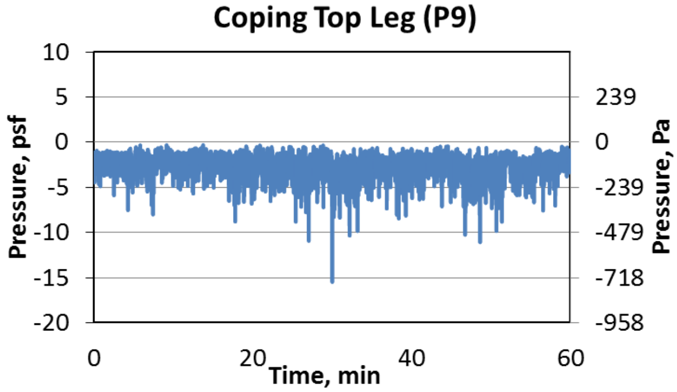

	Wind Speed, mph(kph)		Cleat (P7)	Coping Front Leg (P8)	Coping Top Leg (P9)
Peak	58 (93)	Pressure, psf (Pa)	3.6 (172)	5.8 (276.4)	0.0 (0)
Mean	29 (47)	Mean, psf (Pa)	-0.1 (-2.7)	0.4 (17.3)	-2.4 (-114.8)
		Suction, psf (Pa)	-3.1 (-149.9)	-7.9 (-376.2)	-15.5 (-740.5)

NOV 16, 2013

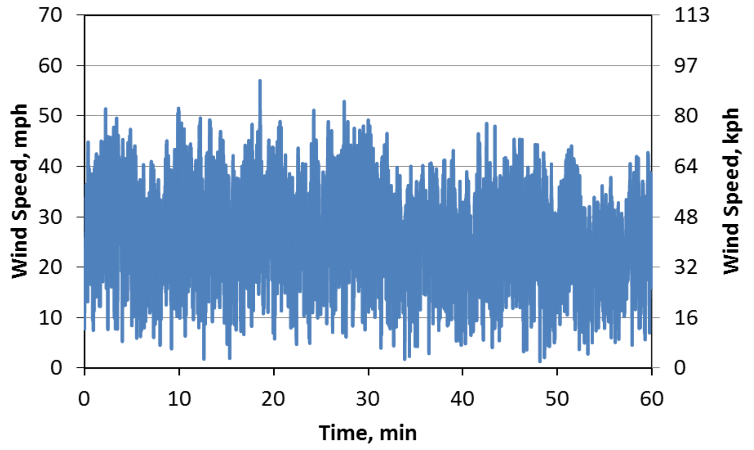

Wind Speed

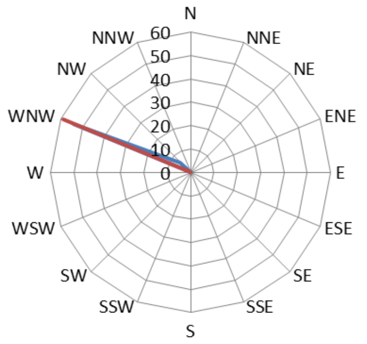

Wind Direction

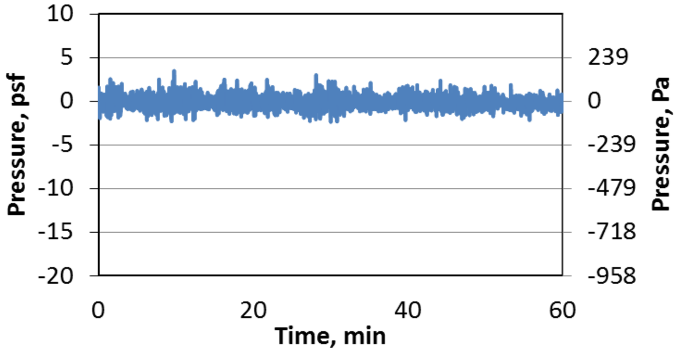

Cleat (P7)

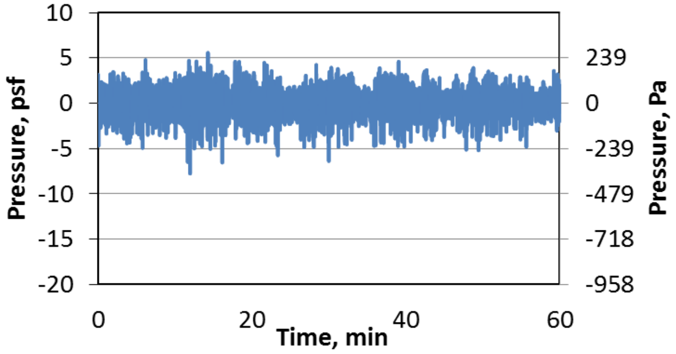

Coping Front Leg (P8)

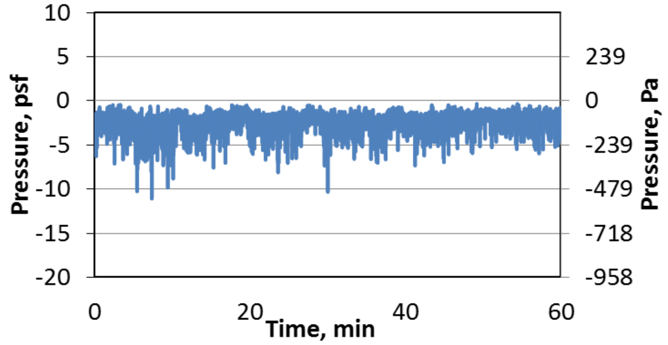

Coping Top Leg (P9)

	Wind Speed, mph(kph)		Cleat (P7)	Coping Front Leg (P8)	Coping Top Leg (P9)
Peak	49 (79)	Pressure, psf (Pa)	3.5 (165.8)	5.6 (266.4)	0.0 (0)
Mean	28 (45)	Mean, psf (Pa)	0.0 (0)	0.3 (14.4)	-2.3 (-109.5)
		Suction, psf (Pa)	-2.4 (-114)	-6.4 (-369.3)	-10.3 (-529.5)

NOV 19, 2013

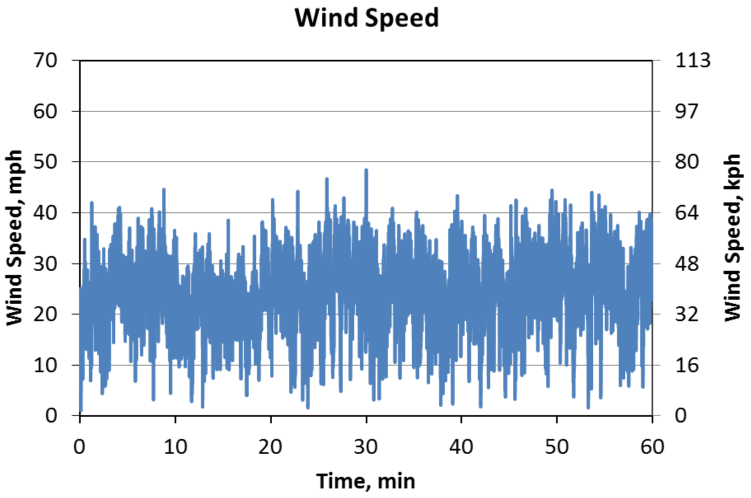

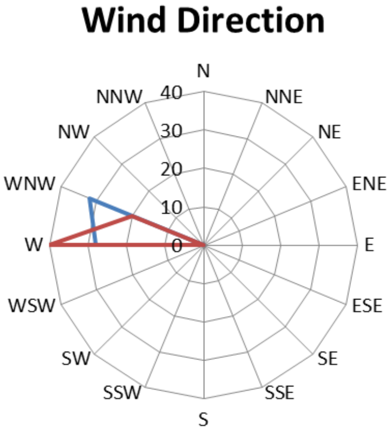

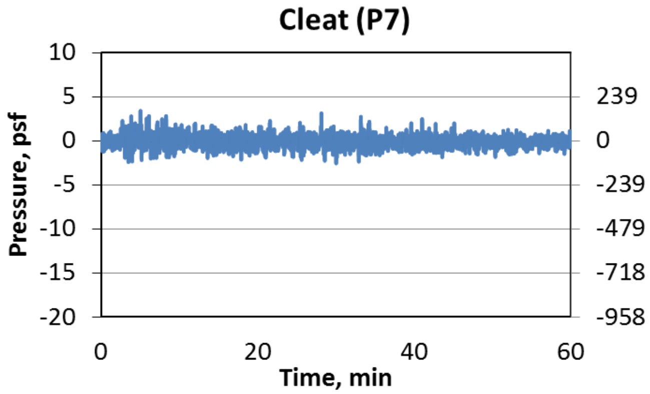

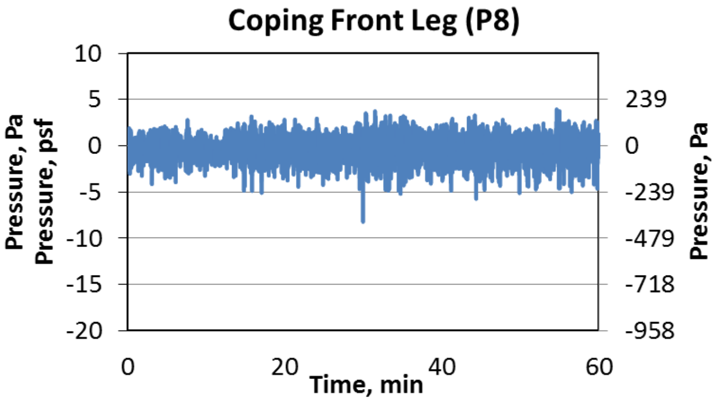

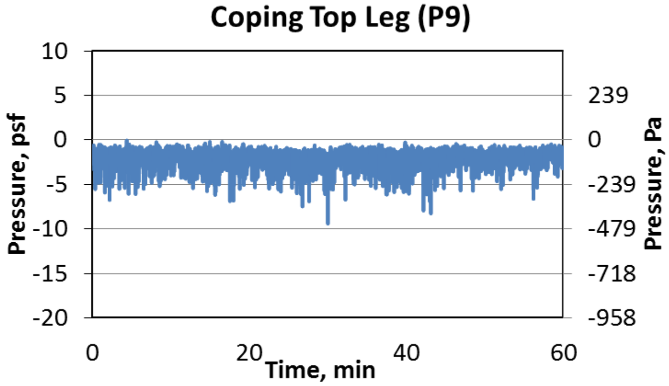

	Wind Speed, mph(kph)		Cleat (P7)	Coping Front Leg (P8)	Coping Top Leg (P9)
Peak	49 (79)	Pressure, psf (Pa)	3.4 (162.0)	3.9 (188.5)	0.0 (0)
Mean	25 (40)	Mean, psf (Pa)	0.0 (0)	-0.1 (-3.2)	-1.9 (-91.1)
		Suction, psf (Pa)	-2.6 (-123.3)	-8.2 (391.1)	-9.2 (441.5)

Dec 1, 2013

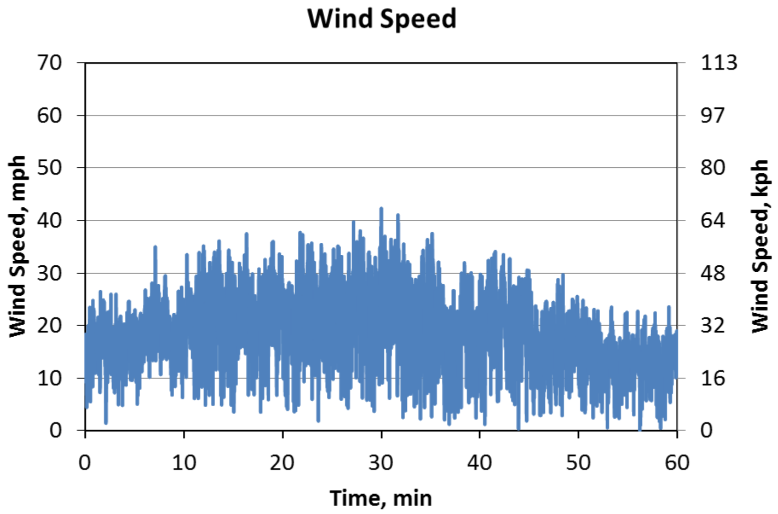

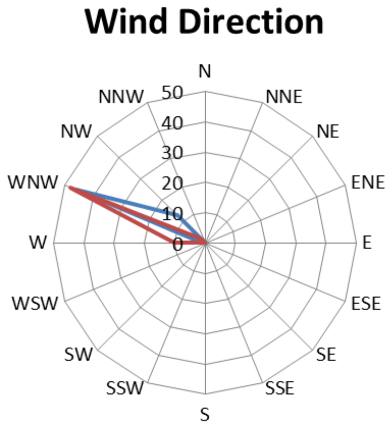

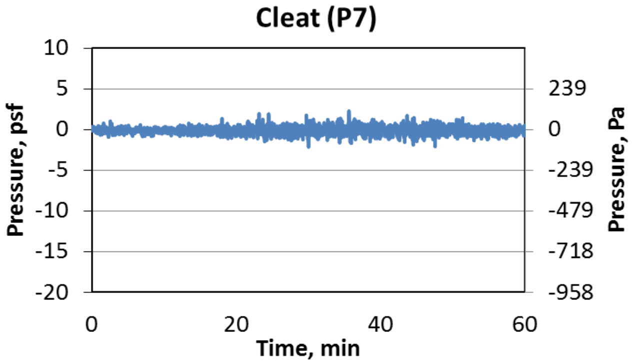

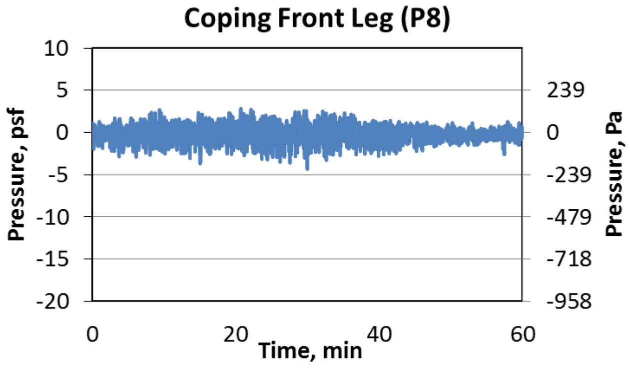

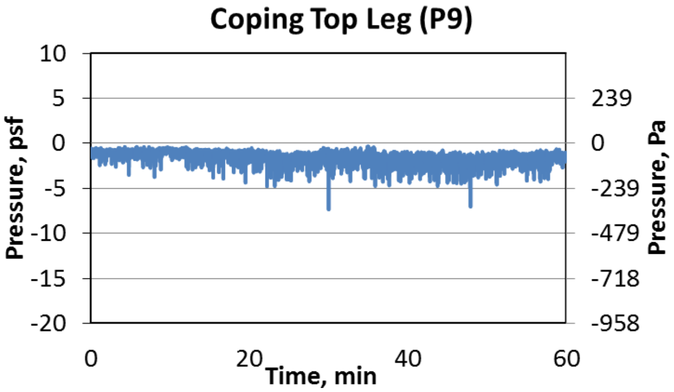

	Wind Speed, mph(kph)		Cleat (P7)	Coping Front Leg (P8)	Coping Top Leg (P9)
Peak	42 (68)	Pressure, psf (Pa)	2.2 (107.7)	2.8 (135.2)	0.0 (0)
Mean	19 (30)	Mean, psf (Pa)	-0.1 (-3.3)	0.1 (2.4)	-1.5 (-71.1)
		Suction, psf (Pa)	-2.2 (-103.5)	-4.3 (-206.2)	-7.3 (-351.6)

Dec 2, 2013

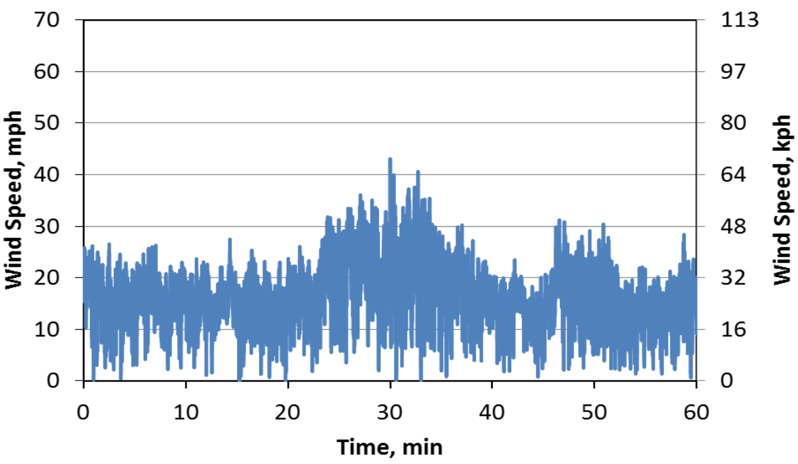

Wind Speed

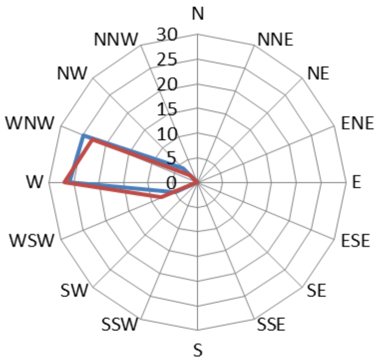

Wind Direction

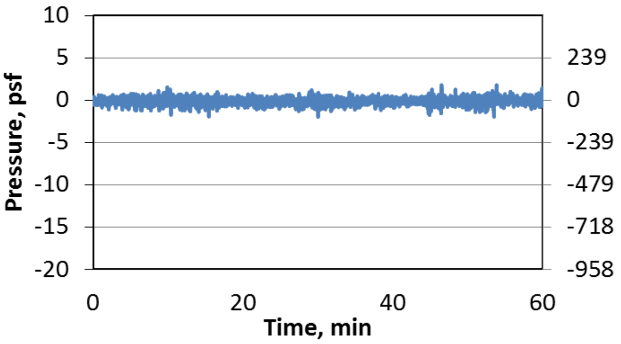

Cleat (P7)

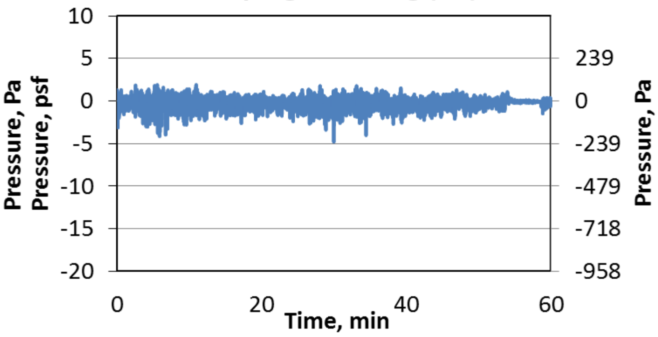

Coping Front Leg (P8)

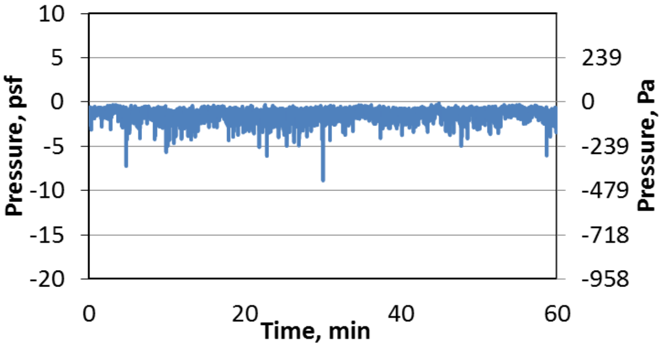

Coping Top Leg (P9)

	Wind Speed, mph(kph)		Cleat (P7)	Coping Front Leg (P8)	Coping Top Leg (P9)
Peak	43 (69)	Pressure, psf (Pa)	1.8 (84.9)	1.9 (90.8)	0.0 (0)
Mean	17 (27)	Mean, psf (Pa)	-0.1 (-3.9)	-0.1 (-7.2)	-1.2 (-59.3)
		Suction, psf (Pa)	-2.0 (-95.9)	-4.8 (-229.2)	-8.8 (-420.8)

Dec 18, 2013

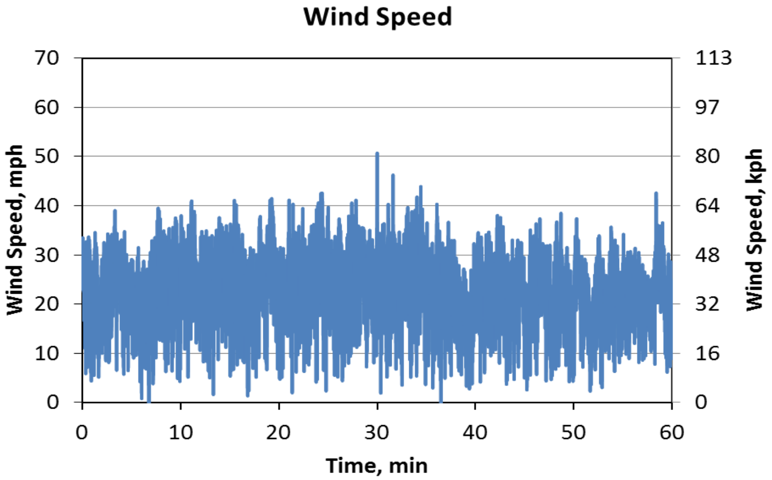

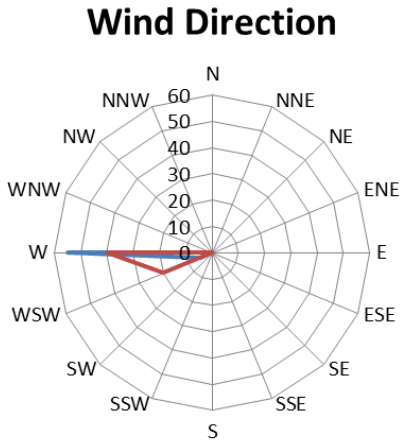

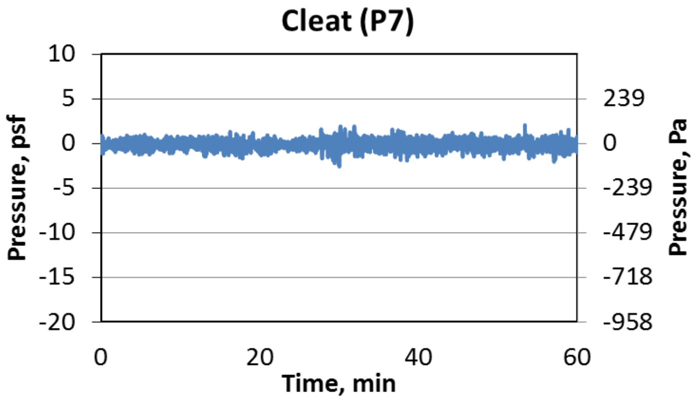

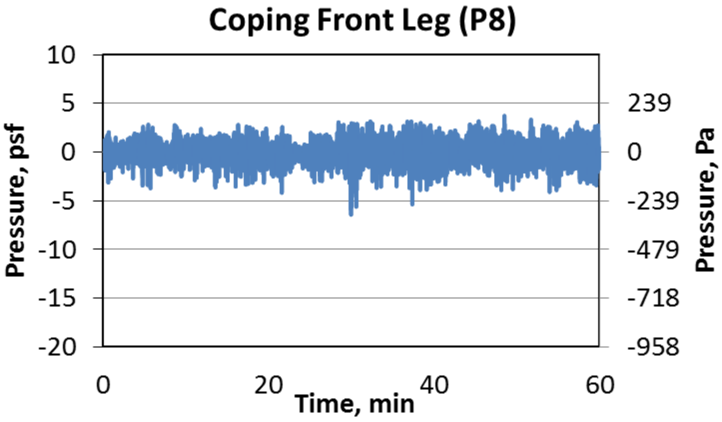

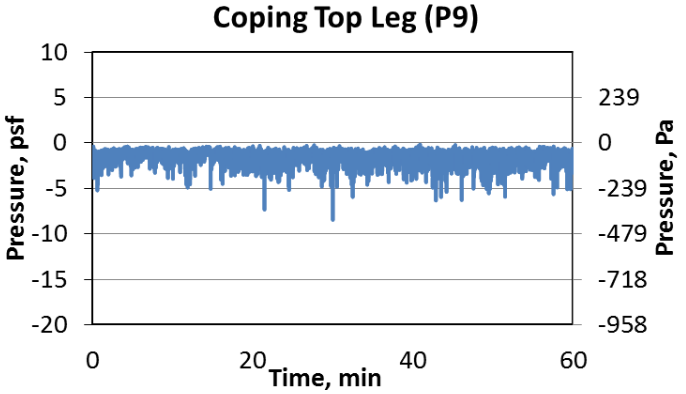

	Wind Speed, mph(kph)		Cleat (P7)	Coping Front Leg (P8)	Coping Top Leg (P9)
Peak	50 (81)	Pressure, psf (Pa)	2.0 (97.2)	3.7 (177.4)	0.0 (0)
Mean	23 (37)	Mean, psf (Pa)	-0.1 (-3.8)	0.2 (11.9)	-1.4 (-69.2)
		Suction, psf (Pa)	-2.6 (-124)	-6.4 (-307.3)	-8.4 (-402.9)

Dec 23, 2013

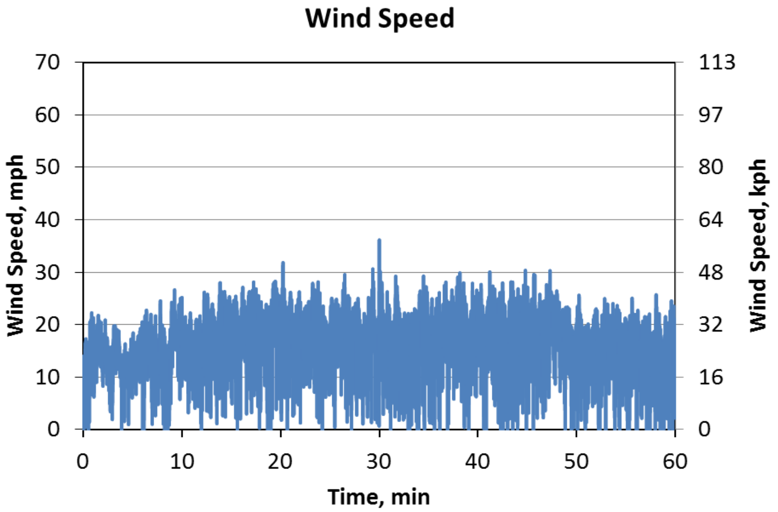

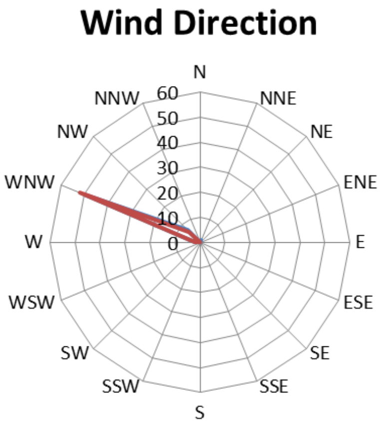

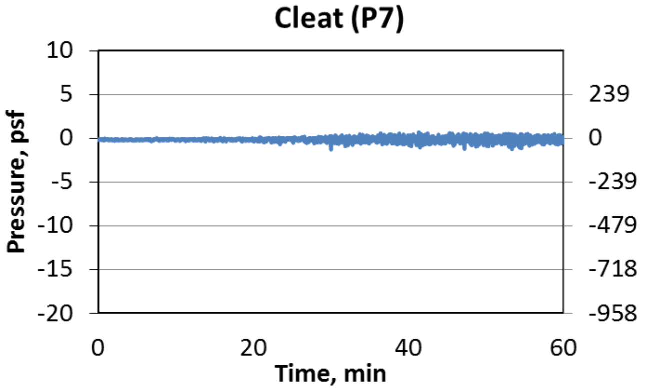

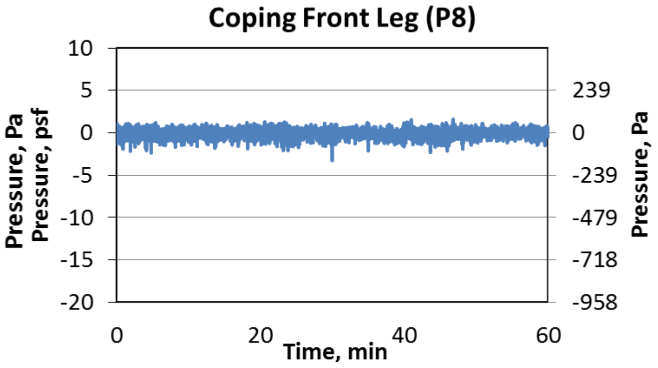

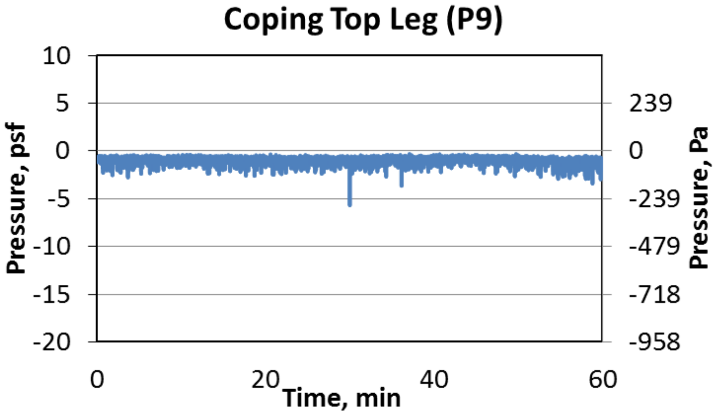

	Wind Speed, mph(kph)		Cleat (P7)	Coping Front Leg (P8)	Coping Top Leg (P9)
Peak	36 (58)	Pressure, psf (Pa)	0.7 (31.9)	1.6 (75.9)	0.0 (0)
Mean	17 (27)	Mean, psf (Pa)	-0.1 (-6.9)	0.1 (3.2)	-0.9 (-45.2)
		Suction, psf (Pa)	-1.3 (-62.9)	-3.3 (-156.4)	-5.7 (-271.5)

Feb 20, 2014

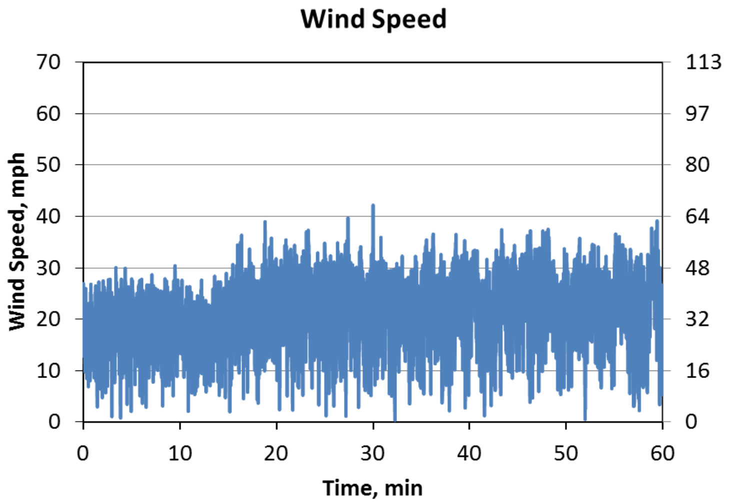
Wind Speed

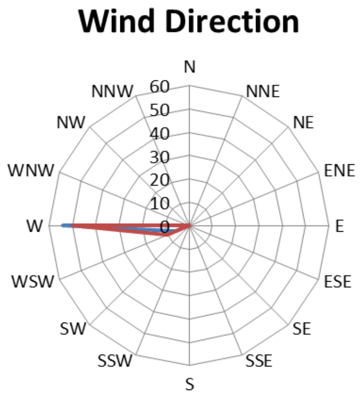
Wind Direction

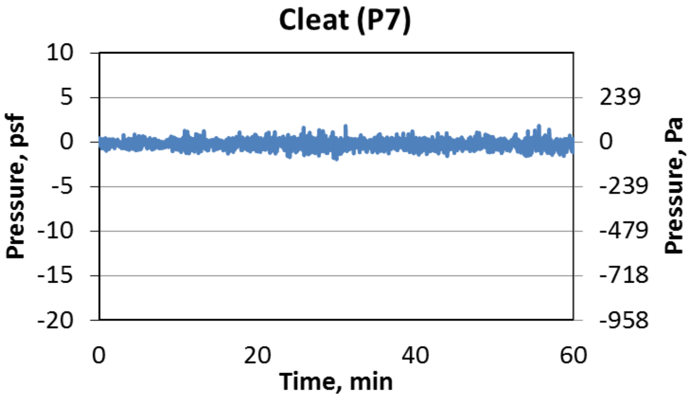
Cleat (P7)

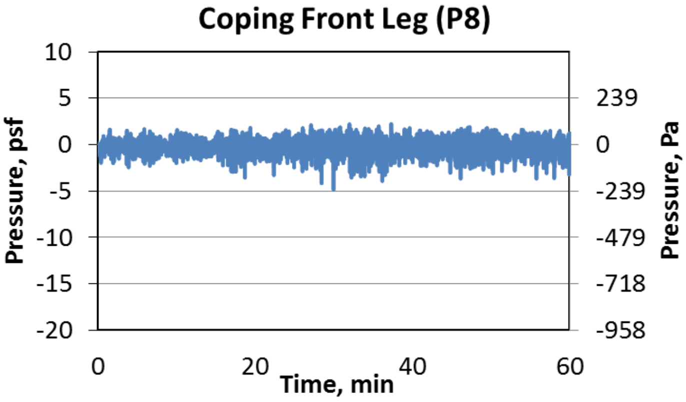
Coping Front Leg (P8)

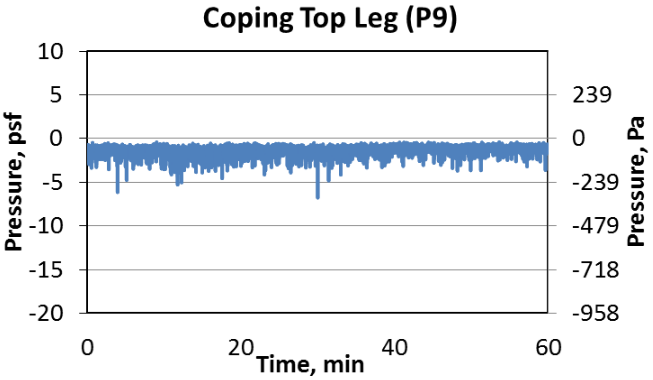
Coping Top Leg (P9)

	Wind Speed, mph(kph)		Cleat (P7)	Coping Front Leg (P8)	Coping Top Leg (P9)
Peak	42 (68)	Pressure, psf (Pa)	1.8 (86.2)	2.2 (106)	0.0 (0)
Mean	22 (35)	Mean, psf (Pa)	-0.2 (-9.0)	0.0 (0)	-1.3 (-61.6)
		Suction, psf (Pa)	-2.0 (-93.6)	-4.8 (-230.1)	-6.8 (-324.2)

Feb 21, 2014

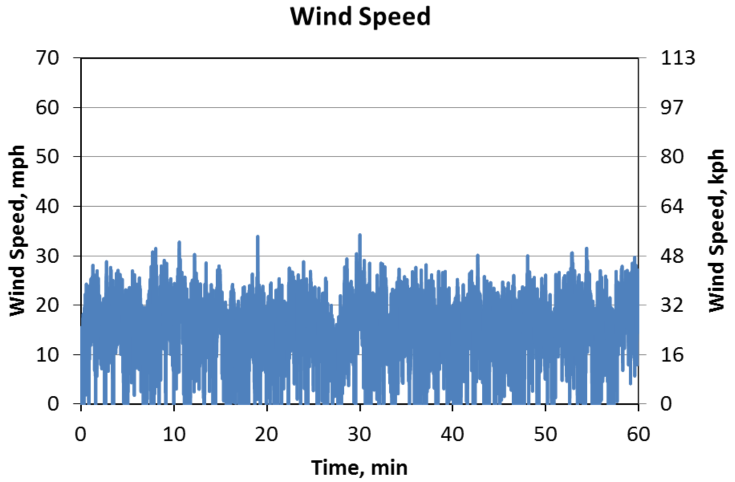
Wind Speed

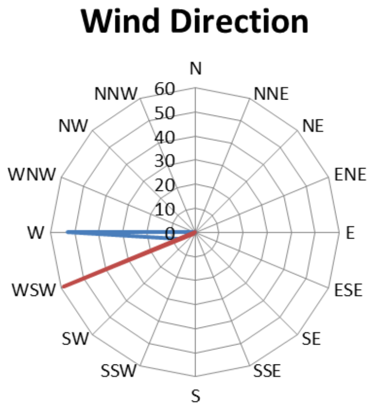
Wind Direction

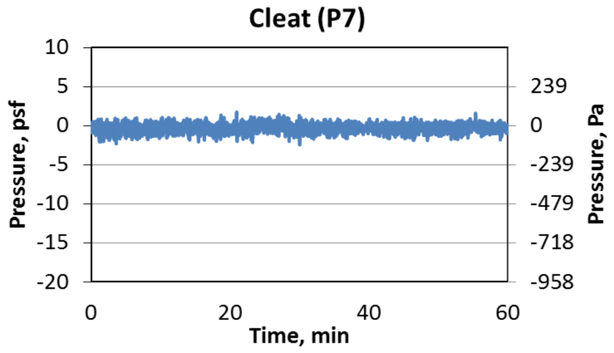
Cleat (P7)

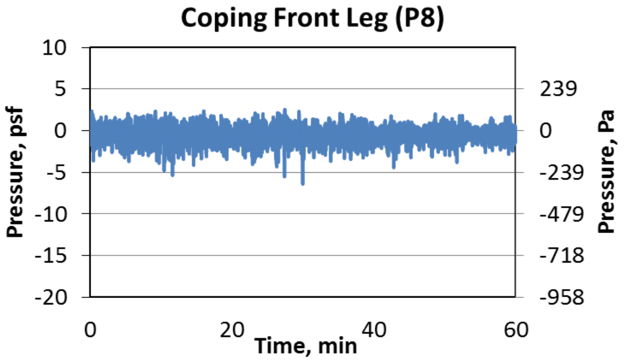
Coping Front Leg (P8)

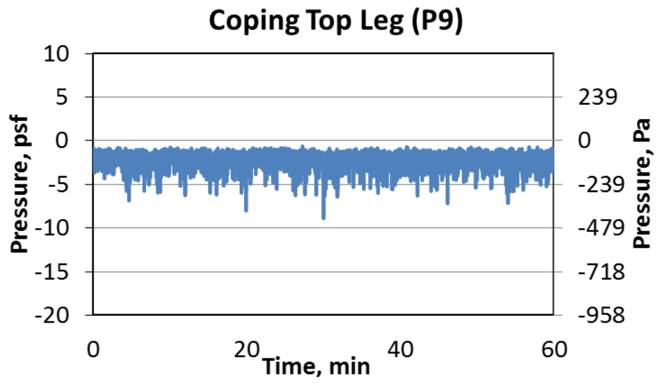
Coping Top Leg (P9)

	Wind Speed, mph(kph)		Cleat (P7)	Coping Front Leg (P8)	Coping Top Leg (P9)
Peak	34 (55)	Pressure, psf (Pa)	1.7 (81.7)	2.5 (121.3)	0.0 (0)
Mean	16 (26)	Mean, psf (Pa)	-0.2 (-11.4)	-0.3 (-14.3)	-2.0 (-97.1)
		Suction, psf (Pa)	-2.5 (-118.1)	-6.4 (-305.8)	-8.9 (-424.9)

April 17, 2014

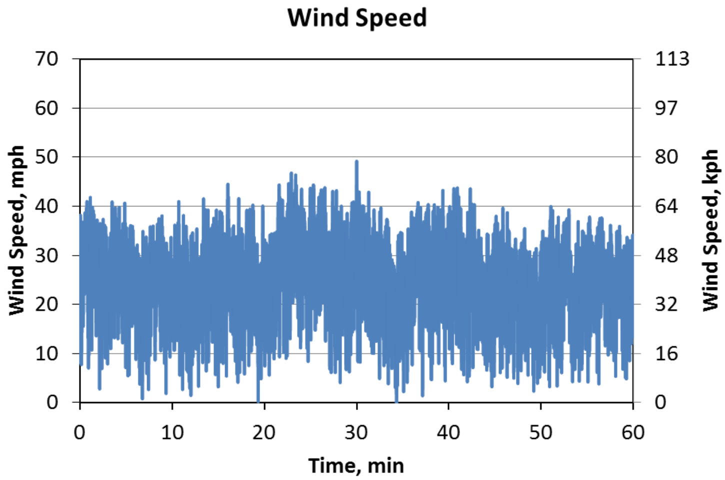
Wind Speed

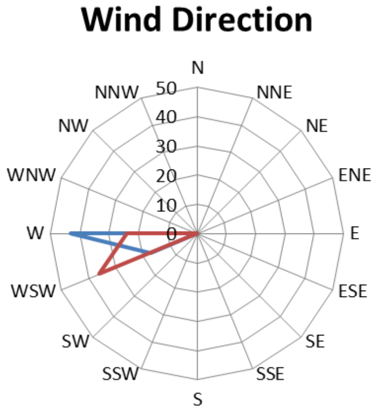
Wind Direction

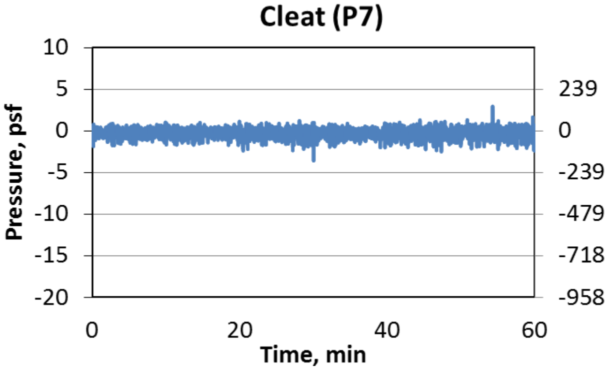
Cleat (P7)

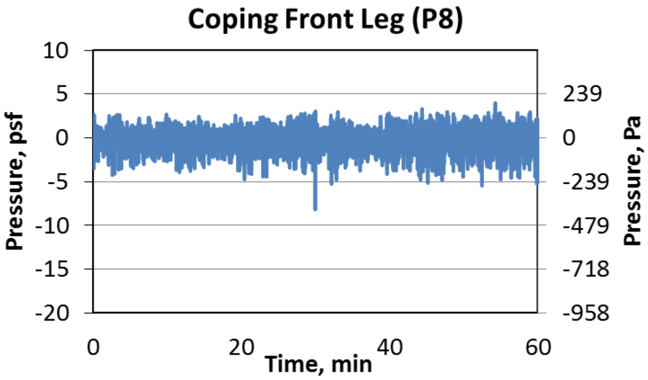
Coping Front Leg (P8)

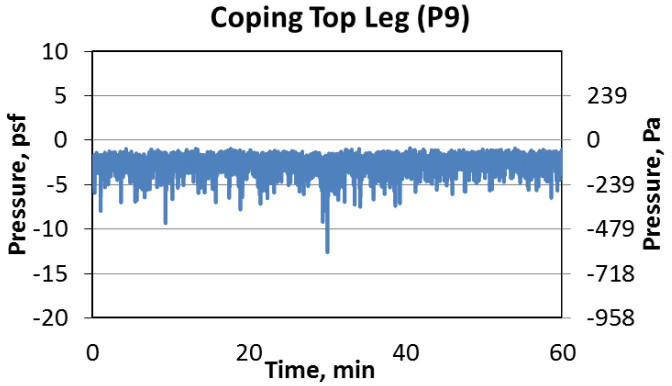
Coping Top Leg (P9)

	Wind Speed, mph(kph)		Cleat (P7)	Coping Front Leg (P8)	Coping Top Leg (P9)
Peak	49 (79)	Pressure, psf (Pa)	2.9 (140.5)	4.0 (189.8)	0.0 (0)
Mean	25 (41)	Mean, psf (Pa)	-0.3 (-12.7)	0.0 (0)	-2.4 (113.4)
		Suction, psf (Pa)	-3.6 (-172.4)	-8.1 (-385.6)	-12.6 (-603.1)

April 21, 2014

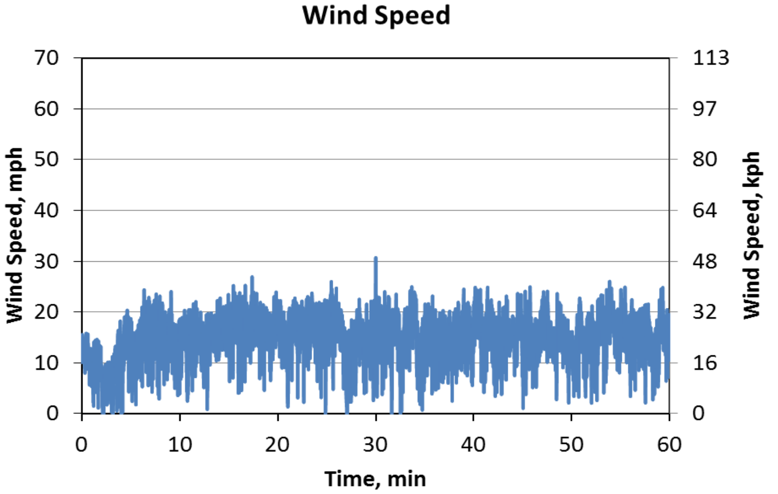

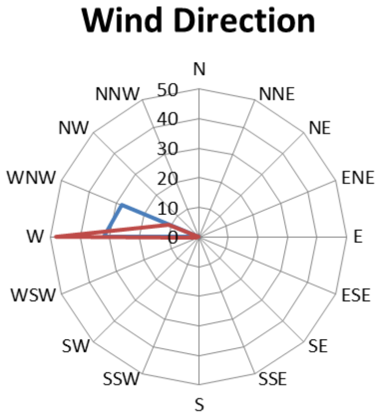

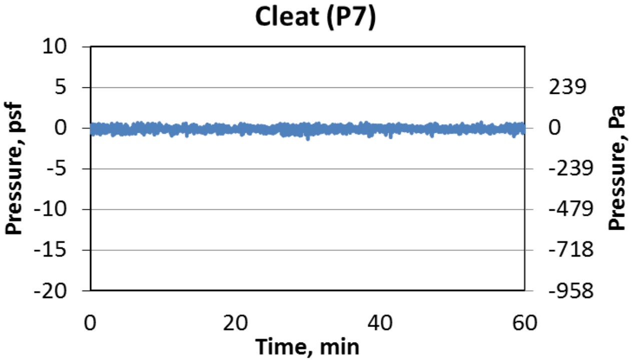

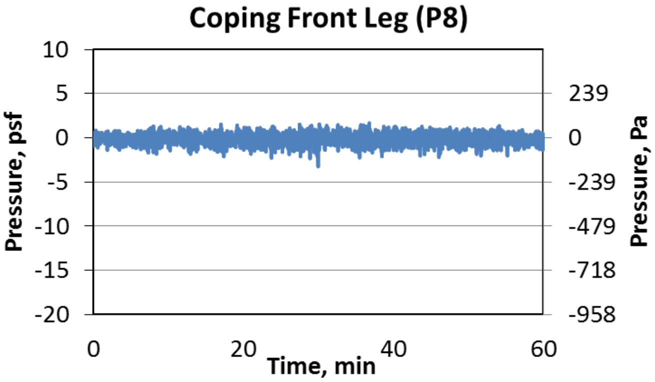

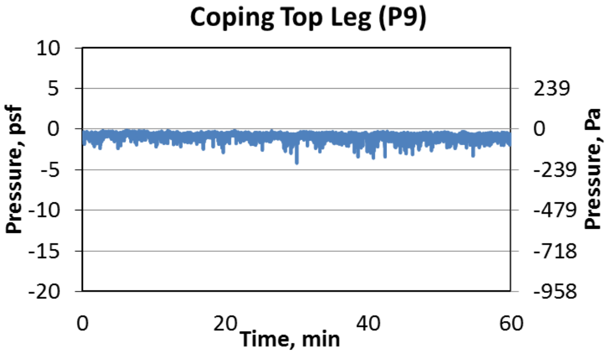

	Wind Speed, mph(kph)		Cleat (P7)	Coping Front Leg (P8)	Coping Top Leg (P9)
Peak	30 (49)	Pressure, psf (Pa)	0.7 (34)	1.7 (79.2)	0.0 (0)
Mean	15 (24)	Mean, psf (Pa)	-0.1 (-3.5)	0.0 (0)	-0.8 (-39.7)
		Suction, psf (Pa)	-1.4 (-67.2)	-3.2 (-155.1)	-4.2 (-199.3)

April 22, 2014

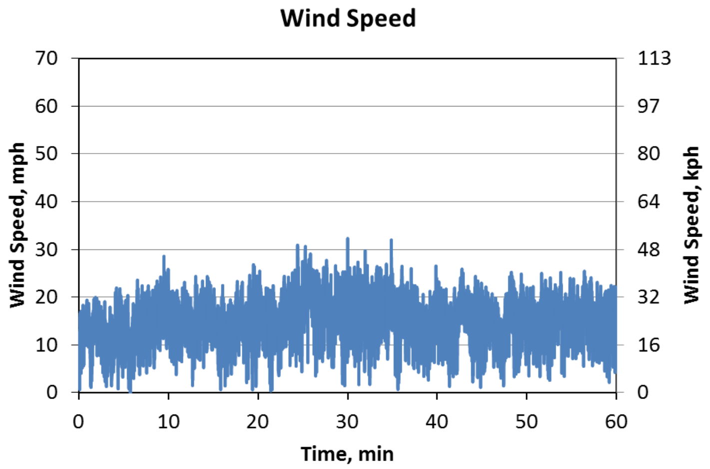
Wind Speed

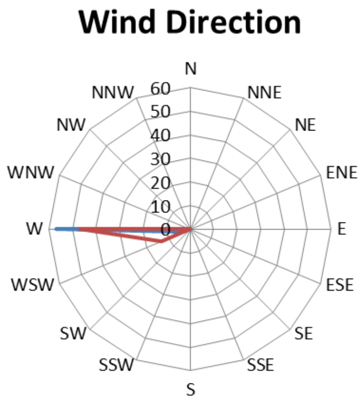
Wind Direction

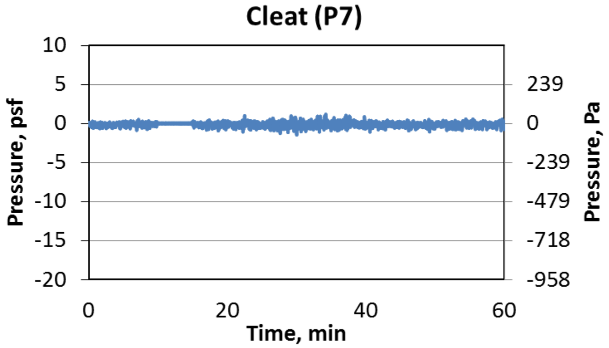
Cleat (P7)

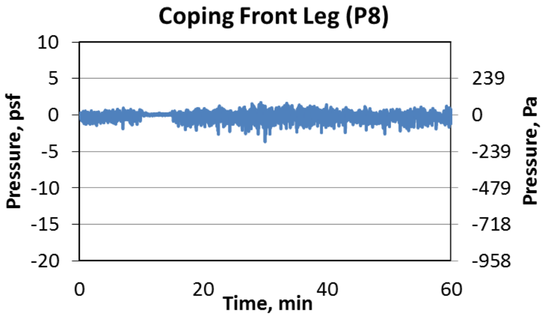
Coping Front Leg (P8)

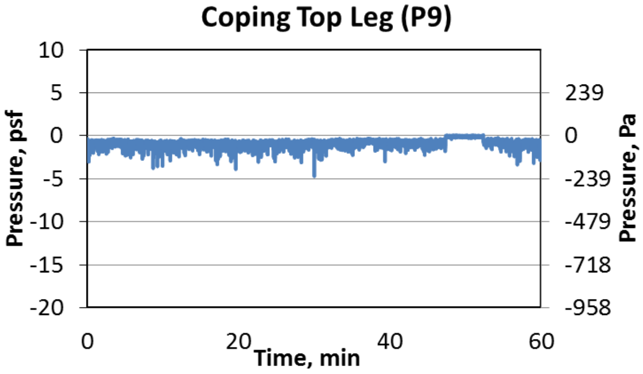
Coping Top Leg (P9)

	Wind Speed, mph(kph)		Cleat (P7)	Coping Front Leg (P8)	Coping Top Leg (P9)
Peak	32 (52)	Pressure, psf (Pa)	1.2 (56.2)	1.7 (82.4)	0.1 (4.4)
Mean	15 (25)	Mean, psf (Pa)	-0.1 (-5.3)	-0.1 (-4.4)	-0.8 (-38.9)
		Suction, psf (Pa)	-1.5 (-70.7)	-3.7 (-174.9)	-4.6 (-222.5)

June 9, 2014

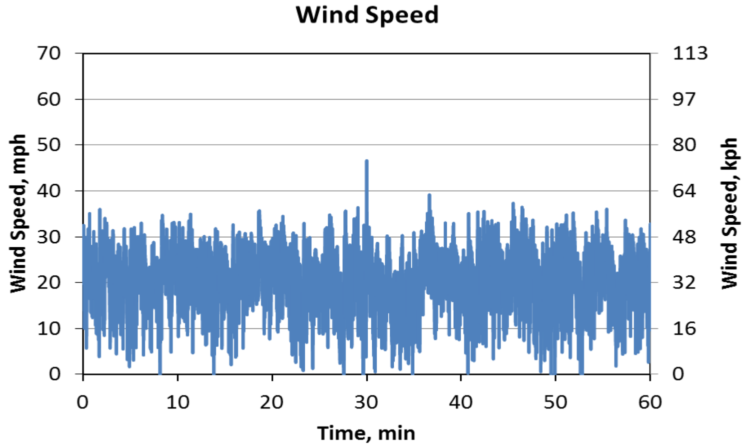
Wind Speed

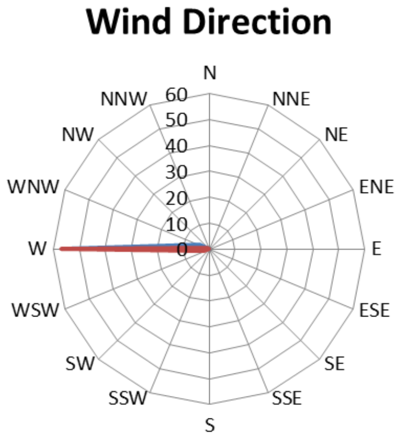
Wind Direction

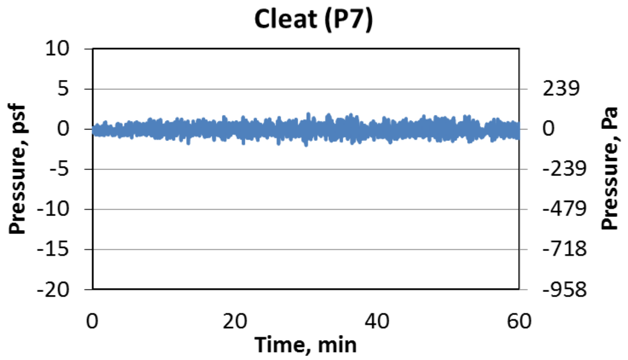
Cleat (P7)

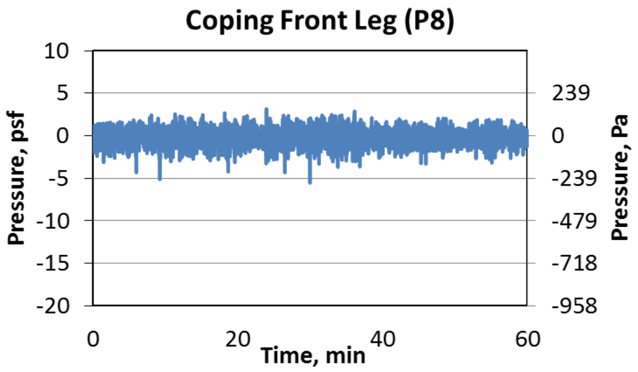
Coping Front Leg (P8)

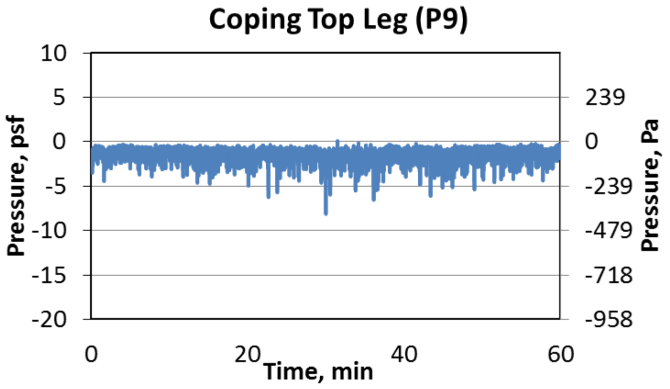
Coping Top Leg (P9)

	Wind Speed, mph(kph)		Cleat (P7)	Coping Front Leg (P8)	Coping Top Leg (P9)
Peak	46 (74)	Pressure, psf (Pa)	1.9 (89.9)	3.1 (149.5)	0.1 (3.9)
Mean	21 (33)	Mean, psf (Pa)	-0.1 (-4.4)	0.1 (3.6)	-1.4 (-65.8)
		Suction, psf (Pa)	-2.0 (-97.8)	-5.5 (-262.9)	-8.1 (387.6)

June 20, 2014

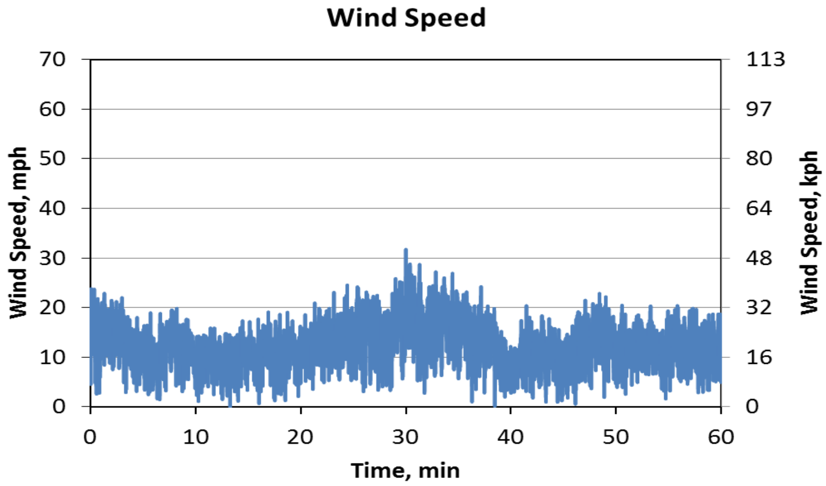

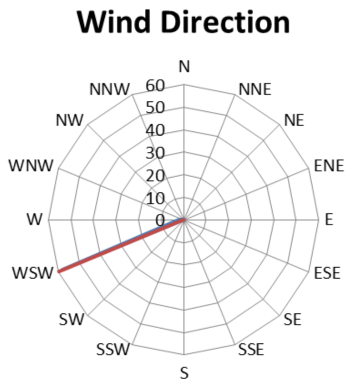

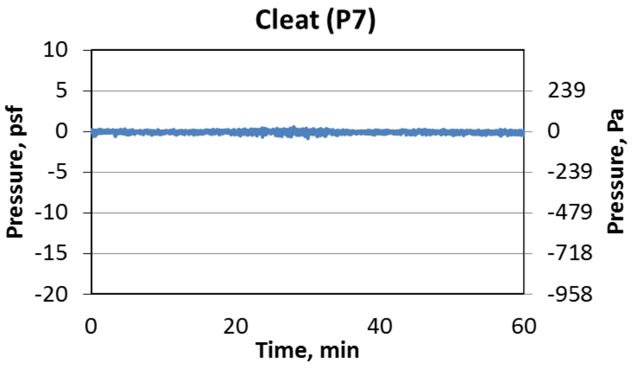

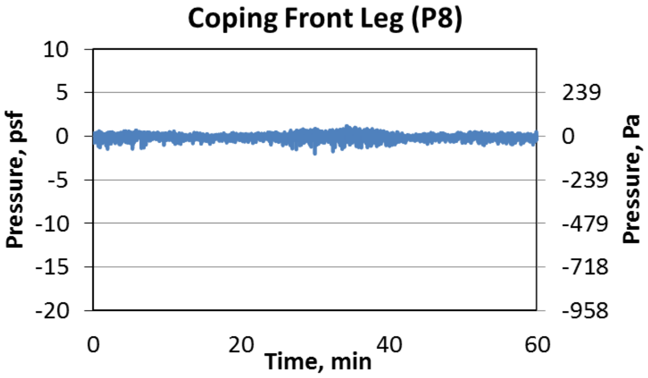

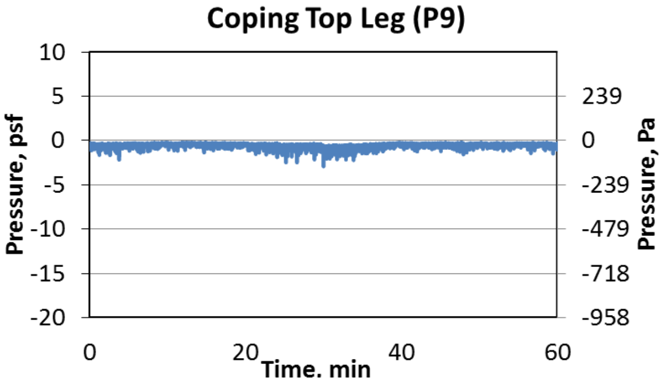

	Wind Speed, mph(kph)		Cleat (P7)	Coping Front Leg (P8)	Coping Top Leg (P9)
Peak	32 (51)	Pressure, psf (Pa)	0.6 (26.6)	1.2 (57)	0.0 (0)
Mean	13 (20)	Mean, psf (Pa)	-0.1 (-3)	0.0 (0)	-0.6 (-26.5)
		Suction, psf (Pa)	-0.9 (-41.8)	-2.0 (-95.3)	-2.9 (-139.7)

Appendix E

ASCE Calculations

The following Appendix shows the ASCE calculations in order to compare them to the data of the present study, seen in Section 5.4. It determines the velocity pressure at different wind speeds and the design wind loads acting on the parapet.

The calculations for the determining the velocity pressure at different wind speeds. Equation 2 from section 2.3.2 will be used:

$$q_h = 0.00256 \times K_d \times K_z \times K_{zt} \times V^2 \times I \quad (\text{psf})$$

Sample calculations for wind speed 30 mph (48.3 kph) with the load parameters stated in Section 5.4

Where K_d= Wind directionality factor = 1.0

K_z= Velocity pressure exposure coefficient = 1.13

K_{zt}= Topographic factor = 1.0

V = Basic Wind Speed= 30 mph

$$q_p = 0.00256 * 1.13 * 0.85 * 1.0 * (30)^2$$

$$q_p = 2.2 \text{ psf} (105.3 \text{ Pa})$$

Table E.1: Velocity pressure at different wind speeds

Velocity, mph (kph)	Velocity pressure, psf (kPa)
30 (48.3)	2.6 (0.12)
40 (64.4)	4.6 (0.22)
50 (80.5)	7.2 (0.35)
60 (96.6)	10.4 (0.50)
70 (112.7)	14.2 (0.68)
80 (128.7)	18.5 (0.89)
90 (144.8)	23.4 (1.12)

Now using Equation 1 to determine the design wind pressure acting on the parapet:

$$P = q_p[(GC_p) - (GC_{pi})]$$

The velocity pressures that were calculated for 30 mph (48.3 kph) will be put into Equation 1 to find the design wind pressure. The interior and exterior pressure coefficient stated in Section 5.4 are used

Where q_p = Velocity pressure evaluated at the top of the parapet = 2.6

GC_p = exterior pressure coefficient given for leeward side = -2.8 or +0.3

GC_p = exterior pressure coefficient given for windward side = -1.4 or +1.0

GC_{pi} = interior pressure coefficient = ±0.55

Suction for 30 mph and 90 mph Windward:

$$P = 2.6 \text{ x } [(-1.4) - (0.55)]$$

$$P = 2.6\ x\ (-1.95) = -5.1\ psf\ (-0.24\ kPa)$$

$$P = 23.4\ x\ (-1.95) = -45.6\ psf\ (-2.19\ kPa)$$

Suction for 30 mph and 90 mph Leeward:

$$P = 2.6 \text{ x } [(-2.8) - (0.55)]$$

$$P = 2.6\ x\ (-3.35) = -8.7\ psf\ (-0.42\ kPa)$$

$$P = 23.4\ x\ (-3.35) = -78.4\ psf\ (-3.76\ kPa)$$

Pressure for 30 mph and 90 mph Windward:

$$P = 2.6 \text{ x } [(1.0) - (-0.55)]$$

$$P = 2.6\ x\ (1.55) = 4.0\ psf\ (0.19\ kPa)$$

$$P = 23.4\ x\ (1.55) = 36.3\ psf\ (1.74\ kPa)$$

Pressure for 30 mph and 90 mph Leeward:

$$P = 2.6 \text{ x } [(0.3) - (-0.55)]$$

$$P = 2.6 \ x \ (0.85) = 2.2 \ psf \ (0.11 \ kPa)$$

$$P = 23.4 \ x \ (0.85) = 19.9 \ psf \ (0.95 \ kPa)$$

Table E.2: Parapet wind loads on the Windward side

Velocity, mph (kph)	Velocity pressure, psf (Pa)	Pressure, psf (kPa)	Suction, psf (kPa)
30 (48.3)	2.6 (0.12)	4.0 (0.19)	-5.1 (-0.24)
40 (64.4)	4.6 (0.22)	7.2 (0.34)	-9.0 (-0.43)
50 (80.5)	7.2 (0.35)	11.2 (0.54)	-14.1 (-0.68)
60 (96.6)	10.4 (0.50)	16.1 (0.77)	-20.3 (-0.97)
70 (112.7)	14.2 (0.68)	22.0 (1.05)	-27.6 (-1.32)
80 (128.7)	18.5 (0.89)	28.7 (1.37)	-36.1 (-1.73)
90 (144.8)	23.4 (1.12)	36.4 (1.74)	-45.7 (-2.19)

Table E.3: Parapet wind loads on the Leeward side

Velocity, mph (kph)	Velocity pressure, psf (Pa)	Pressure, psf (kPa)	Suction, psf (kPa)
30 (48.3)	2.6 (0.12)	2.2 (0.11)	-8.7 (-0.42)
40 (64.4)	4.6 (0.22)	3.9 (0.19)	-15.5 (-0.74)
50 (80.5)	7.2 (0.35)	6.1 (0.29)	-24.2 (-1.16)
60 (96.6)	10.4 (0.50)	8.9 (0.43)	-34.9 (-1.67)
70 (112.7)	14.2 (0.68)	12.0 (0.57)	-47.5 (-2.27)
80 (128.7)	18.5 (0.89)	15.7 (0.75)	-62.0 (-2.97)
90 (144.8)	23.4 (1.12)	19.9 (0.95)	-78.5 (-3.76)

Appendix F

WIND-RCI

The following Appendix shows the wind uplift loads acting on the roof by the use of the software Wind-RCI. Wind-RCI uses the NBCC 2010 building code to determine the wind loads acting on the roof of the buildings. Each figure in the appendix displays each step of the software to calculate the wind loads acting on the roof for the building of the present study.

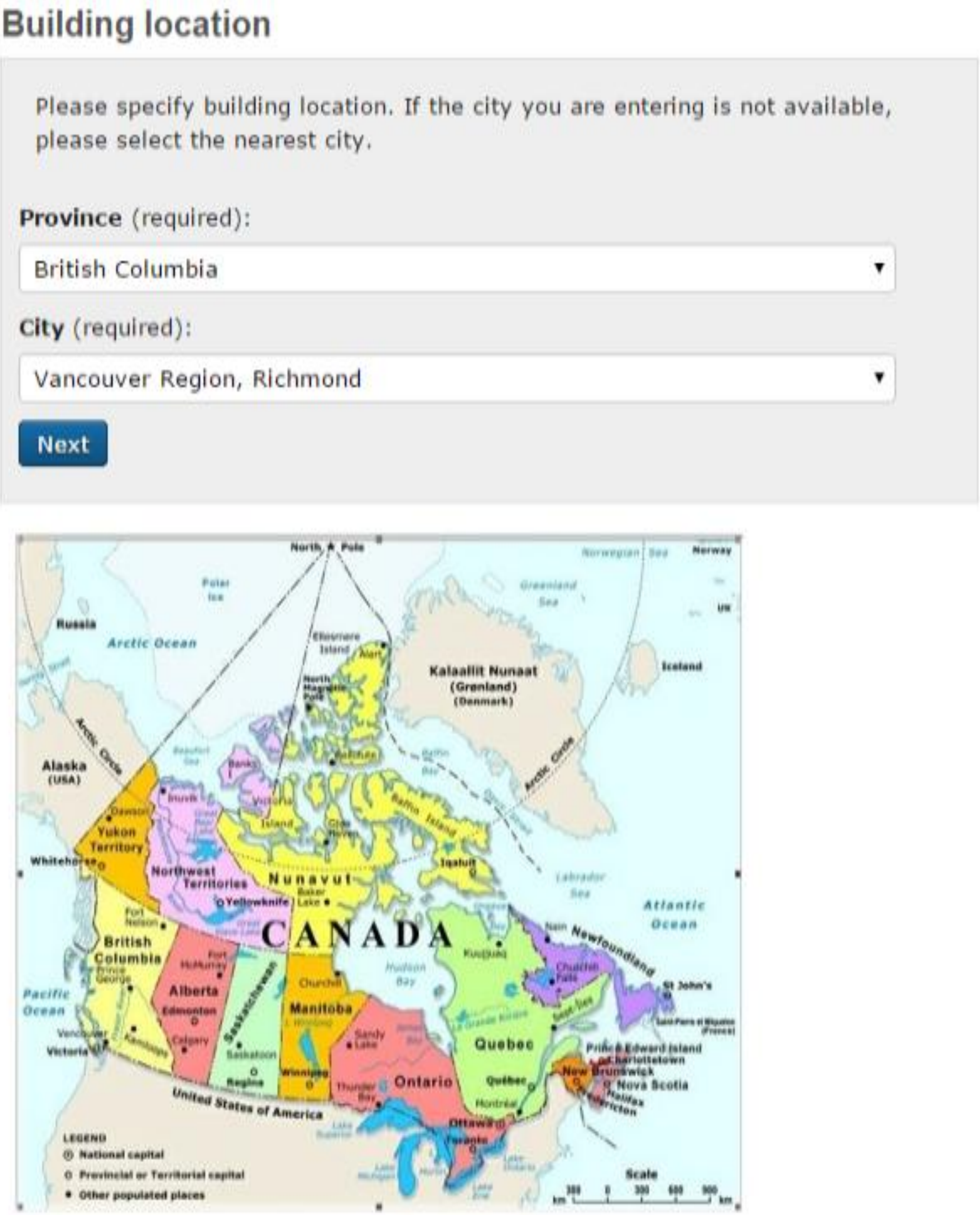

Building location

Please specify building location. If the city you are entering is not available, please select the nearest city.

Province (required):

British Columbia ▾

City (required):

Vancouver Region, Richmond ▾

Figure F.1: Screen 1-Building Location

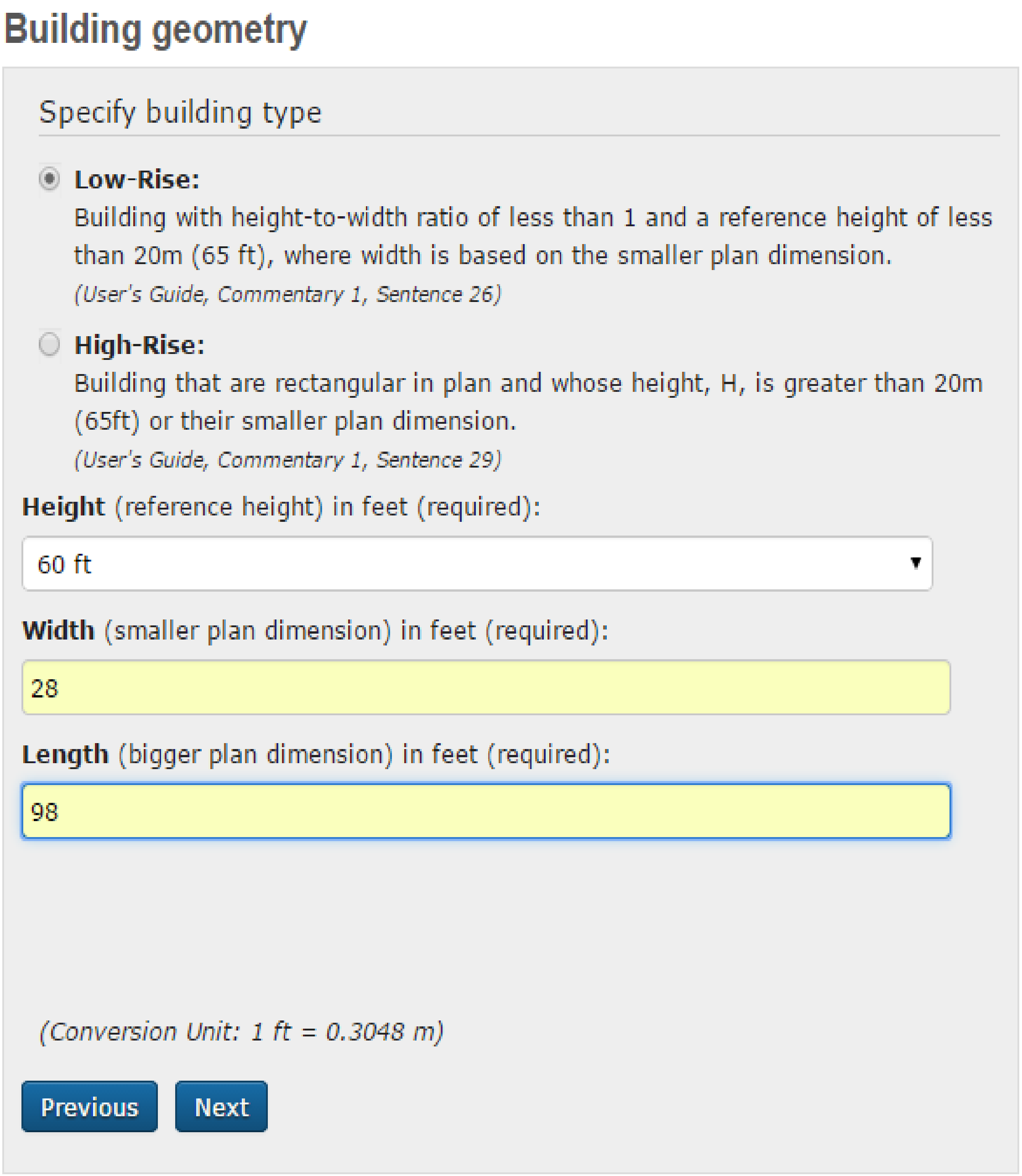

Building geometry

Specify building type

● **Low-Rise:**
Building with height-to-width ratio of less than 1 and a reference height of less than 20m (65 ft), where width is based on the smaller plan dimension.
(User's Guide, Commentary 1, Sentence 26)

○ **High-Rise:**
Building that are rectangular in plan and whose height, H, is greater than 20m (65ft) or their smaller plan dimension.
(User's Guide, Commentary 1, Sentence 29)

Height (reference height) in feet (required): 60 ft

Width (smaller plan dimension) in feet (required): 28

Length (bigger plan dimension) in feet (required): 98

(Conversion Unit: 1 ft = 0.3048 m)

Figure F.2: Screen 2-Building geometry

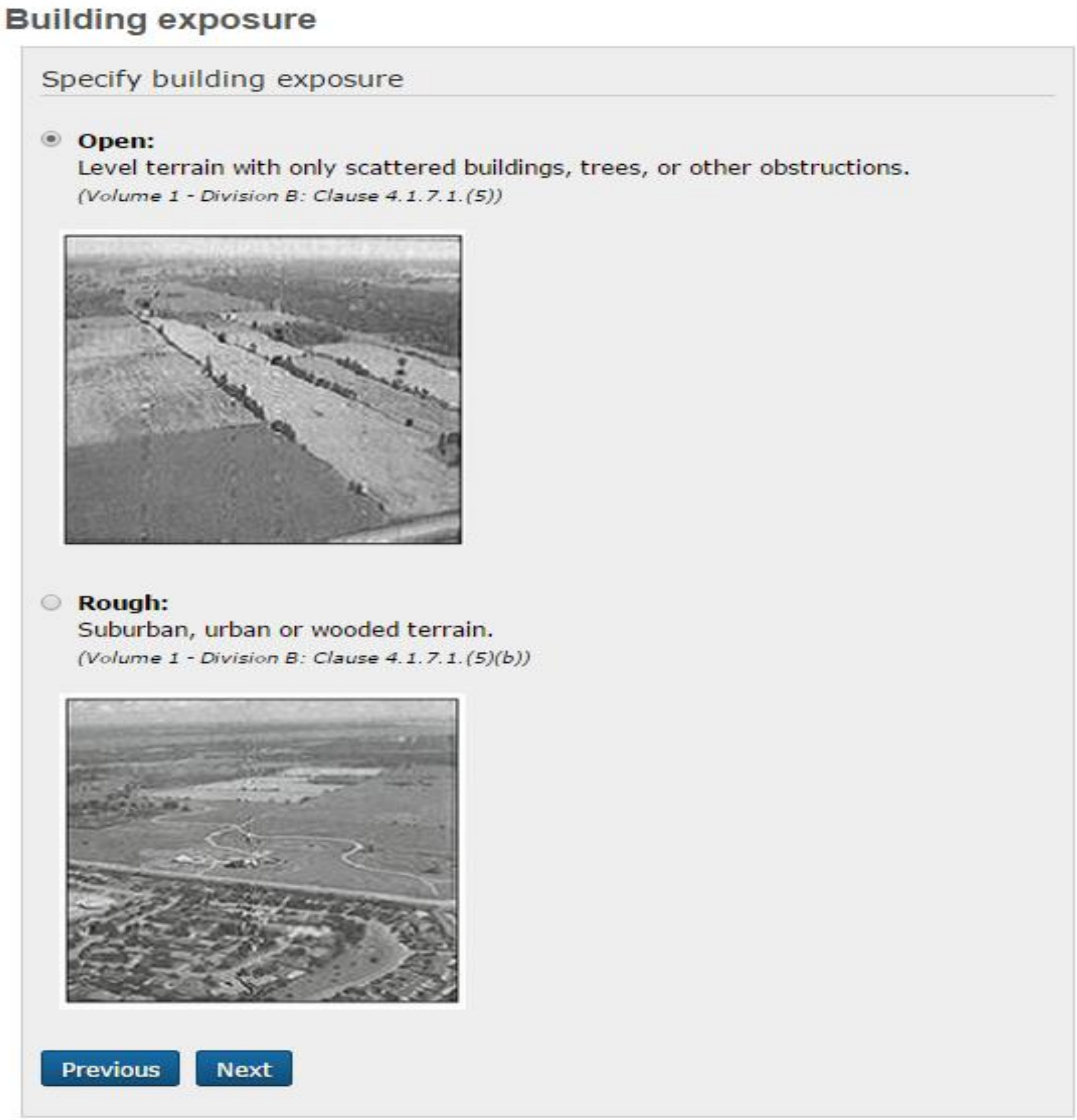

Building exposure

Specify building exposure

● **Open:**
Level terrain with only scattered buildings, trees, or other obstructions.
(Volume 1 - Division B: Clause 4.1.7.1.(5))

○ **Rough:**
Suburban, urban or wooded terrain.
(Volume 1 - Division B: Clause 4.1.7.1.(5)(b))

Figure F.3: Screen 3-Building Exposure

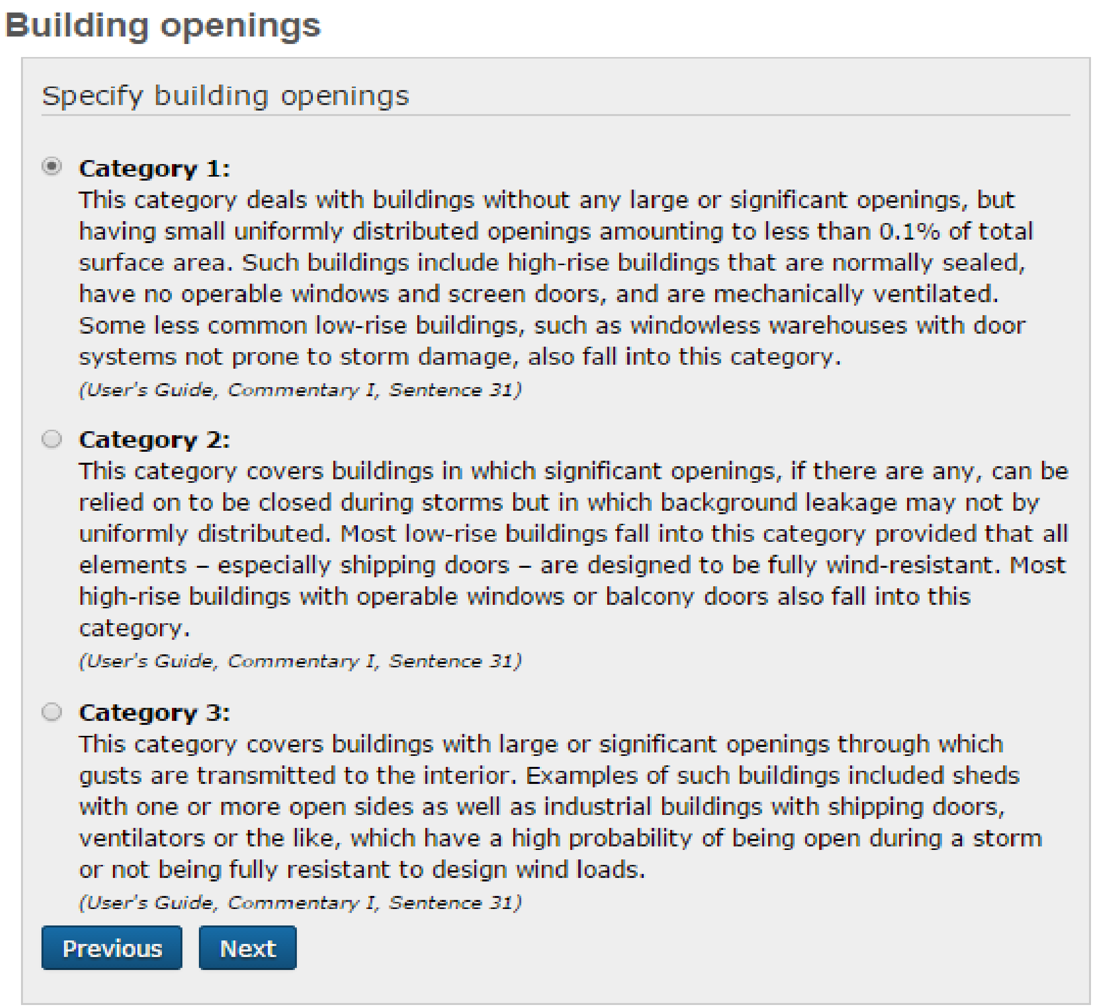

Building openings

Specify building openings

● **Category 1:**
This category deals with buildings without any large or significant openings, but having small uniformly distributed openings amounting to less than 0.1% of total surface area. Such buildings include high-rise buildings that are normally sealed, have no operable windows and screen doors, and are mechanically ventilated. Some less common low-rise buildings, such as windowless warehouses with door systems not prone to storm damage, also fall into this category.
(User's Guide, Commentary I, Sentence 31)

○ **Category 2:**
This category covers buildings in which significant openings, if there are any, can be relied on to be closed during storms but in which background leakage may not by uniformly distributed. Most low-rise buildings fall into this category provided that all elements – especially shipping doors – are designed to be fully wind-resistant. Most high-rise buildings with operable windows or balcony doors also fall into this category.
(User's Guide, Commentary I, Sentence 31)

○ **Category 3:**
This category covers buildings with large or significant openings through which gusts are transmitted to the interior. Examples of such buildings included sheds with one or more open sides as well as industrial buildings with shipping doors, ventilators or the like, which have a high probability of being open during a storm or not being fully resistant to design wind loads.
(User's Guide, Commentary I, Sentence 31)

Figure F.4: Screen 4-Building opening

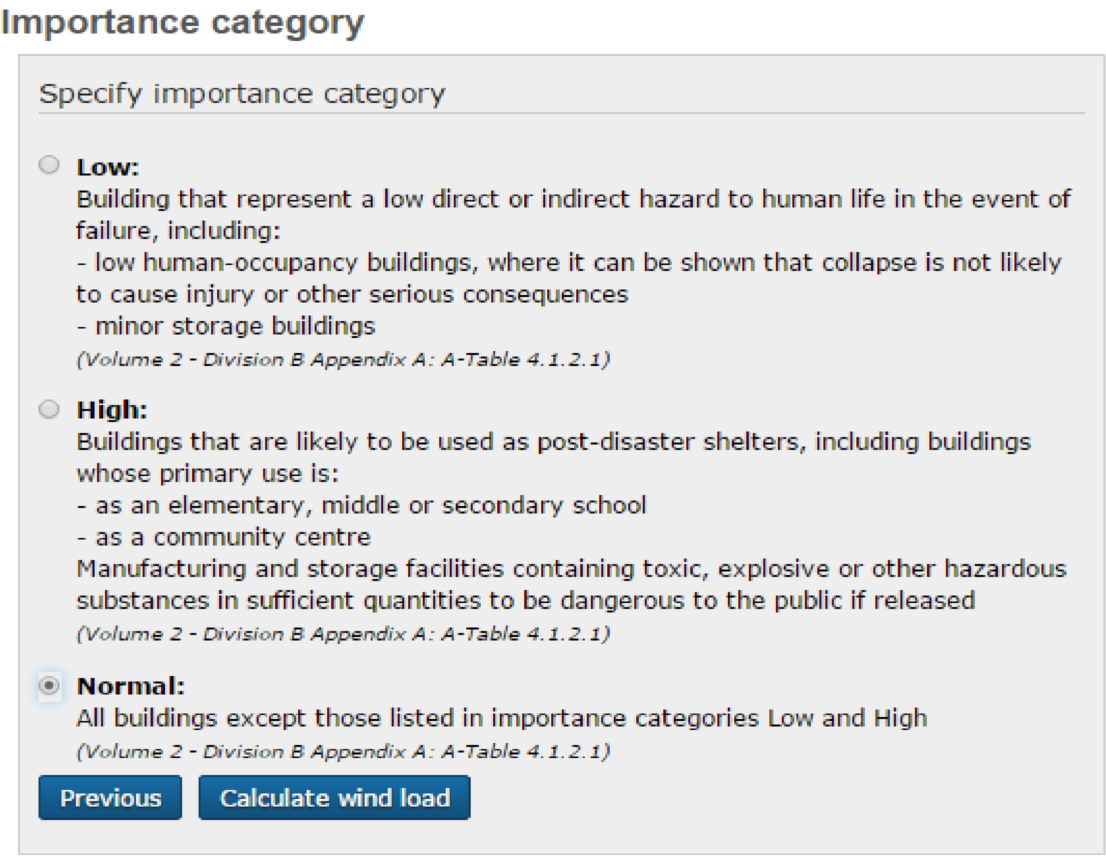

Importance category

Specify importance category

○ **Low:**
Building that represent a low direct or indirect hazard to human life in the event of failure, including:
- low human-occupancy buildings, where it can be shown that collapse is not likely to cause injury or other serious consequences
- minor storage buildings

(Volume 2 - Division B Appendix A: A-Table 4.1.2.1)

○ **High:**
Buildings that are likely to be used as post-disaster shelters, including buildings whose primary use is:
- as an elementary, middle or secondary school
- as a community centre

Manufacturing and storage facilities containing toxic, explosive or other hazardous substances in sufficient quantities to be dangerous to the public if released
(Volume 2 - Division B Appendix A: A-Table 4.1.2.1)

● **Normal:**
All buildings except those listed in importance categories Low and High
(Volume 2 - Division B Appendix A: A-Table 4.1.2.1)

Figure F.5: Screen 5-Importance category

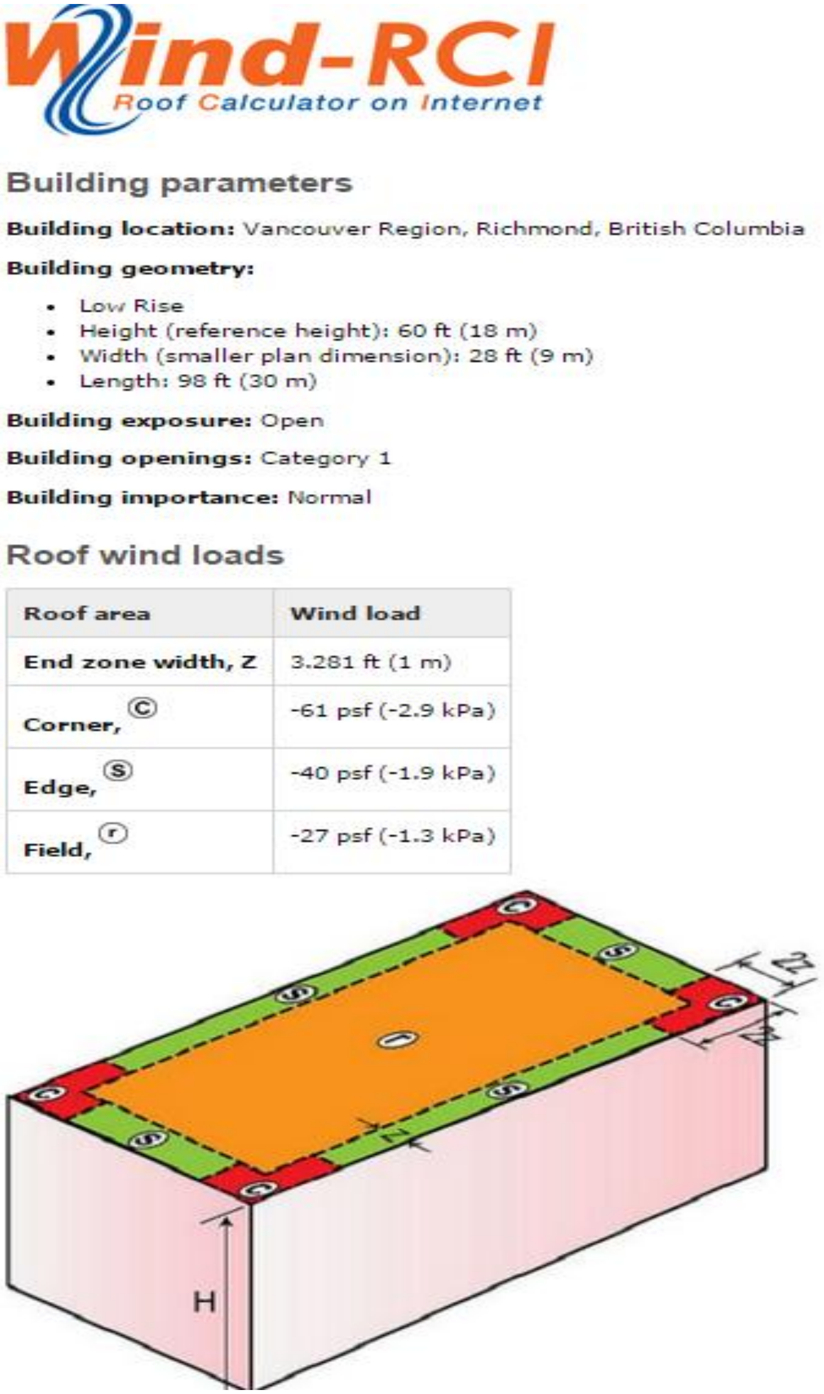

Wind-RCI
Roof Calculator on Internet

Building parameters

Building location: Vancouver Region, Richmond, British Columbia

Building geometry:

- Low Rise
- Height (reference height): 60 ft (18 m)
- Width (smaller plan dimension): 28 ft (9 m)
- Length: 98 ft (30 m)

Building exposure: Open

Building openings: Category 1

Building importance: Normal

Roof wind loads

Roof area	Wind load
End zone width, Z	3.281 ft (1 m)
Corner, Ⓒ	-61 psf (-2.9 kPa)
Edge, Ⓢ	-40 psf (-1.9 kPa)
Field, ⓡ	-27 psf (-1.3 kPa)

Figure F.6: Wind-RCI report

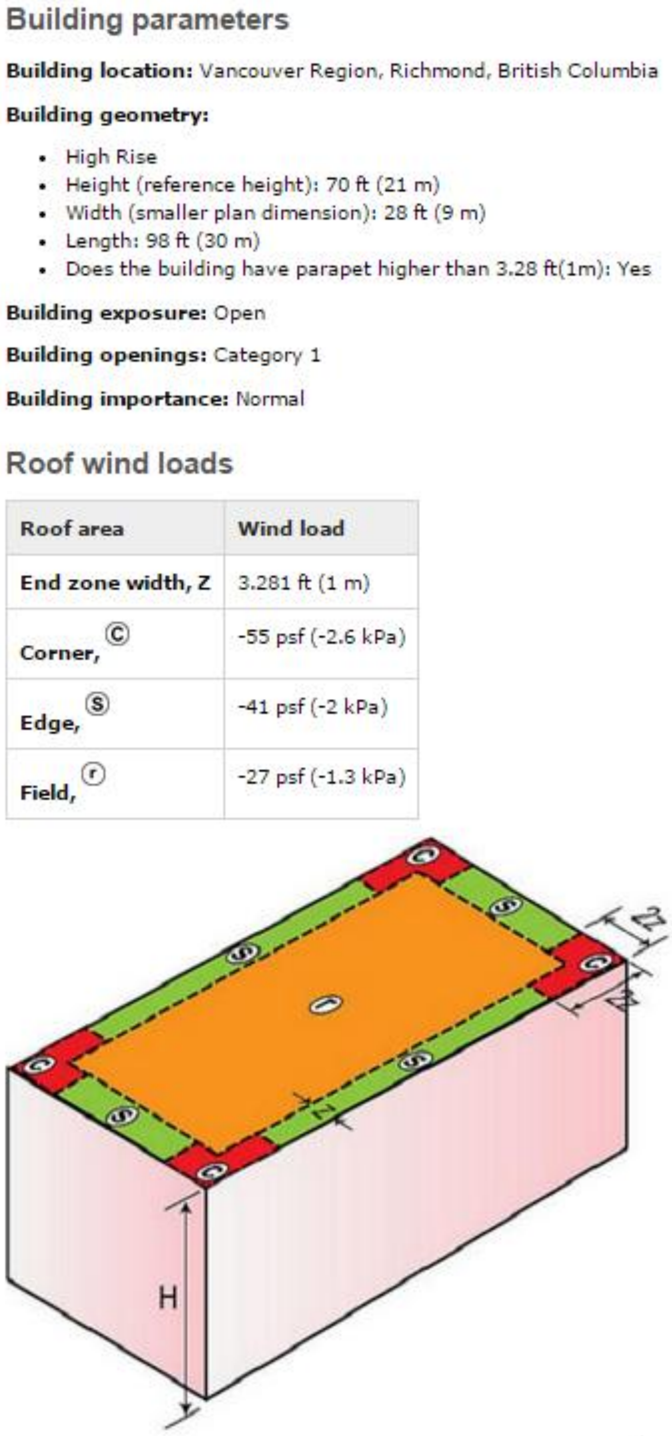

Building parameters

Building location: Vancouver Region, Richmond, British Columbia

Building geometry:

- High Rise
- Height (reference height): 70 ft (21 m)
- Width (smaller plan dimension): 28 ft (9 m)
- Length: 98 ft (30 m)
- Does the building have parapet higher than 3.28 ft(1m): Yes

Building exposure: Open

Building openings: Category 1

Building importance: Normal

Roof wind loads

Roof area	Wind load
End zone width, Z	3.281 ft (1 m)
Corner, ⓒ	-55 psf (-2.6 kPa)
Edge, ⓢ	-41 psf (-2 kPa)
Field, ⓡ	-27 psf (-1.3 kPa)

Figure F.7: Wind report for high-rise building

Appendix G

NBCC Code Change Request

The details of the submitted code change request form to the NBCC is seen in the appendix.

Table G.1: Code change request

Code change to:	new
Code Name:	2010nbc
Code Reference:	
Subject:	Design wind loads on roof metal edges
Problem:	The current building code does not specify design wind loads for roof metal edges or parapets. Recent studies based on full-scale field measurements have shown that roof metal edges are subjected to negative pressures on windward, top and leeward faces (Bysice 2015). Failure of roof edge components have led to major roof failures due to strong wind events (Baskaran et al. 2007). In order to properly design these roof components, their wind design load needs to be specified.
Proposed Change/Addition:	A roof metal edge shall be designed to sustain wind load on all of its faces (windward, top and leeward). For conservatism, the value of design wind load to be used should be that prescribed for roof field.
Justification/Explanation:	Roof metal edges are subjected to wind-induced negative pressures on all of its faces, as observed by Jiang (1995), McDonald et al. (1997) and Bysice (2015). The highest suction observed for three different types of roof edge configurations consistently acts on the top face of the metal edge. Furthermore, the values for this suction are of lower magnitude than those observed in the roof, as experimentally observed by Stathopoulos et al. (1999) and calculated by Bysice (2015). For conservatism, it is therefore suggested that the prescribed roof pressure be applied as a design load on all faces of the metal edges.
Objectives:	2010 NBC OP2 Structural Sufficiency of the Building

	2010 NBC OP2.1 loads bearing on the building elements that exceed their 2010 NBC OP2.3 damage to or deterioration of building elements 2010 NBC OS2 Structural Safety 2010 NBC OS2.1 loads bearing on the building elements that exceed their loadbearing capacity 2010 NBC OS2.3 damage to or deterioration of building elements
Cost Implications:	The roof edge systems would have to be designed by a professional engineer. The system will be designed appropriately for imposed loads, and roof failures originating at the edge will be reduced. This will result in a reduction of future costs of repair/replacement.
Enforcement Implications:	Only professional engineers will be allowed to sign for roof edges designs.
Other Comments:	Baskaran, A., Molleti, S. and Roodvoets, D. (2007) “Understanding low-slope roofs under hurricane Charley from field to practice.” *Journal of ASTM International*, 4, (10). Bysice, J. (2013). “Wind Uplift Resistance of Roof Edge Components.” Master’s Thesis, University of Ottawa, Canada. Jiang, H. (1995). “Wind Effects on Metal Edge Flashings.” Master’s thesis, Texas Tech University, Lubbock, Texas, USA. Mcdonald, J., P. Sarkar, and H. Gupta (1997). "Wind-induced Loads on Metal Edge Flashings." *Journal of Wind Engineering and Industrial Aerodynamics* 72: 367-77. Stathopoulos, T., Marathe, R., Wu, H (1999). “Mean wind pressures on flat roof corners affected by parapets: field and wind tunnel studies.” *Engineering Structures* 21: 629–638.